R-10-18

Hydrological and hydrogeological effects of an open repository in Forsmark

Final MIKE SHE flow modelling results for the Environmental Impact Assessment

Erik Mårtensson, Lars-Göran Gustafsson
DHI Sverige AB

July 2010

Svensk Kärnbränslehantering AB
Swedish Nuclear Fuel
and Waste Management Co

Box 250, SE-101 24 Stockholm
Phone +46 8 459 84 00

ISSN 1402-3091
SKB R-10-18

Hydrological and hydrogeological effects of an open repository in Forsmark

Final MIKE SHE flow modelling results for the Environmental Impact Assessment

Erik Mårtensson, Lars-Göran Gustafsson
DHI Sverige AB

July 2010

Abstract

This report presents methodology and modelling results concerning a deep-rock repository for spent nuclear fuel in Forsmark. Specifically, the modelling tools MIKE SHE, MIKE 11 and MOUSE are used to quantify the groundwater inflow to the repository and associated hydrological and hydrogeological effects during the construction and operation phases. The modelling results presented in the report provide input to the Environmental Impact Assessment (EIA) that will be part of a permit application according to the Environmental Code.

Based on an existing MIKE SHE model for Forsmark, the first step of the modelling process was to implement an updated hydrogeological model of the bedrock and to increase the vertical and horizontal extents of the model domain. Other model updates involve the vegetation classification, and implementation of SFR (final repository for short-lived radioactive waste) and the subsurface-drainage system at the nearby nuclear power plant.

The updated model was calibrated using measured data on groundwater levels in the Quaternary deposits and the bedrock, water levels in lakes, and stream discharges. The calibrated model was then used for simulation of undisturbed conditions (i.e. without the repository) as a reference for modelling results obtained for disturbed conditions (with the repository). The modelling results for undisturbed conditions that are presented in the report closely resemble those of the final MIKE SHE site descriptive modelling (SDM-Site Forsmark).

The repository layout was implemented as pipe links (segments) in the modelling tool MOUSE, and the implemented layout was used for the modelling of disturbed conditions. The study uses an updated and verified MIKE SHE-MOUSE coupling routine that is specifically adapted for calculation of groundwater inflow to grouted rock tunnels. The vertical shafts of the repository are implemented in the form of MIKE SHE grid cells with atmospheric pressure.

Modelling results for disturbed conditions show that the magnitude and the geographical extent of the groundwater-table drawdown are smaller than the hydraulic-head drawdown in the bedrock. The influence area for the groundwater-table drawdown primarily coincides with locations where the Quaternary deposits are in contact with bedrock containing fracture zones with high vertical hydraulic conductivity.

The groundwater inflow to the repository, the groundwater-table drawdown and the drawdown of hydraulic heads in the bedrock were analysed for different values of the hydraulic conductivity of the grouted zone (K_{grout}) and also for layouts that aim to represent different repository-development phases. For a hypothetical case with a fully open repository, the model-calculated inflow is in the interval 15–47 L/s depending on the value of K_{grout}. Using meteorological data and sea-level data for the year 2006, the associated influence area for the groundwater-table drawdown (annual average drawdown exceeding 0.3 m) has a size of 1.4 km^2 for $K_{grout} = 10^{-7}$ m/s and less than half for $K_{grout} = 10^{-9}$ m/s.

According to the modelling results, the groundwater inflow to the repository has very small effects on water levels in lakes and discharges in streams. However, for $K_{grout} = 10^{-7}$ m/s the annually accumulated discharge in the stream upstream from Lake Bolundsfjärden is reduced by 13%, which is due to draw-down of the groundwater table within the catchment area of the stream.

Sensitivity analyses show that the groundwater inflow to the repository and the size of the groundwater-table influence area are not very sensitive to the tested variants concerning the hydrogeological properties of the upper 200 m of the bedrock and the boundary conditions (including the sea level). The model-calculated influence area demonstrates some sensitivity to the choice of methodology for modelling water flow in the unsaturated zone. Moreover, the influence area is larger if the hydrogeological properties in the upper 20 m of the model domain are the same as those used in a parallel DarcyTools modelling activity.

According to the MIKE SHE modelling results, the inflow to a planned extension of SFR will have no or very limited impact on the inflow to the repository and also on the location of the groundwater table, compared to a situation with the repository and the present SFR layout. Moreover, results of so called

particle tracking show that there is a low probability for spreading of water-soluble substances from the grouted zone to the ground surface. A simplified approach was used for modelling of the backfill saturation and the groundwater-level recovery subsequent to the operational phase of the repository. The results indicate that the location of the groundwater table will be fully recovered within a few years after termination of the groundwater diversion from the repository.

Sammanfattning

Denna rapport presenterar metodik och modelleringsresultat gällande ett slutförvar för använt kärnbränsle i djupt berg i Forsmark. Specifikt används modelleringsverktygen MIKE SHE, MIKE 11 och MOUSE för att kvantifiera inläckaget av grundvatten till förvaret och därtill kopplade hydrologiska och hydrogeologiska effekter i samband med skedena uppförande och drift. De modelleringsresultat som presenteras i rapporten utgör underlag för den miljökonsekvensbeskrivning (MKB) som ska ingå i en tillståndsansökan enligt miljöbalken.

Baserat på en befintlig MIKE SHE-modell för Forsmark gjordes som ett första steg i modelleringsprocessen en implementering av en uppdaterad hydrogeologisk modell för berget och en utökning av modelldomänens horisontella och vertikala utsträckningar. Andra modelluppdateringar berör vegetationsklassificeringen och implementering av SFR (slutförvar för kortlivat radioaktivt avfall) och dräneringssystemet under mark vid det närbelägna kärnkraftverket.

Den uppdaterade modellen kalibrerades mot uppmätta data på grundvattennivåer i jordlagren och berget, vattennivåer i sjöar och vattenföring i bäckar. Den kalibrerade modellen användes därefter för simulering av opåverkade förhållanden (det vill säga, utan förvaret) som en referens för modelleringsresultaten för påverkade förhållanden (med förvaret). De modelleringsresultat som presenteras i rapporten uppvisar stora likheter med motsvarande resultat från den platsbeskrivande MIKE SHE-modelleringen (SDM-Site Forsmark).

Förvarets utformning implementerades som rörlänkar (segment) i modelleringsverktyget MOUSE, och den implementerade utformningen användes för modelleringen av påverkade förhållanden. I studien används en uppdaterad och verifierad rutin för kopplingen mellan MIKE SHE och MOUSE, specifikt anpassad för beräkning av inläckage av grundvatten till injekterade bergtunnlar. Förvarets vertikala schakt är implementerade i MIKE SHE som beräkningsceller med atmosfärstryck.

Modelleringsresultaten för påverkade förhållanden visar att storleken och den geografiska utsträckningen av grundvattenytans avsänkning är mindre än sänkningen av grundvattennivåerna i berget. Påverkansområdet för grundvattenytans avsänkning sammanfaller främst med lägen där jordlagren är i kontakt med sprickzoner med hög vertikal hydraulisk konduktivitet.

Inläckaget av grundvatten till förvaret, grundvattenytans avsänkning och sänkningen av grundvattennivåerna i berget analyserades för olika värden på den hydrauliska konduktiviteten i den injekterade zonen (K_{grout}) och även för utformningar som syftar till att representera förvarets olika utbyggnadssteg. För ett hypotetiskt fall med ett helt öppet förvar är det modellberäknade inläckaget 15–47 l/s beroende på värdet på K_{grout}. Med meteorologiska data och havsnivådata för året 2006 har det tillhörande påverkansområdet för grundvattenytans avsänkning (avsänkningens årsmedelvärde > 0,3 m) en storlek på 1,4 km^2 för $K_{grout} = 10^{-7}$ m/s och mindre än hälften för $K_{grout} = 10^{-9}$ m/s.

Enligt modelleringsresultaten ger inläckaget mycket små effekter på vattennivåer i sjöar och vattenföring i bäckar. För $K_{grout} = 10^{-7}$ m/s reduceras dock den årliga ackumulerade vattenföringen i bäcken uppströms från sjön Bolundsfjärden med 13 %, vilket beror på avsänkningen av grundvattenytan inom bäckens avrinningsområde.

Känslighetsanalyser visar att inläckaget av grundvatten till förvaret och storleken på grundvattenytans avsänkning inte är känsliga för de testade varianterna vad gäller de hydrogeologiska egenskaperna i de övre 200 m av berget och randvillkoren (inklusive havets nivå). Det modellberäknade påverkansområdet uppvisar viss känslighet för valet av metodik för modellering av vattenflöde i den omättade zonen. Vidare är påverkansområdet större om de hydrogeologiska egenskaperna är samma som de som används i en parallell modelleringsaktivitet med DarcyTools.

Enligt resultaten från MIKE SHE-modelleringen kommer inläckaget till en planerad utbyggnad av SFR endast att ge en liten eller ingen inverkan på inläckaget till förvaret och likaså på grundvattenytans läge, jämfört med situationen med förvaret och befintligt SFR. Vidare visar resultat från så kallad partikelspårning att det är mycket liten sannolikhet för spridning av vattenlösliga ämnen från den injekterade zonen till markytan. Ett förenklat angreppsätt användes för modellering av återfyllnadsmaterialets mättnad och återhämtningen av grundvattennivåer efter förvarets driftskede. Resultaten indikerar att grundvattenytans läge kommer att ha återhämtats helt inom några år efter det att grundvattenbortledningen från förvaret upphört.

Contents

1 Introduction

1.1 Background

The Swedish Nuclear Fuel and Waste Management Co (SKB) has performed site investigations at two different locations in Sweden, referred to as the Forsmark and Laxemar-Simpevarp areas, with the objective of siting a final repository for spent nuclear fuel. In 2009 Forsmark was chosen as site for the repository. Data from the site investigations are used in a variety of modelling activities, and the results are utilised within the frameworks of Site Descriptive Modelling (SDM), Safety Assessment (SA) and Environmental Impact Assessment (EIA). The SDM provides a description of the present conditions at the site, and is used as a basis for developing models of future conditions in the area. The effects of an open repository on the hydrological and near-surface hydrogeological conditions in Forsmark have previously been studied in /Gustafsson et al. 2009/. In this report, known deficiencies of the SDM-Site model /Bosson et al. 2008/ and the open repository model of /Gustafsson et al. 2009/ are corrected. Moreover, the model is updated with the latest hydrogeological bedrock model and vegetation classification, both identical with the ones used within the safety assessment (SR-Site).

The numerical modelling was performed with the modelling tools MIKE SHE and MOUSE, and is based on the conceptual description of the Forsmark site provided in /Johansson 2008/ and /Follin et al. 2008/. The modelling performed in this project is based on the SDM-Site Forsmark model /Bosson et al. 2008/. All the different subject areas within the site descriptive modelling project are summarised in /SKB 2008a/, whereas the surface systems are described in more detail in /Lindborg (ed) 2008/.

The repository will be kept drained during the construction and operation phases, and there will therefore be atmospheric pressure in the open tunnels, shafts and rock caverns of the repository. This will cause disturbances in the pressure field around the subsurface constructions and an inflow of groundwater. The size of this inflow and its possible effects on surrounding groundwater and surface-water systems need to be quantified. The issues related to the effects of the open repository concern both the conditions in the repository (inflows and hydrochemical conditions) and in the surrounding environment (groundwater levels, surface-water levels and -discharges). Thus, the open repository modelling provides results to both SA and EIA. The modelling work presented here is a continuation and update of the open repository modelling work described in /Gustafsson et al. 2009/ and replaces the results presented in previous reports /Bosson and Berglund 2006, Gustafsson et al. 2009/. However, some specific analyses in /Gustafsson et al. 2009/, such as sensitivity analyses concerning hydraulic properties and evaluation of seasonal effects, are considered sufficient for their purposes and are therefore not repeated in the present report. The work presented here is an input to the final EIA, whereas the study by /Gustafsson et al. 2009/ provided input to the preliminary EIA, which was presented in the end of 2009.

1.2 Scope and objectives

The present work can be subdivided into the following four parts:

- Comparison between the updated MIKE SHE-MOUSE coupling routine and an analytical solution of groundwater inflow to a grouted tunnel. Further, this updated coupling routine is implemented in the open repository model of /Gustafsson et al. 2009/, in order to determine the influence of the routine on the calculated inflow to the repository and the drawdown of the groundwater table.
- Updating of the SDM-Site Forsmark numerical flow model and simulation of undisturbed conditions. The model updates include a new hydrogeological bedrock model compared to the one used in /Bosson et al. 2008, Gustafsson et al. 2009/, enlargement of the model area, a new vegetation classification, an updated representation of SFR (final repository for short-lived radioactive waste) and representation of the drainage system at the nuclear power plant.
- Implementation of the open repository in the updated flow model, and analysis of the hydrological effects of an open repository and of an extension of SFR, including effects on the surface hydrology and the hydrogeological conditions in the Quaternary deposits and the upper bedrock.

- Analysis of the sensitivity of the modelling results to the hydrogeological properties of the upper bedrock and the Quaternary deposits, the boundary conditions, the procedure for modelling water flow in the unsaturated zone and a future scenario with an increased sea level.

The general objectives of the present modelling are the following:

- Develop and present an updated open repository flow model based on the SDM-Site Forsmark MIKE SHE model, using an updated MIKE SHE-MOUSE coupling routine.
- Provide final quantitative results for the EIA regarding the repository in Forsmark, in terms of the influence of the open repository on groundwater levels, surface-water levels and -discharges within the model area.
- Evaluate the inflow to different parts of the open repository for three different grouting cases and for different phases of repository construction and development.
- Evaluate the influence of an extension of SFR on groundwater inflows and groundwater levels.

1.3 Setting

The Forsmark area is located approximately 120 km north of Stockholm, in northern Uppland in the municipality of Östhammar. Figure 1-1 shows parts of the regional model area and the so called candidate area. It also shows some lakes and other objects of importance for the hydrological modelling.

The candidate area is the area initially prioritised for potentially hosting the geological repository, which means that the repository possibly could be built somewhere within this area, not that it would occupy the whole area. This implies that more detailed investigations have been performed within the candidate area than outside it, at least for some of the site investigation disciplines, see /SKB 2008a/ for details.

The candidate area is situated in the immediate vicinity of the Forsmark nuclear power plant and the underground final repository for short-lived radioactive waste, SFR. The candidate area is located along the shoreline of Öregrundsgrepen (part of the Baltic Sea), and extends from the nuclear power plant and the access road to SFR in the northwest to the Kallrigafjärden bay in the southeast. The candidate area is approximately 6 km long and 2 km wide.

A description of climate and hydrological and hydrogeological conditions in the Forsmark area is presented in /Johansson 2008/. /Lindborg (ed.) 2008/ gives a description of the surface and near-surface system, including models of e.g. topography and Quaternary deposits.

In this report, the datum plane is RHB 70. Depending on the type of data, levels will be given in metres above sea level (m.a.s.l.) or metres below sea level (m.b.s.l.) according to the RHB 70 system.

1.4 Modelling procedure

The modelling work is based on the SDM-Site Forsmark MIKE SHE model /Bosson et al. 2008/. A reference simulation for undisturbed conditions was performed using an updated version of the calibrated final model version as described in /Bosson et al. 2008/. In the next step, the tunnels, shafts and rock caverns were introduced into the model to investigate how these constructions will affect the hydrology and near-surface hydrogeology in the model area. The last step was a sensitivity analysis which aimed to investigate the sensitivity of the modelling results to the hydrogeological properties of the upper bedrock and Quaternary deposits, the boundary conditions, the modelling procedure of the unsaturated zone and a future scenario with an increased sea level.

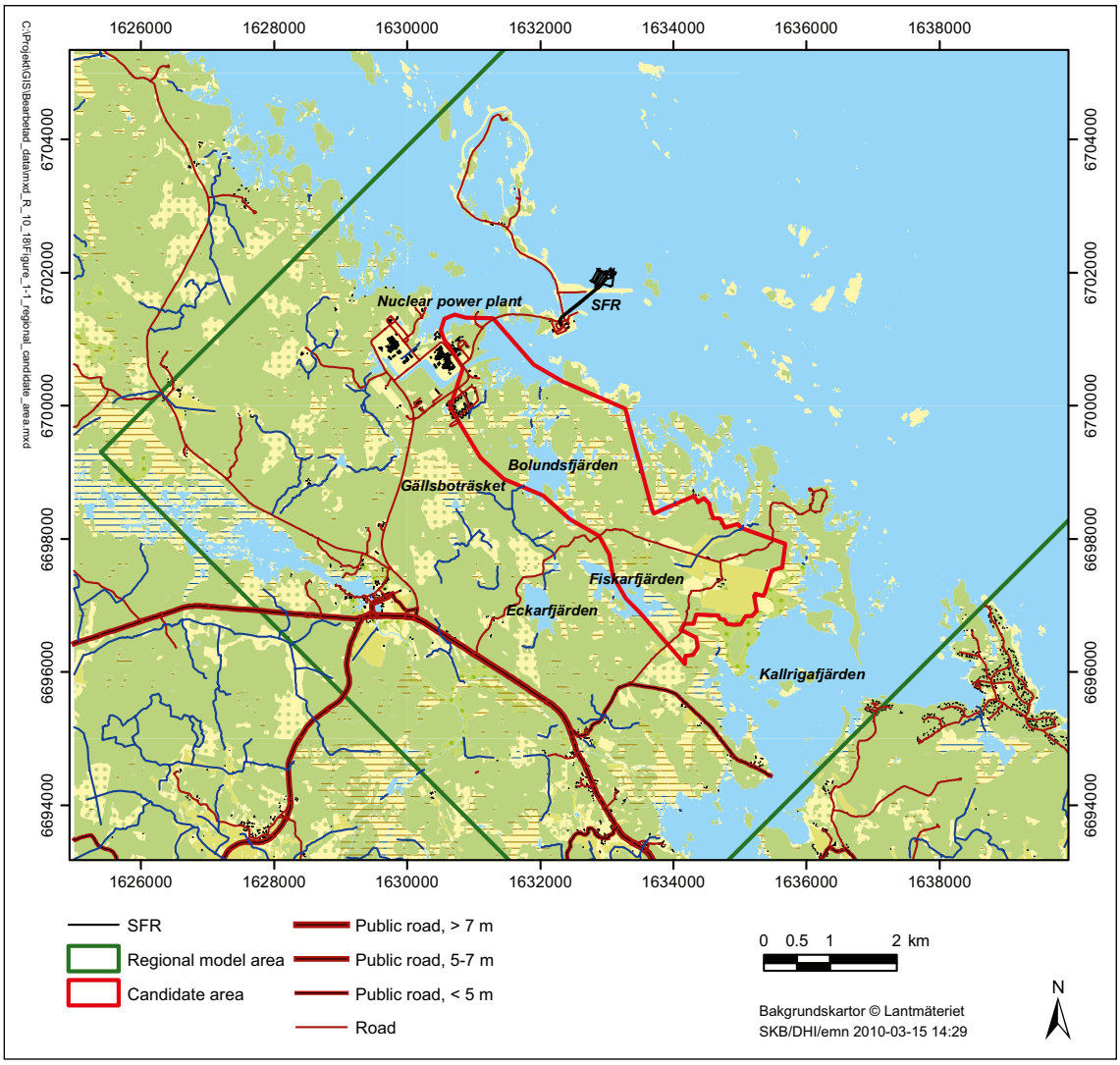

Figure 1-1. *Detailed map of the land part of the regional model area and some objects of particular interest for the hydrological modelling.*

1.5 Related modelling activities

Several modelling activities have provided external input data and models required for the present modelling. Whereas most of these inputs are described in /Bosson et al. 2008/, we here briefly discuss interactions with modelling activities that consider flow of the integrated bedrock-Quaternary deposits system and modelling activities analysing the influences of an open repository and the design of the planned repository.

The numerical model was developed using the MIKE SHE tool, coupled with the modelling tool MOUSE that describes the geometry of the repository and the interactions with the surrounding groundwater system. The ground surface, represented by the topographic model (DEM) of the site, was the upper model boundary and the lower boundary was set at 1,200 m.b.s.l. The modelling activities that provided inputs to the various parts of this work can be summarised as follows:

- The Forsmark SR-Site hydrogeological modelling performed with the CONNECTFLOW modelling tool /Joyce et al. 2010/ delivered the hydrogeological properties of the bedrock.
- The SDM-Site conceptual modelling of the surface hydrology and near-surface hydrogeology at Forsmark /Johansson 2008/ provided a basic hydrogeological parameterisation and a hydrological-hydrogeological description to be tested in the numerical modelling. The relations between the near-surface and bedrock hydrogeological models are discussed in /Follin et al. 2008, SKB 2008a/.

- The MIKE SHE SDM-Site Forsmark numerical modelling of the surface hydrology and near-surface hydrogeology at Forsmark /Bosson et al. 2008/. All the simulations in this report are based on an update of the final version of the MIKE SHE model described in /Bosson et al. 2008/.
- The MIKE SHE numerical flow modelling of hydrological and near-surface hydrogeological effects of groundwater inflow to an open repository /Gustafsson et al. 2009/. As mentioned previously, the present report is a continuation and an update of the work presented in /Bosson and Berglund 2006, Gustafsson et al. 2009/, and the results in this report therefore supersede those presented in the previous studies.
- The open repository simulations performed in DarcyTools /Svensson and Follin 2010/. The DarcyTools modelling focuses on the bedrock and the conditions at repository level, including detailed studies of the groundwater inflow during construction and operation, and the inflow and backfill saturation subsequent to repository decommissioning.
- The MIKE SHE SR-Site Forsmark numerical flow modelling and transport modelling of surface water and near-surface groundwater for present and future conditions (2000 AD, 5000 AD and 10,000 AD) /Bosson et al. 2010/.
- The DarcyTools modelling related to SFR and its planned extension /Odén 2009/.

1.6 This report

This report provides an integrated presentation of the modelling activities listed in Section 1.2. Chapter 2 describes the modelling tool and the numerical flow model. Chapter 3 presents the results from simulations with the open repository model of /Gustafsson et al. 2009/, using an updated MIKE SHE-MOUSE coupling routine. The results are compared with an analytical solution and the results presented in /Gustafsson et al. 2009/. Chapter 4 presents model updates, simulation specifications as well as conditions and simulation cases for disturbed conditions, i.e. with the open repository included in the model. Chapter 5 provides model-calibration results. The results of a reference simulation for undisturbed conditions are presented in Chapter 6. Chapter 7 presents results from simulations of disturbed conditions, whereas Chapter 8 describes and presents results from a sensitivity analysis with respect to the impact from an open repository. Chapter 9 discusses different types of uncertainties. Chapter 10 summarises the results and presents the conclusions of the work.

2 Overview of modelling tools

2.1 MIKE SHE

MIKE SHE is a physically based, distributed model that simulates water flows from rainfall to river flow. It is a commercial code, developed by the Danish Hydraulic Institute (DHI). This sub-section summarises the basic processes and the governing equations in MIKE SHE. The code used in this project is software release version 2010. For a more detailed description, see the technical reference and the user's guide /Graham and Butts 2005, DHI Software 2010a/.

MIKE SHE describes the main processes in the land phase of the hydrological cycle. The precipitation can either be intercepted or fall to the ground. The water on the ground surface can infiltrate, evaporate or form overland flow. Once the water has infiltrated the soil, it enters the unsaturated zone. In the unsaturated zone, it can either be extracted by roots and leave the system as transpiration, or it can percolate down to the saturated zone (Figure 2-1). MIKE SHE is fully integrated with the channel-flow code MIKE 11. The exchange of water between the two modelling tools takes place during the whole simulation, i.e. the two programs run simultaneously.

MIKE SHE is developed primarily for modelling of groundwater flow in porous media. In the present modelling, the bedrock is included as a porous medium. MIKE SHE consists of the following model components:

- Precipitation (rain or snow).
- Evapotranspiration, including canopy interception, which is calculated according to the principles in /Kristensen and Jensen 1975/.
- Overland flow, which is calculated with a 2D finite difference diffusive wave approximation of the Saint-Venant equations, using the same 2D mesh as in the horizontal mesh used in the (3D) groundwater flow component. Overland flow interacts with rivers, the unsaturated zone, and the saturated (groundwater) zone.
- Channel flow is described by MIKE 11, which is a modelling system for river hydraulics. MIKE 11 is a dynamic, 1D modelling tool for the design, management and operation of rivers and channel systems. MIKE 11 supports any level of complexity and offers simulation tools that cover the entire range from simple Muskingum routing to high-order dynamic wave formulations of the Saint-Venant equations.
- Unsaturated water flow, which in MIKE SHE is described as a vertical soil profile model that interacts with both the overland flow (through ponding) and the groundwater flow (the groundwater table provides the lower boundary condition for the unsaturated zone). MIKE SHE offers three different modelling approaches, including a simple two-layer root-zone mass balance approach, a gravity flow model, and a full Richards equation model.
- Saturated (groundwater) flow, which allows for 3D flow in heterogeneous media, with conditions shifting between unconfined and confined. The spatial and temporal variations of the dependent variable (the hydraulic head) are described mathematically by the 3D Darcy equation and solved numerically by an iterative implicit finite difference technique.

For a detailed description of the processes included in MIKE SHE and MIKE 11, see /DHI Software 2010a/.

2.2 The coupling between MIKE 11 and MIKE SHE

The coupling between MIKE 11 and MIKE SHE is made via river links, which are located on the edges that separate adjacent grid cells. The location of each river link is determined from the co-ordinates of the MIKE 11 river points. Since the MIKE SHE river links are located on the edges between grid cells, the details of the MIKE 11 river geometry can be only partly included in MIKE SHE, depending on the grid size. The smaller the grid size, the more accurately the river network can be reproduced. This also leads to the restriction that each MIKE SHE grid cell can only be coupled to one coupling reach in MIKE 11 per river link in MIKE SHE.

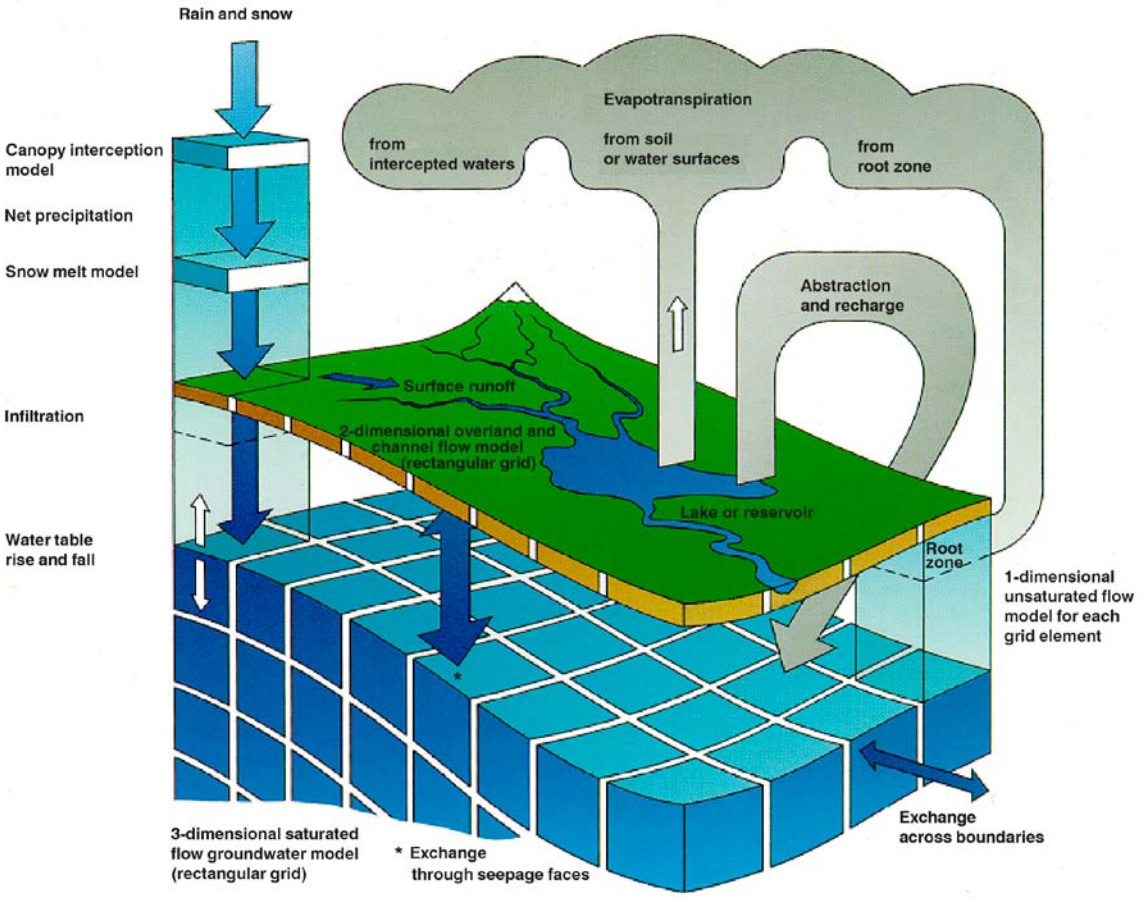

Figure 2-1. *Overview of the MIKE SHE model /DHI Software 2010a/.*

2.2.1 Overland water

The communication between the river network in MIKE 11 and the overland component in MIKE SHE can be defined in two different ways:

- Using so called flood codes, where water levels from MIKE 11 simply are transferred to MIKE SHE.
- Using a two-way communication based on a so-called overbank spilling option.

In this version of the Forsmark model, the two-way overbank spilling option is applied. This option allows river water to spill onto the MIKE SHE model as overland flow. The overbank spilling option treats the river bank as a weir. When the overland flow water level or the river water level is above the left or right bank elevation, water will spill across the bank based on the weir formula in Equation 2-1. The principle is illustrated in Figure 2-2.

$$Q = dx \cdot C \cdot (H_{us} - H_w)^k \cdot \left[1 - \left(\frac{H_{ds} - H_w}{H_{us} - H_w}\right)^k\right]^{0.385} \qquad 2\text{-}1$$

Q Flow across the weir (m^3/s).

dx Grid size (m).

C Weir coefficient (–), set to the default value 1.838.

H_{us} Height of water on the upstream side of the weir (m).

H_{ds} Height of water on the downstream side of the weir (m).

H_w Height of the weir (m).

k Head exponent (–), set to the default value 1.5, in order to account for both the flow area and the head gradient according to the Manning equation.

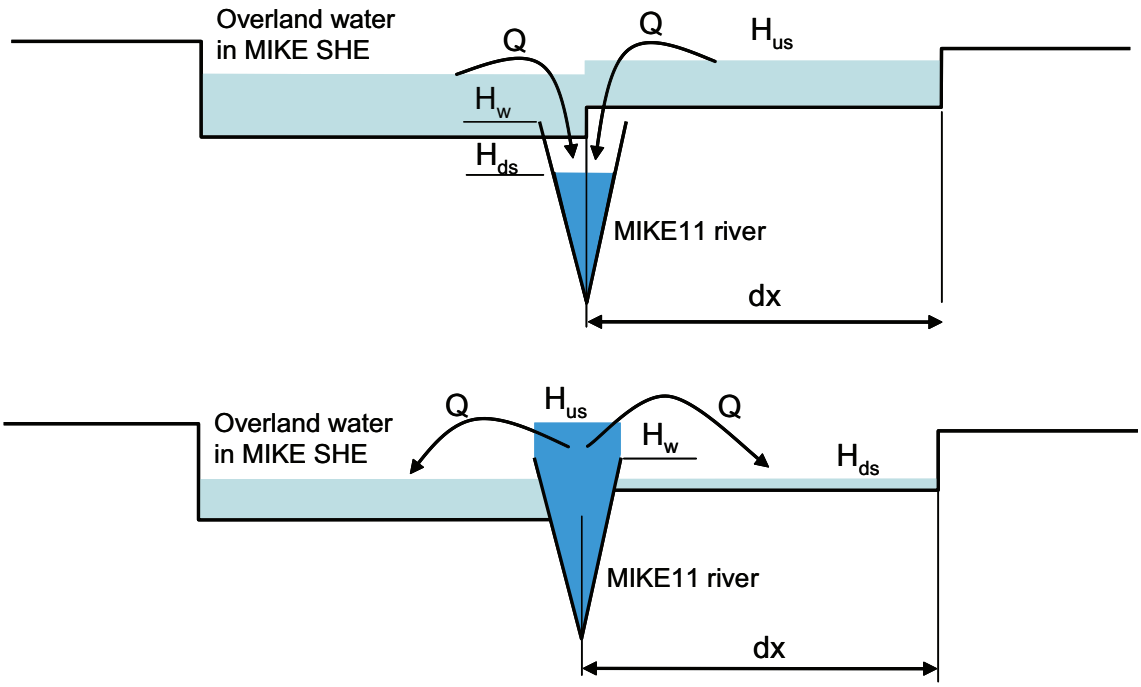

Figure 2-2. *Illustration of the overland coupling between MIKE 11 and MIKE SHE, and representation of parameters for calculating the exchange of water.*

Note that Equation 2-1 is calculated twice, i.e. once for each cell on either side of the river link. This allows for different flow to/from either side of the river if there is an overland water level gradient across the river, or if the right and left river bank levels are different.

If overland water levels are such that overland water is flowing to the river, overland flow to the river is added to MIKE 11 as lateral inflow. If the water level in the river is higher than the level of ponded water, river water will spill onto the MIKE SHE cell and become part of the overland flow. If the upstream water depth over the weir approaches zero, the flow over the weir becomes undefined. Therefore, the calculated flow is reduced to zero linearly when the upstream height is below a certain threshold.

2.2.2 Groundwater

The communication between the river network and the groundwater is calculated in the same way as in previous versions of the code /DHI Software 2010a/. The groundwater coupling between MIKE 11 and MIKE SHE is made via river links, on the edges that separate adjacent grid cells. The exchange flow between a saturated zone grid cell, in contact with the river system, and a river link is included as a source/sink term in the governing flow equation in MIKE SHE for three-dimensional saturated flow. The exchange flow is calculated as a conductance multiplied by the head difference between the river and the grid cell according to Equation 2-2. The principle is illustrated in Figure 2-3.

$$Q_{cell} = dh \cdot C \qquad 2\text{-}2$$

Q_{cell} Exchange flow from one neighbouring grid cell to the river link (m^3/s).

dh Head difference between the river link and the neighbouring grid cell (m).

C Total conductance (m^2/s).

Note that Equation 2-2 is calculated twice, once for each cell on either side of the river link. This allows for different flow to/from either side of the river if there is a groundwater head gradient across the river, or if the aquifer properties are different. The conductance between the grid cell and the river link is a function of the water level in the river, the river width, the elevation of the riverbed, as well as the hydraulic properties of the riverbed and the aquifer material, according to Equation 2-3 and Figure 2-3.

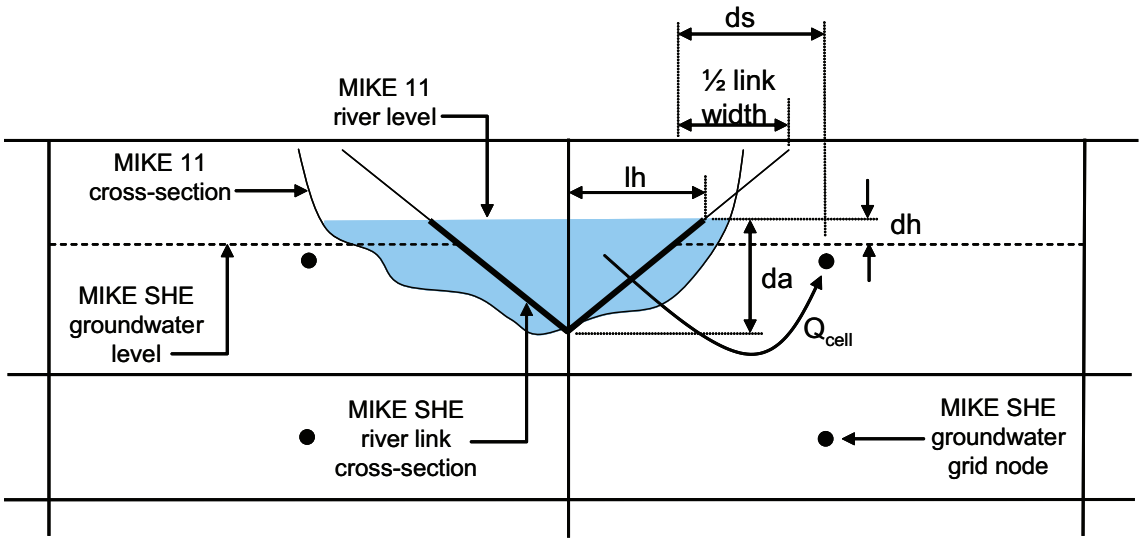

Figure 2-3. *Illustration of the groundwater coupling between MIKE 11 and MIKE SHE, and representation of parameters for calculating the exchange of water.*

$$C = \frac{1}{\frac{ds}{K_h \cdot da \cdot dx} + \frac{1}{LC \cdot P \cdot dx}} \qquad 2\text{-}3$$

K_h Horizontal hydraulic conductivity (m/s).

da Vertical surface available for exchange flow (m).

dx Grid size (m).

ds Average flow length (m), i.e. the distance from the grid node to the middle of the river bank.

P Wetted perimeter of the cross-section (m), assumed to be equal to the sum of the vertical (da) and horizontal (lh) lengths available for exchange flow (Figure 2-3).

LC Leakage coefficient of the bed material (s^{-1}).

The MIKE 11 model uses the precise cross-sections as defined in MIKE 11 for calculating river water levels and -volumes. However, the exchange of water between MIKE 11 and MIKE SHE is calculated based on the river link cross section, which is a simplified, triangular cross-section. The top width is equal to the distance between the left and right bank in the cross-section. The elevation of the bottom of the triangle equals the smallest depth of the MIKE 11 cross-section, see Figure 2-3.

2.3 The coupling between MOUSE and MIKE SHE

In the present open repository modelling, the program MOUSE /DHI Software 2010b/ has been used for modelling inflow to the repository. MOUSE is a modelling tool developed for urban hydrology and pipe-flow hydraulics. The coupling between MOUSE and MIKE SHE is typically used for calculating groundwater infiltration to sewers. In this project, the access tunnel from the ground surface down to the repository, the tunnels and rock caverns in the central area, the main- and transport tunnels and the deposition tunnels have been described as a number of pipe links in MOUSE. The program calculates the flow of water between the MIKE SHE groundwater model and the MOUSE model, i.e. the inflow of groundwater to the repository, according to Section 2.3.1. The exchange flow between a saturated zone grid cell (MIKE SHE) and a tunnel link (MOUSE) intersecting the grid cell is included as a source/sink term in the governing flow equation in MIKE SHE for three-dimensional saturated flow.

In the present version of the coupling between MOUSE and MIKE SHE, inflow of water to vertical shafts (manholes in MOUSE) is not allowed. Therefore, the inflow of water to the shafts is calculated in MIKE SHE only, see Section 2.3.2.

2.3.1 Leakage flows

In /Gustafsson et al. 2009/ the accuracy of the MIKE SHE-MOUSE coupling routine was tested and compared with an analytical solution (Equation 3-1) of groundwater inflow to a grouted tunnel. According to the test simulations, the groundwater inflow was found to be underestimated with approximately 20–40% compared to the analytical solution. The most likely reason behind these discrepancies between the MIKE SHE results and the analytical solution is that the flow resistance in the grouted zone around the tunnels was added to the bedrock properties, instead of replacing the bedrock with the grouted zone. If the interface between the subsurface cavity and the surrounding geological material is thin, like in the case of a concrete sewer pipe, this will not be a problem. However, in the case of a rather thick grouted zone (several metres), this zone a considerable part of the MIKE SHE grid cells.

A development of the MIKE SHE-MOUSE coupling routine has been performed as part of the present modelling work. Chapter 3 presents a comparison with an analytical solution and the effects of the new coupling routine on the calculated inflow to the open repository and on the drawdown of the groundwater table. Also, the reasons behind the discrepancies in the results between the old and new solution are further discussed (Section 3.1.3).

The new solution of groundwater inflow to a grouted tunnel implies that the exchange flow between MIKE SHE and MOUSE is calculated according to Equation 2-4. The principle is illustrated in Figure 2-4.

$$Q_{cell} = dh \cdot \frac{K \cdot 2 \cdot \pi}{\ln(\frac{r + d_{grout}}{r})} \cdot L \qquad 2\text{-}4$$

Q_{cell} Leakage flow from grid cell to tunnel (m^3/s).

dh Difference in hydraulic head between the grid cell where the tunnel is located (h_{aq}) and the tunnel link (h_t) (m).

L Length of a tunnel segment intersecting the grid cell (m).

K Hydraulic conductivity (m/s).

r Tunnel radius (m).

d_{grout} Thickness of the grouted zone (m).

The level of grouting and the ungrouted hydraulic conductivity of the bedrock, in both the vertical and the horizontal direction, are taken into consideration by setting the hydraulic conductivity, K, in Equation 2-4, according to Equation 2-5.

$$K = min\,[K_{grout},\, max\,[K_h,\, K_v]] \qquad 2\text{-}5$$

K_{grout} Hydraulic conductivity (m/s) of the grouted zone, i.e. the hydraulic conductivity of the bedrock near the tunnel after grouting.

K_h Horizontal hydraulic conductivity of the grid cell (m/s).

K_v Vertical hydraulic conductivity of the grid cell (m/s).

Equation 2-5 governs whether the hydraulic conductivity of the grouted zone, K_{grout}, or the aquifer, K_h or K_v, should be used when calculating the inflow to the tunnel (Equation 2-4). Only one of these conductivities is hence used in Equation 2-4. The hydraulic conductivity of the aquifer varies with depth and is set according to the conductivity in the actual calculation layer. The exchange of water also depends on the head difference between the tunnel and the aquifer, as well as the tunnel radius (Equation 2-4). The only input data needed for the coupled MIKE SHE-MOUSE simulation, except for the geometry and location of the tunnel, is the hydraulic conductivity of the grouted zone around the tunnel, K_{grout}, and the thickness of the grouted zone, d_{grout}, which may be specified as a unique value for each tunnel link.

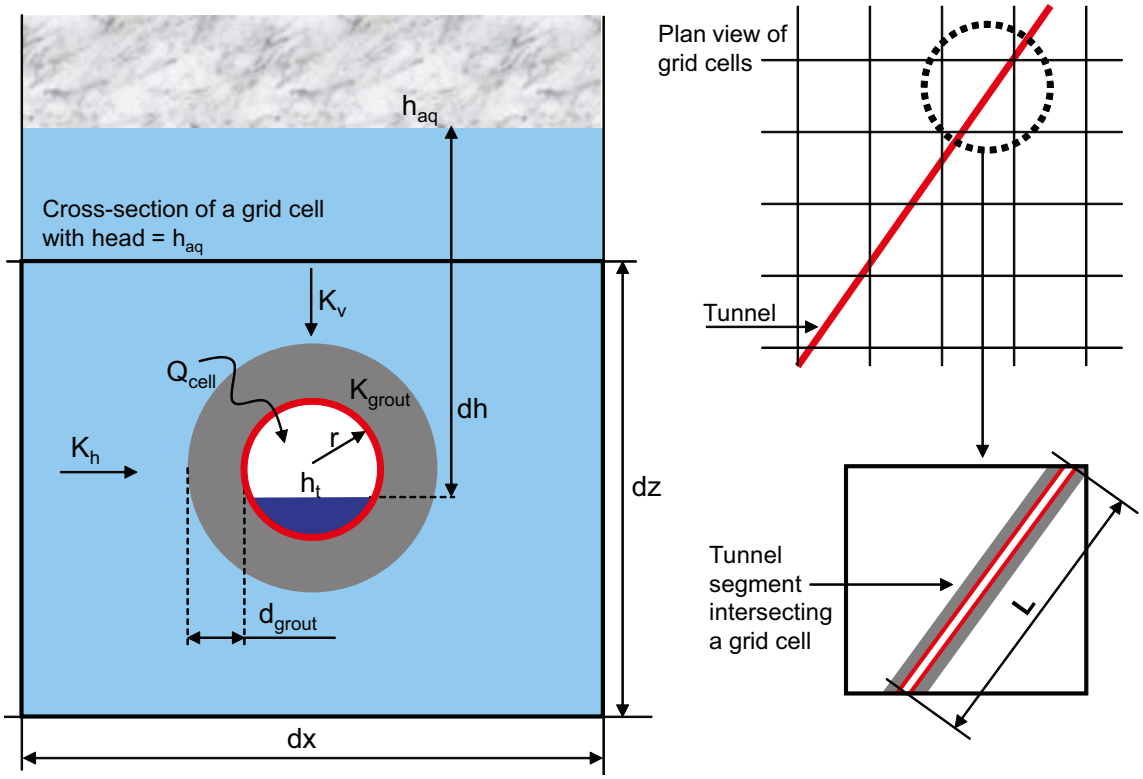

Figure 2-4. *Illustration of the groundwater coupling between MOUSE and MIKE SHE, and representation of parameters for calculating the exchange of water.*

2.3.2 Grouting of shafts

The shafts are described as grid cells in MIKE SHE with a specified head (equal to atmospheric pressure) in the calculation layers intersected by the shafts. The leakage flow from the aquifer to a shaft is then calculated as the sum of flows from each calculation layer intersecting the shaft, based on a specified conductance, C, for each calculation layer. The leakage flow from a saturated zone grid cell, containing one or several shafts, is included as a sink term in the governing flow equation for three-dimensional saturated flow. The leakage flow is calculated according to Equation 2-6. The principle is illustrated in Figure 2-5.

$$Q_{cell} = dh \cdot C \qquad 2\text{-}6$$

Q_{cell} Leakage flow from grid cell containing the shaft (m^3/s).

dh Difference between the calculated head in the grid cell containing the shaft and the specified head boundary, equal to the lower level of the calculation layer when the shaft is deeper than the lower level of the calculation layer, and equal to the bottom of the shaft if the bottom is above the lower level of the calculation layer (m).

C Total conductance (m^2/s).

The total conductance, C, is calculated according to Equation 2-7.

$$C = \frac{K \cdot 2 \cdot \pi}{\ln\left(\frac{r + d_{grout}}{r}\right)} \cdot dz \qquad 2\text{-}7$$

K Hydraulic conductivity (m/s).

dz Height of calculation layer, or height of the shaft contained in the layer if the shaft bottom is above the lower level of the calculation layer (m).

r Radius of the shaft (m).

d_{grout} Thickness of the grouted zone (m).

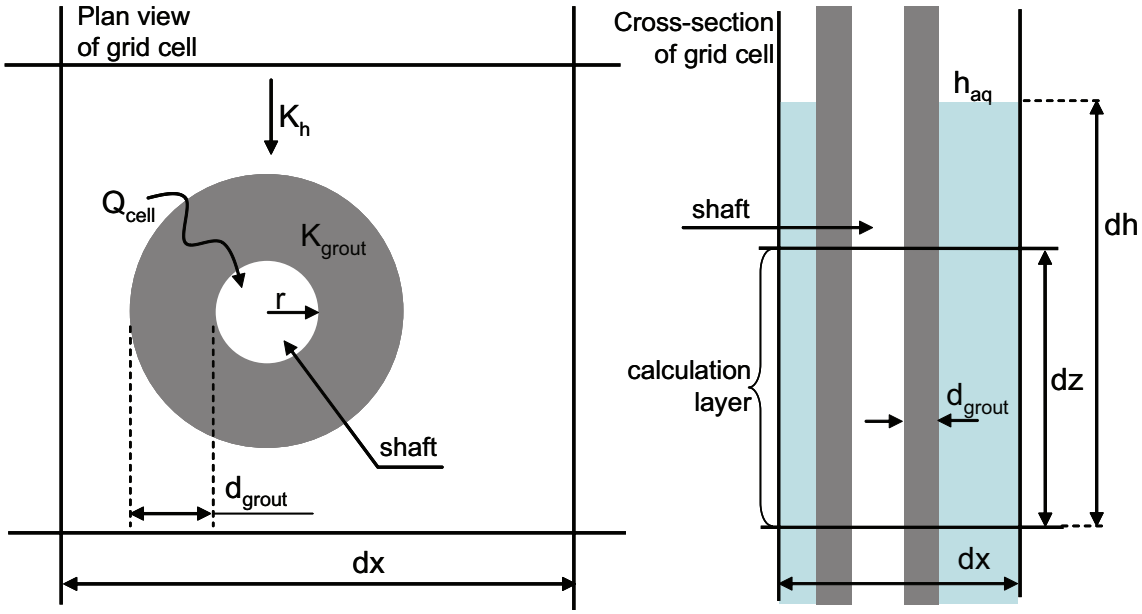

Figure 2-5. *Calculation of exchange of water for the shafts.*

According to Equation 2-8, the level of grouting and the ungrouted horizontal hydraulic conductivity of the bedrock are both taken into consideration by setting the hydraulic conductivity, K, in Equation 2-7. A vertical inflow to a vertical shaft is not possible and therefore only the horizontal conductivity of the bedrock is considered.

$$K = min\ [K_{grout}, K_h] \qquad 2\text{-}8$$

K_{grout} Hydraulic conductivity of the grouted zone, i.e. the conductivity of the bedrock near the shaft after grouting to a certain level (m/s).

K_h Horizontal hydraulic conductivity of the grid cell (m/s).

The total conductance, C, for each calculation layer, is listed in Appendix 2 for each shaft and for different grouting cases.

3 Impact of the updated routine for coupling MIKE SHE and MOUSE

As described in Section 2.3, a development of the MIKE SHE-MOUSE coupling routine (here abbreviated MS-M) has been performed. /Gustafsson et al. 2009/ tested a previous version of the MS-M coupling routine by comparison with an analytical solution for groundwater inflow to a grouted tunnel. The results showed that using the previous routine, here denoted MS-M_{old}, the groundwater inflow was 20–40% lower than the analytically calculated inflow. Section 3.1 presents simulation results using an updated MIKE SHE-MOUSE coupling routine (MS-M_{new}) and compares these results with those obtained using the analytical solution. The importance of the MS-M coupling routine for the calculated inflow to the repository and the groundwater-table drawdown is presented in Section 3.2 and 3.3, respectively, in the form of comparisons with the results using the Forsmark model setup in /Gustafsson et al. 2009/.

3.1 Comparison with analytical solution

The same model-test setup as that in /Gustafsson et al. 2009/ is here used to test the accuracy of the updated MIKE SHE-MOUSE coupling routine. The following sections present the analytical solution, the test-model setup and the simulation results.

3.1.1 Analytical solution

The utilized analytical solution of groundwater inflow from bedrock to a grouted tunnel is given by Equation 3-1. The solution assumes that the bedrock is a homogenous porous medium and that the groundwater table above the tunnel is fixed.

$$q_{an} = \frac{2\pi \cdot K_0 \cdot H}{\ln(\frac{2H}{r_w}) + (\frac{K_0}{K_{grout}} - 1) \cdot \ln(1 + \frac{d_{grout}}{r_w})} \qquad 3\text{-}1$$

q_{an} Groundwater flow from bedrock to grouted tunnel ($m^3/(s \cdot m)$).

K_0 Hydraulic conductivity of bedrock (m/s).

K_{grout} Hydraulic conductivity of grouted zone (m/s).

H Depth from groundwater table to tunnel centre (m).

r_w Tunnel radius (m).

d_{grout} Thickness of grouted zone (m).

3.1.2 Model setup

Figure 3-1 shows the layout of the MIKE SHE test-domain, representing such idealized conditions for which Equation 3-1 is applicable. The model domain has dimensions 4,000 m in one of the horizontal directions (x) and 2,000 m in the vertical direction (z). The grid size is set to 40 m in all three dimensions down to the level z = –600 m. In the second horizontal direction (y) only three grid rows are used (size 120 m), of which two rows form the model boundary. A fixed hydraulic head is applied at the top boundary (z = 0), whereas all other boundaries are no-flow boundaries). A MOUSE tunnel segment with a radius of 2.5 m and atmospheric pressure is located with its centre at the level z = –500 m.

The tests include totally nine cases, including the combinations 10^{-7}, 10^{-8} or 10^{-9} m/s in terms of K_0 (= K_h = K_v) and K_{grout}. In the test simulations, the thickness of the grouted zone (d_{grout}) was set to 4 m. In order to reach steady-state conditions, all MIKE SHE simulation cases were run for a minimum time period of 10 years.

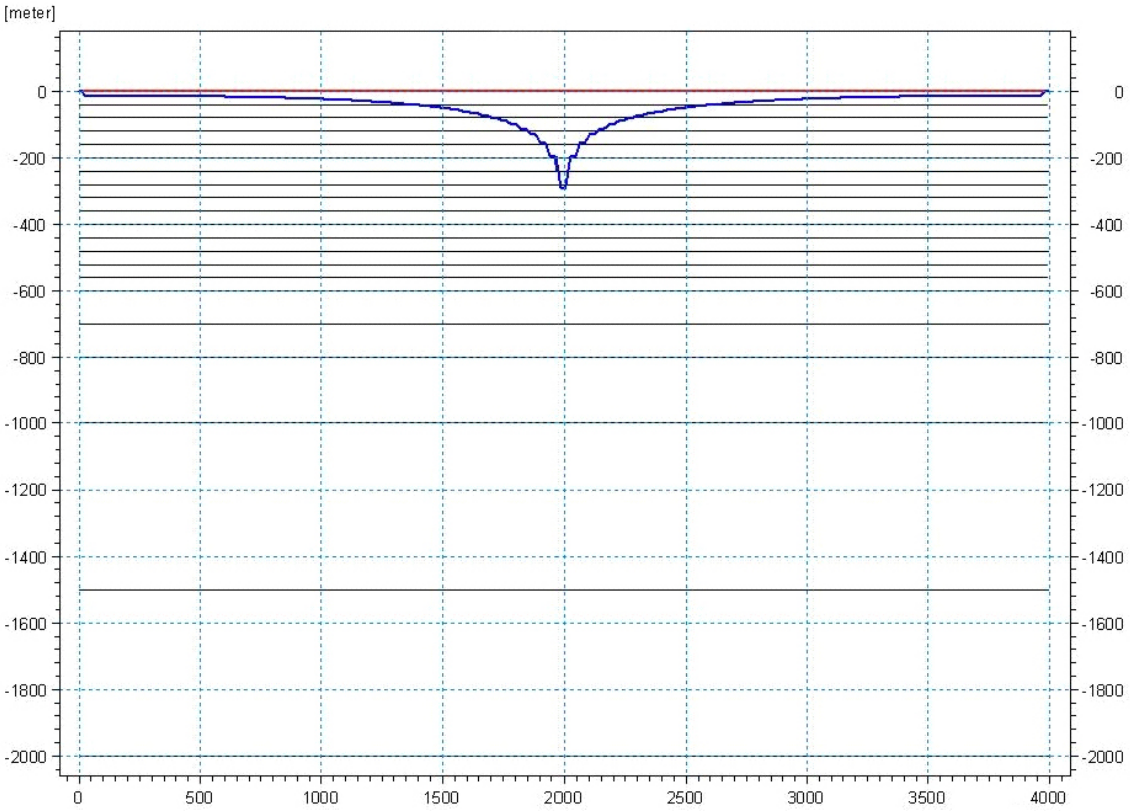

Figure 3-1. *Cross-section through the MIKE SHE test-model domain. The groundwater level is fixed at z = 0 m. The horizontal black lines show the lower level of each calculation layer. The blue line is an example of the calculated head in the layer where the tunnel is located (with its centre at z = –500 m).*

3.1.3 Comparison with analytical solution

Table 3-1 presents the calculated inflows to the tunnel for the nine test cases. The ratio between the MIKE SHE-calculated and the analytically calculated inflow is presented for both the previous /Gustafsson et al. 2009/ and the updated MIKE SHE-MOUSE coupling routines. As mentioned previously, using MS-M_{old} the MIKE SHE-calculated inflow is 20–40% smaller than the analytically calculated inflow. Using MS-M_{new} there is a closer match to the analytically calculated inflow. In all tested simulation cases, the MIKE SHE-calculated inflow differs by only a few percent compared to that obtained using the analytical solution.

Table 3-1. Summary of calculated inflows (m^2/s) using MIKE SHE and the analytical solution (Equation 3-1) for the nine test cases. MS-M = MIKE SHE-MOUSE coupling routine.

	Test case								
	1	**2**	**3**	**4**	**5**	**6**	**7**	**8**	**9**
Bedrock cond. (m/s)	10^{-7}	10^{-7}	10^{-7}	10^{-8}	10^{-8}	10^{-8}	10^{-9}	10^{-9}	10^{-9}
K_{grout} (m/s)	10^{-7}	10^{-8}	10^{-9}	10^{-7}	10^{-8}	10^{-9}	10^{-7}	10^{-8}	10^{-9}
MS-M_{new}	$4.9\cdot10^{-5}$	$2.2\cdot10^{-5}$	$3.1\cdot10^{-6}$	$6.1\cdot10^{-6}$	$5.4\cdot10^{-6}$	$2.2\cdot10^{-6}$	$6.3\cdot10^{-7}$	$6.1\cdot10^{-7}$	$5.4\cdot10^{-7}$
Eq. 3-1	$5.2\cdot10^{-5}$	$2.2\cdot10^{-5}$	$3.1\cdot10^{-6}$	$6.1\cdot10^{-6}$	$5.2\cdot10^{-6}$	$2.2\cdot10^{-6}$	$6.2\cdot10^{-7}$	$6.1\cdot10^{-7}$	$5.2\cdot10^{-7}$
	Ratio (%) between MIKE SHE and the analytical solution (Equation 3-1)								
MS-M_{new}	93	101	101	100	103	102	101	100	103
MS-M_{old}	71	64	61	73	71	64	77	77	74

The reason for the discrepancies between the MS-M_{old} results and the analytical results is likely that the flow resistance (which is proportional to the inverse of the hydraulic conductivity) of the grouted zone is added to the flow resistance of the bedrock. The new routine (Equations 2-4 and 2-5) implies that the grouted zone replaces the bedrock within the grouted zone if the flow resistance of the bedrock is lower than the flow resistance of the grouted zone. If the flow resistance of the bedrock is higher than that of the grouted zone, the grouted zone is disregarded. This condition essentially mimics a real situation, in which no rock grouting is performed if the original hydraulic conductivity of the rock around the tunnel periphery is below a certain hydraulic conductivity threshold.

3.2 Inflow to the repository

This section investigates the importance of the MS-M coupling routine for the calculated inflow to the repository. Model simulations were done for the three grouting cases $K_{grout} = 10^{-7}$, 10^{-8} and 10^{-9} m/s, using the same MIKE SHE Forsmark model for disturbed conditions as in /Gustafsson et al. 2009/ but replacing the previous MS-M coupling routine (MS-M_{old}) with the updated one (MS-M_{new}). It should be noted the results presented in this section are for comparison purposes only; the final results are presented in Chapter 7.

Table 3-2 presents the model-calculated inflow to the repository for the three grouting cases. As can be seen in the table, $K_{grout} = 10^{-8}$ m/s yields an inflow of 32.2 L/s, which can be compared with 22.1 L/s using MS-M_{old} /Gustafsson et al. 2009/. Hence, the MS-M update in itself yields an increase of the inflow of approximately 31% for $K_{grout} = 10^{-8}$ m/s. The corresponding results for $K_{grout} = 10^{-7}$ and 10^{-9} m/s are 24 and 35%, respectively. Hence, the difference between the two coupling routines is larger for lower values of K_{grout}.

3.3 Drawdown of the groundwater table

Table 3-3 summarises the model-calculated groundwater-table drawdown and the associated influence area for the three grouting cases $K_{grout} = 10^{-7}$, 10^{-8} and 10^{-9} m/s. For a drawdown exceeding 0.3 m, grouting case $K_{grout} = 10^{-7}$ m/s yields an influence area that is almost three times larger than that for grouting case $K_{grout} = 10^{-9}$ m/s, whereas it for $K_{grout} = 10^{-8}$ m/s is two times larger. Compared to the results of /Gustafsson et al. 2009/, the influence area is between 13 and 31% larger if MS-M_{new} is used. As for the inflow to the repository, the difference between the influence areas calculated using MS-M_{old} and MS-M_{new} is higher for smaller values of K_{grout}. Figure 3-2 shows the model-calculated influence area for $K_{grout} = 10^{-8}$ m/s, using the previous and the updated MIKE SHE-MOUSE coupling routine. According to this figure, the overall shape and size of the influence area is no very sensitive to the MS-M coupling routine. The largest difference can be seen in areas in the vicinity of the nuclear power plant.

Table 3-2. Annual average groundwater inflow (L/s) to the repository. The right-hand column shows the absolute (L/s) and relative (%) underestimations in the model of /Gustafsson et al. 2009/.

Case	Inflow to the repository (L/s)	Underestimation of inflow (L/s) in /Gustafsson et al. 2009/
$K_{grout} = 1 \cdot 10^{-7}$ m/s	46.9	11.1 (24%)
$K_{grout} = 1 \cdot 10^{-8}$ m/s	32.2	10.1 (31%)
$K_{grout} = 1 \cdot 10^{-9}$ m/s	15.8	5.6 (35%)

Table 3-3. Influence areas (km²) for different limits of the annual average groundwater-table drawdown and values of K_{grout}. The results refer to a fully open repository and year 2006. The lower part of the table shows absolute (km²) and relative (%) underestimations of the influence areas in /Gustafsson et al. 2009/.

Grouting case	Influence area (km²) > 0.1 m	> 0.3 m	> 0.5 m	> 1 m	> 2 m	> 4 m
$K_{grout} = 10^{-7}$ m/s	3.31	1.80	1.36	0.91	0.69	0.57
$K_{grout} = 10^{-8}$ m/s	2.56	1.37	1.02	0.67	0.46	0.30
$K_{grout} = 10^{-9}$ m/s	1.43	0.71	0.49	0.28	0.14	0.06
	Underestimation in /Gustafsson et al. 2009/					
$K_{grout} = 10^{-7}$ m/s	0.35 km² (11%)	0.23 km² (13%)	0.23 km² (17%)	0.16 km² (18%)	0.13 km² (19%)	0.18 km² (32%)
$K_{grout} = 10^{-8}$ m/s	0.45 km² (18%)	0.35 km² (26%)	0.27 km² (26%)	0.21 km² (31%)	0.21 km² (46%)	0.18 km² (60%)
$K_{grout} = 10^{-9}$ m/s	0.13 km² (9%)	0.22 km² (31%)	0.17 km² (35%)	0.14 km² (50%)	0.08 km² (57%)	0.04 km² (67%)

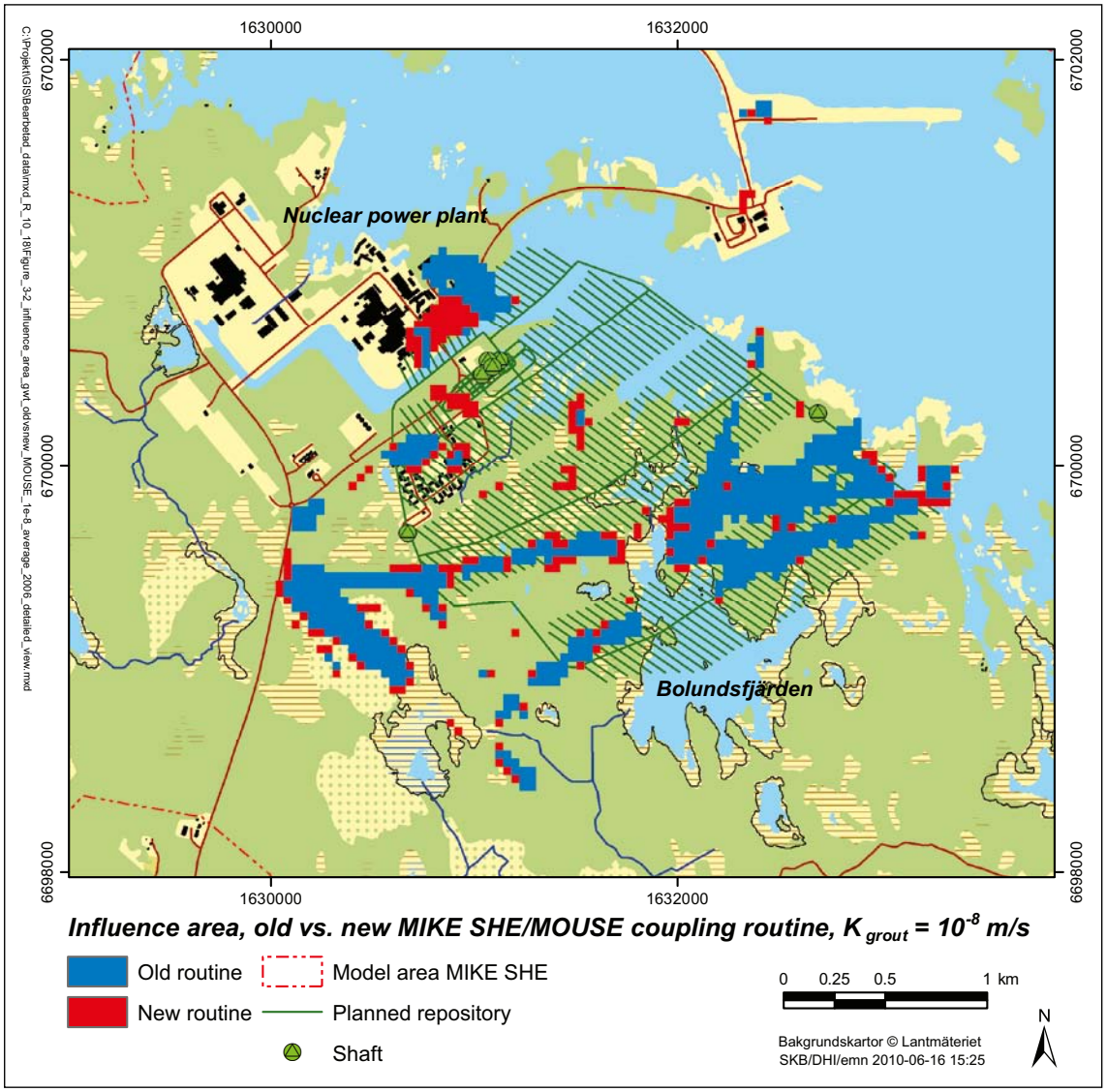

Figure 3-2. *Influence areas (annual average groundwater-table drawdown > 0.3 m, year 2006) using the previous (old routine; blue areas only) and the updated MIKE SHE-MOUSE coupling routine (new routine; red and blue areas), $K_{grout} = 10^{-8}$ m/s.*

4 Description of models and simulation cases

This chapter presents model updates in relation to those of /Bosson et al. 2008, Gustafsson et al. 2009/. The model updates concern the bedrock part of the geological model (Section 4.1) and the horizontal and vertical extents of the model domain (Section 4.2). Further, the model implementation of SFR was updated and the subsurface drainage system at the nuclear power plant was included in the model (Section 4.2.1). The simulation period and the initial conditions are described in Section 4.2.2. Table 4-1 summarises the model updates relative to the SDM-Site Forsmark MIKE SHE model /Bosson et al. 2008/ and the previous MIKE SHE open repository model /Gustafsson et al. 2009/. A reference simulation using the present model updates was run for the chosen simulation period. The results from this simulation are presented in Chapter 6.

The second step in the modelling process was to implement the repository in the model, and to quantify disturbed conditions, i.e. the groundwater inflow and the associated hydrological and hydrogeological effects for different cases and conditions. The geometry of the implemented repository layout is presented in Section 4.3.1, and the different simulation cases for disturbed conditions are presented in Section 4.3.2. The results from these simulations are presented in Chapter 7.

4.1 Input data updates

4.1.1 Bedrock hydrogeology

An updated hydrogeological model of the bedrock compared to the one used in the SDM-Site modelling /Bosson et al. 2008/ and the previous open repository modelling /Gustafsson et al. 2009/ was delivered from the CONNECTFLOW modelling team /Joyce et al. 2010/ and implemented in the present MIKE SHE model. The delivered data set contains data on horizontal and vertical hydraulic conductivities (m/s), specific storage coefficients (1/m) and porosities (–) with a horizontal resolution of 40 m. The name of the delivered bedrock model is SRS_HCD2h100A2b_HRD5r1_phi7F_HSD5d_IC4Mat_MD2_MOW_RMD1000.

The upper 200 m of the bedrock contains horizontal fractures/sheet joints with large horizontal hydraulic conductivity. In these areas the groundwater flow in the upper part of the bedrock is dominated by the horizontal component. Figures 4-1 and 4-2 show the anisotropy ratio K_h/K_v at the levels 110 and 450 m.b.s.l., respectively. At the level 110 m.b.s.l. the horizontal hydraulic conductivity (K_h) is up to 10^4 times higher than the vertical conductivity (K_v) in areas close to the nuclear power plant. Specifically, the horizontal hydraulic conductivity at the level 110 m.b.s.l. is in the range of 10^{-6}–10^{-5} m/s in the fracture zones and 10^{-8}–10^{-7} m/s in the surrounding bedrock. At repository level (450 m.b.s.l.) the anisotropy ratio is much smaller, with K_h and K_v in the range 10^{-12}–10^{-9} m/s.

Table 4-1. Summary of updates of the SDM-Site Forsmark model /Bosson et al. 2008/ and the previous open repository model /Gustafsson et al. 2009/.

	SDM-Site Forsmark model /Bosson et al. 2008/	Open repository model /Gustafsson et al. 2009/	Present study
Hydrogeological model of the bedrock	SDM23_HCD2h100A2b_HRD5r1_phi4F_HSD5d_IC3Mat_MD2_MOW18 /Follin et al. 2007, 2008/	SDM23_HCD2h100A2b_HRD5r1_phi4F_HSD5d_IC3Mat_MD2_MOW18 /Follin et al. 2007, 2008/	SRS_HCD2h100A2b_HRD5r1_phi7F_HSD5d_IC4Mat_MD2_MOW_RMD1000 /Joyce et al. 2010/
Vertical extent	600 m.b.s.l.	990 m.b.s.l.	1,200 m.b.s.l.
Number of calculation layers	14	20	22
Model area	37 km^2 (25.5 km^2 land, 11.5 km^2 sea)	37 km^2 (25.5 km^2 land, 11.5 km^2 sea)	56 km^2 (30.5 km^2 land, 25.5 km^2 sea)
Vegetation classes	4	4	8
SFR implementation	Pumping wells	Internal head boundary	MOUSE
Drainage system at the nuclear power plant	Not included	Not included	Included

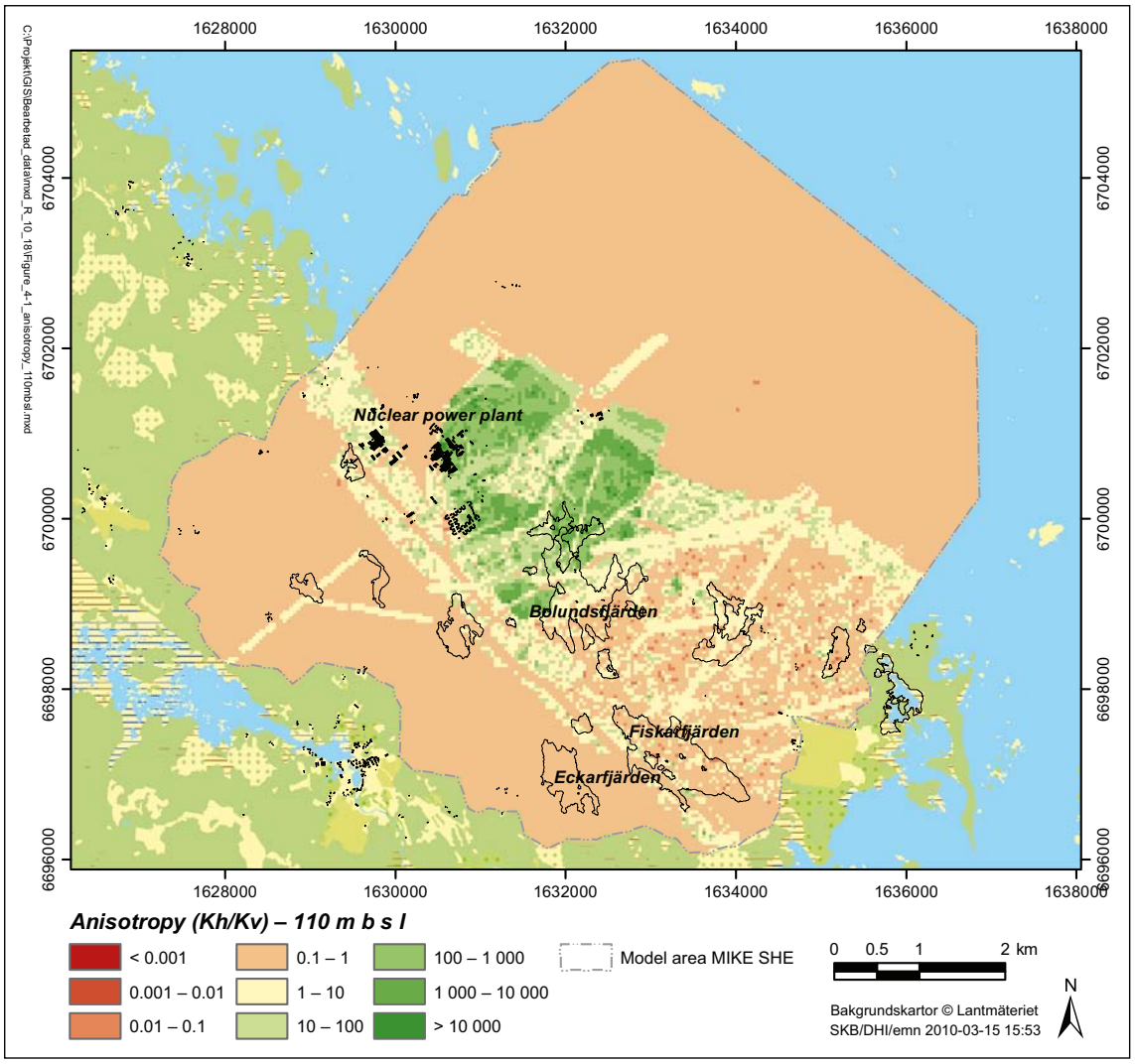

Figure 4-1. *Anisotropy ratio (horizontal/vertical hydraulic conductivity) at the level 110 m.b.s.l.*

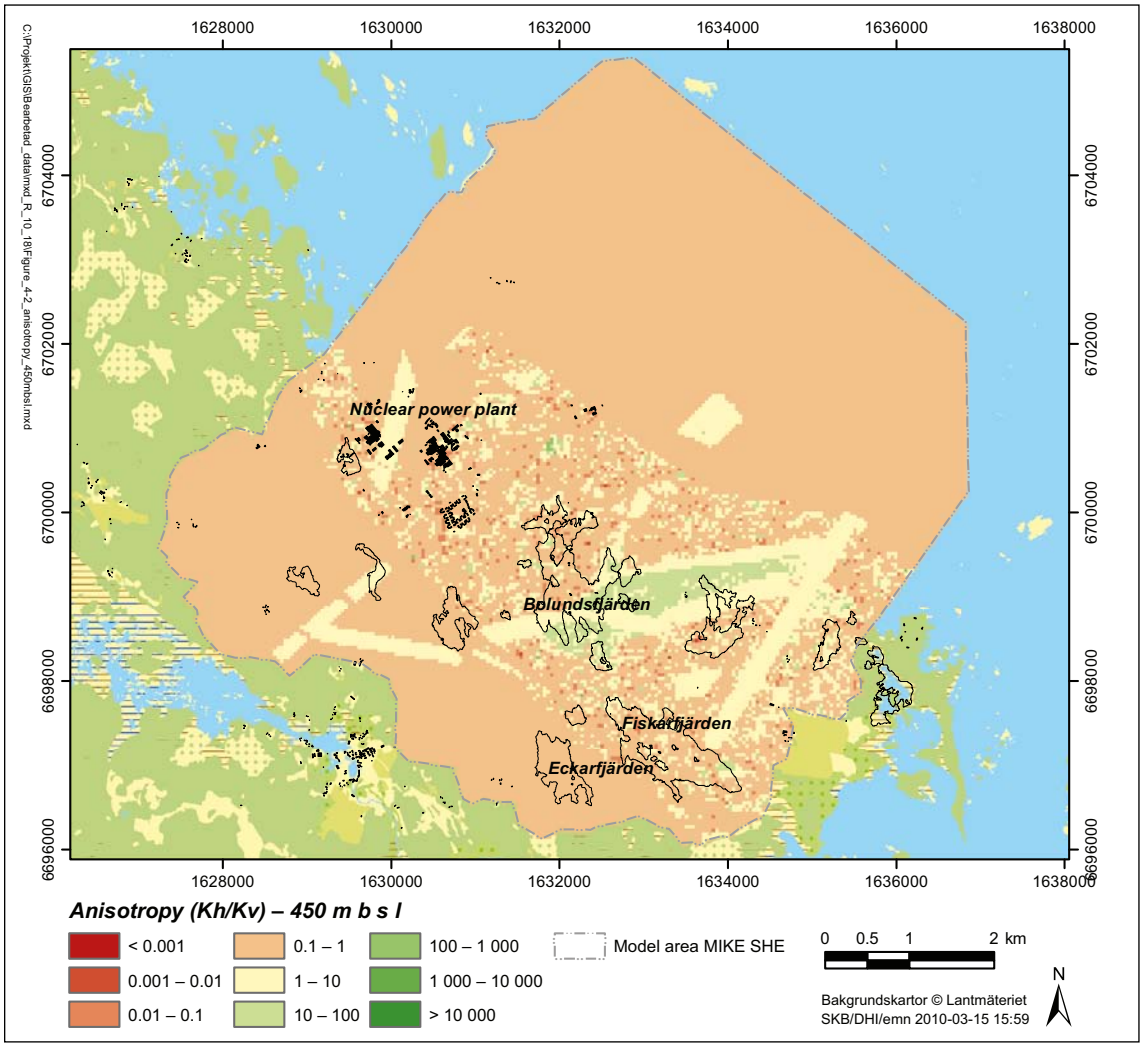

Figure 4-2. *Anisotropy ratio at the level 450 m.b.s.l.*

4.1.2 Vegetation classification

As part of the present study, the vegetation classification in MIKE SHE was updated compared to the classifications of /Bosson et al. 2008, Gustafsson et al. 2009/. Based on the underlying vegetation map that was also used in those previous modelling studies, the land areas that were defined as open land in /Bosson et al. 2008/ were here divided into four vegetation classes, namely open land, arable land, wetland and impermeable land. In addition, the vegetation class mixed forest was added to the classification. Figure 4-3 shows the updated vegetation classification that is used in the present modelling. As can be seen from this figure, the largest part of the land areas consists of coniferous forest, whereas areas classified as impermeable land mainly are located at the industrial area at the nuclear power plant. Table 4-2 shows the parameter values for different vegetation classes. The new vegetation classes are highlighted in the table. For descriptions of the parameters, see /Bosson et al. 2008/.

4.2 Numerical model and initial base case

4.2.1 Model area, boundaries and grid

The MIKE SHE model area comprises most of the on-shore (land) part of the Forsmark regional model area. The land part of the model area was enlarged compared to the SDM-Site model /Bosson et al. 2008/, mainly in the southeast. The sea part of the model area was also enlarged to the northeast. In the previous open repository modelling /Gustafsson et al. 2009/ the inflow to the repository caused a hydraulic-head drawdown at the level 50 m.b.s.l. that reached the model boundary in the sea.

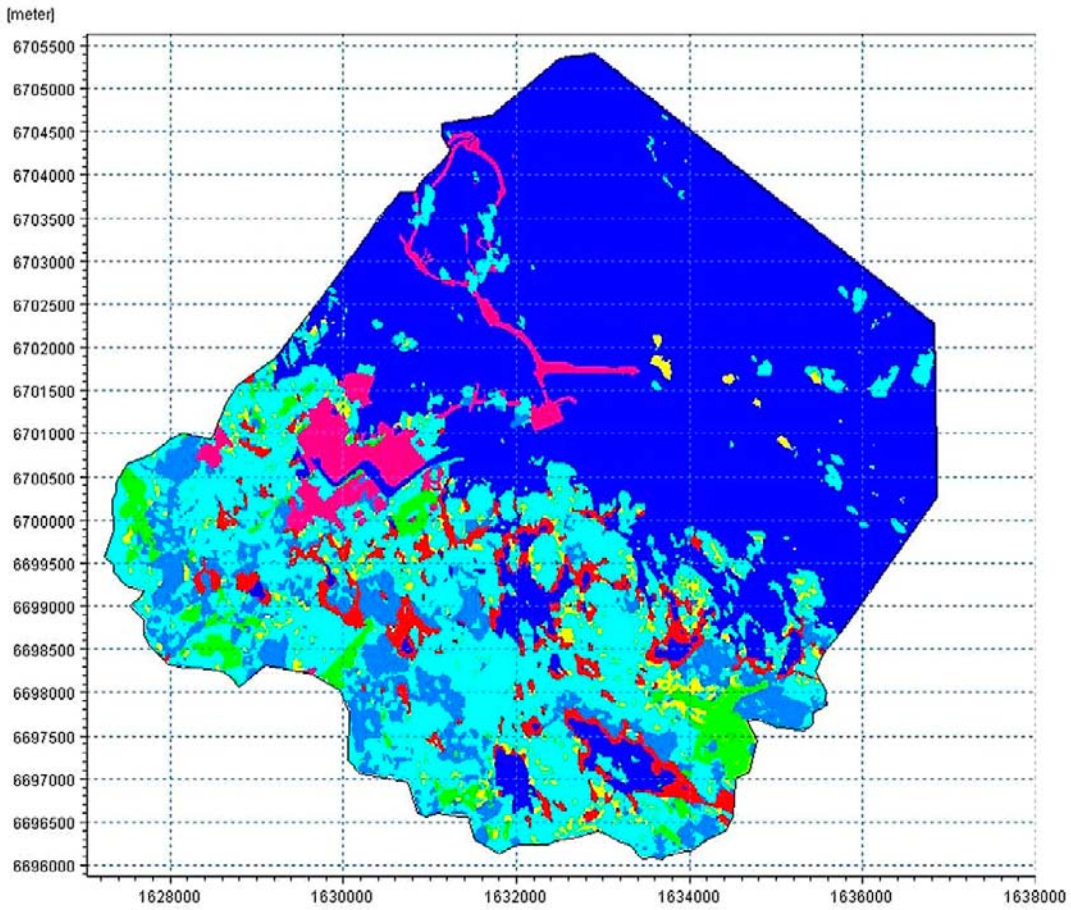

Figure 4-3. *Vegetation classes in the MIKE SHE model. Dark blue = surface water, light blue = deciduous forest, turquoise = coniferous forest, dark green = open land, light green = arable land, yellow = mixed forest, red = wetland, pink = impermeable land.*

Table 4-2. Vegetation-parameter values for different vegetation classes. New classes are highlighted.

	Vegetation parameter			
Vegetation class	C_{int} (mm)	LAI (–)	A_{root} (1/m)	K_c (–)
Water	0	0	1	1
Deciduous forest	0.2	0–6	1	1
Coniferous forest	0.5	7	1	1
Mixed forest	0.3	4–6	1	1
Open land	0.1	4–7	1	1
Arable land	0.05	0–6	1	1
Wetland	0.05	3–4	1	1
Impermeable land	0	0	1	1

Similar to the previous MIKE SHE model versions, the upstream (inland) boundary follows the surface-water divide towards the river Forsmarksån catchment, and not the inland boundary of the Forsmark regional model area. Figure 4-4 shows the present MIKE SHE model area (size 56 km^2) and the SDM-Site model area (37 km^2) in /Bosson et al. 2008/. The model area of /Gustafsson et al. 2009/ is the same as that of /Bosson et al. 2008/. As described in Table 4-1, the bottom of the model domain has been extended from 600 m.b.s.l. /Bosson et al. 2008/ and 990 m.b.s.l. /Gustafsson et al. 2009/ to 1,200 m.b.s.l. in the present model, i.e. well below repository level.

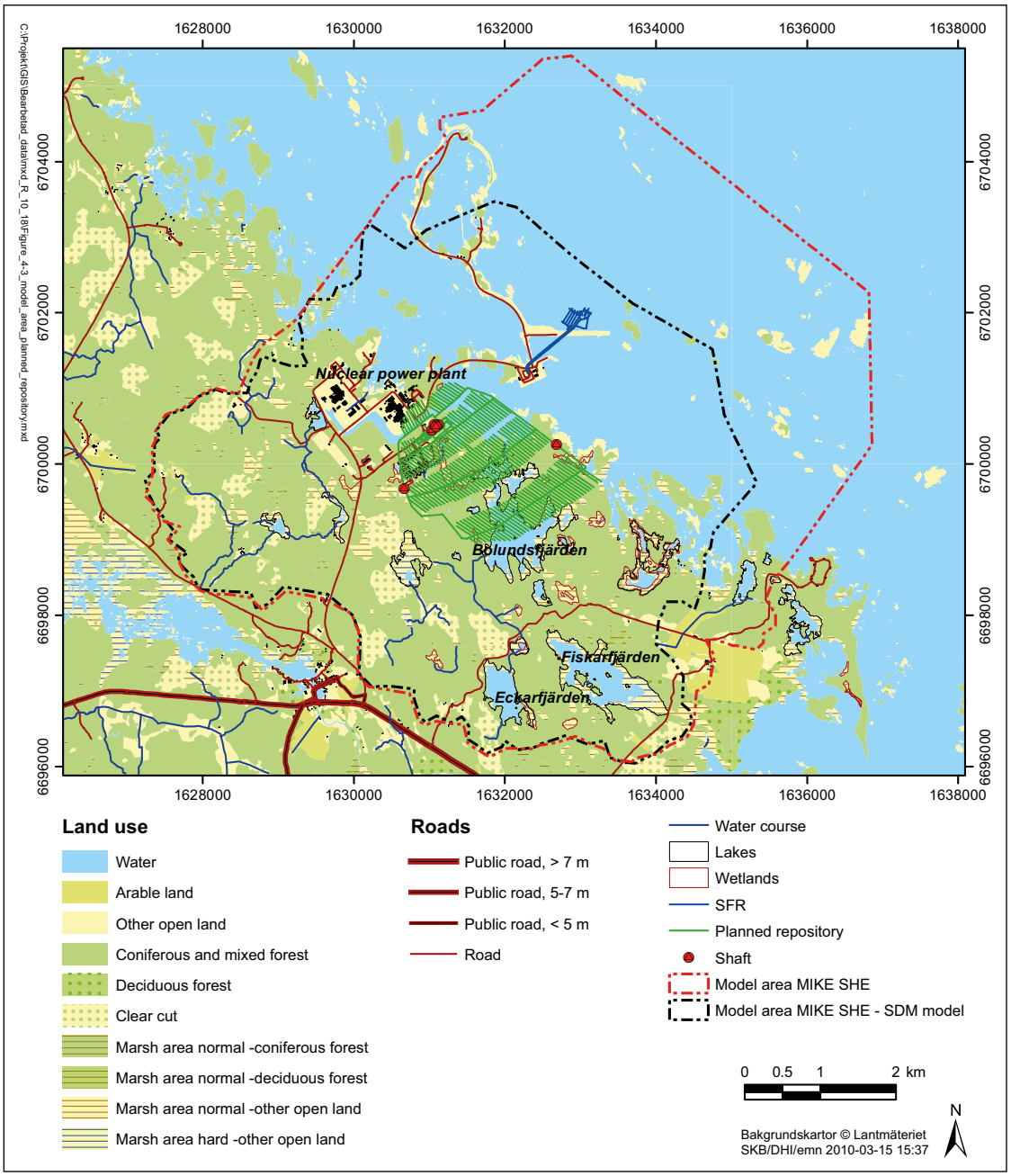

Figure 4-4. *MIKE SHE model area, SFR and the planned repository (layout D2, version 1.0, April, 2008).*

The geometry of the two uppermost calculation layers are the same as those of /Bosson et al. 2008/, with a minimum thickness of layer 1 of 2.5 m. The third calculation layer and those below follow the geological layers of the bedrock model. Down to 200 m.b.s.l., the layers have a thickness of 20 m, and in the range 200–1,200 m.b.s.l. the layer thickness is 100 m. This implies that the vertical resolution of the calculation layers is higher compared to the SDM-Site model, in which the range 250–600 m.b.s.l. consisted of a single layer. The horizontal resolution of the grid cells is 40 m by 40 m in the whole model area. A detailed description of the geological layers and calculation layers of the SDM-Site Forsmark model is given in /Bosson et al. 2008/.

Groundwater divides are assumed to coincide with surface-water divides, which means that a no-flow boundary condition is used for the on-shore part of the model boundary. The sea forms the uppermost calculation layer in the off-shore parts of the model. Due to that large flows of overland water in MIKE SHE can lead to numerical instabilities, the sea is described as a geological layer consisting of highly conductive material, with a hydraulic conductivity of 0.001 m/s. The sea part of the uppermost

calculation layer, as well as the outer sea boundary for all calculation layers, has a time-varying prescribed head boundary condition that is set equal to the measured time-varying sea level. The top boundary condition is expressed in terms of the precipitation and potential evapotranspiration (PET), which are assumed to be uniformly distributed over the model area and given as time series with daily values. The actual evapotranspiration is calculated during the simulation. The bottom boundary of the model is a no-flow boundary.

Current groundwater diversion in the Forsmark area includes a drainage system at the nuclear power plant and the underground facility SFR. The drainage system was not implemented in previous modelling, whereas /Bosson et al. 2008/ described the groundwater inflow to SFR in the form of pumping from a well at different levels. This well became inactive during parts of the simulation period, and it was therefore in the /Gustafsson et al. 2009/ modelling replaced by an internal head boundary. Using the latter approach the model-calculated inflow to SFR was 3.9 L/s, which can be compared to the measured inflow of 6 L/s. In order to obtain a more accurate quantification of the inflow, in the present study SFR is implemented as tunnel links (segments) in MOUSE in the same way as the repository (cf. Section 2.3.1). The hydraulic conductivity of the grouted zone around SFR (here denoted $K_{grout, SFR}$) was calibrated using the measured inflow as a calibration target, which resulted in a model-calculated inflow of 5.7 L/s for $K_{grout, SFR} = 2.5 \cdot 10^{-9}$ m/s.

As mentioned above, the drainage system at the nuclear power plant was disregarded in the previous modelling studies. A pumping well that was implemented and supposed to represent the drainage system was inactive throughout the whole simulation period in /Bosson et al. 2008/. The measured drainage flow is on the order of 1–2 L/s /Johansson 2008/. In the present model, the drainage system was implemented in the form of a subsurface drainage at the level 20 m.b.s.l. below all reactor buildings, which yield a model calculated drainage flow of 1.3 L/s using a so called drainage time constant of $5 \cdot 10^{-6}$ s^{-1}.

4.2.2 Simulation period

The simulation period covers the two-year period January 4, 2005–January 14, 2007. Specifically, year 2005 was used as an initialisation period, whereas the results presented in this report are derived from year 2006. Meteorologically, this year was relatively normal, however with unusually intense snowmelt during April and dry conditions during the summer (July–August).

4.3 Input to the simulations of disturbed conditions

The second step in the modelling process was to implement the repository into the model and to quantify the disturbed conditions, i.e. the groundwater inflow to the repository and the associated hydrological and hydrogeological effects. Section 4.3.1 describes the implemented repository layout, whereas Section 4.3.2 presents the various simulation cases that were studied for disturbed conditions.

4.3.1 Repository geometry

The implemented repository layout was delivered in April, 2008 (Forsmark layout D2, version 1.0). This layout (Figure 4-4) takes into account 27% additional deposition holes as a reserve for excluded deposition holes. Figure 4-5 details the layout of the access tunnel (ramp), tunnels and rock caverns in the central area at repository level, and main tunnels, transport tunnels and deposition tunnels, also at repository level. The deposition holes (c. 6,000) are not included in the model. The layout is the same as that used in /Gustafsson et al. 2009/. As mentioned previously, the repository is implemented as pipe links (segments) in the modelling tool MOUSE (Section 2.3.1). Table 4-3 presents geometrical data for the implemented tunnels, including the rock caverns in the central area. The total tunnel length is c. 84 km, with the majority located at approximately 450 m.b.s.l.

The repository layout also includes six vertical shafts that extend from ground surface down to repository level. These shafts are not implemented in MOUSE but in the form of MIKE SHE grid cells with atmospheric pressure (cf. Section 2.3.2). Geometrical data for the implemented shafts are shown in Table 4-4. Note that two of the shafts (SF00 and ST00) are very close and therefore located in the same MIKE SHE grid cells. Due to recent minor design changes, the diameter of the shafts SC00 and SF00 has been enlarged with 0.5 and 1 m, respectively, compared to /Gustafsson et al. 2009/.

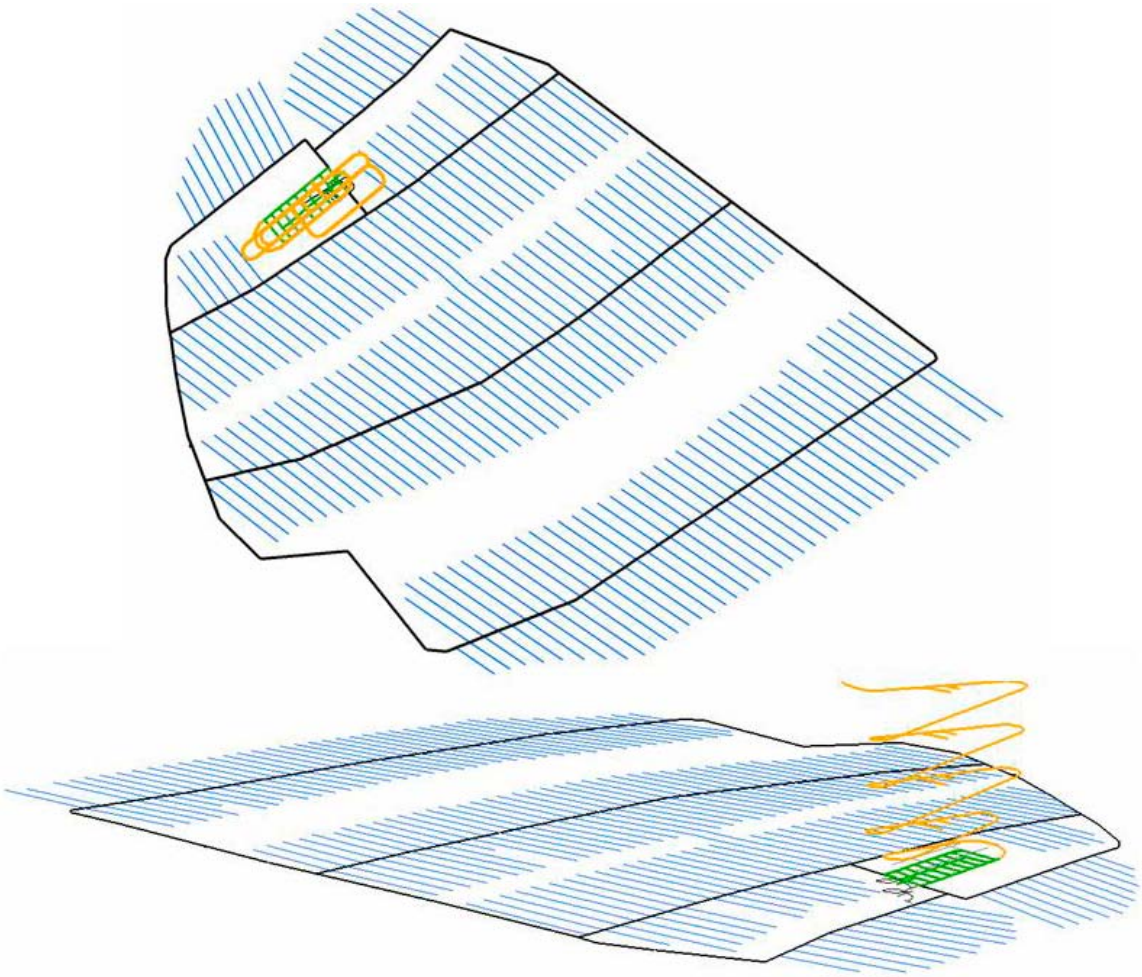

Figure 4-5. Layout of the access tunnel from the ground surface down to repository level (yellow line), tunnels and rock caverns in the central area at repository level (green lines), and main and transport tunnels (black lines) and deposition tunnels (blue lines), also at repository level.

Table 4-3. Geometrical data on the implemented repository layout (layout D2, version 1.0, April, 2008).

Calculation layer	Lower level (m.b.s.l.)	Tunnel-segment length (m)	Tunnel-casing area (m^2)
Layer 1–3	20	239	5,747
Layer 4	40	209	5,028
Layer 5	60	166	3,983
Layer 6	80	374	6,655
Layer 7	100	209	4,489
Layer 8	120	218	5,228
Layer 9	140	214	5,142
Layer 10	160	205	4,925
Layer 11	180	236	4,405
Layer 12	200	535	11,254
Layer 13	300	1,491	31,345
Layer 14	400	798	16,800
Layer 15	500	78,908	1,483,578
Layer 16	600	213	3,863
Layer 17	700		
Layer 18	800		
Layer 19	900		
Layer 20	1,000		
Layer 21	1,100		
Layer 22	1,200		
Sum		**84,016**	**1,592,441**

Table 4-4. Geometrical data on the implemented shafts (layout D2, version 1.0, April, 2008).

Shaft	Lower level (m.b.s.l.)	X-coordinate (m)	Y-coordinate (m)	Diameter (m)	Circumference (m)
SA01	467.08	1630669	6699672	3.00	9.42
SA02	467.36	1632686	6700261	3.00	9.42
SB00	490.00	1631036	6700450	6.00	18.85
SC00	520.00	1631122	6700519	5.50	17.28
SF00	442.20	1631088	6700489	3.50	11.00
ST00	442.20	1631064	6700518	3.50	11.00

4.3.2 Description of simulation cases

This section describes the simulation cases that were studied for disturbed conditions. The cases are summarised in Table 4-5. Three cases have been studied in terms of the hydraulic conductivity (K_{grout}) of the grouted zone around tunnels and shafts, $K_{grout} = 10^{-7}$, 10^{-8} and 10^{-9} m/s. In all simulation cases for disturbed conditions, the thickness of the grouted zone (d_{grout}) is set to 5 m /Brantberger and Janson 2009/. As described in Section 2.3.1, the inflow to the repository is calculated based on both the hydraulic conductivity of the grouted zone and that of the surrounding bedrock. In cases when the bedrock has a lower hydraulic conductivity compared to the grouted zone, the conductivity of the bedrock controls the inflow, and vice versa.

Unless stated otherwise, disturbed conditions have been studied under the assumption that the whole repository is open at the same time. This is a purely hypothetical worst case that will not occur in reality. In order to investigate the importance of the actual construction and operation of the repository, three development phases that are approximations of reality have been defined and studied in terms of groundwater inflow and groundwater-table drawdown. Figure 4-6 shows the repository layouts during the (initial) construction phase (here denoted phase 0), and during the three subsequent development phases (phases 1–3) during repository operation. The definition of the construction phase is that the access tunnel and the tunnels, rock caverns and shafts in the central area are open, but no other parts of the repository. The definitions of development phases 1–3 are that one deposition area is open at a time (Figure 4-6).

Table 4-5. Summary of the studied simulation cases. Results are presented for the highlighted years.

Simulation case	Hydraulic conductivity of the grouted zone	Meteorological data							
Construction phase	$K_{grout} = 10^{-7}$ m/s	2005	2006						
Construction phase	$K_{grout} = 10^{-8}$ m/s	2005	2006						
Fully open repository excl. main and deposition tunnels	$K_{grout} = 10^{-8}$ m/s	2005	2006						
Development phase 3	$K_{grout} = 10^{-8}$ m/s	2005	2006						
Fully open repository	$K_{grout} = 10^{-7}$ m/s	2005	2006						
Fully open repository	$K_{grout} = 10^{-8}$ m/s	2005	2006						
Fully open repository	$K_{grout} = 10^{-9}$ m/s	2005	2006						
Extended SFR	No repository	2005	2006						
Fully open repository and extended SFR	$K_{grout} = 10^{-8}$ m/s	2005	2006						
Natural conditions	No repository or SFR	2005	2006						
Backfill saturation and groundwater-level recovery (initial conditions: $K_{grout} = 10^{-8}$ m/s and extended SFR)	$K_{grout} = 10^{-8}$ m/s, no SFR			2005	2006	2005	2006	2005	2006
Reference to saturation simulation (initial conditions: extended SFR)	No repository, no SFR			2005	2006	2005	2006	2005	2006
Reference simulation	No repository	2005	2006						
	Simulation cycle	1st		2nd		3rd		4th	

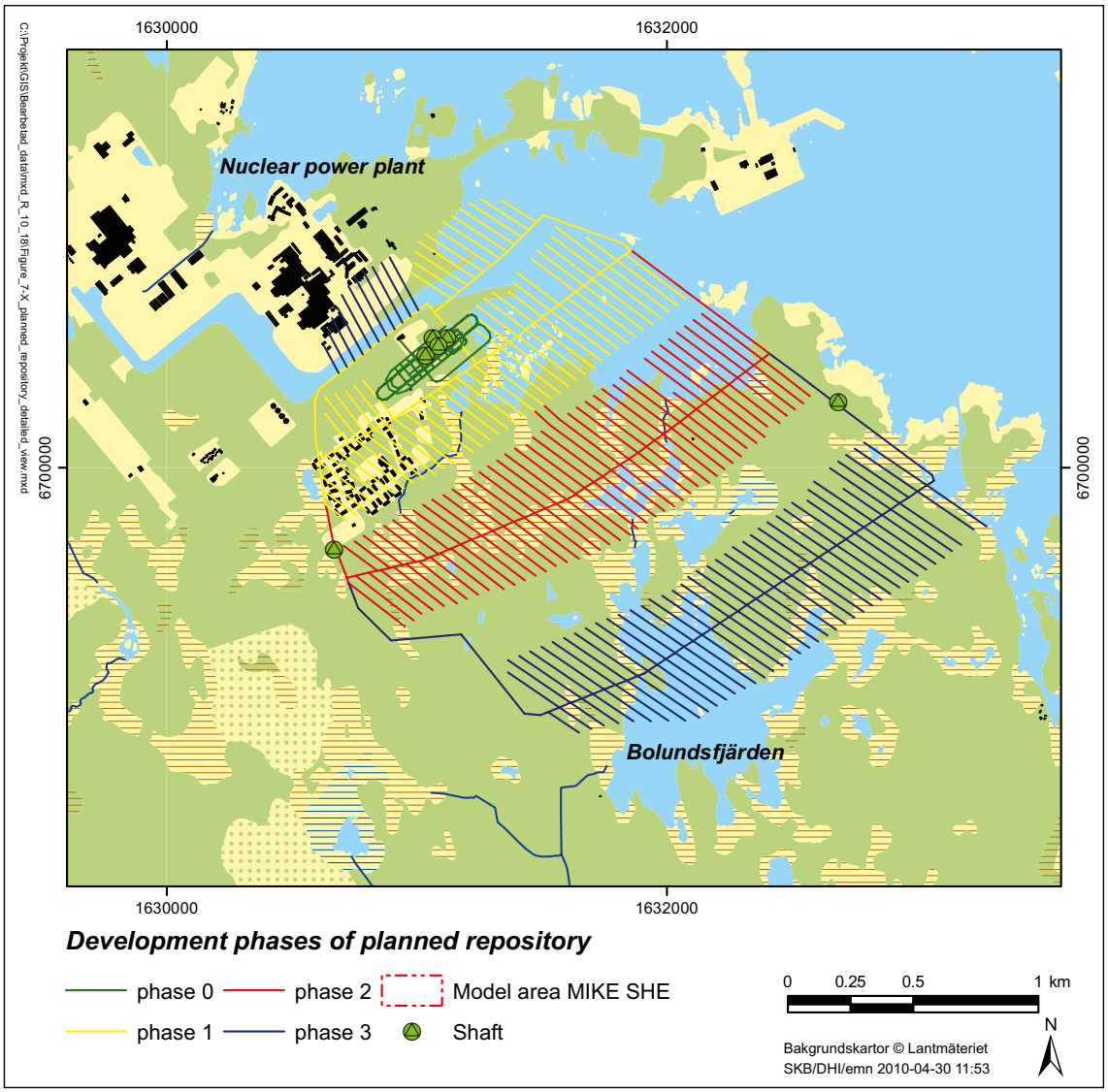

Figure 4-6. *Definitions of the investigated development phases during construction and operation of the repository.*

Moreover, one small deposition-area sector north of the central area is open during phase 1, whereas a neighbouring section (a reserve area) will be open during phase 3. The transport tunnels are opened gradually such that all transport tunnels are open during phase 3.

In addition to simulations with a fully open repository, the above-mentioned phases have been simulated individually. Further, one simulation case considers a hypothetical case with a fully open repository, but excluding the main tunnels and deposition tunnels (i.e. without deposition areas). The objective of this (unrealistic) case is to investigate the importance of the deposition areas versus other underground parts of the repository for the inflow and the associated hydrological and hydrogeological effects.

An extension of SFR is in the planning stages, and an extended SFR is expected to be in operation by 2020 /SKB 2008b/. In this report, SFR (which also is a repository) is simply denoted SFR not to confuse it with the deep-rock repository for spent nuclear fuel. Two simulations (with and without the repository) were carried out to investigate the importance of the SFR extension. As described previously, SFR and its extension are described as tunnel links (segments) in MOUSE in the same way as the repository. The layout of SFR and a preliminary layout of its extension are shown in Figure 4-7. Moreover, one simulation case that represents natural conditions (without SFR) was run and used as reference to evaluate the influence of the groundwater inflow to the present SFR. The results from the SFR simulations are presented in Section 7.6.

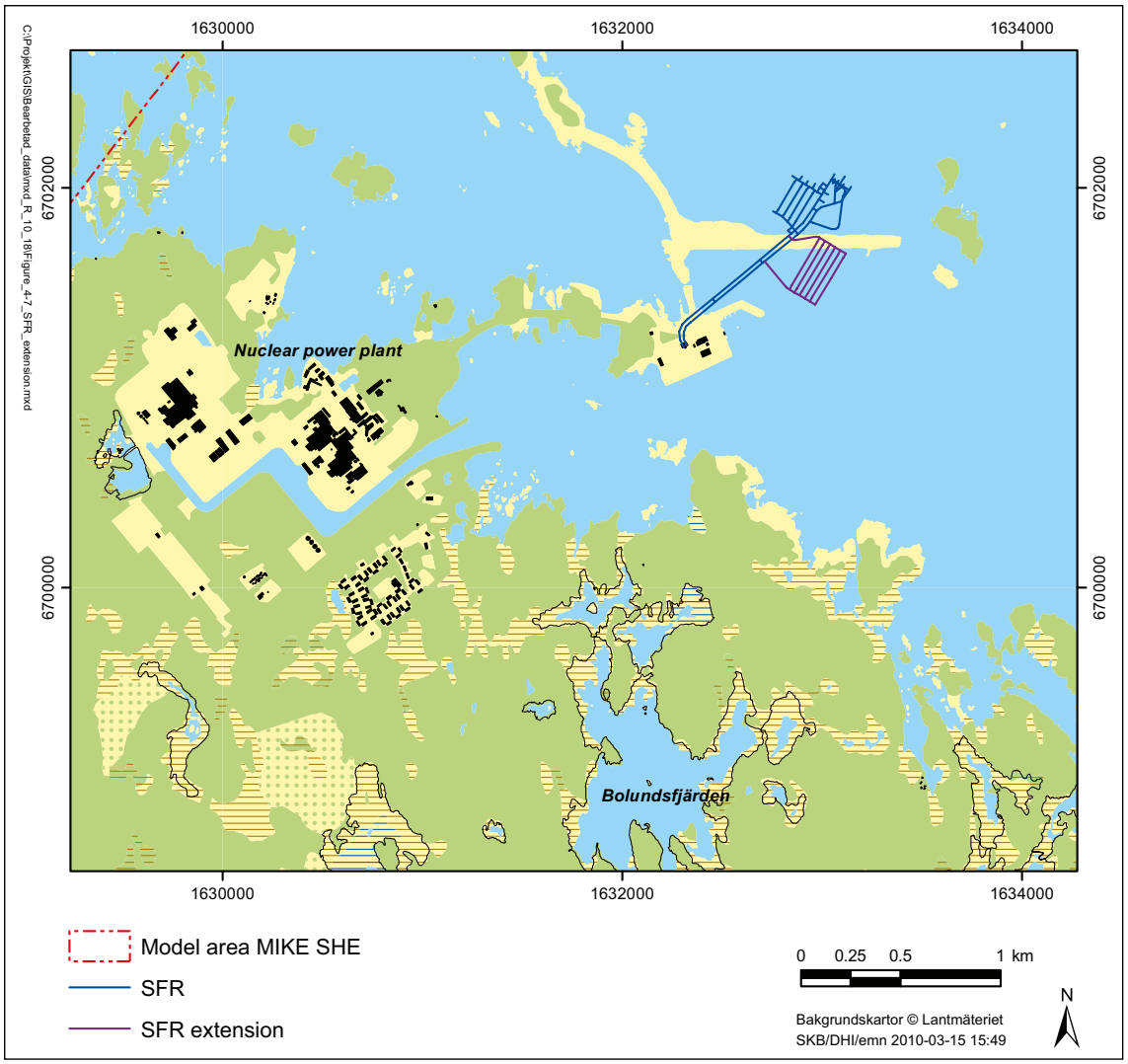

Figure 4-7. *Layout of the present SFR and a preliminary layout of the planned SFR extension.*

The final part of the modelling study concerns the backfill saturation process and the recovery of the groundwater table and hydraulic heads in the bedrock, after termination of the pumping from the repository. Section 7.7 (see also Appendix 4) describes the methodology and results from this study. The initial conditions for the saturation simulation are obtained from the last time step in the simulation for disturbed conditions ($K_{grout} = 10^{-8}$ m/s) with a fully open repository and an extended SFR. The simulation was done for a six-year period (the two-year period 2005–2006 was cycled three times).

5 Model calibration

5.1 Parameter variations

As part of the present modelling, several model changes have been made compared to the SDM-Site model /Bosson et al. 2008/ and the previous open repository model /Gustafsson et al. 2009/. For instance, a new hydrogeological bedrock model has been implemented (for further details regarding model updates, see Sections 4.1 and 4.2). Therefore, the model performance had to be tested and compared with the SDM-Site model /Bosson et al. 2008/ prior to the execution of the open repository modelling.

Initial modelling of an interference test (which involved pumping of groundwater from percussion borehole HFM14) showed that the calculated drawdown was too small and slow compared to the measured drawdown. The same problems were initially experienced during the calibration of the SDM-Site model. In addition, initial modelling showed that the calculated surface-water discharge was too low. As a basis for the model calibration, four different calibration cases were defined in order to analyse the sensitivity of the modelling results for undisturbed conditions to the hydraulic properties of the bedrock, see Table 5-1.

With the intention of increasing the model calculated surface-water discharge, the so-called time constant of the subsurface drainage was in all four cases multiplied by a factor of 5 compared to the SDM-Site model. In calibration case 2, the specific storage coefficient was also changed to $5 \cdot 10^{-8}$ m^{-1} throughout the whole bedrock, in order to decrease the model-calculated response time in the studied interference test. In cases 3 and 4 the horizontal hydraulic conductivity (K_h) and the vertical hydraulic conductivity (K_v) were modified in the upper 200 m of the bedrock. K_h was increased and K_v was decreased with a factor of 5 and 10 in case 3 and 4, respectively. This was done with the aim of lowering the too high model-calculated head elevations in the bedrock. The same specific storage coefficient as mentioned above was applied in cases 3 and 4. The simulations were run for the period 1th of September 2004 to 31th of March 2007. In addition, modelling of the interference test in percussion borehole HFM14 was performed for all calibration cases.

5.2 Modelling results

Figure 5-1 shows the locations of the groundwater-monitoring wells (SFM) and the percussion boreholes (HFM) used in the model calibration. The MAE (mean absolute error) and ME (mean error) for each monitoring well and borehole are listed in Tables 5-2 and 5-3. Results for the monitoring wells (Table 5-2) are presented in terms of the hydraulic head or the depth to the groundwater table, depending on which gives the best correlation with measured data /Bosson et al. 2008/. The percussion boreholes are divided into sections with packers at different depths. The sections are numbered from the bottom of the borehole and upwards, i.e. borehole section HFM01_1 is located below section HFM01_2.

As shown by the mean of the MAE- and ME-values in Table 5-2, the model-calculated average hydraulic head in the Quaternary deposits show little variation between the different cases. Changes in the hydraulic conductivities of the bedrock (cases 3 and 4) yield a higher MAE for wells SFM0001, SFM0003 and SFM0017 and smaller MAE for wells SFM0049 and SFM0057. For all other monitoring wells, the model-calculated hydraulic head is more or less unaffected by the hydraulic conductivity of the bedrock.

Table 5-1. Changes in hydraulic properties in sensitivity cases 1–4 compared to the reference bedrock model delivered from CONNECTFLOW /Joyce et al. 2010/.

Case	K_h, bedrock above –200 m	K_v, bedrock above –200 m	Specific storage coefficient in the bedrock (m^{-1})
1	Unchanged	Unchanged	Unchanged
2	Unchanged	Unchanged	$5 \cdot 10^{-8}$
3	$K_h \cdot 5$	$K_v/5$	$5 \cdot 10^{-8}$
4	$K_h \cdot 10$	$K_h/10$	$5 \cdot 10^{-8}$

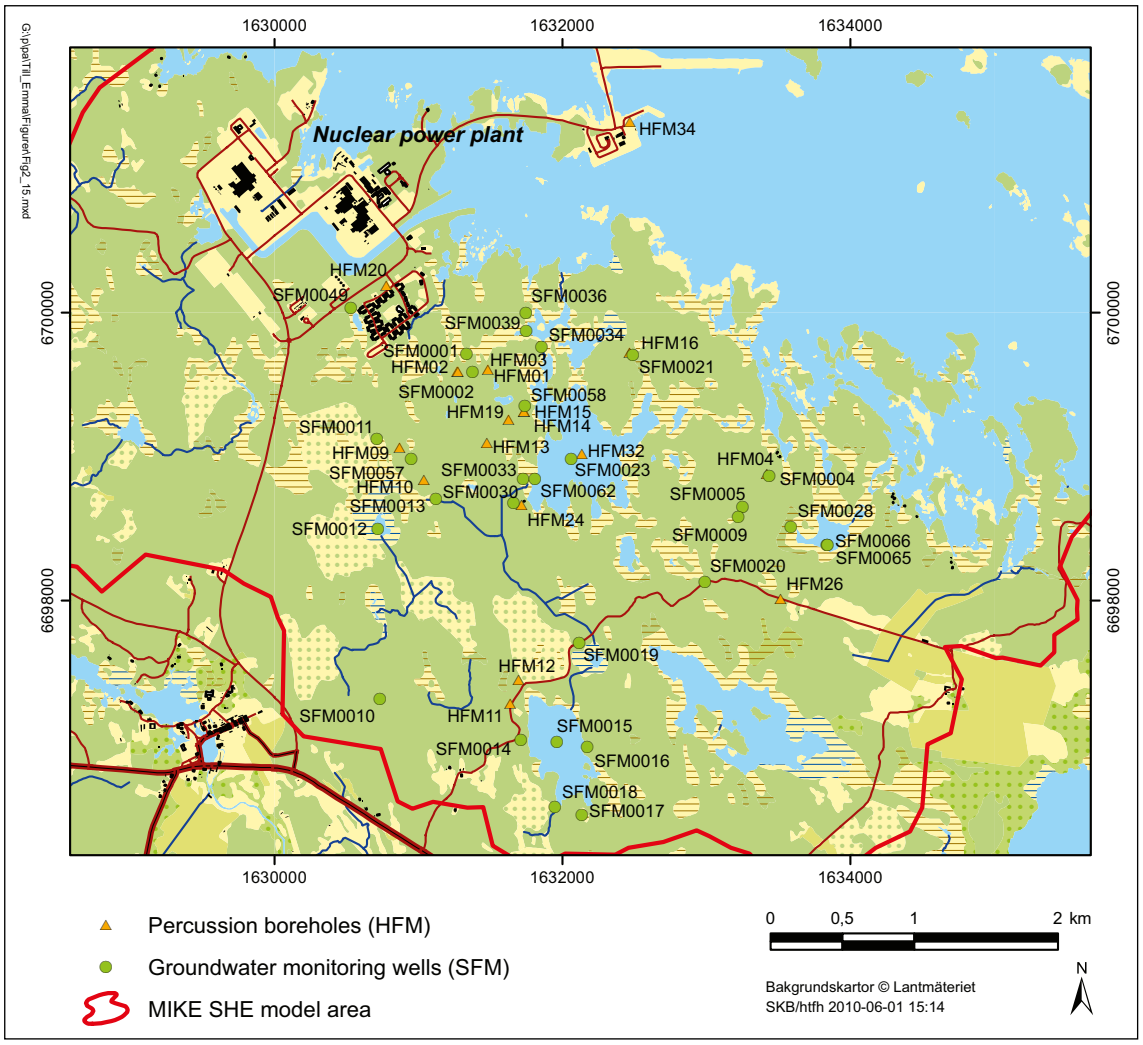

Figure 5-1. *Locations of groundwater monitoring wells (SFM) and percussion boreholes (HFM) within the MIKE SHE model area that were used in the model calibration.*

Table 5-2. MAE and ME for groundwater monitoring wells (SFM) for sensitivity cases 1–4. Results are evaluated in terms of hydraulic head and depth to the groundwater table.

Well id	Case 1		Case 2		Case 3		Case 4	
	MAE	ME	MAE	ME	MAE	ME	MAE	ME
Head								
SFM0001	0.36	–0.23	0.36	–0.22	0.37	–0.15	0.54	–0.43
SFM0003	0.26	–0.03	0.26	–0.02	0.28	0.21	0.28	0.19
SFM0004	0.46	0.40	0.46	0.40	0.46	0.40	0.46	0.40
SFM0005	0.28	–0.02	0.28	–0.02	0.28	–0.03	0.28	–0.04
SFM0009	0.39	–0.39	0.39	–0.39	0.40	–0.39	0.40	–0.39
SFM0010	0.46	0.45	0.47	0.45	0.50	0.49	0.50	0.49
SFM0011	0.16	0.16	0.16	0.16	0.16	0.16	0.16	0.16
SFM0012	0.08	0.00	0.09	0.01	0.08	0.00	0.08	0.01
SFM0013	0.34	0.02	0.34	0.03	0.34	0.02	0.34	0.01
SFM0014	0.25	–0.21	0.25	–0.21	0.24	–0.21	0.24	–0.20
SFM0015	0.05	–0.01	0.05	–0.01	0.05	–0.01	0.05	–0.01
SFM0016	0.08	–0.08	0.08	–0.08	0.08	–0.08	0.08	–0.07
SFM0017	0.33	–0.03	0.33	–0.02	0.52	–0.49	0.60	–0.60
SFM0018	0.27	–0.21	0.28	–0.21	0.27	–0.19	0.27	–0.18
SFM0020	0.48	0.09	0.48	0.09	0.48	0.09	0.42	0.38
SFM0021	0.45	–0.10	0.45	–0.10	0.46	–0.14	0.47	–0.16
SFM0023	0.13	–0.12	0.13	–0.12	0.12	–0.12	0.12	–0.11
SFM0030	0.50	–0.41	0.50	–0.41	0.50	–0.42	0.51	–0.43
SFM0033	0.41	0.41	0.41	0.41	0.42	0.41	0.42	0.41
SFM0034	0.43	0.43	0.44	0.43	0.44	0.44	0.49	0.49
SFM0036	0.43	–0.05	0.43	–0.05	0.43	–0.07	0.43	–0.09
SFM0039	0.05	–0.03	0.05	–0.03	0.05	–0.03	0.05	–0.02
SFM0057	0.63	–0.49	0.63	–0.49	0.56	–0.38	0.51	–0.01
SFM0062	0.12	0.05	0.12	0.05	0.12	0.05	0.12	0.05
SFM0065	0.25	–0.20	0.25	–0.21	0.25	–0.20	0.25	–0.20
SFM0066	0.09	–0.02	0.09	–0.02	0.09	–0.02	0.09	–0.02
Depth to gw. table								
SFM0002	0.45	–0.45	0.45	–0.45	0.43	–0.43	0.44	–0.44
SFM0019	0.18	0.11	0.18	0.10	0.18	0.10	0.18	0.10
SFM0028	0.16	–0.13	0.16	–0.13	0.17	–0.15	0.18	–0.15
SFM0049	0.24	–0.18	0.24	–0.18	0.18	0.00	0.17	0.00
SMF0058	0.61	0.57	0.60	0.57	0.61	0.57	0.61	0.57
Mean	**0.30**	**–0.02**	**0.30**	**–0.02**	**0.31**	**–0.02**	**0.31**	**–0.01**

Table 5-3. MAE and ME for percussion borehole (HFM) sections for sensitivity cases 1–4. Results are evaluated in terms of hydraulic head.

Borehole section id	Case 1		Case 2		Case 3		Case 4	
	MAE	ME	MAE	ME	MAE	ME	MAE	ME
HFM01_1	0.49	–0.49	0.64	–0.64	0.15	–0.15	0.16	0.16
HFM01_2	0.74	–0.74	0.78	–0.78	0.37	–0.37	0.09	0.09
HFM02_1	0.64	–0.64	0.65	–0.65	0.19	–0.10	0.42	0.40
HFM02_2	0.68	–0.68	0.69	–0.69	0.30	–0.27	0.24	0.16
HFM02_3	0.64	–0.64	0.64	–0.64	0.50	–0.50	0.35	–0.32
HFM03_1	0.54	–0.54	0.54	–0.54	0.43	–0.42	0.47	–0.46
HFM03_2	0.52	–0.52	0.52	–0.52	0.42	–0.40	0.46	–0.44
HFM04_1	0.16	–0.13	0.20	–0.19	0.15	0.15	0.24	0.24
HFM04_2	0.34	–0.34	0.36	–0.36	0.21	0.21	0.34	0.34
HFM9	0.18	–0.04	0.18	–0.04	0.14	0.06	0.19	0.18
HFM10_1	0.53	–0.52	0.53	–0.52	0.45	–0.44	0.32	–0.31
HFM10_2	0.27	–0.08	0.24	–0.09	0.25	0.04	0.24	0.02
HFM11_1	0.17	0.06	0.18	0.06	0.43	–0.42	0.29	0.17
HFM11_2	0.53	–0.49	0.52	–0.49	0.30	–0.23	0.26	0.11
HFM12_1	0.48	0.45	0.48	0.46	0.38	0.35	0.37	0.32
HFM12_2	0.37	0.35	0.38	0.35	0.24	0.11	0.34	0.32
HFM13_2	0.80	–0.78	0.78	–0.76	0.19	0.01	0.67	0.67
HFM13_3	0.67	–0.08	0.67	–0.08	0.48	–0.12	0.34	0.09
HFM14	0.70	–0.70	0.69	–0.69	0.32	–0.31	0.18	0.14
HFM15_1	0.73	–0.73	0.72	–0.72	0.32	–0.29	0.28	0.27
HFM15_2	0.63	–0.61	0.61	–0.60	0.29	–0.23	0.27	0.24
HFM16_1	0.34	–0.27	0.34	–0.28	0.22	0.21	0.58	0.58
HFM16_2	0.33	–0.27	0.34	–0.27	0.19	0.15	0.54	0.54
HFM16_3	0.34	–0.28	0.34	–0.28	0.18	0.07	0.41	0.41
HFM19_2	0.64	–0.64	0.63	–0.63	0.21	–0.18	0.40	0.40
HFM20_2	0.36	–0.25	0.29	–0.27	0.64	0.64	0.84	0.84
HFM20_3	0.47	–0.44	0.45	–0.45	0.52	0.52	0.95	0.95
HFM20_4	0.64	–0.61	0.63	–0.62	0.24	0.18	0.67	0.67
HFM24	0.70	0.66	0.70	0.66	0.57	0.53	0.53	0.51
HFM26	0.39	–0.34	0.41	–0.39	0.20	0.19	0.46	0.46
HFM32_1	1.24	–1.24	1.26	–1.26	1.32	–1.32	1.28	–1.28
HFM32_2	1.12	–1.12	1.13	–1.13	1.15	–1.15	0.88	–0.88
HFM32_3	0.89	–0.89	0.88	–0.88	0.84	–0.84	0.66	–0.66
HFM32_4	0.59	–0.59	0.59	–0.59	0.55	–0.55	0.47	–0.47
HFM34_3	0.51	–0.51	0.50	–0.50	0.17	–0.08	0.16	0.01
Mean	**0.55**	**–0.42**	**0.56**	**–0.43**	**0.39**	**–0.14**	**0.44**	**0.13**

An increased horizontal hydraulic conductivity in combination with a decreased vertical hydraulic conductivity lowers the calculated hydraulic heads in almost all percussion boreholes (Table 5-3). For the majority of the boreholes MAE decreases in cases 3 and 4 compared to cases 1 and 2, for which the MAE- and ME-values are almost identical. In cases 1 and 2 the hydraulic head in the bedrock is overestimated, resulting in an average ME of c. –0.4 m. In cases 3 and 4 the corresponding values are –0.14 and +0.13 m, respectively. Case 3 gives the best overall description of the hydraulic head, with an average MAE of +0.39 m compared to +0.44 m in case 4.

The surface-water dynamics are affected by the changes of the hydraulic parameters used for the bedrock. In Figure 5-2 the accumulated discharge in the stream upstream from Lake Bolundsfjärden is presented for calibration cases 1–4. In terms of the accumulated stream discharge, the reference case (case 1) produces the best fit to the measured discharge; the accumulated calculated discharge is 91% of the measured discharge. However, the results are almost as good in cases 3 and 4, with calculated discharges of 88% and 86%, respectively, of the measured discharge.

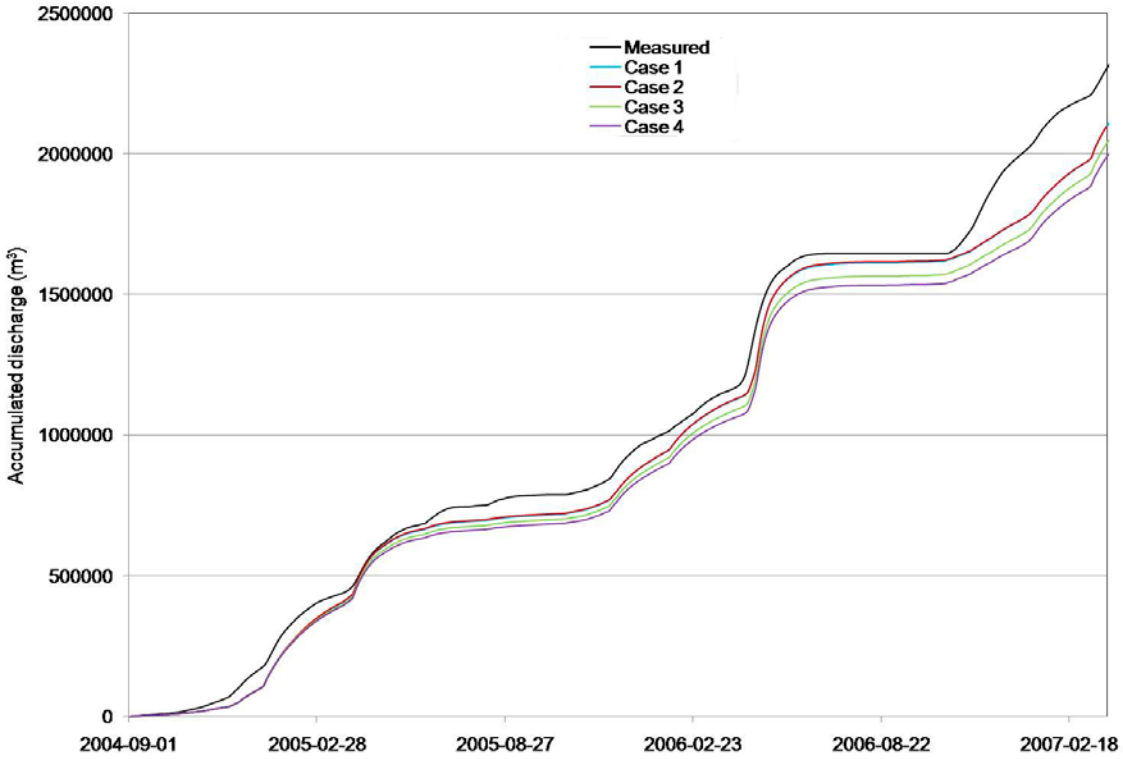

Figure 5-2. *Measured and model-calculated accumulated discharges in the stream upstream from Lake Bolundsfjärden for calibration cases 1–4.*

The interference test with pumping from percussion borehole HFM14 was simulated for all calibration cases. The test started on July 4, 2006, and was terminated on July 25, 2006. Hydraulic responses were monitored in a number of borehole sections in the bedrock and also in some groundwater monitoring wells. The results from the interference test are described in /Gokall-Norman and Ludvigson 2007/. Table 5-4 shows the difference between the measured and the calculated drawdown in surrounding boreholes for each calibration case. Percussion borehole HFM15 is not included in the table, since it is located in the same MIKE SHE model cell as the pumping borehole HFM14.

The model yields a drawdown caused by the pumping in borehole HFM14 that matches the measured drawdown better for calibration case 2 than for case 1, likely due to the reduced storage coefficient that reduces the response time. The decreased vertical hydraulic conductivity in cases 3 and 4 increases the magnitude of the calculated drawdown. Case 4 produces the most accurate average ME, but the average MAE is much better in cases 2 and 3. Overall, case 3 yields the best agreement between the measured and the model calculated drawdown, considering both ME and MAE. Figures 5-3 and 5-4 present two examples of the resulting drawdown curves for calibration case 3.

5.3 Resulting calibration

It can be concluded that calibration case 3 yields the best overall calibration results, considering groundwater levels in groundwater-monitoring wells and percussion boreholes, surface-water discharges and the interference test in borehole HFM14. The accumulated surface-water discharge is 3% lower in case 3 compared to the reference case (case 1) but the result is considered to be acceptable. All calibration cases yield approximately similar results in terms of the overall fit to measured groundwater levels in groundwater-monitoring wells. For the percussion boreholes and the HFM14 interference test, case 3 gives the best fit to measurements in terms of hydraulic heads and drawdowns.

Table 5-4. Difference between measured and calculated maximum drawdown in borehole sections for the HFM14 interference test.

Borehole section id	Case 1	Case 2	Case 3	Case 4
HFM01_1	–0.49	0.50	0.78	1.04
HFM01_2	0.79	1.00	0.34	–0.11
HFM02_1	–0.89	–0.67	–0.16	–0.18
HFM02_2	–0.75	–0.57	–0.34	–0.55
HFM02_3	–1.36	–1.28	–0.60	–0.48
HFM03_1	–1.93	–1.90	–2.10	–2.16
HFM03_2	–2.08	–2.05	–2.25	–2.31
HFM04_1	–0.15	–0.01	0.25	0.57
HFM04_2	–0.39	–0.36	–0.27	–0.07
HFM04_3	–0.25	–0.23	–0.14	0.03
HFM9	0.01	–0.05	0.19	0.35
HFM10_1	0.03	0.13	0.79	1.30
HFM10_2	–1.21	0.20	0.66	1.06
HFM13_2	–1.14	–2.54	–2.23	–2.72
HFM16_1	–0.75	–1.15	–0.12	0.53
HFM16_2	–0.94	–1.08	–0.07	0.52
HFM19_2	0.81	0.26	–1.97	–2.78
HFM20_2	0.39	–0.46	0.10	0.46
HFM20_3	–1.54	–0.73	0.17	0.49
HFM32_1	–3.05	1.47	2.29	2.34
HFM32_2	–0.03	0.83	2.23	2.69
HFM32_3	–0.10	–1.40	–1.29	–1.04
Mean diff.	**–0.68**	**–0.46**	**–0.17**	**–0.05**
Mean abs. diff.	**0.87**	**0.86**	**0.88**	**1.08**

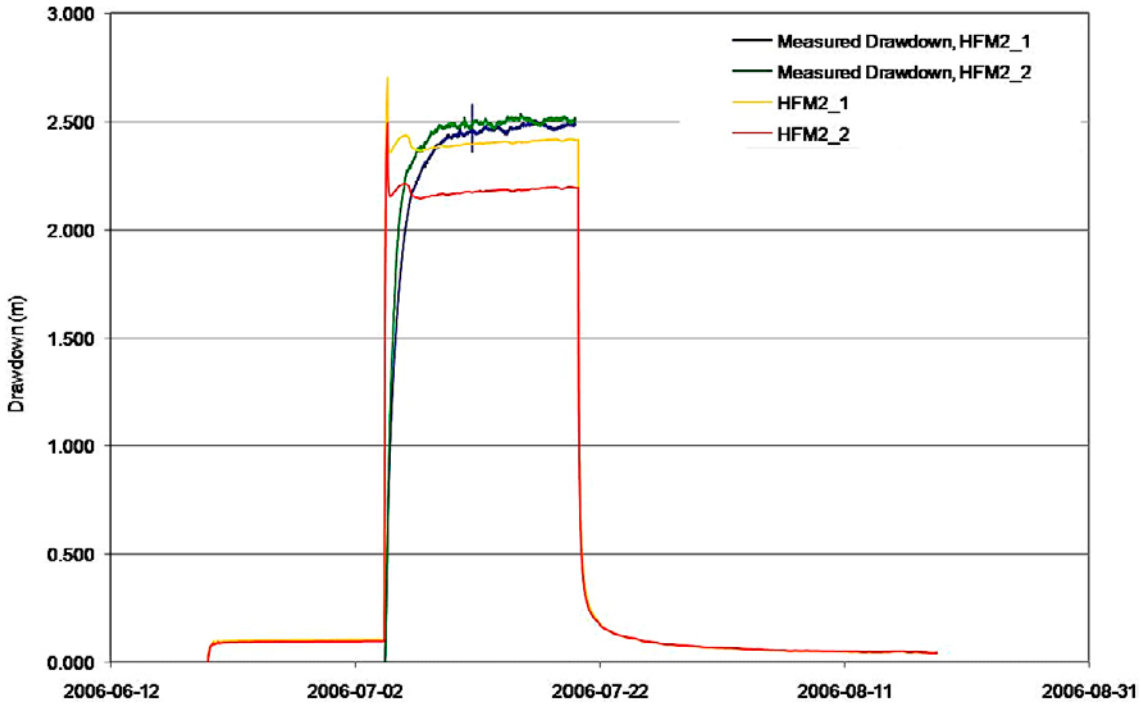

Figure 5-3. *Measured and model-calculated drawdown in borehole HFM02, sections 1 (bottom section) and 2, for calibration case 3.*

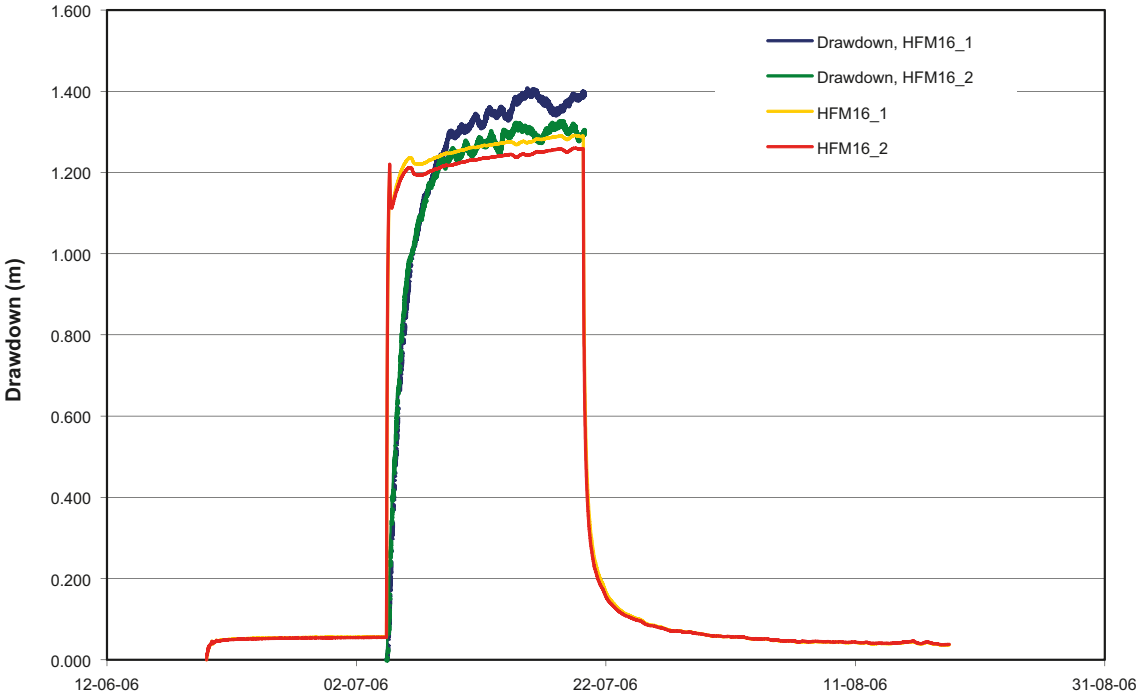

Figure 5-4. *Measured and model-calculated drawdown in borehole HFM16, sections 1 (bottom section) and 2, for calibration case 3.*

Table 5-5 compares calibration case 3 to the final version of the SDM-Site MIKE SHE model /Bosson et al. 2008/, in terms of MAE and ME for groundwater levels in groundwater-monitoring wells and percussion boreholes, and the accumulated discharge in the stream upstream from Lake Bolundsfjärden. According to this table, case 3 and the final SDM-Site model are in good agreement. The two models yield similar ME for the groundwater levels in the groundwater-monitoring wells, whereas MAE is slightly higher in case 3. In terms of groundwater levels in percussion boreholes, case 3 yields a higher ME but a lower MAE compared to the SDM-Site model.

However, ME and MAE represent average deviations and do not give a complete picture of the model performance concerning transients. It is therefore important also to study time series for each groundwater-monitoring well and percussion borehole in order to check that the actual dynamics and response times in the flow system are well described by the model. Figure 5-5 shows model-calculated hydraulic heads for calibration case 3 and the SDM-Site model, and measured hydraulic heads in SFM0003, SFM0014, HFM9 and HFM13_2. Case 3 provides a good replica of the overall transient behaviour, similar to the SDM-Site model. It should also be noted that the evaluated time periods in Table 5-5 differ between case 3 and the SDM-Site model, which may also contribute to the differences between the results from the two models.

Table 5-5. MAE and ME for groundwater levels in groundwater-monitoring wells (SFM) and percussion boreholes (HFM). The right column shows the ratio (%) between the model calculated and the measured accumulated discharge in the stream upstream from Lake Bolundsfjärden. Results are shown for calibration case 3 and for the final version of the SDM-Site model /Bosson et al. 2008/.

	Time period	SFM		HFM		Stream discharge
		MAE	ME	MAE	ME	
Case 3	Sep. 1, 2004–Mar. 31, 2007	0.31	–0.02	0.39	–0.14	88
SDM-Site	May 15, 2003–Mar. 31, 2007	0.26	–0.02	0.41	–0.03	92

SFM0003

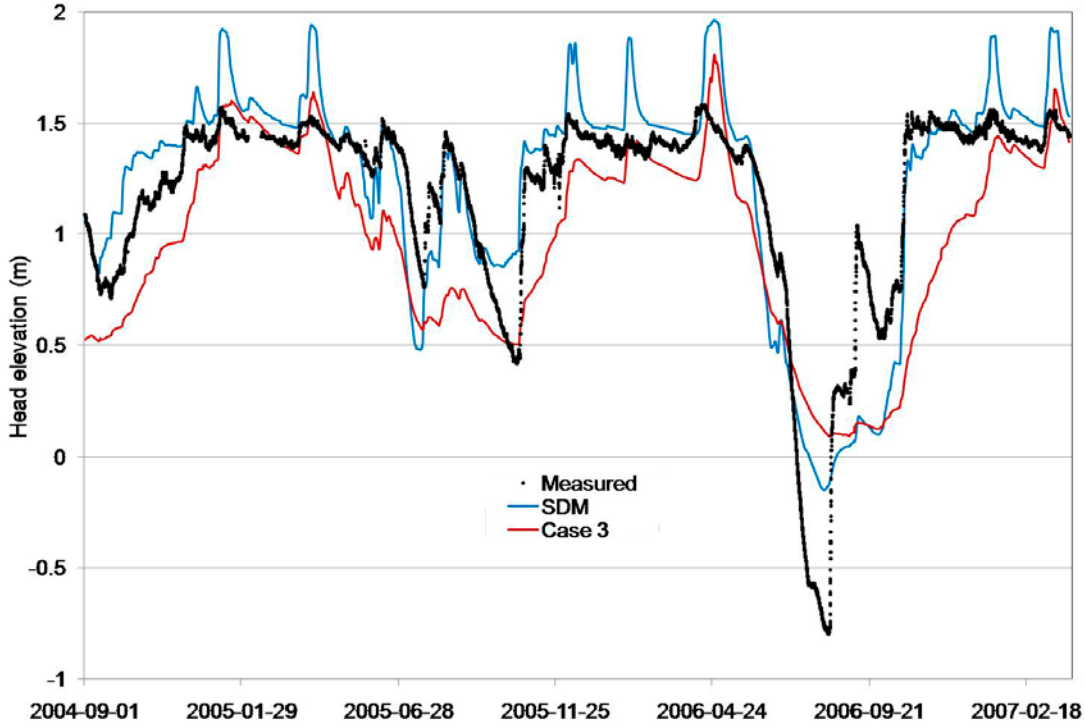

SFM0014

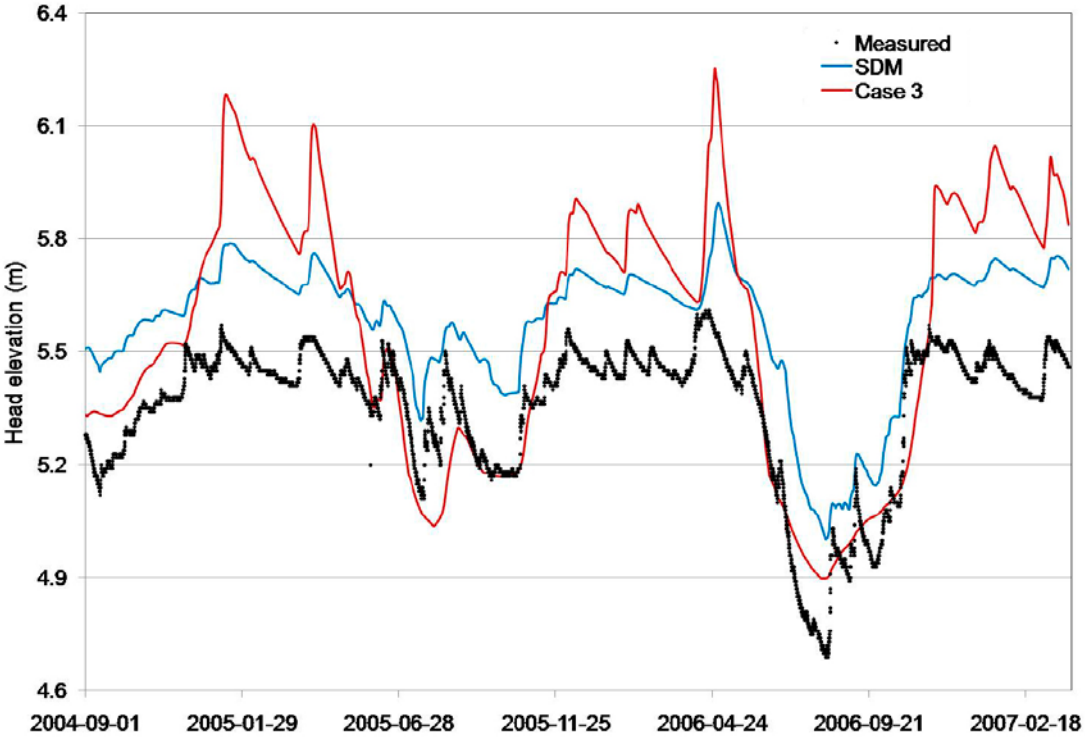

HFM9

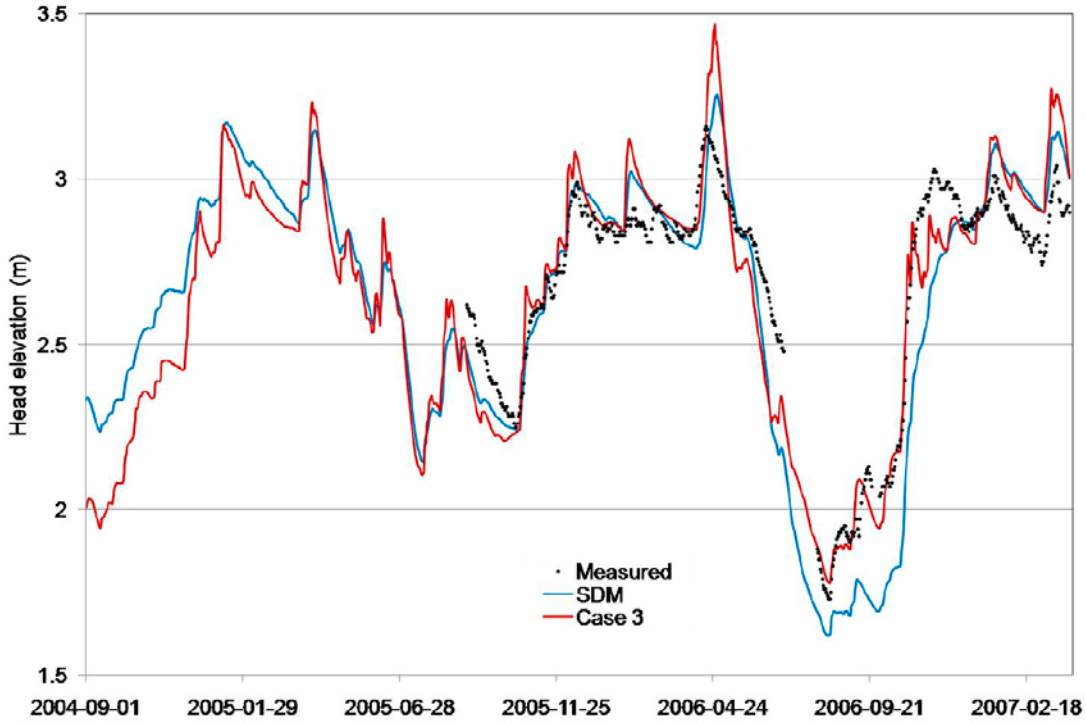

HFM13_2

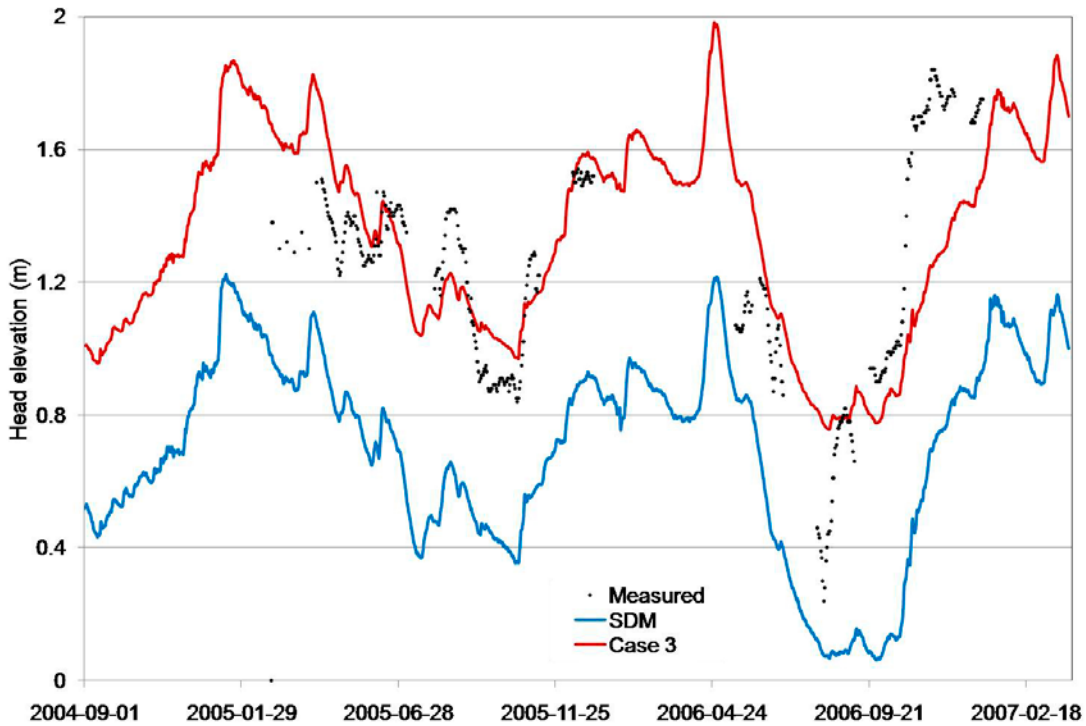

Figure 5-5. *Comparison between measured and model-calculated hydraulic heads for calibration case 3 and the calibrated SDM-Site model for groundwater-monitoring wells SFM0003 and SFM0014 and percussion boreholes HFM9 and HFM13_2 (the upper section of the borehole).*

As a result of the model calibration, an initial base case was defined to be used for the subsequent modelling. To summarise, the following changes were made to the model of the hydrogeological properties of the bedrock that was delivered from the CONNECTFLOW modelling team /Joyce et al. 2010/:

- The horizontal hydraulic conductivity (K_h) was increased by a factor of 5 in the upper 200 m of the bedrock.
- The vertical hydraulic conductivity (K_v) was decreased by a factor of 5 in the upper 200 m of the bedrock.
- The specific storage coefficient was set to $5 \cdot 10^{-8}$ m^{-1} in all bedrock layers.

Apart from the above-mentioned changes, as described in Chapter 4 the base case model also includes an increased subsurface-drainage time constant. Specifically, this constant is increased by a factor of 5 compared to the SDM-Site model.

6 Results for undisturbed conditions

This chapter presents modelling results for undisturbed conditions, i.e. the situation without the repository but with groundwater inflow to SFR and groundwater drainage at the nuclear power plant. The main objective for simulating undisturbed conditions is to provide a reference to the simulations for disturbed conditions, with groundwater inflow to the repository. The presentation includes calculated water balances, surface-water discharges and groundwater levels. Further MIKE SHE modelling results for undisturbed conditions are presented in /Bosson et al. 2008/. Results are presented as mean values for the year 2006.

6.1 Water balance

The water balance presented here represents a sub-volume within the total model volume. Since the sea is represented as a highly conductive geological layer with a prescribed time-varying head, the sea and the model volume below the sea are not included in the water balance calculations. Thus, the water balance is calculated for the land part of the model area, including the littoral zone. In this case the littoral zone refers to the area close to the sea which from time to time is submerged due to sea-level variations.

The calculated water balance for undisturbed conditions is presented in Figure 6-1 and Table 6-1. All water-balance components are expressed as area-normalised total volumetric discharges (mm/year). The accumulated precipitation is 534 mm and the calculated evapotranspiration 406 mm. The total storage change during the year is –34 mm (the total storage decreases), consisting of storage changes in the overland compartment (an increase by 8 mm), the unsaturated zone (an increase by 12 mm), the groundwater zone (–24 mm) and snow (–30 mm). This water balance yields a model-calculated annual runoff of 162 mm (= 534–406 + 34). Some 75% of the precipitation is removed by evapotranspiration, which is in accordance with the results presented by /Bosson et al. 2008/. Compared to /Bosson et al. 2008/ the present results differ in terms of the calculated runoff and storage components. This difference can be explained by the fact that /Bosson et al. 2008/ evaluated a different time period, specifically the three hydrological years September, 2003–September, 2006.

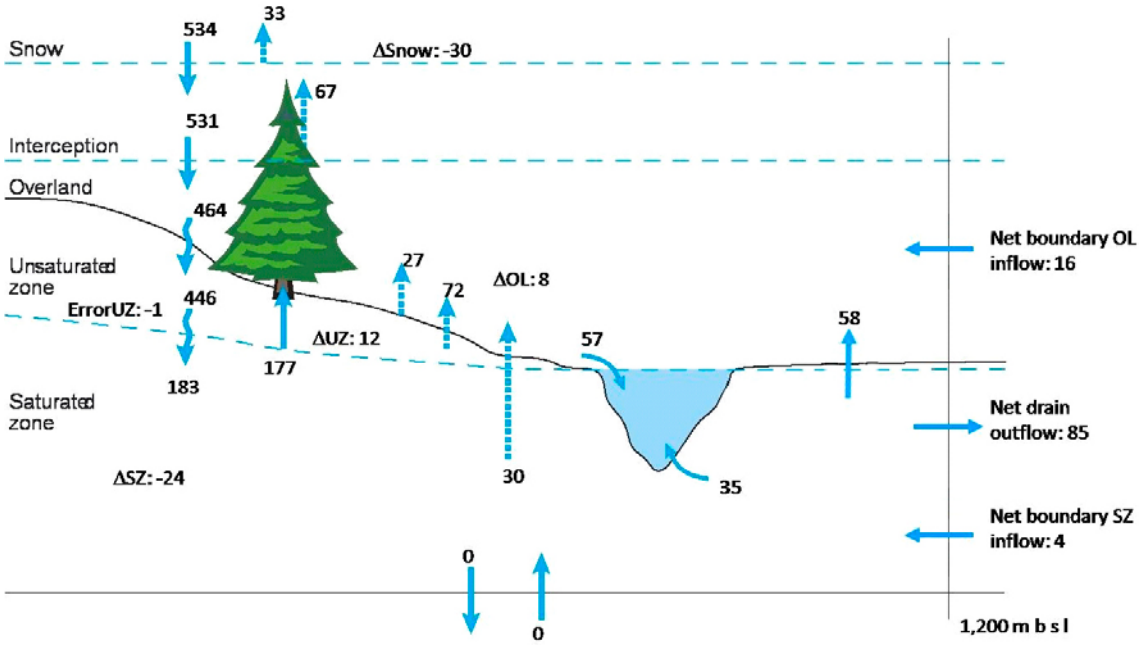

Figure 6-1. *Calculated annual water balance (mm) for the land part of the model area for undisturbed conditions.*

Table 6-1. Total annual accumulated water balance (mm) for the land part of the model area for undisturbed conditions. The date format is YYYY-MM-DD.

Date	Precipitation	Canopy storage change	Evapo-transpiration	Snow storage change	Overland storage change	Overland boundary inflow	Overland boundary outflow	Overland to river	Subsurface storage change	Subsurface boundary Inflow	Subsurface boundary outflow	Drain & net base-flow to river	Drain outflow to sea
2005-12-30	0.0	0.0	0.0	0.0	0.0	0.0	0.0	0.0	0.0	0.0	0.0	0.0	0.0
2006-01-29	–17.5	0.0	0.0	14.1	–26.8	–726.4	748.7	4.5	–5.1	1.2	1.9	2.5	5.3
2006-02-28	–65.9	–0.1	0.6	32.6	–23.2	–1,264.3	1,289.1	11.8	–0.7	2.4	3.8	7.1	11.1
2006-03-30	–112.3	–0.1	3.3	78.0	–25.1	–1,460.5	1,483.1	15.2	–7.6	3.6	5.6	9.5	13.9
2006-04-29	–151.0	–0.1	37.3	–29.8	11.9	–2,451.6	2,484.1	29.0	21.5	5.2	7.4	20.9	23.6
2006-05-29	–168.5	–0.1	97.5	–29.8	–9.8	–2,934.0	2,963.6	43.6	–18.9	6.7	9.2	25.2	27.9
2006-06-28	–199.4	1.8	191.3	–29.8	–28.4	–3,961.0	3,987.5	46.5	–61.7	8.9	10.3	26.4	32.2
2006-07-28	–206.5	0.0	295.8	–29.8	–45.5	–4,481.9	4,504.5	46.5	–129.4	11.1	11.3	27.0	35.8
2006-08-27	–264.1	1.1	360.0	–29.8	–46.3	–5,146.6	5,163.6	46.5	–133.7	13.2	12.2	27.3	39.8
2006-09-26	–316.5	–0.1	401.7	–29.8	–48.0	–6,845.4	6,860.4	46.7	–125.8	15.1	13.1	27.7	46.8
2006-10-26	–424.8	1.7	406.6	–29.8	–33.2	–8,300.6	8,316.6	48.0	–55.7	16.7	14.2	28.5	54.6
2006-11-25	–513.6	0.2	406.6	–29.8	8.5	–12,768.5	12,760.9	51.1	–16.5	18.6	15.6	31.6	68.9
2006-12-30	–534.1	0.1	406.6	–29.8	7.6	–19,275.6	19,259.6	57.4	–11.3	20.7	17.2	34.9	85.2

The calculated evapotranspiration (406 mm) is the sum of transpiration from vegetation (177 mm) and various evaporation components, including evaporation from soil (72 mm), evaporation from snow (33 mm) and evaporation from flooded areas (27 mm), i.e. lakes and wetlands, interception (67 mm), and evaporation from the saturated zone (30 mm). The total runoff is then calculated to 157 mm, consisting of overland flow to streams (57 mm), groundwater flow to streams (35 mm, of which 29 mm is drain flow from the upper soil layer), and net boundary outflow to the sea (85–16–4 = 65 mm).

The presently calculated total runoff is 5 mm higher than the runoff calculated by /Bosson et al. 2008/, and the drainage flow to the sea (85 mm) is much higher in the present model compared to /Bosson et al. 2008, Gustafsson et al. 2009/. The runoff in the uppermost soil layers is described as a subsurface drainage. In coastal areas, this runoff goes directly to the sea. As the sea level varies with time, a loop of water is created between the overland compartment and the saturated zone. This process is more pronounced in the present model, since the drainage time constant has been increased compared to previous models.

The calculated infiltration from the overland compartment to the unsaturated zone is 446 mm, whereas the calculated groundwater recharge from the unsaturated to the saturated zone is 183 mm. The other water-balance components for the saturated zone comprise evaporation (30 mm), flow to streams (35 mm), net discharge to overland (58 mm), net outflow to the sea (81 mm), and storage changes (–24 mm). The reduced saturated-zone storage is mainly due to the dry period June–September, which is not compensated for during the remaining months that year. A more balanced period with similar hydrological conditions in the end and the beginning would result in an increase of the runoff terms but also in an increase of the model-calculated evaporation.

The drainage at the nuclear power plant and the groundwater inflow to SFR totally represent 2 mm, which yield a total drain outflow of 87 mm including the drainage flow of 85 mm to the sea (see Table 6-1). Note that only a small part of SFR is located below the land part of the model area. For further details concerning the inflow to SFR, see Section 7.1.

The quite large snow-storage change is an effect of the studied period (the calendar year 2006). In particular, there is an increase of the snow storage during December 2005, whereas the snow storage is zero in the end of December 2006. The large amount of evaporation from snow comes from the relatively late snow cover during spring 2006. The snow cover did not melt until the beginning of April 2006, and was consequently accessible for evaporation during more than three months, with a rather high potential evapotranspiration (PET) during March and April.

6.2 Surface-water levels and -discharges

Figure 6-2 shows the locations of the surface-water gauging stations in Forsmark. Figure 6-3 shows a time-series plot of model-calculated and measured discharges at the gauging station upstream from Lake Bolundsfjärden (PFM005764) during 2006. In April there is a distinct snowmelt that results in high peak discharges. The summer was very dry, including a dry beginning of the autumn, followed by a rather wet last part of the year. The model captures the overall runoff dynamics but overestimates the spring peak. Moreover, in mid autumn the model response after a long dry period is too slow. Figure 6-4 shows a time-series plot of the accumulated stream discharge. As can be seen from this figure, the model underestimates the accumulated stream discharge over the two-year simulation period.

Appendix 1 presents model-calculated and measured stream discharges for the surface-water discharge gauging stations located downstream from Lake Eckarfjärden, Lake Stocksjön and Lake Gunnarsbo-träsket. Figure 6-5 shows a time-series plot of model-calculated and measured water levels in Lake Bolundsfjärden during year 2006. In general, the model provides a proper description of the actual water-level variations of the lake. The overall results in terms of surface-water levels and surface-water discharges are in accordance with the results presented in /Bosson et al. 2008/, which includes a more detailed comparison between model-calculated and measured data.

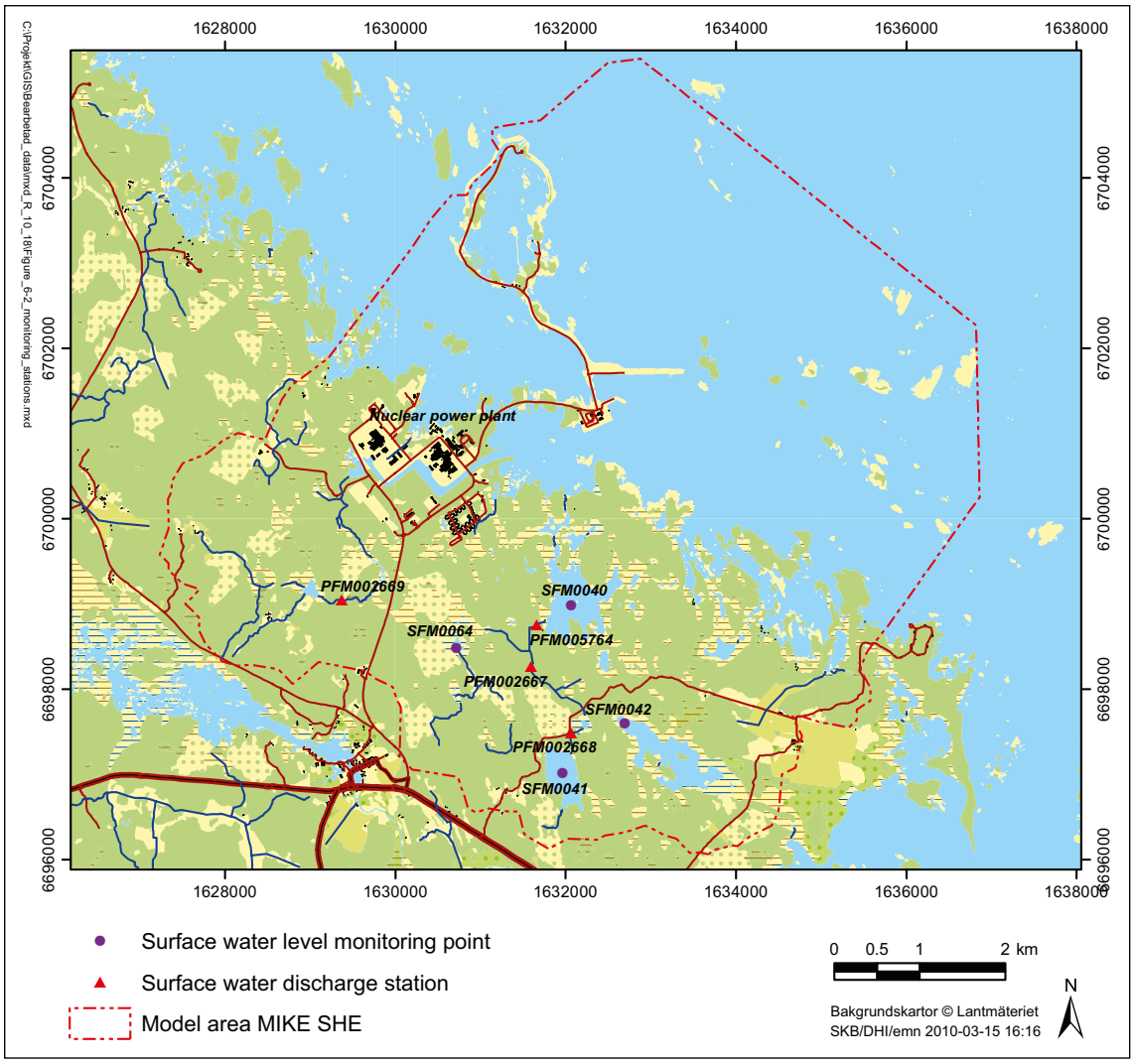

Figure 6-2. *Locations of the surface-water discharge gauging stations PFM002668 (downstream from Lake Eckarfjärden), PFM002667 (downstream from Lake Stocksjön), PFM002669 (downstream from Lake Gunnarsboträsket) and PFM005764 (upstream from Lake Bolundsfjärden). The map also shows the locations of the surface-water level gauging stations SFM0041 (Lake Eckarfjärden), SFM0042 (Lake Fiskarfjärden), SFM0064 (Lake Gällsboträsket) and SFM0040 (Lake Bolundsfjärden).*

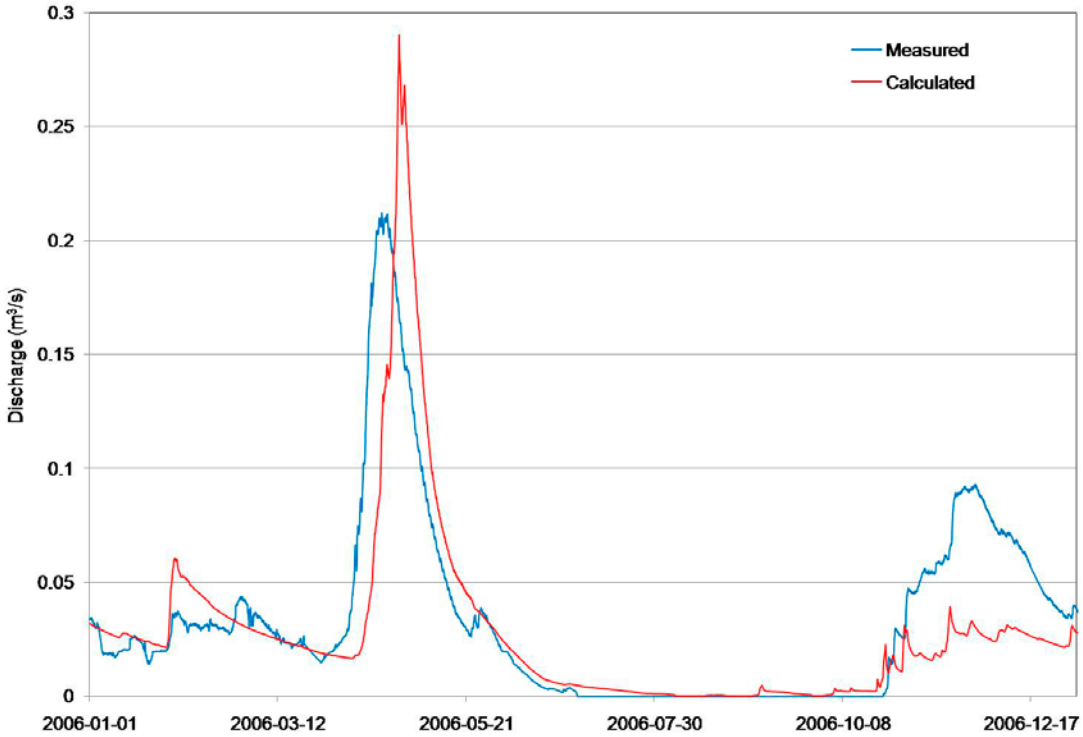

Figure 6-3. *Model-calculated and measured discharges (m^3/s) in the stream upstream from Lake Bolundsfjärden. The date format is YYYY-MM-DD.*

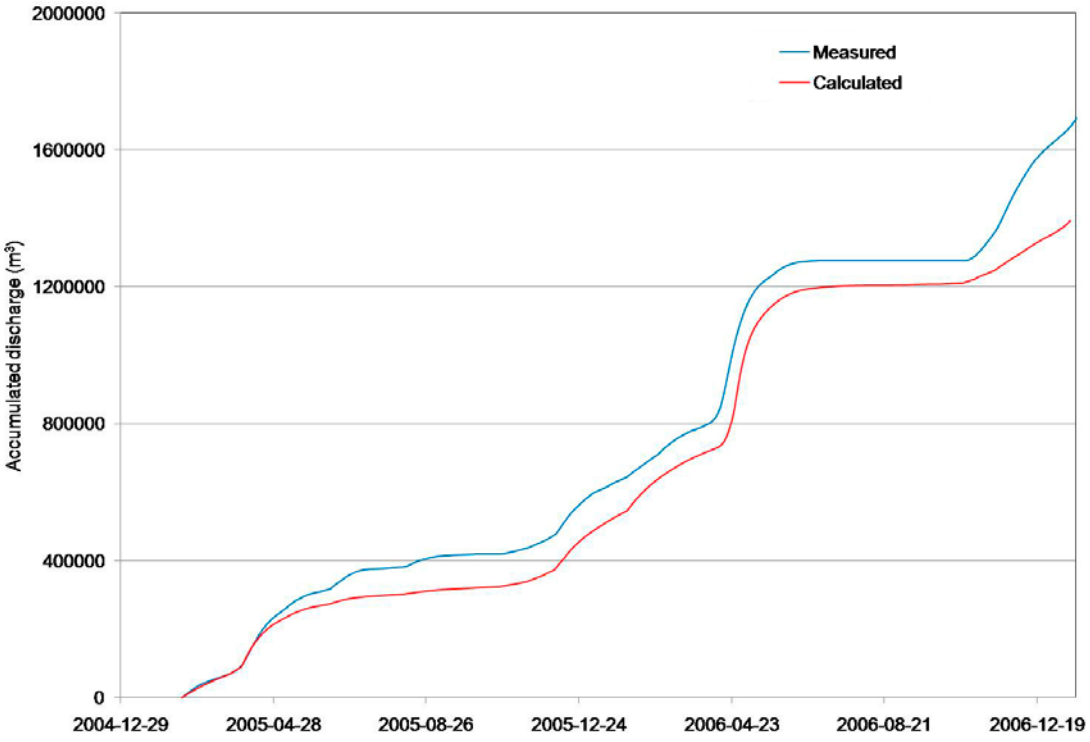

Figure 6-4. *Model-calculated and measured accumulated discharges (m^3) in the stream upstream from Lake Bolundsfjärden.*

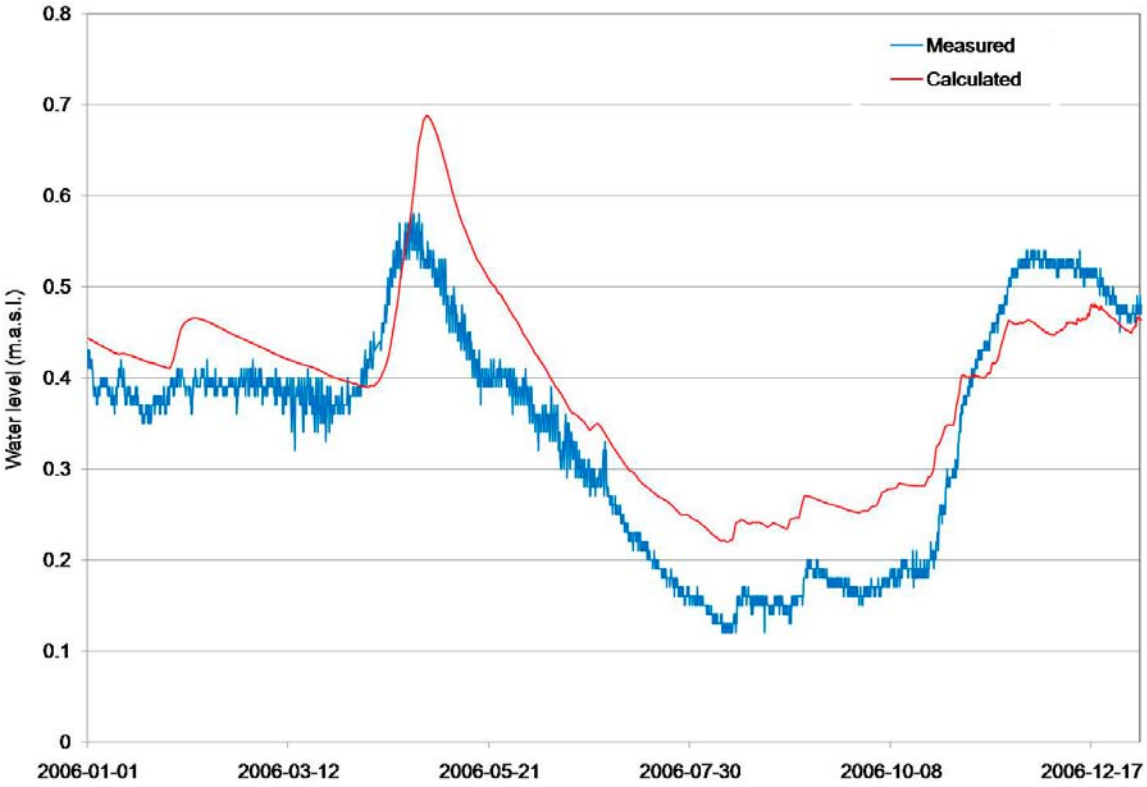

Figure 6-5. *Model-calculated and measured water levels (m.a.s.l.) in Lake Bolundsfjärden.*

6.3 Elevation of the groundwater table

Figure 6-6 shows the calculated annual average (year 2006) groundwater-table elevation (m.a.s.l.). The sea has been excluded from the figure, since it is only of interest to study the groundwater-table elevation in the land part of the model area. The groundwater table in the sea is equal to the time-varying sea level. As can be seen from the figure, the low elevation of the ground surface implies that the groundwater-table elevation is only up to a few meters above sea level in large parts of the area.

Figure 6-7 shows the calculated annual average depth to the groundwater table in the model area. The groundwater table is shallow and located less than 1.5 m below ground in most of the model area, with an average depth of 1.1 m below ground surface (excluding the sea). The groundwater table is located at larger depths in the high-altitude areas, associated with groundwater recharge near groundwater divides. There are also areas with a hydraulic head above the ground surface, for which Figure 6-7 shows the calculated overland water depth. These areas are (local) low-altitude areas where there is groundwater discharge and that coincide with lakes and areas in the vicinity of streams.

Figure 6-8 shows the cumulative frequency distribution (CFD) of the model-calculated depth to the groundwater table (metres relative to the ground surface). Note that the sea is excluded from these data. As can be seen in Figure 6-8, approximately 75% of the land area has a groundwater-table depth between 0 and 2 m below the ground surface. In the remaining part, c. 10% of the area has a groundwater-table depth below 2 m and c. 15% consists of areas with overland water (lakes, wetlands and streams).

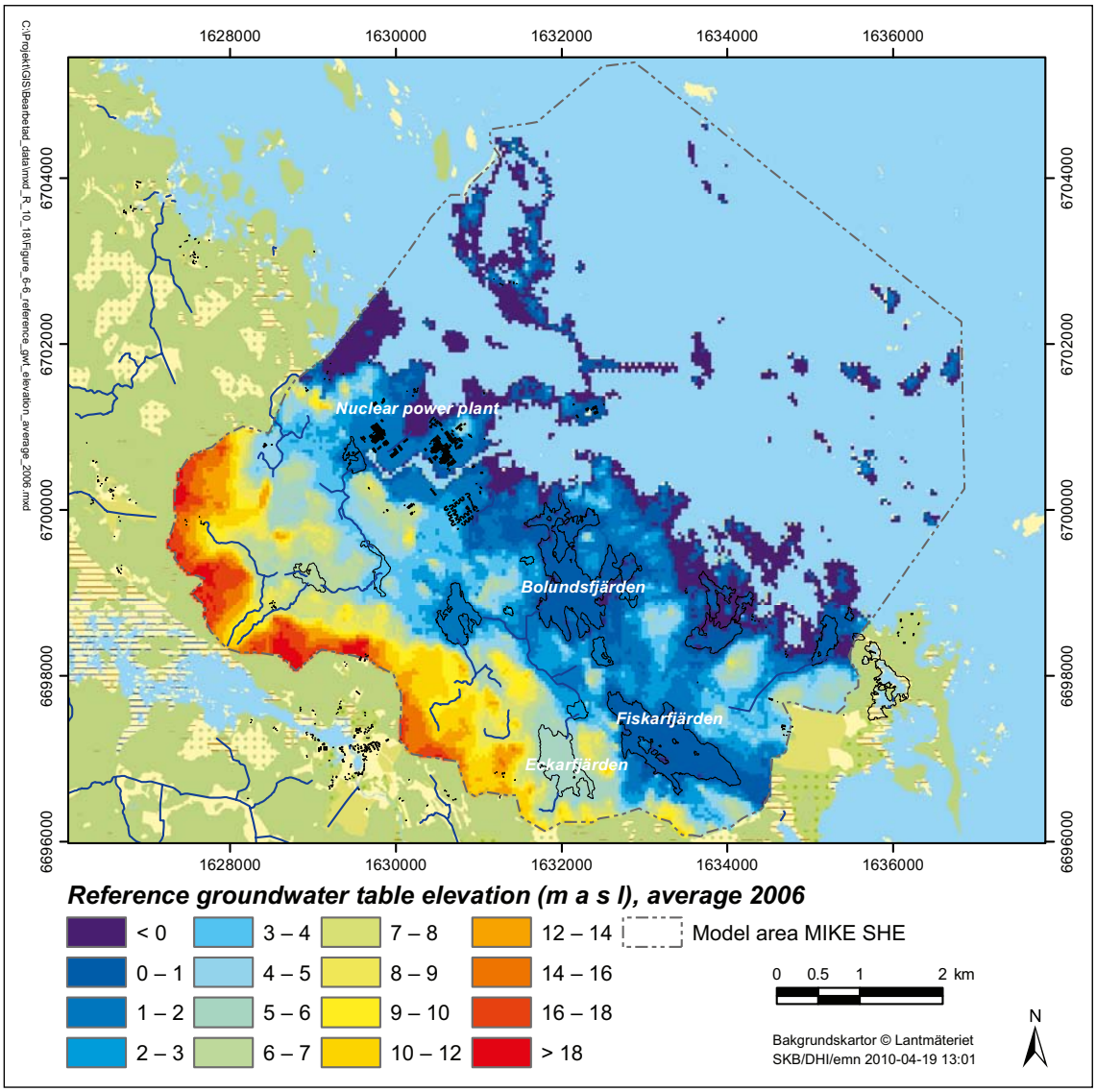

Figure 6-6. *Model-calculated annual average groundwater-table elevation (m.a.s.l.), year 2006.*

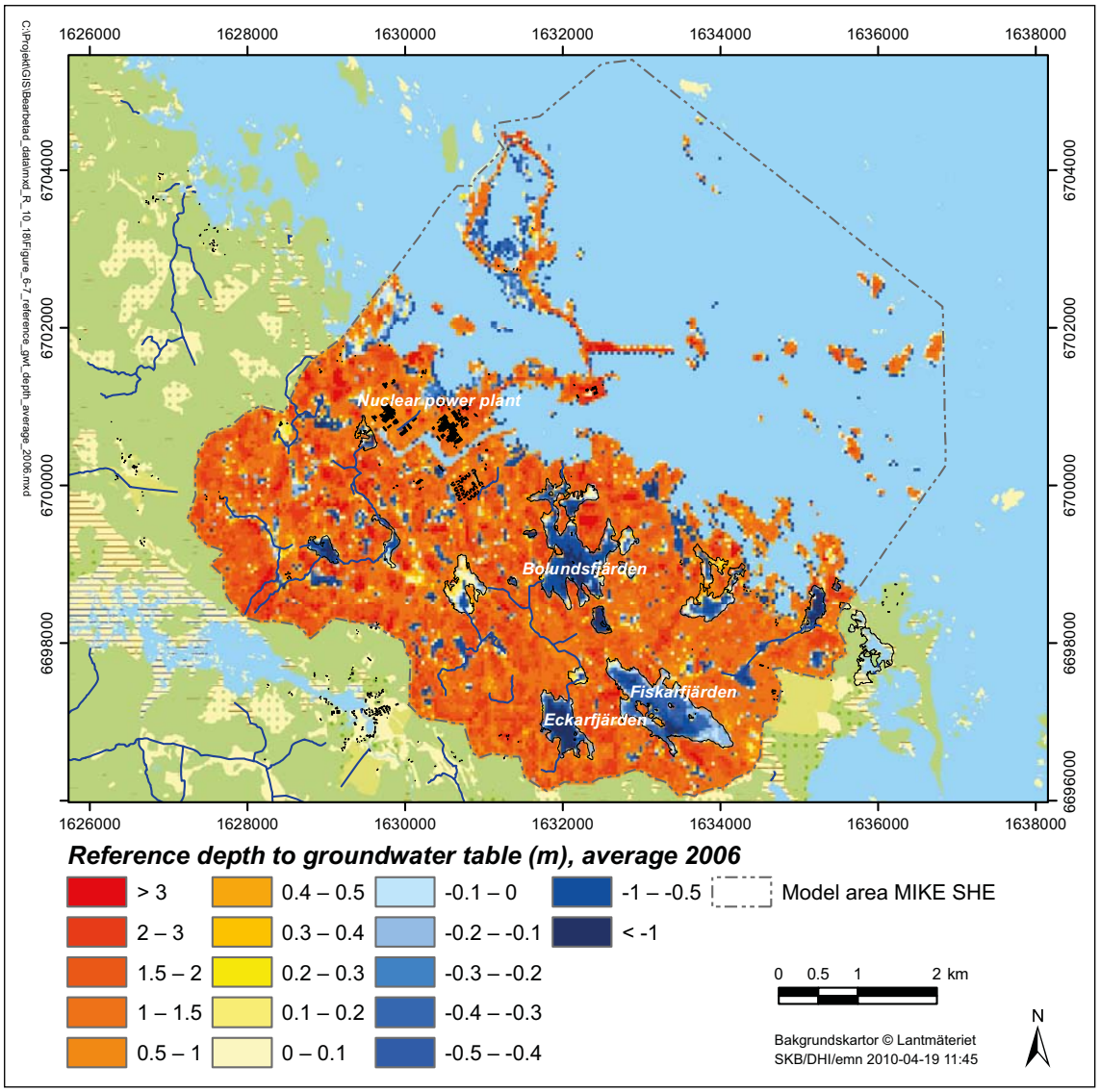

Figure 6-7. *Model-calculated annual average depth to the groundwater table. Negative depths denote areas with water above the ground surface.*

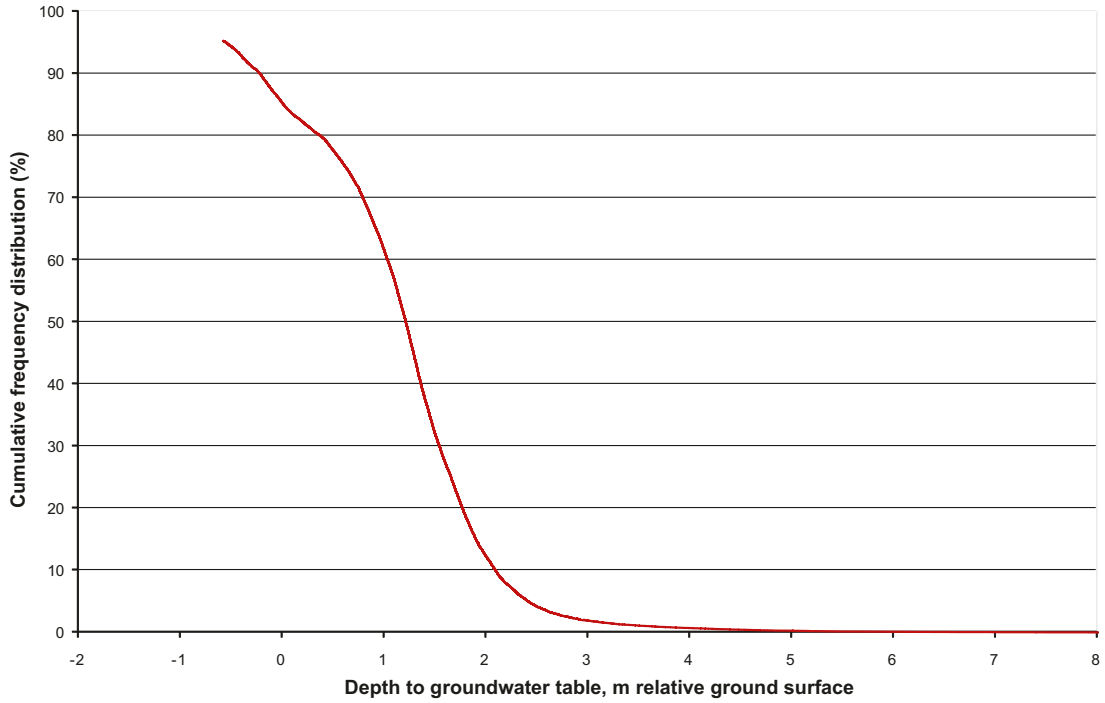

Figure 6-8. *Cumulative frequency distribution (CFD) of the model-calculated depth to the groundwater table relative to the ground surface (excluding the sea).*

6.4 Groundwater recharge and discharge areas

Figure 6-9 shows the model calculated annual average hydraulic-head difference between computational layers 1 and 2. Hence, the figure shows the locations of groundwater recharge and discharge areas in the Quaternary deposits. Figure 6-10 shows the corresponding head difference between layers 4 (30 m.b.s.l.) and 5 (50 m.b.s.l.), hence showing areas with downward and upward groundwater flow in the upper part of the bedrock. According to Figure 6-9, there is groundwater discharge in the Quaternary deposits at the locations of streams and lakes. Due to local-scale topographical variations, the spatial distribution of recharge and discharge areas is rather scattered in the Quaternary deposits.

In the bedrock layers 4–5 areas with upward flow are located in the vicinity of and below the lakes. To some extent, topographical depressions at the ground surface are also areas with upward flow in the bedrock. There is downward flow in the areas around SFR and the nuclear power plant due to the inflow to SFR and the subsurface drainage below the power plant. MIKE SHE modelling results (not reproduced here) show that for natural conditions, i.e. without the groundwater diversion at these facilities, there is no downward flow in the bedrock in these areas. The vertical groundwater flow pattern under natural and the present conditions is further discussed in Section 7.6.3.

The hydraulic-head differences in the Quaternary deposits are somewhat smaller compared to the head differences between the computational layers 4 and 5 in the upper parts of the bedrock. The mean head difference in the recharge areas (areas with downward flow) is 0.05 m between layers 1 and 2 and 0.29 m between layers 4 and 5. The corresponding head differences in the discharge areas (areas with upward flow) are –0.01 m between layers 1 and 2 and –0.12 m between layers 4 and 5. The larger head differences between the bedrock layers can be explained by the greater thickness of layers 4 and 5 (20 m) compared to the Quaternary deposit layers 1 and 2.

The present results are in accordance with the results of the SDM-Site model /Bosson et al. 2008/. The main differences are found in the upper bedrock in the areas around SFR and the nuclear power plant. In the present modelling there are larger vertical hydraulic-head differences in areas with downward flow compared to /Bosson et al. 2008/. The groundwater inflow to SFR and the drainage system at the nuclear power plant were not considered in the corresponding results of /Bosson et al. 2008/.

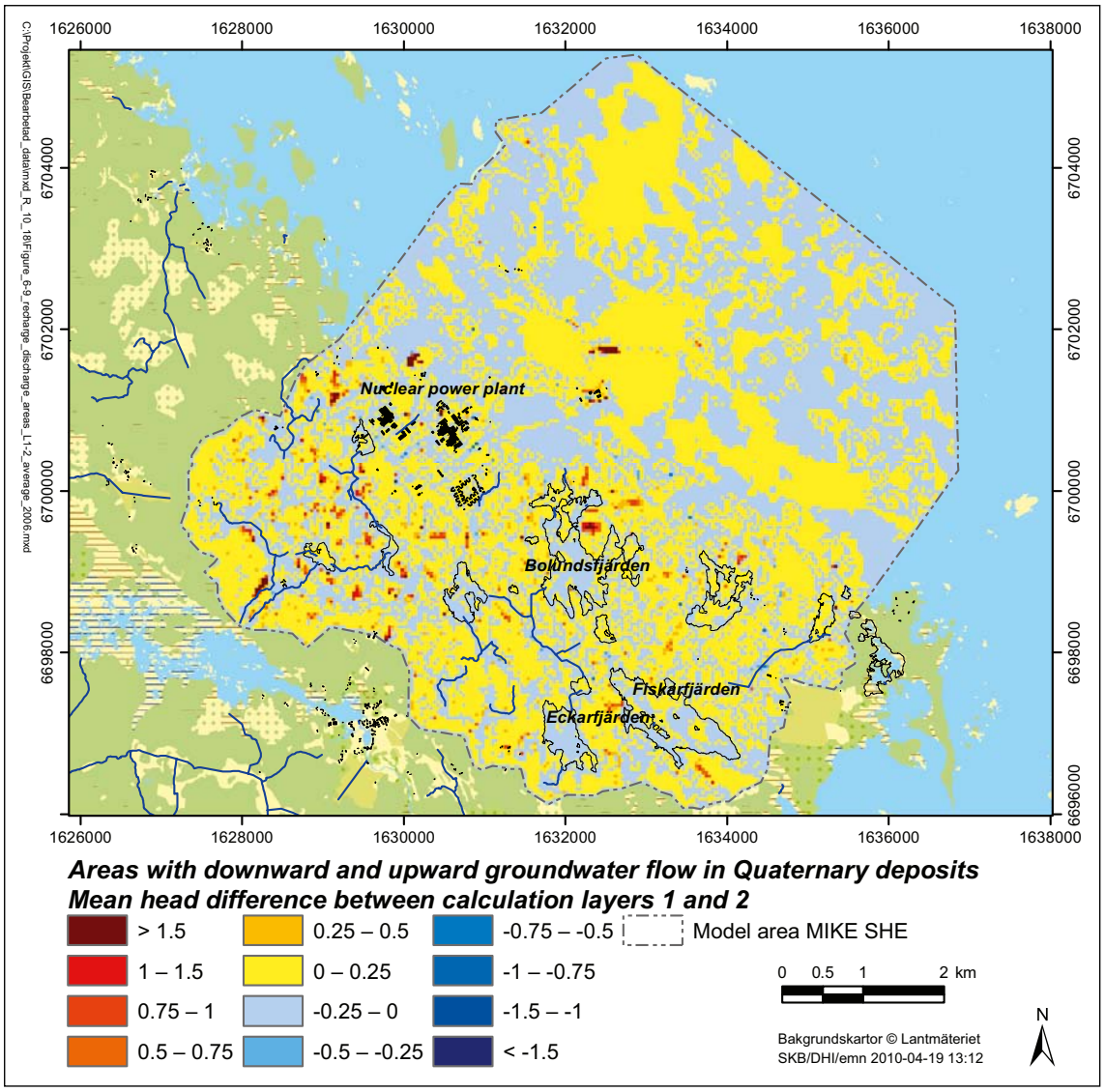

Figure 6-9. *Annual average hydraulic-head difference (m) between computational layers 1 and 2, showing the locations of groundwater recharge and discharge areas in the Quaternary deposits. Blue colours indicate upward flow (discharge) and yellow/red colours indicate downward flow (recharge).*

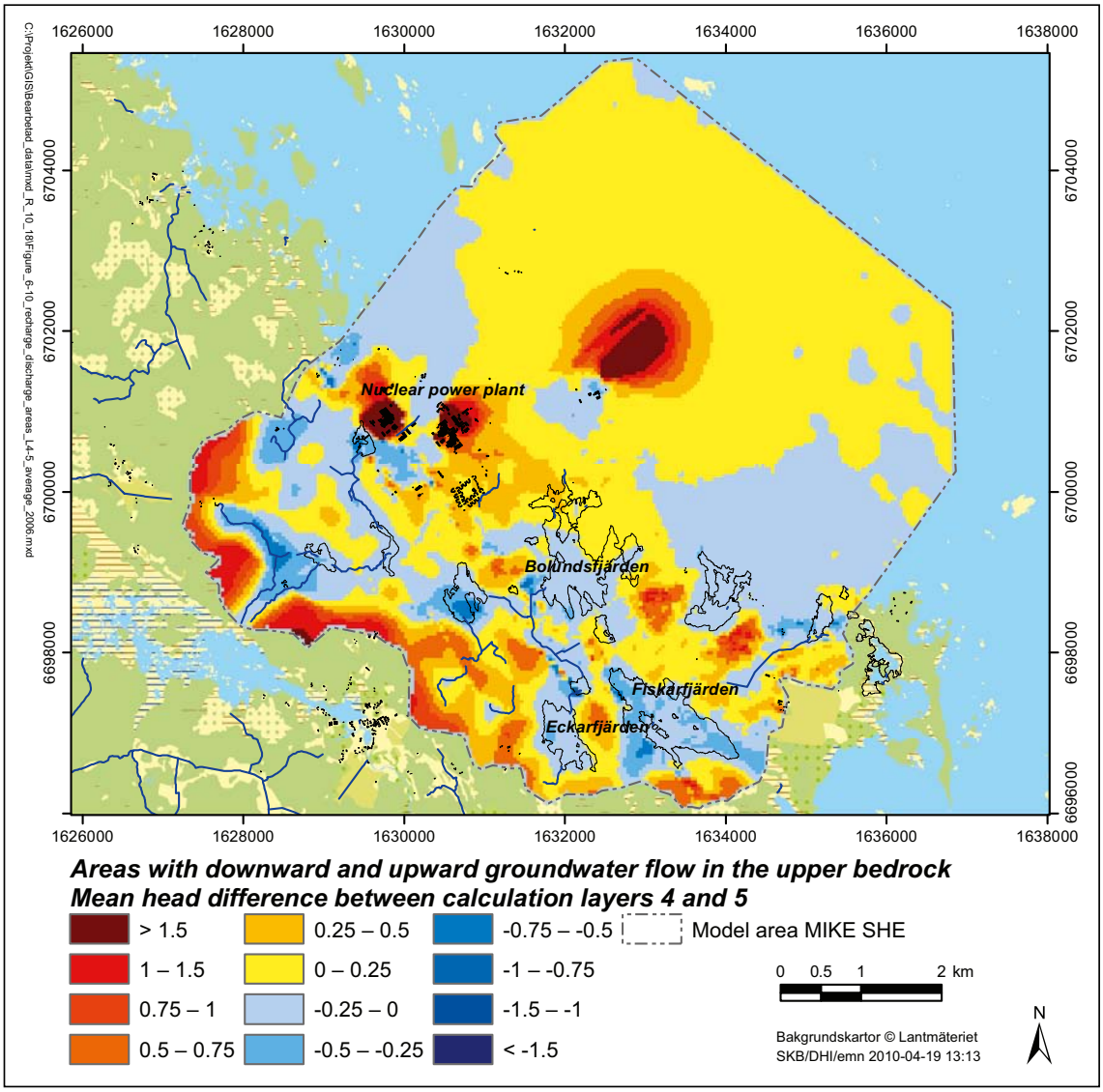

Figure 6-10. *Annual average hydraulic-head difference (m) between computational layers 4 and 5, showing areas with downward and upward groundwater flow in the upper part of the bedrock. Blue colours indicate upward flow and yellow/red colours indicate downward flow.*

7 Results for open repository conditions

This chapter presents results of the modelling of disturbed conditions, i.e. with groundwater inflow to the repository. The simulations consider three grouting cases, $K_{grout} = 10^{-7}$, 10^{-8} and 10^{-9} m/s. Unless stated otherwise, results are presented as annual averages for the year 2006 and for the case with a fully open repository. As explained previously, this is a hypothetical worst case that will not occur in reality. The actual construction and operation of the repository imply that tunnel construction and backfilling will take place simultaneously in different parts of the repository area. In order to study the influence of the actual construction and operation of the repository on its hydrological and hydrogeological effects, results are presented for three phases that are rough approximations of reality. These phases include the (initial) construction phase, development phase 3, and a hypothetical case with a fully open repository excluding main and deposition tunnels. All results for disturbed conditions are compared to the results for undisturbed conditions, i.e. without the repository but including SFR and the drainage system at the nuclear power plant.

Water balances are presented for the entire MIKE SHE model area and for different parts of the model area, including detailed results for the saturated zone. The model-calculated groundwater inflow to the repository is presented for three grouting cases for a fully open repository, the construction phase (two grouting cases) and for the above-mentioned development phases (one grouting case), of which one is purely hypothetical. Moreover, results from particle-tracking simulations are analysed for the construction phase and for a fully open repository, and the hydrological effects of the repository are presented in terms of changes of lake-water levels and stream discharges.

Modelling results in terms of the drawdown of the groundwater table are shown for three grouting cases. The spatial variability of the drawdown of the groundwater table and hydraulic heads in the bedrock are analysed in the form of horizontal cross sections and vertical profiles through the model area and the repository. Effects on the groundwater-table elevation and hydraulic heads in the bedrock are evaluated for different combinations of the repository development and SFR, including the present SFR and an extension of that facility. Finally, the chapter presents the results of a study of backfill saturation, recovery of the groundwater table and recovery of hydraulic heads in the bedrock subsequent to termination of the groundwater diversion from the repository.

7.1 Water balance

The groundwater inflow to the repository affects the water turnover in the model area. Table 7-1 summarises water-balance components for the land part of the model area for undisturbed conditions and for disturbed conditions (three grouting cases). Observe that part of the repository area is located below the sea (cf. Figure 4-4) and is therefore not considered in Table 7-1.

Table 7-1. Water balance (mm) for the land part of the model area for undisturbed and disturbed conditions.

	Undisturbed conditions	$K_{grout} = 10^{-7}$ m/s	$K_{grout} = 10^{-8}$ m/s	$K_{grout} = 10^{-9}$ m/s
Precipitation	534.1	534.1	534.1	534.1
Evapotranspiration	406.6	401.1	404.4	405.3
Canopy storage change	0.1	0.1	0.1	0.1
Snow storage change	–29.8	–29.8	–29.8	–29.8
Overland storage change	7.6	7.0	6.9	9.1
Subsurface storage change	–11.3	–15.0	–12.9	–12.0
Net overland inflow from sea	16.0	19.6	19.9	19.9
Net subsurface inflow from sea	3.6	20.3	12.9	7.2
Drainflow to sea	85.2	84.1	84.6	84.9
Overland flow to river	57.4	46.7	50.0	53.7
Drainflow to river	28.9	26.9	27.3	27.7
Net baseflow to river	5.9	5.7	5.8	5.9
Inflow to the open repository	–	44.5	28.0	13.7

For grouting case $K_{grout} = 10^{-7}$ m/s the model-calculated annual runoff is 124 mm, which can be compared to 158 mm for undisturbed conditions. Hence, the runoff reduction is 34 mm. For this grouting case, the groundwater inflow to the repository corresponds to 45 mm. The remaining 11 mm are due to a slightly reduced evapotranspiration and changes in subsurface storage. The groundwater inflow to the repository is in this grouting case 28% (45/158) of the runoff for undisturbed conditions. The corresponding ratio for $K_{grout} = 10^{-8}$ and 10^{-9} m/s is 18% and 9%, respectively.

The groundwater inflow also affects the runoff to the streams. This runoff component is reduced by 92–79 = 13 mm (–14%) for $K_{grout} = 10^{-7}$ m/s. The largest effect concerns overland flow to streams, which is reduced by 11 mm (–19%) for $K_{grout} = 10^{-7}$ m/s. This effect is most pronounced in the downstream parts of the area, in particular downstream from Lake Bolundsfjärden. In this part of the model area, there is a small depth to the groundwater table for undisturbed conditions and the groundwater table drawdown is large for disturbed conditions (see Section 7.5).

Both for undisturbed and disturbed conditions there is a net subsurface and overland inflow to the land part of the model from the sea. Both these flow components are larger for disturbed conditions compared to undisturbed conditions. The net overland inflow increases with 4 mm (23%), whereas the net subsurface inflow increases by 16 mm, from 4 mm for undisturbed conditions to 20 mm for $K_{grout} = 10^{-7}$ m/s (a factor of five). The net subsurface inflow is the runoff component with the largest relative change. The increased inflow from the sea mainly occurs in the bedrock layers (16 mm). Table 7-2 presents water-balance components for the saturated zone for each calculation layer in the bedrock for the land part of the model area. The principle for calculating in- and outflows (annual volumes) for a specific calculation layer is illustrated in Figure 7-1.

As can be seen in Table 7-2, for grouting case $K_{grout} = 10^{-7}$ m/s the total horizontal inflow in the bedrock from the sea area increases with 16 mm, from an outflow of 2 mm to an inflow of 14 mm. Almost half of this change pertains to the lower sheet-joint layer at approximately 110 m.b.s.l. and there is also a considerable change of the horizontal flow in sheet-joint layer 6 between 60 and 80 m.b.s.l. The vertical groundwater flows are larger than the horizontal flows, and the inflow to the repository yields large changes of the vertical flows. The net vertical inflow from the Quaternary deposits (QD) to the bedrock in layer 3 changes with 25 mm, from 2 mm for undisturbed conditions to 27 mm for grouting case $K_{grout} = 10^{-7}$ m/s.

16 mm (36%) of the inflow to the repository (45 mm for grouting case $K_{grout} = 10^{-7}$ m/s) correspond to an increased horizontal net inflow from the sea, whereas 25 mm (56%) correspond to an increased vertical net inflow from the QD. The remaining 4 mm correspond to reduced storage in the bedrock (steady-state conditions were not reached during the simulation period). Note that these figures refer to the parts of the repository below the land part of the model area (cf. Figure 4-4).

Table 7-3 presents water-balance components (L/s) for each layer in the bedrock for the whole model area. Hence, Table 7-3 considers both land and sea and the whole repository. According to the table, the inflow to the repository yields an increase of the vertical inflow from the QD to the bedrock (from layer 2 to layer 3) of 43, 29 and 15 L/s for grouting case $K_{grout} = 10^{-7}$ m/s, $K_{grout} = 10^{-8}$ m/s and $K_{grout} = 10^{-9}$ m/s, respectively. Considering the land part of the model area (cf. Table 7.2, but expressed in L/s) the corresponding increase is 24, 17 and 9 L/s, respectively. According to Table 7-3, for grouting

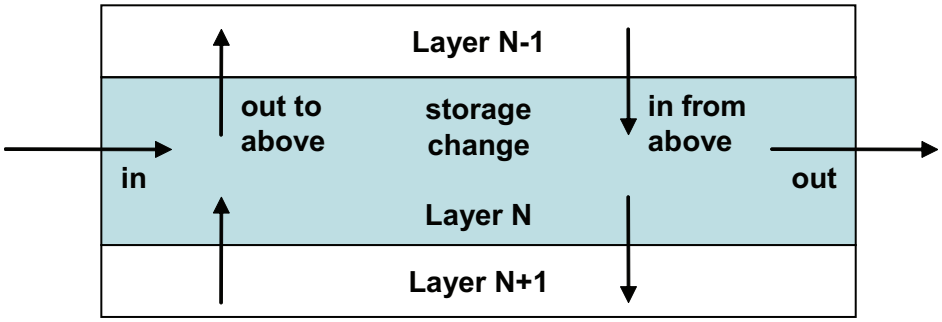

Figure 7-1. *Water-balance components for the saturated zone (see Table 7-2). In- and outflow arrows are labelled for layer N (values for the lower arrows are presented for the layer below in Table 7-2).*

Table 7-2. Water-balance components (mm) for the saturated zone for the land part of the model area and for each bedrock calculation layer. Results are presented for undisturbed and disturbed conditions. The water balance components in the table are defined in Figure 7-1.

		Undisturbed conditions				$K_{grout} = 10^{-7}$ m/s				$K_{grout} = 10^{-8}$ m/s				$K_{grout} = 10^{-9}$ m/s			
Layer	**Lower level (m.b.s.l)**	**Net horizontal outflow**	**Vertical out to above**	**Vertical in from above**	**To open repository**	**Net horizontal outflow**	**Vertical out to above**	**Vertical in from above**	**To open repository**	**Net horizontal outflow**	**Vertical out to above**	**Vertical in from above**	**To open repository**	**Net horizontal outflow**	**Vertical out to above**	**Vertical in from above**	**To open repository**
L3	20	0.16	15.55	17.80		–0.54	10.50	37.70	0.02	–0.18	11.22	31.08	0.05	0.05	12.39	24.33	0.02
L4	40	0.30	5.41	7.92		–0.24	3.00	34.01	2.29	–0.04	3.29	24.69	0.44	0.14	3.73	16.29	0.05
L5	60	0.20	3.13	5.18		–0.93	1.55	30.35	0.97	–0.40	1.71	22.55	0.49	–0.01	1.96	14.17	0.13
L6	80	0.55	2.13	3.98		–2.33	1.00	29.76	9.34	–0.37	1.06	21.80	2.02	0.21	1.21	13.30	0.27
L7	100	0.24	1.77	2.66		–0.69	1.34	22.69	0.99	–0.40	0.89	19.57	0.95	–0.03	0.92	12.11	0.28
L8	120	0.46	1.31	1.96		–7.40	0.61	21.66	11.00	–3.83	0.57	18.70	5.10	–0.79	0.63	11.58	0.81
L9	140	0.07	1.09	1.28		–0.54	0.67	18.12	0.47	–0.46	0.45	17.32	0.36	–0.27	0.45	11.37	0.11
L10	160	0.04	0.83	0.95		–0.21	0.34	17.86	0.41	–0.25	0.29	17.26	0.48	–0.16	0.31	11.40	0.24
L11	180	0.03	0.60	0.68		–0.34	0.19	17.51	0.45	–0.33	0.17	16.92	0.47	–0.19	0.20	11.20	0.26
L12	200	0.02	0.42	0.47		–0.20	0.16	17.37	0.61	–0.20	0.13	16.73	0.64	–0.12	0.12	11.06	0.35
L13	300	0.01	0.26	0.29		–0.15	0.14	16.95	0.70	–0.13	0.10	16.27	0.68	–0.09	0.08	10.77	0.33
L14	400	0.01	0.16	0.17		–0.15	0.25	16.51	0.83	–0.06	0.15	15.77	0.78	0.00	0.07	10.52	0.31
L15	500	0.00	0.08	0.09		–0.26	0.16	15.73	16.34	–0.17	0.12	15.02	15.50	–0.12	0.08	10.22	10.56
L16	600	0.00	0.05	0.06		–0.14	1.38	0.96	0.00	–0.12	1.27	0.91	0.00	–0.08	0.95	0.70	0.00
L17	700	0.00	0.04	0.04		–0.03	0.76	0.50	0.00	–0.02	0.71	0.48	0.00	–0.02	0.53	0.38	0.00
L18	800	0.00	0.03	0.03		–0.02	0.57	0.36	0.00	–0.01	0.53	0.35	0.00	–0.01	0.39	0.27	0.00
L19	900	0.00	0.02	0.02		–0.03	0.42	0.26	0.00	–0.03	0.39	0.25	0.00	–0.02	0.28	0.19	0.00
L20	1,000	0.00	0.02	0.02		–0.03	0.27	0.17	0.00	–0.02	0.25	0.16	0.00	–0.01	0.18	0.13	0.00
L21	1,100	0.00	0.01	0.01		0.00	0.17	0.12	0.00	0.00	0.16	0.12	0.00	0.00	0.11	0.09	0.00
L22	1,200	0.00	0.01	0.01		–0.01	0.09	0.07	0.00	–0.01	0.09	0.06	0.00	0.00	0.06	0.05	0.00
Sum		**2.10**			**0.00**	**–14.24**			**44.43**	**–7.03**			**27.96**	**–1.50**			**13.73**

Table 7-3. Water-balance components (L/s) for the saturated zone in the whole model area and for each bedrock calculation layer. Results are shown for undisturbed and disturbed conditions. The water-balance components are defined in Figure 7-1.

		Undisturbed conditions					$K_{grout} = 10^{-7}$ m/s					$K_{grout} = 10^{-8}$ m/s					$K_{grout} = 10^{-9}$ m/s				
Layer	Lower level (m.b.s.l)	Net horizontal outflow	Vertical out to above	Vertical in from above	To SFR	To open repository	Net horizontal outflow	Vertical out to above	Vertical in from above	To SFR	To open repository	Net horizontal outflow	Vertical out to above	Vertical in from above	To SFR	To open repository	Net horizontal outflow	Vertical out to above	Vertical in from above	To SFR	To open repository
L3	20	0.01	15.94	21.16	0.07		0.00	10.40	58.71	0.05	0.04	0.00	11.15	45.03	0.06	0.06	0.00	12.38	32.27	0.06	0.03
L4	40	0.01	5.69	11.31	0.38		–0.01	2.92	54.41	0.30	3.12	0.00	3.21	38.40	0.34	0.64	0.00	3.66	24.19	0.36	0.08
L5	60	0.00	3.33	8.56	0.73		–0.02	1.50	49.58	0.62	0.95	–0.01	1.66	35.88	0.66	0.49	0.00	1.91	21.99	0.69	0.14
L6	80	0.00	2.49	6.99	3.26		–0.03	1.09	47.61	2.97	9.13	–0.02	1.11	34.19	3.06	2.03	–0.01	1.29	20.55	3.14	0.33
L7	100	0.00	2.72	3.96	0.33		–0.04	1.83	36.29	0.30	0.96	–0.03	1.47	29.47	0.31	0.92	–0.01	1.59	17.40	0.32	0.28
L8	120	0.00	1.87	2.79	0.55		–0.05	0.81	34.04	0.52	10.65	–0.03	0.79	27.58	0.53	4.94	–0.02	0.90	16.12	0.53	0.79
L9	140	0.00	1.62	1.99	0.39		–0.06	3.07	25.19	0.36	0.53	–0.04	1.84	23.20	0.37	0.44	–0.02	1.03	14.94	0.38	0.14
L10	160	0.00	1.44	1.43	0.00		–0.06	2.05	23.33	0.00	0.39	–0.04	1.32	21.91	0.00	0.47	–0.02	0.84	14.26	0.00	0.23
L11	180	–0.01	1.01	1.00	0.00		–0.07	1.20	22.16	0.00	0.44	–0.05	0.74	20.91	0.00	0.46	–0.02	0.49	13.69	0.00	0.25
L12	200	–0.01	0.66	0.65	0.00		–0.07	0.64	21.23	0.00	0.59	–0.05	0.38	20.14	0.00	0.61	–0.02	0.27	13.24	0.00	0.34
L13	300	0.00	0.36	0.36	0.00		–0.01	0.24	20.31	0.00	0.69	–0.01	0.15	19.34	0.00	0.67	0.00	0.12	12.77	0.00	0.34
L14	400	0.00	0.21	0.21	0.00		–0.01	0.30	19.69	0.00	0.81	–0.01	0.18	18.70	0.00	0.77	0.00	0.09	12.41	0.00	0.31
L15	500	0.00	0.11	0.10	0.00		0.00	0.17	18.76	0.00	18.90	0.00	0.13	17.89	0.00	18.05	0.00	0.09	12.11	0.00	12.22
L16	600	0.00	0.07	0.07	0.00		0.00	1.74	1.52	0.00	0.00	0.00	1.61	1.41	0.00	0.00	0.00	1.23	1.08	0.00	0.00
L17	700	0.00	0.05	0.05	0.00		0.00	1.02	0.82	0.00	0.00	0.00	0.96	0.78	0.00	0.00	0.00	0.75	0.61	0.00	0.00
L18	800	0.00	0.04	0.04	0.00		0.00	0.76	0.60	0.00	0.00	0.00	0.72	0.58	0.00	0.00	0.00	0.56	0.45	0.00	0.00
L19	900	0.00	0.03	0.03	0.00		–0.01	0.56	0.43	0.00	0.00	0.00	0.53	0.42	0.00	0.00	0.00	0.40	0.32	0.00	0.00
L20	1,000	0.00	0.02	0.02	0.00		–0.01	0.38	0.29	0.00	0.00	0.00	0.36	0.28	0.00	0.00	0.00	0.27	0.22	0.00	0.00
L21	1,100	0.00	0.02	0.01	0.00		–0.01	0.26	0.20	0.00	0.00	0.00	0.25	0.20	0.00	0.00	0.00	0.19	0.15	0.00	0.00
L22	1,200	0.00	0.01	0.01	0.00		–0.01	0.15	0.12	0.00	0.00	0.00	0.14	0.11	0.00	0.00	0.00	0.11	0.09	0.00	0.00
Sum		**–0.01**			**5.70**	**0.00**	**–0.47**			**5.13**	**47.21**	**–0.30**			**5.33**	**30.54**	**–0.15**			**5.48**	**15.48**

case $K_{grout} = 10^{-7}$ m/s the total horizontal inflow in the bedrock from the sea boundary increases with 0.5 L/s, from zero to an inflow of 0.5 L/s (the whole change occurs above 200 m.b.s.l.). Considering the bedrock only, the groundwater inflow to the repository (further discussed in Section 7.2) is 47.2 L/s for grouting case $K_{grout} = 10^{-7}$ m/s, 30.5 L/s for $K_{grout} = 10^{-8}$ m/s, and 15.5 L/s for $K_{grout} = 10^{-9}$ m/s.

Table 7-3 also includes the calculated groundwater inflow to SFR. As described previously (Section 4.2.1), SFR is described as pipe segments in MOUSE in the same manner as the open repository. This approach yields a calculated inflow to SFR of 5.7 L/s for undisturbed conditions (without the repository) and slightly less for disturbed conditions with the repository. SFR-related issues are further discussed in Section 7.6.

As will be shown in Section 7.5, the influence area of the groundwater-table drawdown only represents a small part of the MIKE SHE model area. Table 7-4 presents the calculated water balance specifically for the influence area (groundwater-table drawdown exceeding 0.3 m) for grouting case $K_{grout} = 10^{-7}$ m/s. As can be seen from this table, the inflow to the repository has a large impact on the water balance of the influence area (note that the same area is considered in all grouting cases). For grouting case $K_{grout} = 10^{-7}$ m/s the inflow to the repository is 186 mm or 35% of the precipitation. Also within the influence area there is only a small change of the evapotranspiration. On the other hand, the total runoff decreases with 93 mm, from 148 mm to 55 mm, whereas other changes mainly are associated with the subsurface-storage terms.

For grouting cases $K_{grout} = 10^{-8}$ and 10^{-9} m/s the total runoff from the influence area for $K_{grout} = 10^{-7}$ m/s is 13.5 mm and 49 mm, respectively, hence lower than the runoff for both undisturbed conditions and grouting case $K_{grout} = 10^{-8}$ m/s. An explanation to this is that in grouting case $K_{grout} = 10^{-7}$ m/s, the net subsurface outflow from the specified area increases compared to the net subsurface outflow from the same area for undisturbed conditions. This increase occurs in layer 4 and the layers below (cf. Table 7-5) and is due to the horizontal hydraulic gradient towards the access tunnel, which is located outside the influence area of the groundwater-table drawdown. The inflow to the access tunnel is higher for grouting case $K_{grout} = 10^{-7}$ m/s compared to the other two grouting cases (cf. Table 7-3, layers 6 and 8). This implies that the horizontal hydraulic gradient and thus also the increase of the net subsurface outflow from the specified area are larger for $K_{grout} = 10^{-7}$ m/s. For $K_{grout} = 10^{-7}$ m/s, the decrease of the drain outflow in the uppermost layer is larger than the increase in the subsurface outflow, which hence explains the decrease of the total runoff compared to the undisturbed case.

Table 7-5 presents water-balance components (L/s) for the influence area for each layer in the bedrock. The calculated changes of the vertical net groundwater inflow from the QD to the bedrock are 13, 10 and 6 L/s for grouting case $K_{grout} = 10^{-7}$ m/s, $K_{grout} = 10^{-8}$ m/s and $K_{grout} = 10^{-9}$ m/s, respectively. According to Table 7-3, the corresponding results for the whole model area are 43, 29 and 15 L/s. The total horizontal outflow in the bedrock (primarily in the sheet-joint layers 4–6 and 8) from the influence area to surrounding areas increases; the increase is 7 L/s for grouting case $K_{grout} = 10^{-7}$ m/s.

Table 7-4. Water balance (mm) for the influence area (groundwater-table drawdown > 0.3 m, grouting case $K_{grout} = 10^{-7}$ m/s). Results are shown for undisturbed and disturbed conditions. Note that the same influence-area definition is used in all four cases.

	Undisturbed conditions	$K_{grout} = 10^{-7}$ m/s	$K_{grout} = 10^{-8}$ m/s	$K_{grout} = 10^{-9}$ m/s
Precipitation	534.1	534.1	534.1	534.1
Evapotranspiration	433.9	424.6	431.2	432.3
Canopy storage change	0.1	0.1	0.1	0.1
Snow storage change	–29.8	–29.8	–29.8	–29.8
Overland storage change	–2.8	–1.2	–1.1	–0.3
Subsurface storage change	–14.6	–88.1	–44.3	–26.5
Net overland inflow	135.3	152.0	154.9	142.7
Net subsurface outflow	23.1	124.8	50.9	25.0
Drain outflow	238.8	72.8	104.7	149.1
Overland flow to river	15.0	7.7	9.0	12.1
Drainflow to river	5.9	2.3	4.2	5.1
Net baseflow to river	0.5	–1.0	–0.4	0.1
Inflow to the open repository	–	186.4	177.1	117.1

Table 7-5. Water-balance components (L/s) for the saturated zone in the influence area (groundwater-table drawdown > 0.3 m, grouting case $K_{grout} = 10^{-7}$ m/s) and for each bedrock calculation layer. Results are shown for undisturbed and disturbed conditions. Note that the same influence-area definition is used in all cases. The water-balance components are defined in Figure 7-1.

		Undisturbed conditions				$K_{grout} = 10^{-7}$ m/s				$K_{grout} = 10^{-8}$ m/s				$K_{grout} = 10^{-9}$ m/s			
Layer	Lower level (m.b.s.l)	Net horizontal outflow	Vertical out to above	Vertical in from above	To open repository	Net horizontal outflow	Vertical out to above	Vertical in from above	To open repository	Net horizontal outflow	Vertical out to above	Vertical in from above	To open repository	Net horizontal outflow	Vertical out to above	Vertical in from above	To open repository
L3	20	0.26	2.05	3.14		–1.79	0.06	13.84	0.00	–0.83	0.14	11.02	0.00	–0.15	0.47	7.40	0.00
L4	40	0.30	0.57	1.44		2.91	0.00	17.93	0.00	1.61	0.00	12.59	0.00	0.97	0.01	7.37	0.00
L5	60	0.11	0.31	0.89		1.90	0.00	15.02	0.00	1.31	0.00	10.98	0.00	0.76	0.00	6.39	0.00
L6	80	0.36	0.22	0.69		3.12	0.00	13.13	0.00	0.78	0.00	9.67	0.00	0.29	0.00	5.63	0.00
L7	100	–0.03	0.23	0.33		–0.11	0.07	10.07	0.00	–0.17	0.01	8.90	0.00	–0.13	0.01	5.35	0.00
L8	120	0.27	0.18	0.31		0.80	0.06	10.18	0.00	–0.02	0.01	9.06	0.00	–0.12	0.00	5.48	0.00
L9	140	–0.02	0.19	0.05		0.13	0.07	9.39	0.00	0.14	0.00	9.08	0.00	0.06	0.00	5.60	0.00
L10	160	–0.03	0.14	0.03		0.13	0.01	9.20	0.00	0.17	0.00	8.94	0.00	0.09	0.00	5.54	0.00
L11	180	–0.04	0.10	0.02		0.13	0.00	9.06	0.00	0.20	0.00	8.77	0.00	0.12	0.00	5.45	0.00
L12	200	–0.05	0.07	0.03		0.11	0.00	8.93	0.00	0.19	0.00	8.57	0.00	0.05	0.00	5.33	0.00
L13	300	0.01	0.04	0.05		0.32	0.00	8.82	0.00	0.35	0.00	8.38	0.00	0.19	0.00	5.27	0.00
L14	400	0.00	0.02	0.01		0.86	0.01	8.50	0.00	0.81	0.00	8.04	0.00	0.38	0.00	5.08	0.00
L15	500	0.00	0.01	0.00		0.04	0.00	7.63	7.82	0.04	0.00	7.23	7.43	–0.04	0.00	4.70	4.91
L16	600	0.00	0.01	0.00		0.03	0.48	0.27	0.00	0.00	0.48	0.26	0.00	–0.02	0.34	0.18	0.00
L17	700	0.00	0.00	0.00		–0.06	0.33	0.09	0.00	–0.06	0.31	0.09	0.00	–0.03	0.20	0.06	0.00
L18	800	0.00	0.00	0.00		–0.06	0.23	0.06	0.00	–0.06	0.21	0.05	0.00	–0.03	0.14	0.04	0.00
L19	900	0.00	0.00	0.00		–0.02	0.14	0.03	0.00	–0.02	0.13	0.03	0.00	–0.01	0.09	0.02	0.00
L20	1,000	0.00	0.00	0.00		–0.03	0.09	0.01	0.00	–0.03	0.08	0.01	0.00	–0.02	0.06	0.01	0.00
L21	1,100	0.00	0.00	0.00		–0.02	0.05	0.01	0.00	–0.02	0.05	0.01	0.00	–0.01	0.03	0.01	0.00
L22	1,200	0.00	0.00	0.00		–0.02	0.02	0.01	0.00	–0.01	0.02	0.01	0.00	–0.01	0.02	0.00	0.00
Sum		**1.13**			**0.00**	**8.37**			**7.82**	**4.38**			**7.43**	**2.32**			**4.91**

In the upper bedrock layer (layer 3), the inflow to the influence area increases 2 L/s. Note that the inflow to the repository in Table 7-5 only considers those parts of the repository that are located within the influence area (large parts of the repository are located outside the influence area).

Table 7-6 summarises the model-calculated changes of the vertical net inflow and the horizontal net inflow from the sea boundary (i.e. the differences between disturbed and undisturbed conditions). The results concerning vertical net inflows are divided into the influence area (groundwater-table drawdown exceeding 0.3 m for grouting case $K_{grout} = 10^{-7}$ m/s), the land area excluding the influence area, and the sea area. The changed vertical inflow from the land area corresponds to 50–60% of the inflow to the repository, with a higher relative contribution for lower values of K_{grout}. Approximately 50–60% of the change of the vertical inflow in the land part of the model area is associated to the influence area, whereas the contribution from the influence area to the inflow to the repository is 25–40%. The remaining contribution is mainly from the sea, of which the largest contribution is due to an increased vertical inflow in the sea part of the model area. The contribution due to horizontal inflow across the model boundary in the sea is small. Subsurface-storage changes in the bedrock correspond to 3–7% of the inflow to the repository.

7.2 Groundwater inflow to the repository

Table 7-7 presents the model-calculated groundwater inflow to the repository in each layer of MIKE SHE for three grouting cases. The inflow is larger for higher values of the hydraulic conductivity of the grouted zone. The magnitude of the calculated inflow also differs between different layers of the MIKE SHE model. For grouting case $K_{grout} = 10^{-7}$ m/s, the mean inflow for the simulation period (year 2006) is 40.2 L/s to tunnels and 7.2 L/s to shafts, whereas the lowest inflow (14.7 L/s to tunnels and 0.8 L/s to shafts) is obtained for $K_{grout} = 10^{-9}$ m/s. The mean inflow to the repository hence varies between 47.4 L/s ($K_{grout} = 10^{-7}$ m/s) and 15.5 L/s ($K_{grout} = 10^{-9}$ m/s). These results are similar to those obtained using the updated MIKE SHE-MOUSE coupling routine and the MIKE SHE model of /Gustafsson et al. 2009/; the difference is only 1–5%. The small differences are mainly attributed the model updates presented in Chapters 4 and 5, in particular those related to the hydrogeological model of the bedrock.

Most of the total inflow occurs at repository level (layer 15 at approximately 450 m.b.s.l.). There are also large inflows to tunnels and shafts in the sheet-joint layers 4, 6 and 8. In these layers, there are large inflow differences between different grouting cases, whereas the inflow in layer 15 is almost the same for grouting cases $K_{grout} = 10^{-7}$ and 10^{-8} m/s. The reason for this is the low hydraulic conductivity of the bedrock at repository level. On the other hand, in the sheet-joint layers the hydraulic conductivity of the grouted zone has a large influence on the inflow. The specific inflow (L/(s·km)) is substantially higher in the sheet-joint layers compared to repository level (Table 7-8).

Table 7-6. Changes of water-flow components (L/s) in the bedrock for disturbed conditions for three grouting cases. Note that the same influence-area definition is used in all cases (groundwater-table drawdown > 0.3 m for $K_{grout} = 10^{-7}$ m/s).

Flow-component change	$K_{grout} = 10^{-7}$ m/s		$K_{grout} = 10^{-8}$ m/s		$K_{grout} = 10^{-9}$ m/s	
	(L/s)	Relative contribution	(L/s)	Relative contribution	(L/s)	Relative contribution
Vertical net inflow to bedrock in the influence area	12.70	27%	9.80	32%	5.84	38%
Vertical net inflow to bedrock in the land area (excl. the influence area)	11.48	24%	7.27	24%	3.55	23%
Vertical net inflow to bedrock from the sea area	18.91	40%	11.59	38%	5.28	34%
Horizontal net inflow to bedrock from the sea boundary	0.46	1%	0.29	1%	0.13	1%
Storage change in bedrock	–3.10	7%	–1.22	4%	–0.46	3%
Reduced inflow to SFR	–0.57	1%	–0.37	1%	–0.22	1%
Inflow to the repository	47.21		30.54		15.48	

Table 7-7. Mean inflow (L/s) to tunnels and shafts.

Calculation layer	Lower level (m.b.s.l.)	Tunnels, K_{grout} = 10^{-7} m/s	Tunnels, K_{grout} = 10^{-8} m/s	Tunnels, K_{grout} = 10^{-9} m/s	Shafts, K_{grout} = 10^{-7} m/s	Shafts, K_{grout} = 10^{-8} m/s	Shafts, K_{grout} = 10^{-9} m/s
Layers 1–3	20	0.1	0.0	0.0	0.1	0.0	0.0
Layer 4	40	2.2	0.5	0.1	0.9	0.2	0.0
Layer 5	60	0.7	0.4	0.1	0.3	0.1	0.0
Layer 6	80	7.5	1.7	0.3	1.7	0.3	0.0
Layer 7	100	0.4	0.7	0.2	0.6	0.2	0.0
Layer 8	120	9.1	4.5	0.7	1.6	0.4	0.1
Layer 9	140	0.4	0.3	0.1	0.1	0.1	0.1
Layer 10	160	0.2	0.3	0.2	0.2	0.2	0.1
Layer 11	180	0.2	0.3	0.2	0.3	0.2	0.1
Layer 12	200	0.2	0.4	0.3	0.4	0.2	0.1
Layer 13	300	0.1	0.1	0.2	0.6	0.5	0.2
Layer 14	400	0.1	0.1	0.1	0.7	0.6	0.2
Layer 15	500	18.9	18.0	12.2	0.0	0.0	0.0
Layer 16	600	0.0	0.0	0.0	0.0	0.0	0.0
Layer 17	700	0.0	0.0	0.0	0.0	0.0	0.0
Layer 18	800	0.0	0.0	0.0	0.0	0.0	0.0
Layer 19	900	0.0	0.0	0.0	0.0	0.0	0.0
Layer 20	1,000	0.0	0.0	0.0	0.0	0.0	0.0
Layer 21	1,100	0.0	0.0	0.0	0.0	0.0	0.0
Layer 22	1,200	0.0	0.0	0.0	0.0	0.0	0.0
Sum		**40.2**	**27.3**	**14.7**	**7.2**	**3.2**	**0.8**

Table 7-8. Specific mean inflow (L/(s·km)).

Calculation layer	Lower level (m.b.s.l.)	Tunnel length (m)	K_{grout} = 10^{-7} m/s	K_{grout} = 10^{-8} m/s	K_{grout} = 10^{-9} m/s
Layers 1–3	20	239	0.46	0.13	0.09
Layer 4	40	209	10.66	2.21	0.29
Layer 5	60	166	4.19	2.29	0.68
Layer 6	80	374	19.98	4.54	0.77
Layer 7	100	209	1.96	3.26	1.11
Layer 8	120	218	41.64	20.87	3.35
Layer 9	140	214	1.82	1.38	0.40
Layer 10	160	205	1.12	1.44	0.89
Layer 11	180	236	0.80	1.24	0.80
Layer 12	200	535	0.43	0.69	0.52
Layer 13	300	1,491	0.08	0.09	0.12
Layer 14	400	798	0.15	0.16	0.18
Layer 15	500	78,908	0.24	0.23	0.15
Layer 16	600	213	0.01	0.01	0.01
Layer 17	700		0.00	0.00	0.00
Layer 18	800		0.00	0.00	0.00
Layer 19	900		0.00	0.00	0.00
Layer 20	1,000		0.00	0.00	0.00
Layer 21	1,100		0.00	0.00	0.00
Layer 22	1,200		0.00	0.00	0.00
Sum		**≈ 84,000**			
Total			**0.48**	**0.33**	**0.17**

Figure 7-2 shows the groundwater inflow at repository level (450 m.b.s.l.). The highest inflow is observed along the highly conductive fractures zones (yellow areas in Figure 7-2). These results show what could be denoted "cage effect", i.e. large inflows along the boundaries of the repository (the outer transport tunnels), in particular along the boundary towards the sea. Note that the inflow to the central area at repository level is very small when the transport tunnels are open.

The construction and operation of the repository are here divided into an initial construction phase (phase 0) and three subsequent development phases (phases 1–3), and a hypothetical case with a fully open repository excluding the main and deposition tunnels; the objective of the latter case is to investigate the importance of the main and deposition tunnels for the total inflow. Table 7-9 shows the inflow to the repository for grouting case $K_{grout} = 10^{-8}$ m/s. For the construction phase, results are also shown for $K_{grout} = 10^{-7}$ m/s. According to the table, the inflow is smaller during all individual phases compared to the case with a fully open repository. During phase 0 ($K_{grout} = 10^{-8}$ m/s) the inflow is 37% of the inflow to the fully open repository. The corresponding results are 68% for the fully open repository excluding main and deposition tunnels, and 89% for phase 3. The differences mainly pertain to the repository level. Only the four central shafts are open during phase 0, which explains the small inflow to the shafts compared to the other two phases.

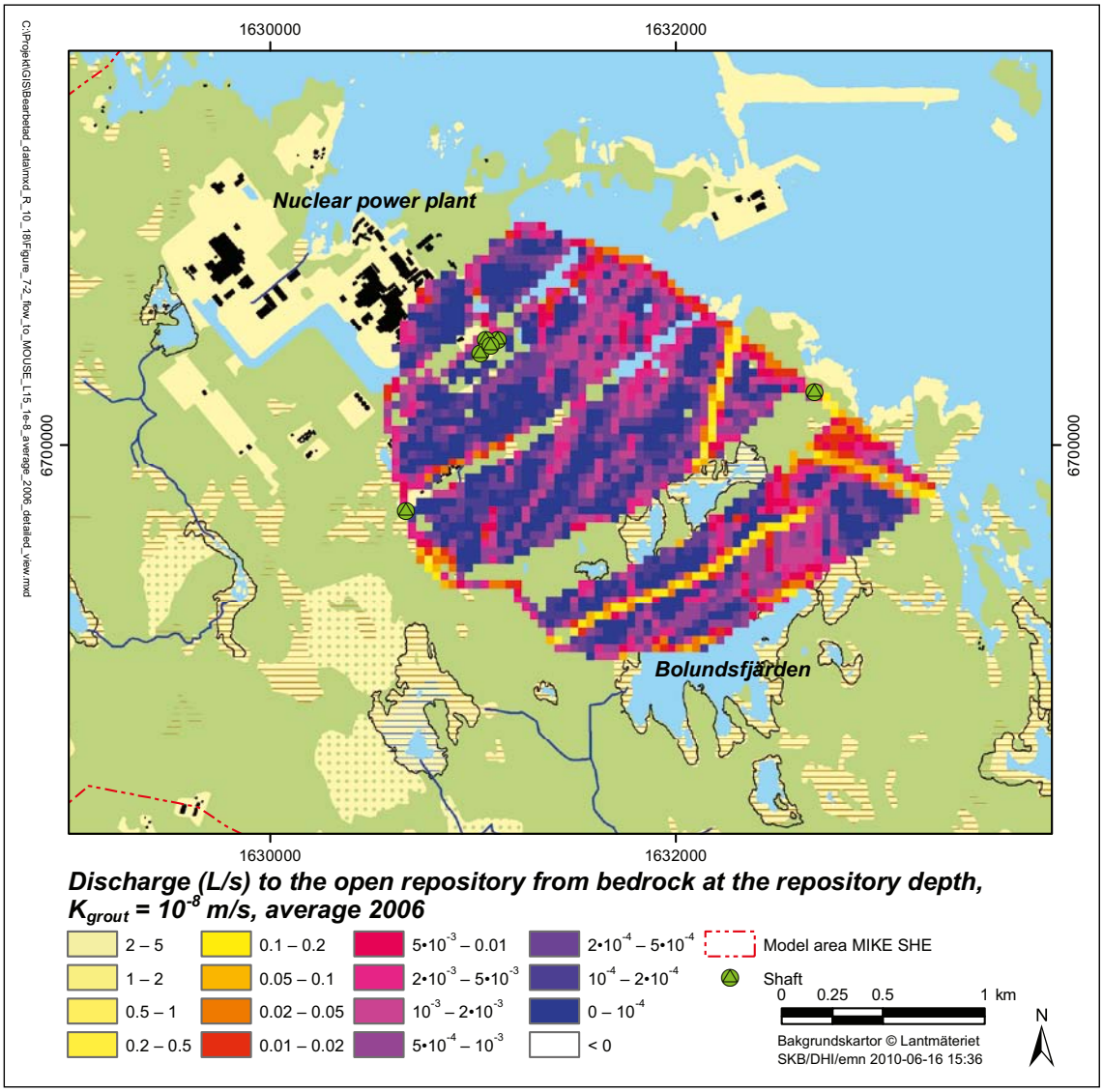

Figure 7-2. *Calculated discharge (L/s) to the repository from each MIKE SHE grid cell at repository level ($K_{grout} = 10^{-8}$ m/s). The results represent the date Aug. 15, 2006.*

Table 7-9. Groundwater inflow to the repository (L/s) for each calculation layer. Results are shown for the construction phase (phase 0), for a fully open repository excluding main and deposition tunnels, and for development phase 3, $K_{grout} = 10^{-8}$ m/s (and also $K_{grout} = 10^{-7}$ m/s for the construction phase).

Calculation layer	Lower level (m.b.s.l.)	Tunnels, phase 0, $K_{grout} = 10^{-7}$ m/s	Tunnels, phase 0, $K_{grout} = 10^{-8}$ m/s	Tunnels, fully open excl. main and dep. tunnels, $K_{grout} = 10^{-8}$ m/s	Tunnels, phase 3, $K_{grout} = 10^{-8}$ m/s	Shafts, phase 0, $K_{grout} = 10^{-7}$ m/s	Shafts, phase 0, $K_{grout} = 10^{-8}$ m/s	Shafts, fully open excl. main and dep. tunnels, $K_{grout} = 10^{-8}$ m/s	Shafts, phase 3, $K_{grout} = 10^{-8}$ m/s
Layers 1–3	20	0.1	0.0	0.0	0.0	0.0	0.0	0.0	0.0
Layer 4	40	2.5	0.5	0.5	0.5	0.9	0.2	0.2	0.2
Layer 5	60	0.8	0.4	0.4	0.4	0.0	0.0	0.1	0.1
Layer 6	80	8.4	1.8	1.8	1.7	1.1	0.2	0.3	0.3
Layer 7	100	0.5	0.7	0.7	0.7	0.6	0.2	0.3	0.2
Layer 8	120	9.7	4.8	4.7	4.6	0.7	0.3	0.4	0.4
Layer 9	140	0.4	0.3	0.3	0.3	0.0	0.0	0.2	0.1
Layer 10	160	0.3	0.3	0.3	0.3	0.0	0.1	0.2	0.2
Layer 11	180	0.2	0.3	0.3	0.3	0.2	0.1	0.2	0.2
Layer 12	200	0.3	0.4	0.4	0.4	0.3	0.1	0.3	0.3
Layer 13	300	0.2	0.2	0.2	0.2	0.0	0.0	0.6	0.5
Layer 14	400	0.2	0.2	0.2	0.2	0.0	0.0	0.7	0.7
Layer 15	500	0.0	0.0	9.0	14.9	0.0	0.0	0.0	0.0
Layer 16	600	0.0	0.0	0.0	0.0	0.0	0.0	0.0	0.0
Layer 17	700	0.0	0.0	0.0	0.0	0.0	0.0	0.0	0.0
Layer 18	800	0.0	0.0	0.0	0.0	0.0	0.0	0.0	0.0
Layer 19	900	0.0	0.0	0.0	0.0	0.0	0.0	0.0	0.0
Layer 20	1,000	0.0	0.0	0.0	0.0	0.0	0.0	0.0	0.0
Layer 21	1,100	0.0	0.0	0.0	0.0	0.0	0.0	0.0	0.0
Layer 22	1,200	0.0	0.0	0.0	0.0	0.0	0.0	0.0	0.0
Sum		**23.6**	**10.2**	**18.7**	**24.5**	**3.9**	**1.3**	**3.4**	**3.3**

7.3 Particle-tracking simulations

Particle-tracking simulations imply that a set of imaginary particles are released and then advected (transported with the groundwater flow) in the model-calculated groundwater flow field. Such simulations were run using flow fields generated for a fully open repository and for the construction phase, in both cases for grouting case $K_{grout} = 10^{-8}$ m/s. In each case, one particle was initially introduced in each saturated-zone grid cell and the model was run for a simulation period of 100 years, approximately corresponding to the lifetime of the repository. Specifically, the model-calculated transient flow field for year 2006 was cycled 100 times. A detailed description of the particle-tracking methodology is presented in /Gustafsson et al. 2008/.

A number of particle-registration zones were defined, including the repository (with the shafts), SFR, and the drainage system at the nuclear power plant. Each MIKE SHE grid cell from which there is an inflow to the repository (represented in MOUSE) was included in the repository registration zone, and the SFR registration zone was defined in the same manner. So called sinks, at which the particle tracking in MIKE SHE is terminated, include the unsaturated zone/overland compartment (in MIKE SHE, it is not possible to separate these two sinks), streams, drain to streams, the sea, and drain to boundary.

Table 7-10 presents the final distribution of particles on different registration zones/sinks after a simulation period of 100 years. Appendix 3 presents detailed results for each MIKE SHE calculation layer. In the case with a fully open repository, the results show that 35% of the released particles have reached the repository at the end of the simulation. The remaining 65% of the released particles are left in the model (51%), or have reached the unsaturated zone/overland compartment (8%) or SFR (4%). Of the particles that have reached the repository after a simulation period of 100 years, approximately 3% have their starting positions in the Quaternary deposits (layers 1 and 2) and hence 97% start in the bedrock. Particles released in all layers reach the repository.

The particle-tracking results for the construction phase (only the access tunnel and the tunnels, rock caverns and shafts in the central area are open) show that approximately 21% of the released particles have reached the repository after 100 years. Compared to the hypothetical case with a fully open repository, twice the number of particles reach SFR. At the end of the construction-phase simulations, 58% of the particles remain in the saturated zone.

Figures 7-3 and 7-4 show the starting points for the particles that reach the fully open repository in the four calculation layers 2, 5 (50 m.b.s.l.), 10 (150 m.b.s.l.) and 15 (450 m.b.s.l.). Corresponding results for the construction phase are shown in Figures 7-5 and 7-6. It can be noted that in both simulation cases, no particles with starting points in layers 2, 5 or 10 close to SFR or the sea area northeast of SFR reach the repository. The vast majority of particles with starting points in these layers/areas reach SFR. Hence, according to these results there is no solute transport by groundwater from SFR to the repository during construction and operation of the repository.

Table 7-10. Distribution of particles on registration zone/sinks with a simulation period of 100 years. Results are presented for a fully open repository and the construction phase, $K_{grout} = 10^{-8}$ m/s. NPP = Forsmark nuclear power plant.

Registration zone/sink	Fully open repository Number of particles	%	Construction phase Number of particles	%
Unsaturated zone/overland	58,788	7.9	73,739	9.9
Streams	2,921	0.4	4,046	0.5
Drain to river	3,084	0.4	4,217	0.6
Sea	1,795	0.2	2,688	0.4
Drain to boundary	1,425	0.2	2,498	0.3
Drainage system at NPP	140	0.0	147	0.0
SFR	32,837	4.4	65,091	8.7
Repository	260,025	35	157,354	21
Left in the model	383,192	51	434,457	58
Sum	**744,207**	**100**	**744,237**	**100**

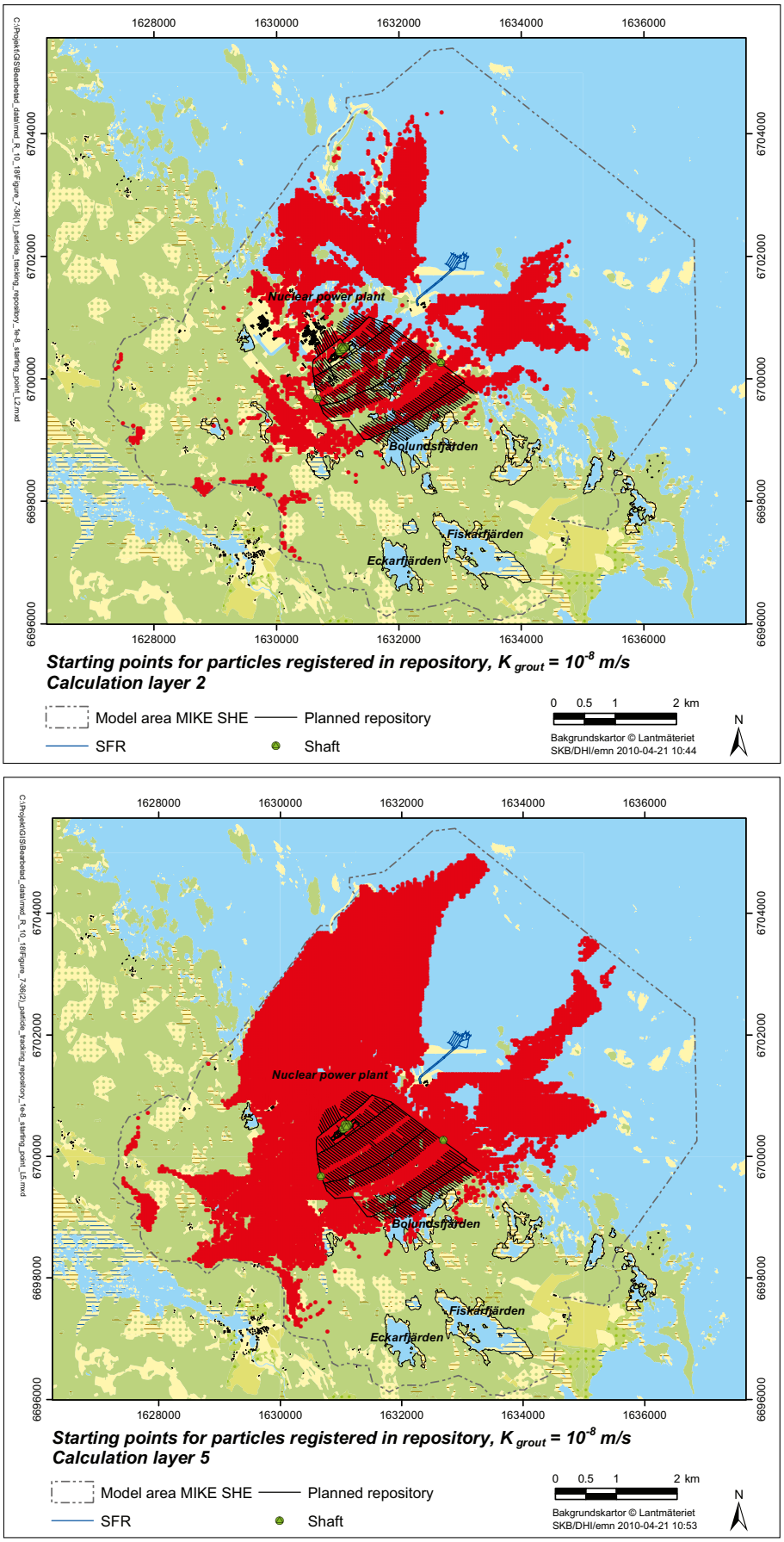

Figure 7-3. *Starting points in layer 2 (upper map) and layer 5 (lower map) for particles that reach the repository, $K_{grout} = 10^{-8}$ m/s.*

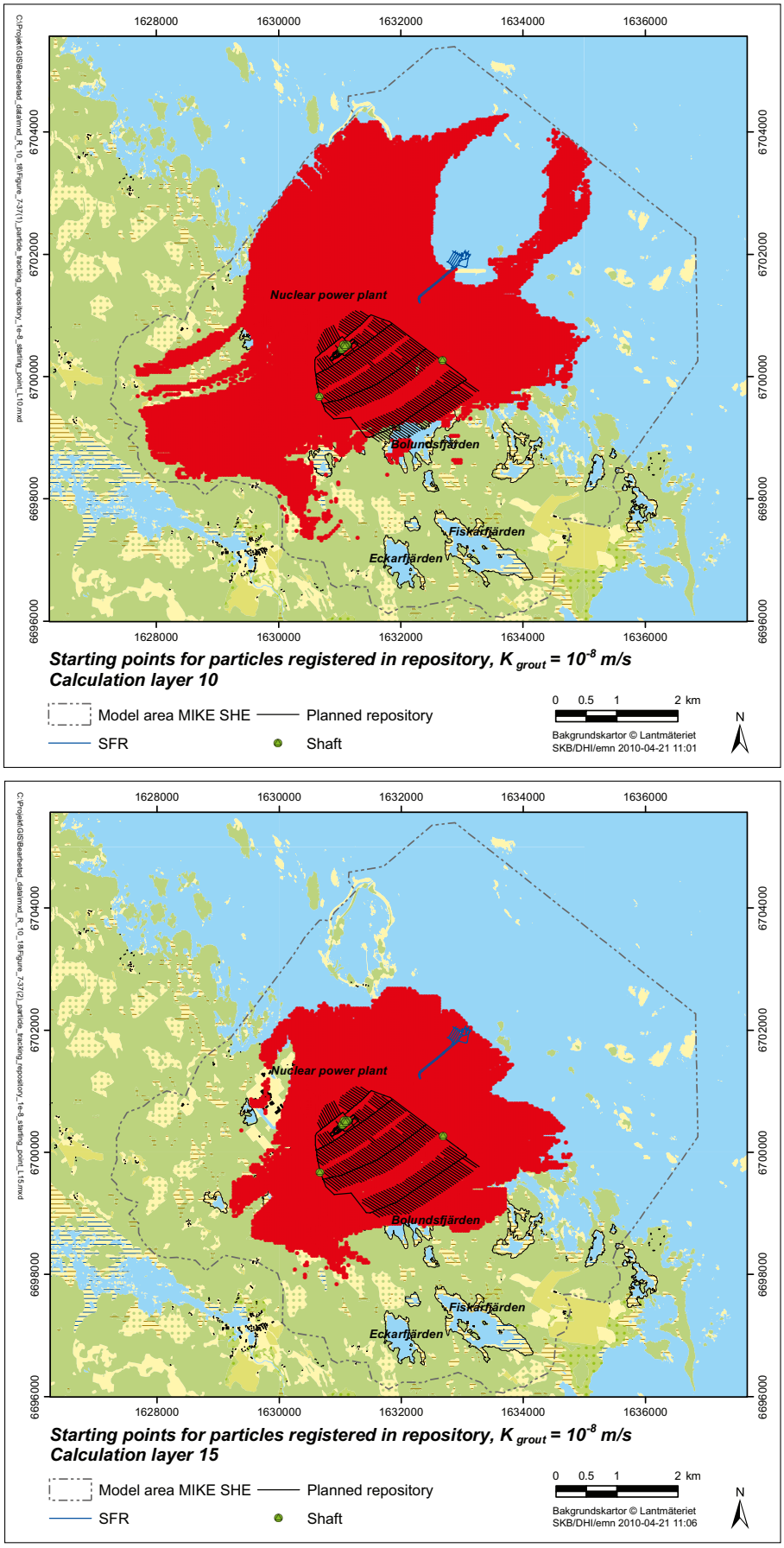

Figure 7-4. *Starting points in layer 10 (upper map) and layer 15 (lower map) for particles that reach the repository, $K_{grout} = 10^{-8}$ m/s.*

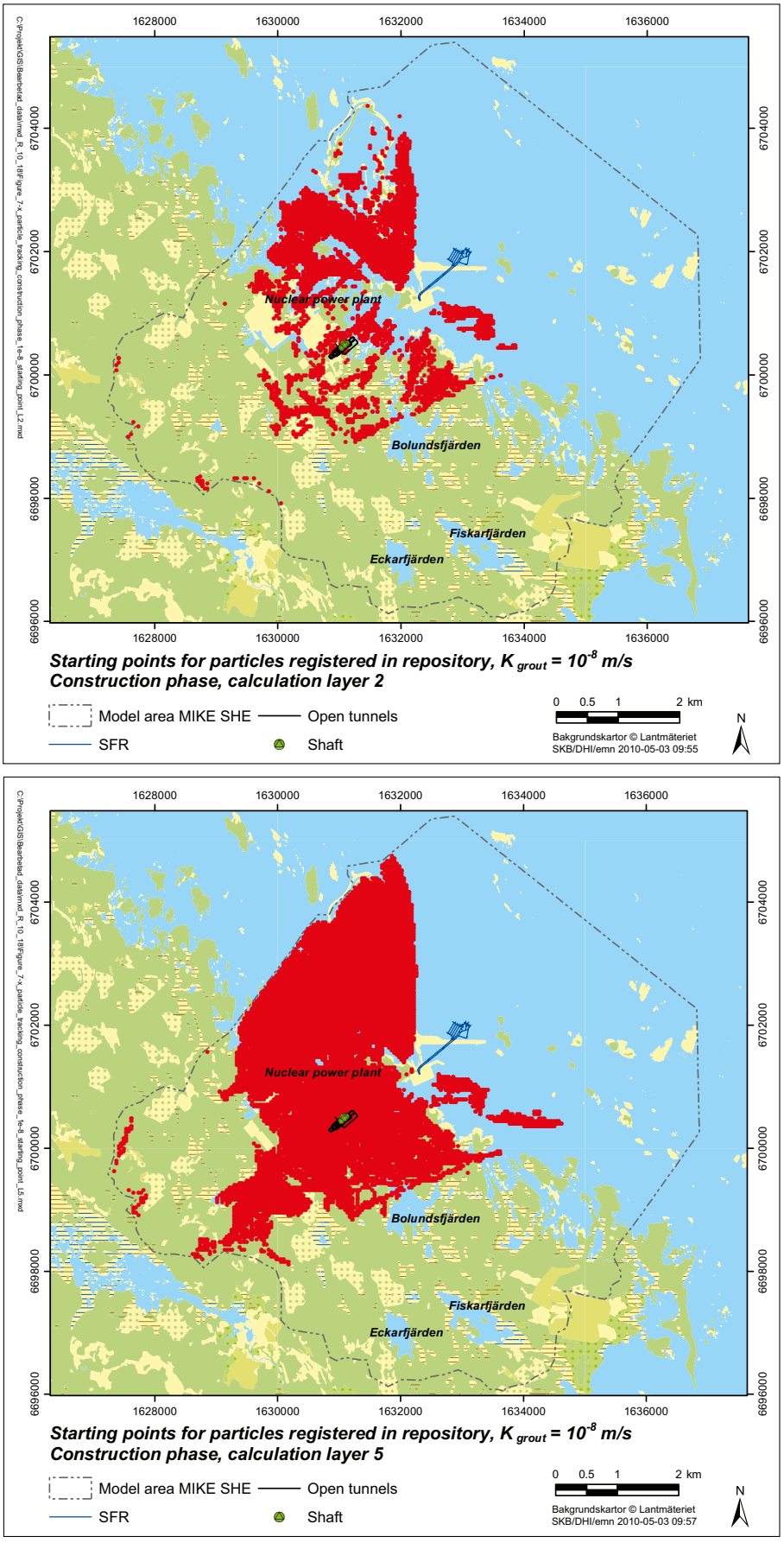

Figure 7-5. *Starting points in layer 2 (upper map) and layer 5 (lower map) for particles that reach the repository for the construction phase, $K_{grout} = 10^{-8}$ m/s.*

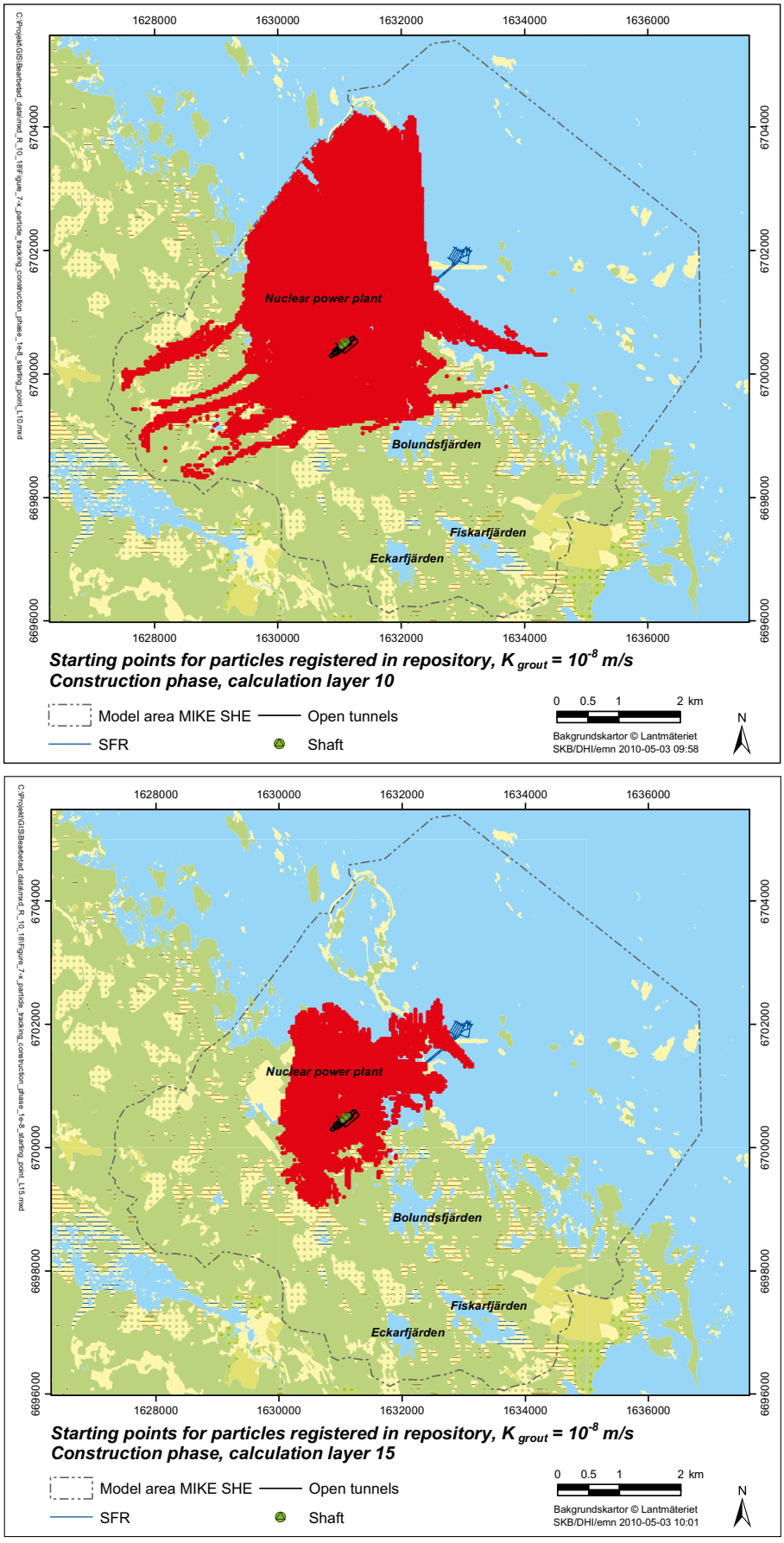

Figure 7-6. *Starting points in layer 10 (upper map) and layer 15 (lower map) for particles that reach the repository for the construction phase, $K_{grout} = 10^{-8}$ m/s.*

As shown in the lower map in Figure 7-4, no particles with starting points in the southern part of the model area (where Lake Eckarfjärden and Lake Fiskarfjärden are located) reach the repository. A majority of the particles that reach the repository above layer 15 have their starting points in areas west, east and north of the repository.

During rock grouting, it is possible that grouting material is spread also outside the intended grouted zone around the tunnel periphery. At least in theory, water-soluble substances in the grouting material could spread in the bedrock and end up in streams and wetlands at the ground surface. Figure 7-7 shows an enlarged view of the starting points in layer 5 (upper map) and layer 10 (lower map) of particles that reach the repository for the construction phase. According to this figure, particles that are released adjacent to the central area reach the repository within a time period of 100 years. The closest starting points of particles that do not reach the repository are located some 400–500 m from the central area. However, these particles still remain in the model volume (in the saturated zone) at the end of the 100-year simulation period. This implies that the probability for unintended spreading of water-soluble substances in the grouting material to the ground surface is considered to be small.

Figure 7-8 shows an enlarged view of particles with starting points in layer 1 (upper map) and layer 2 (lower map) that in the simulation case with a fully open repository are removed from the model domain by the drainage system at the level 20 m.b.s.l. below the nuclear power plant (model-calculated drainage flow 1.3 L/s). There are particles with starting points in layers 1 and 2 (representing the Quaternary deposits) within the industrial area that are not removed by the drainage system. The vast majority of these particles in layer 1 reach the unsaturated zone, whereas some particles that are released in this area in layer 2 reach the repository.

7.4 Surface-water levels and -discharges

According to the MIKE SHE calculations, the groundwater inflow to the repository only has small effects on the water levels of the lakes in the area (for their locations, see Figure 6-2 in Section 6-2). For Lake Eckarfjärden, Lake Fiskarfjärden and Lake Lillfjärden the effect on the water level is negligible. For all studied grouting cases, the average water-level difference between undisturbed and disturbed conditions for these lakes is less than 0.001 m. The largest difference is less than 0.005 m in Lake Eckarjärden and Lake Fiskarfjärden, and less than 0.025 m in Lake Lillfjärden.

For Lake Bolundsfjärden and Lake Gällsboträsket, which are located closer to the repository in the downstream part of the model area, there are some differences between the different grouting cases (see Figures 7-9 to 7-12), with the largest drawdown of the water level for $K_{grout} = 10^{-7}$ m/s. The average drawdown in Lake Gällsboträsket varies between 0.01 and 0.03 m depending on K_{grout}, with a maximum drawdown between 0.05 and 0.12 m (Figure 7-10). For Lake Bolundsfjärden, the average drawdown and the largest drawdown is in the range 0.007–0.02 m and 0.02–0.07 m, respectively (Figure 7-12). The largest drawdown occurs during a period with a high water level in the end of April. Compared to the amplitude of the natural water-level fluctuations, the water-level drawdown due to the inflow to the repository is relatively small. An example is the spring flood in April. During this period, the water level of Lake Gällsboträsket rises c. 0.5 m, which can be compared to a largest drawdown of 0.12 m due to the inflow ($K_{grout} = 10^{-7}$ m/s).

The larger water-level drawdown in Lake Bolundsfjärden and Lake Gällsboträsket compared to the other lakes is due to the groundwater-table drawdown around and the hydraulic-head change below these lakes (see Figure 7-18 in Section 7.5.2). The drawdown of the groundwater table in the catchment areas of these lakes reduces the inflow to the lakes from surrounding areas, which in turn lowers the lake water levels.

The two small lakes Norra Bassängen and Puttan are situated north of Lake Bolundsfjärden. The groundwater-table drawdown is significant in this area, in particular in the vicinity of Lake Puttan (see Figure 7-28 in Section 7.5.3). The water-level drawdown of Lake Norra Bassängen is on the same order as that of Lake Bolundsfjärden, with a maximum drawdown between 0.02 and 0.07 m depending on the hydraulic conductivity of the grouted zone. In Lake Puttan, the annual average water-level drawdown is between 0.06 and 0.39 m (Figures 7-13 and 7-14). For the grouting case $K_{grout} = 10^{-7}$ m/s, the maximum drawdown is 0.84 m. Overall, these results are similar to those presented by /Gustafsson et al. 2009/. However, the maximum water-level drawdown of Lake Bolundsfjärden and Lake Gällsboträsket are larger compared to /Gustafsson et al. 2009/.

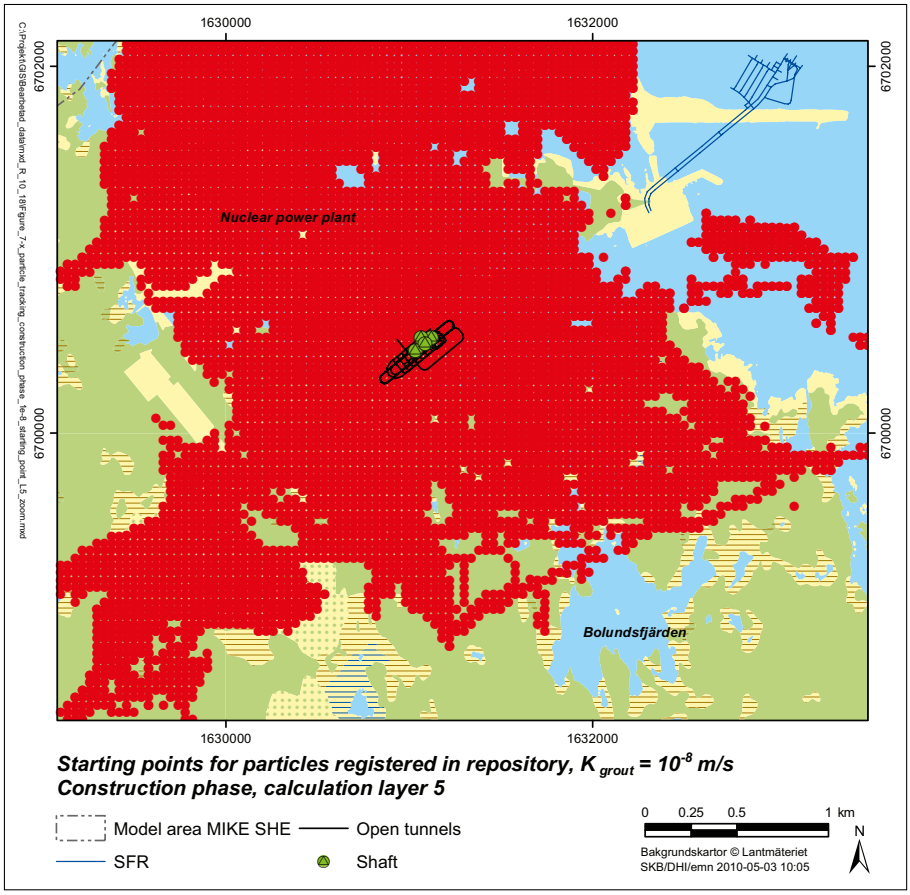

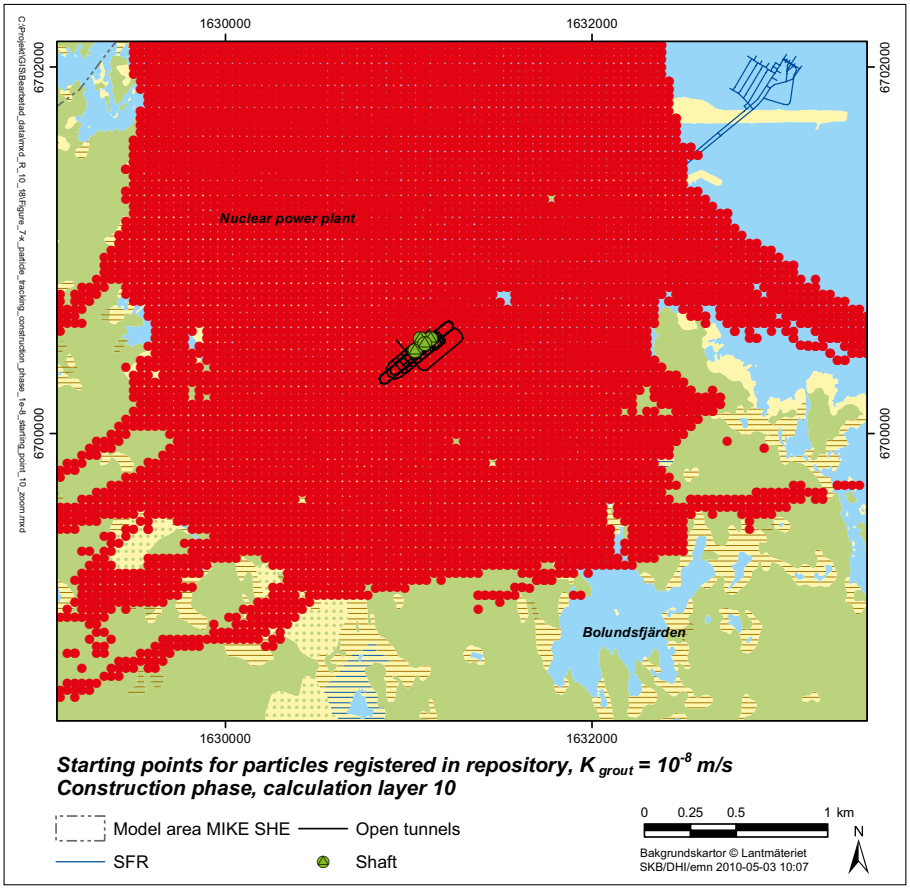

Figure 7-7. *Detailed view of starting points in layer 5 (upper map) and layer 10 (lower map) for particles that reach the repository for the construction phase, $K_{grout} = 10^{-8}$ m/s.*

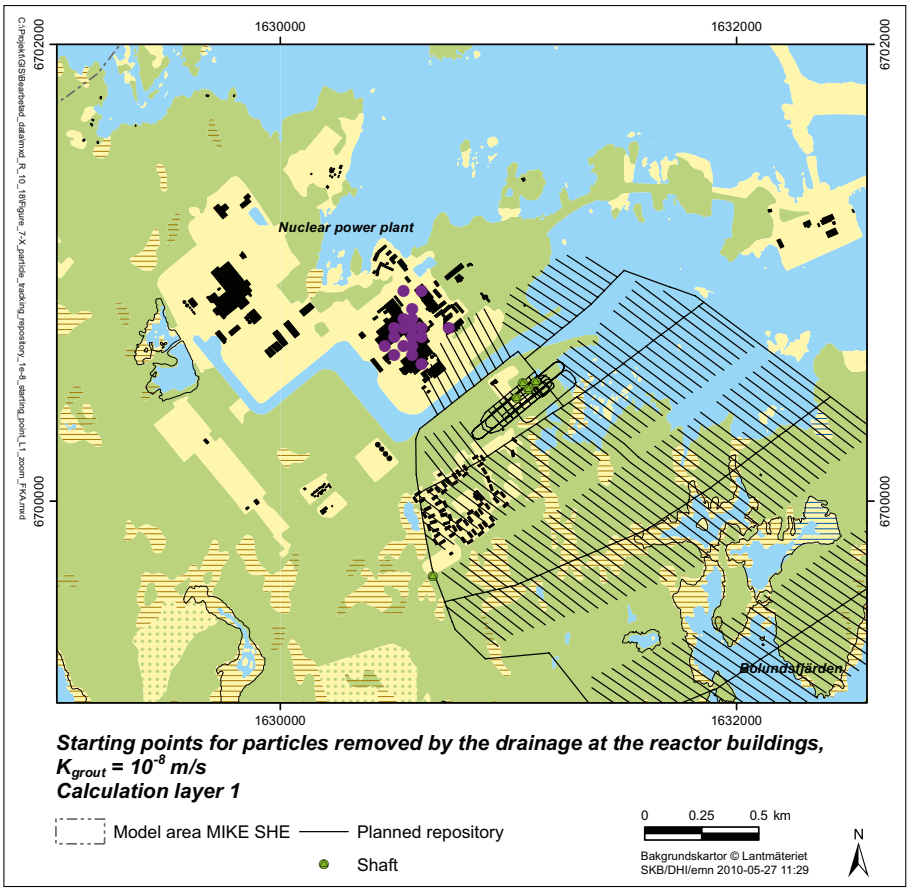

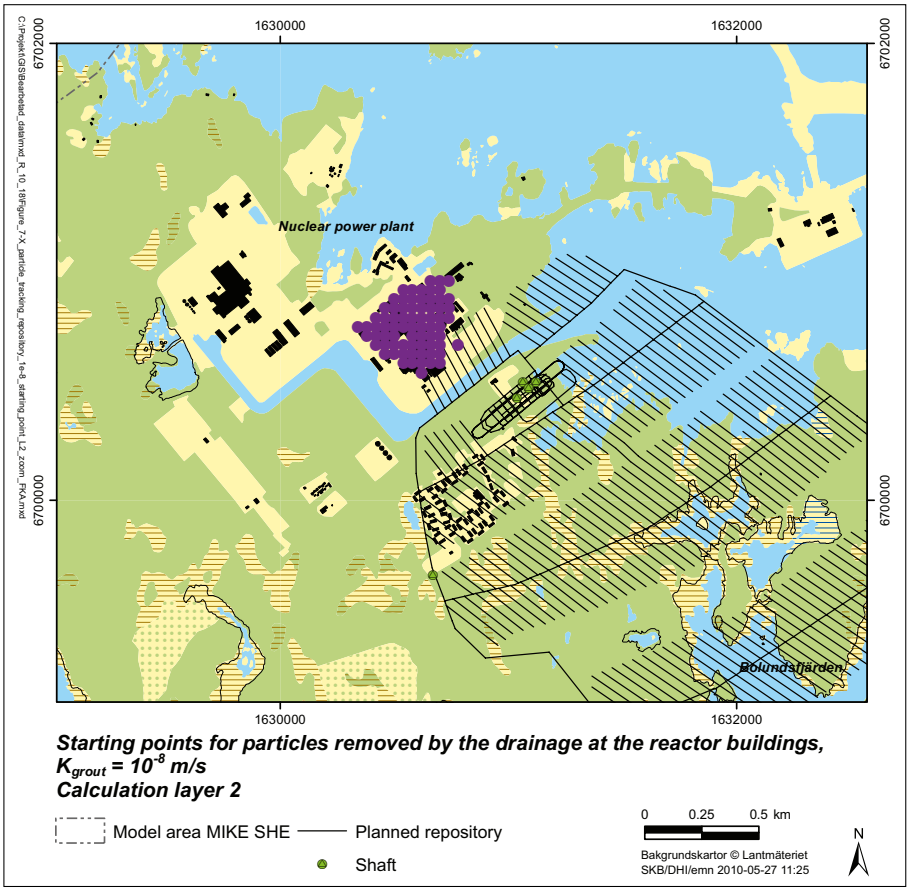

Figure 7-8. *Detailed view of starting points in Quaternary deposit layers 1 (upper map) and 2 (lower map) for particles that are removed by the drainage system at the nuclear power plant, $K_{grout} = 10^{-8}$ m/s.*

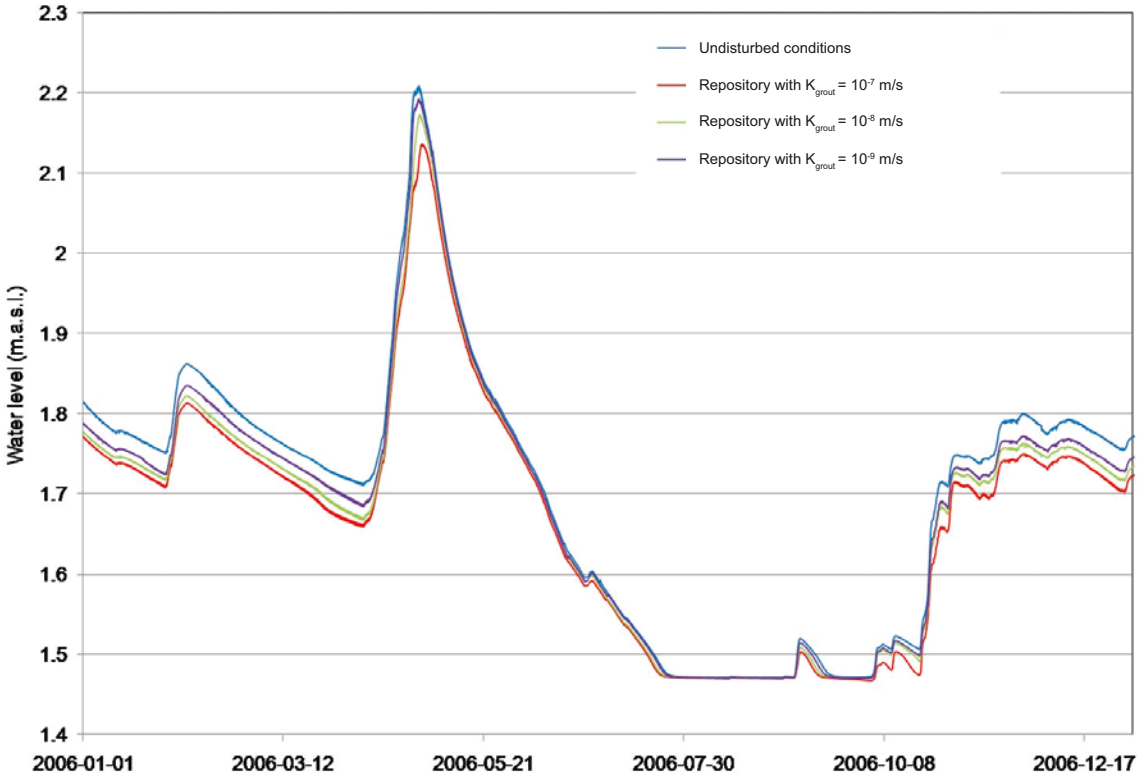

Figure 7-9. *Water level of Lake Gällsboträsket for different values of K_{grout}.*

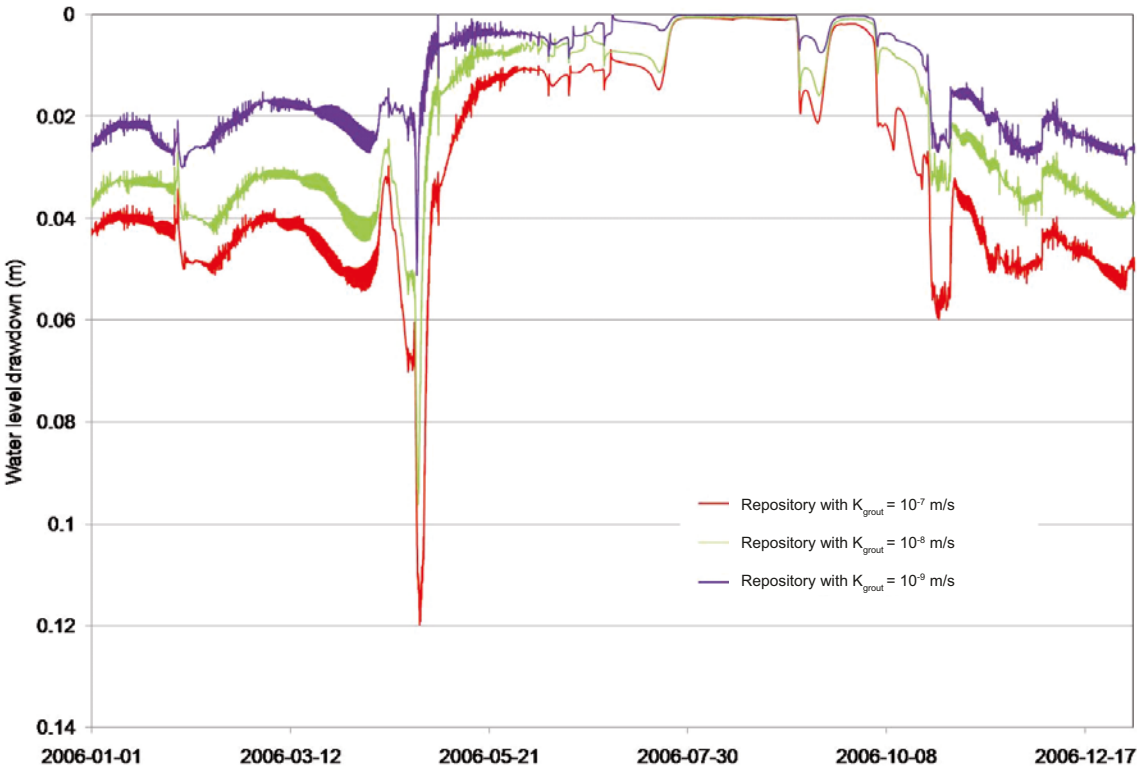

Figure 7-10. *Water-level drawdown of Lake Gällsboträsket for different values of K_{grout}.*

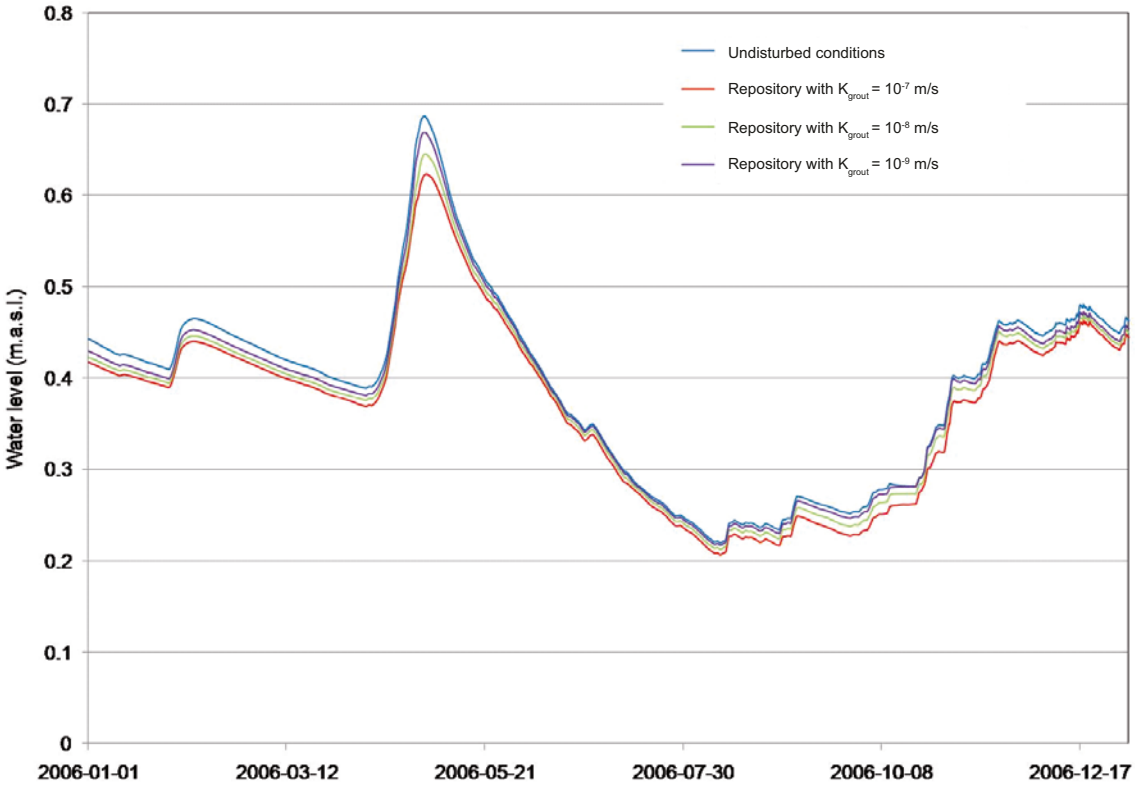

Figure 7-11. *Water level of Lake Bolundsfjärden for different values of K_{grout}.*

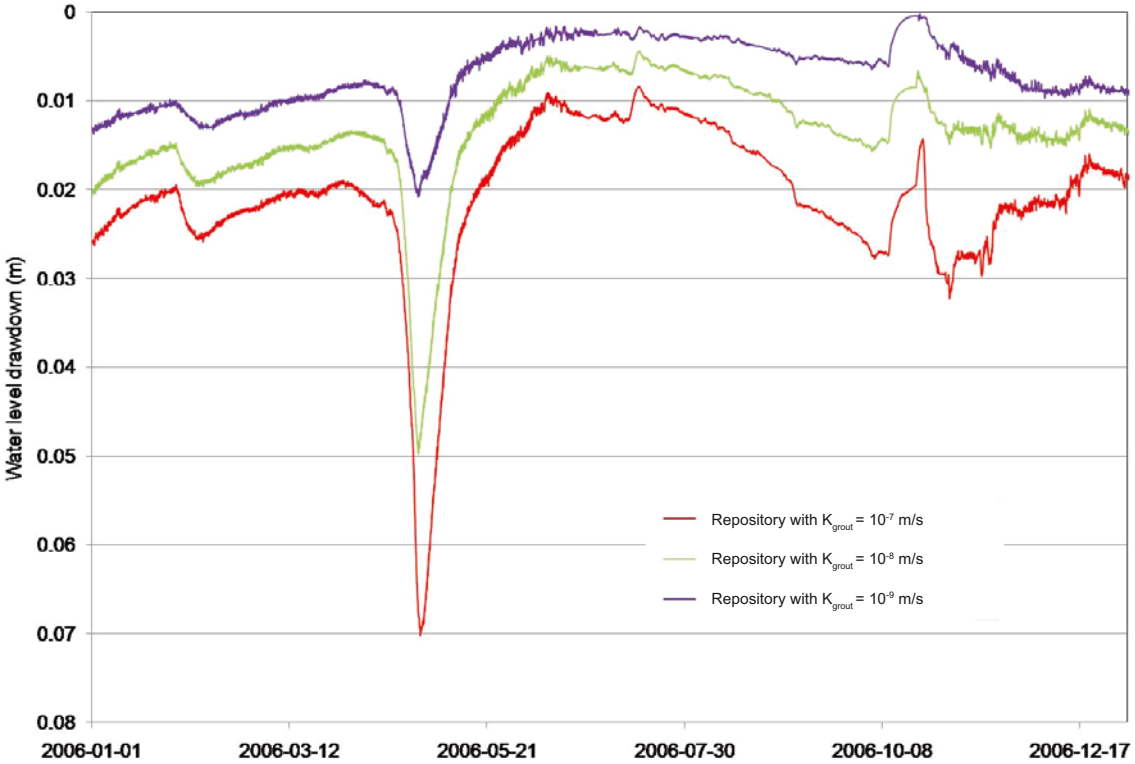

Figure 7-12. *Water-level drawdown of Lake Bolundsfjärden for different values of K_{grout}.*

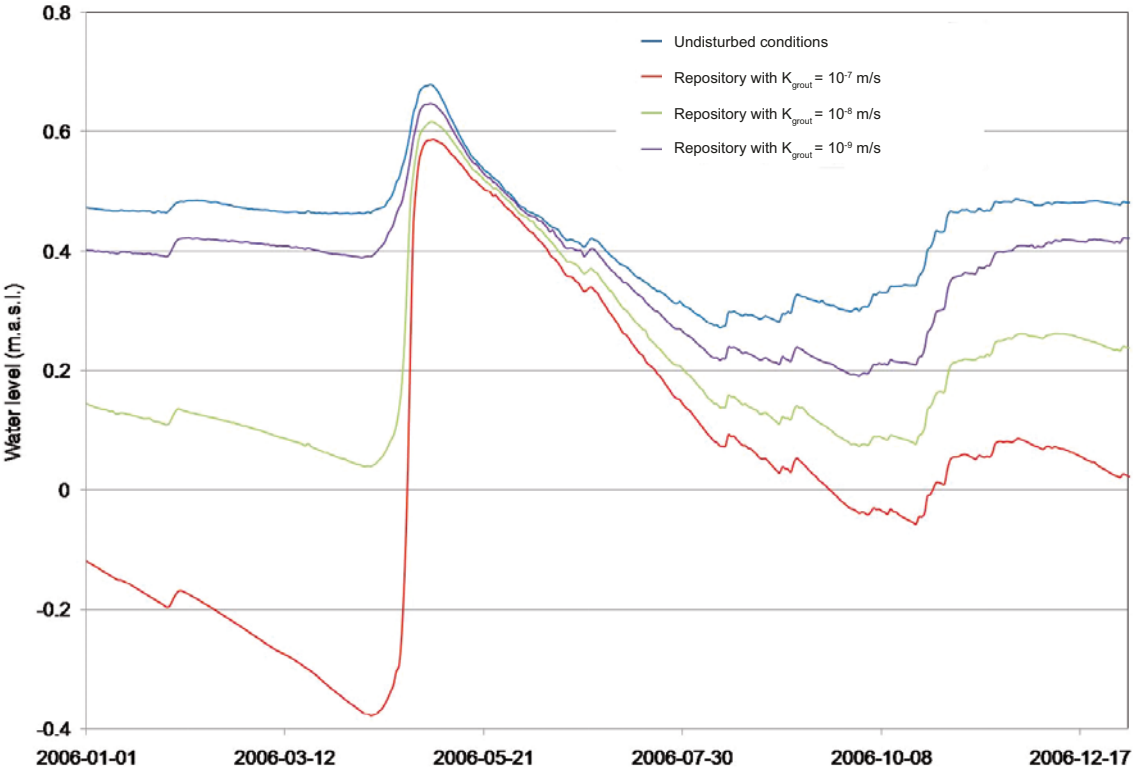

Figure 7-13. *Water level of Lake Puttan for different values of K_{grout}.*

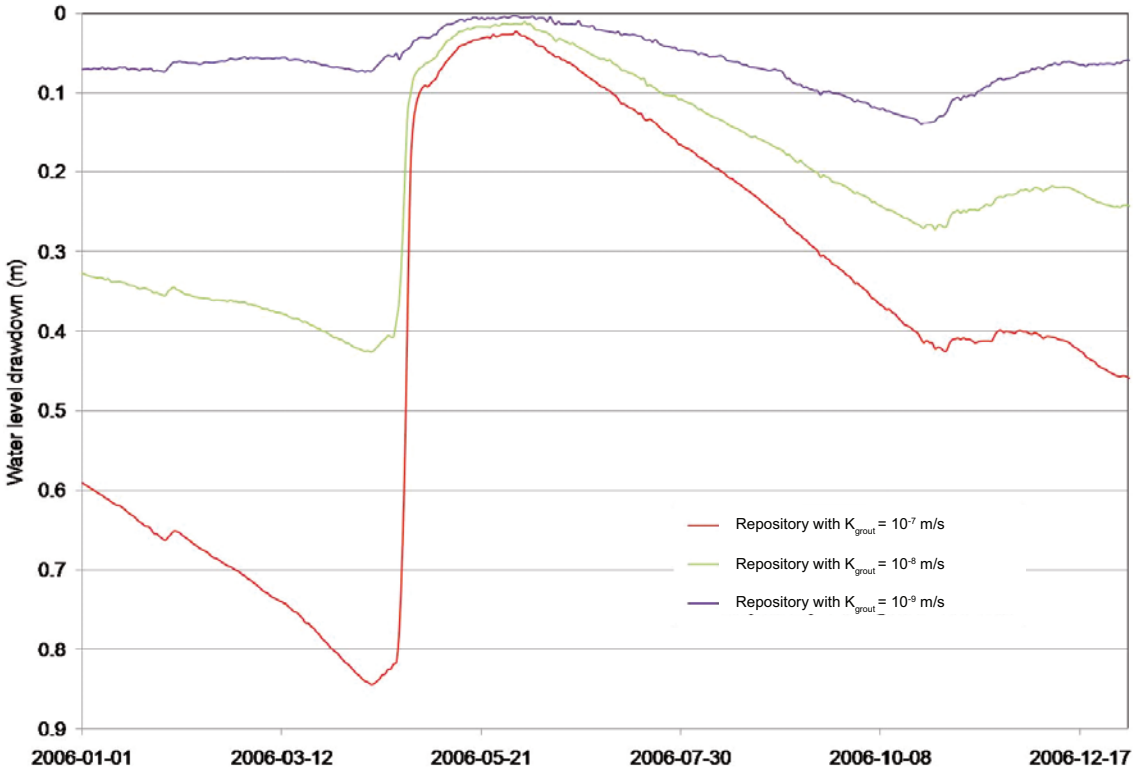

Figure 7-14. *Water-level drawdown of Lake Puttan for different values of K_{grout}.*

The inflow to the repository has small effects on the discharges in the streams. Table 7-11 compares model-calculated annually accumulated discharges at the locations of the four discharge-gauging stations (Figure 6-2 in Section 6-2), for undisturbed conditions and for disturbed conditions using different values of K_{grout}. As can be seen in this table, the difference between undisturbed and disturbed conditions is negligible. The exception is the station upstream from Lake Bolundsfjärden, which is located in the downstream part of the model area close to the repository. Figure 7-15 shows model calculated accumulated discharges at this location. Grouting case $K_{grout} = 10^{-7}$ m/s yields a 13% decrease of the accumulated discharge. The reduction is due to the groundwater-table drawdown in areas upstream from this location, whereas there is no or very little drawdown in areas upstream from the other studied locations. The present results are similar to those of /Gustafsson et al. 2009/, except a larger reduction of the stream discharge upstream from Lake Bolundsfjärden compared to the previous results.

Table 7-11. Relative decrease (%) of annually accumulated stream discharges.

	$K_{grout} = 10^{-7}$ m/s	$K_{grout} = 10^{-8}$ m/s	$K_{grout} = 10^{-9}$ m/s
Downstream Lake Eckarfjärden	1%	< 1%	< 1%
Downstream Lake Stocksjön	1%	< 1%	< 1%
Downstream Lake Gunnarsboträsket	< 1%	< 1%	< 1%
Upstream Lake Bolundsfjärden	13%	9%	5%

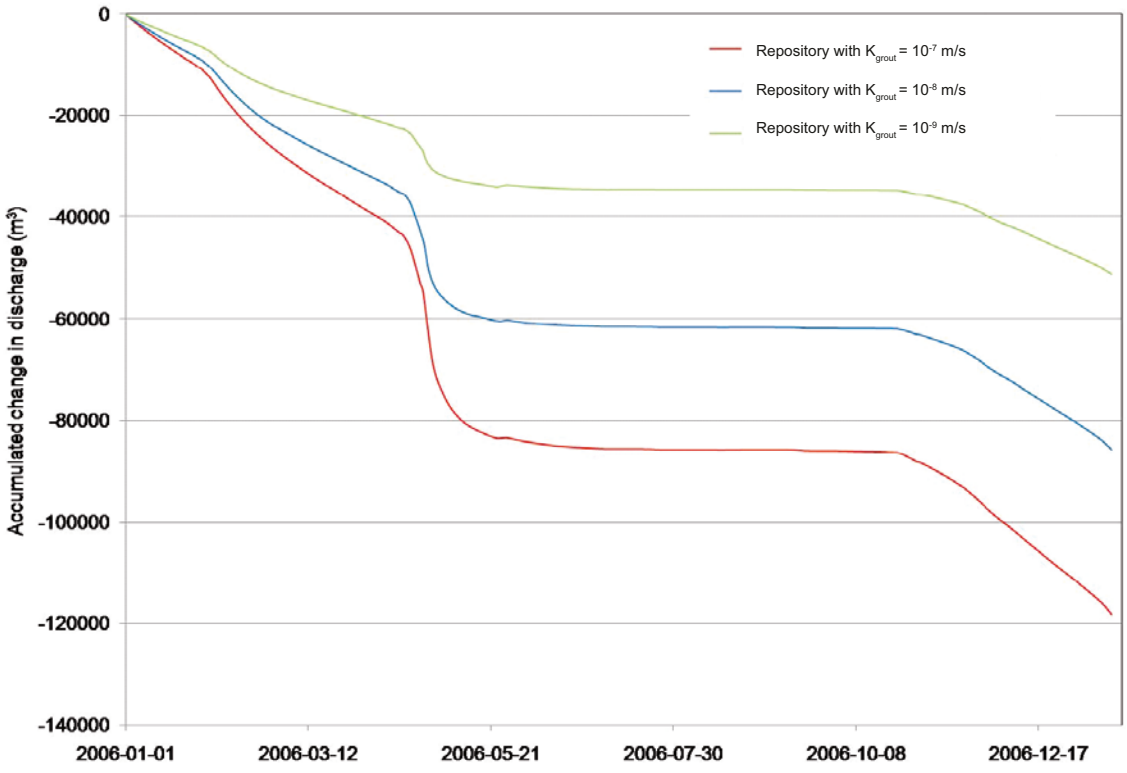

Figure 7-15. *Accumulated reduction of the discharge in the stream upstream from Lake Bolundsfjärden for different values of K_{grout}.*

7.5 Drawdown of groundwater table and hydraulic heads

7.5.1 Drawdown of the groundwater table

The influence area for the groundwater-table drawdown is here defined as the area in which the drawdown due to the groundwater inflow to the repository exceeds 0.3 m. Figure 7-16 shows the model-calculated groundwater-table drawdown for grouting case $K_{grout} = 10^{-8}$ m/s (an enlarged view is shown in Figure 7-17). The influence area mainly comprises band-shaped areas around Lake Bolundsfjärden. The upper part of the bedrock in these areas contains fracture zones with high vertical hydraulic conductivity that are in contact with the Quaternary deposits. Modelling results in terms of hydraulic-head drawdown in the bedrock are presented in Section 7.5.2.

According to the model calculations, the largest groundwater-table drawdown occurs north of Lake Bolundsfjärden, with a drawdown of up to 9 m for $K_{grout} = 10^{-8}$ m/s. In /Gustafsson et al. 2009/ the largest drawdown occurs northeast of the nuclear power plant. However, with the present MIKE SHE model setup there is no groundwater-table drawdown in that specific area. This is likely due to the drainage system at the nuclear power plant, which was not included in the model of /Gustafsson et al. 2009/. This is further discussed in Section 7.5.3. As is also described in that section, the hydraulic conductivity of the grouted zone is an important factor in terms of the size of the groundwater-table drawdown. Section 7.5.4 presents the model-calculated groundwater-table drawdown for different phases of the repository development phases.

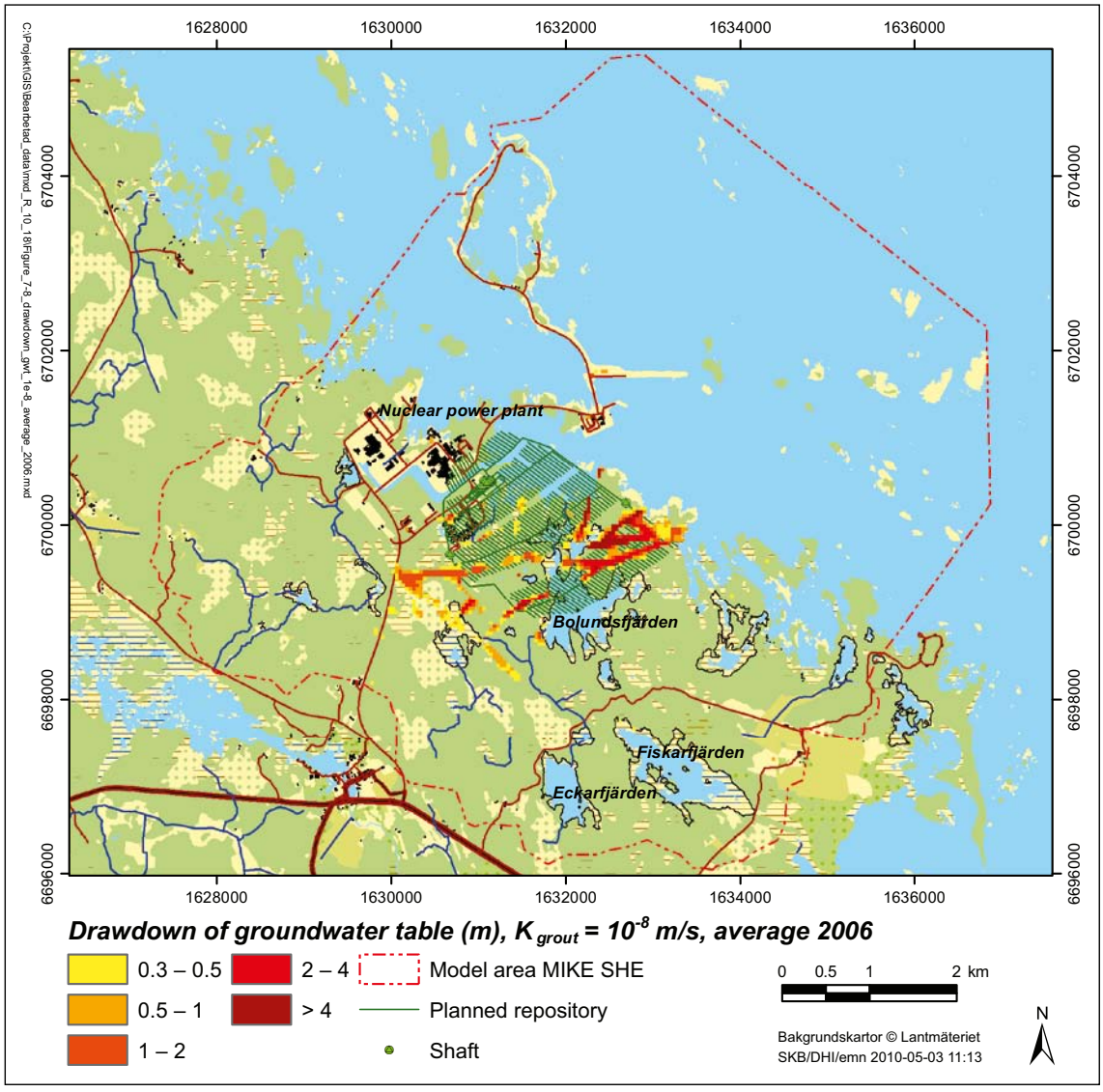

Figure 7-16. *Groundwater-table drawdown, $K_{grout} = 10^{-8}$ m/s.*

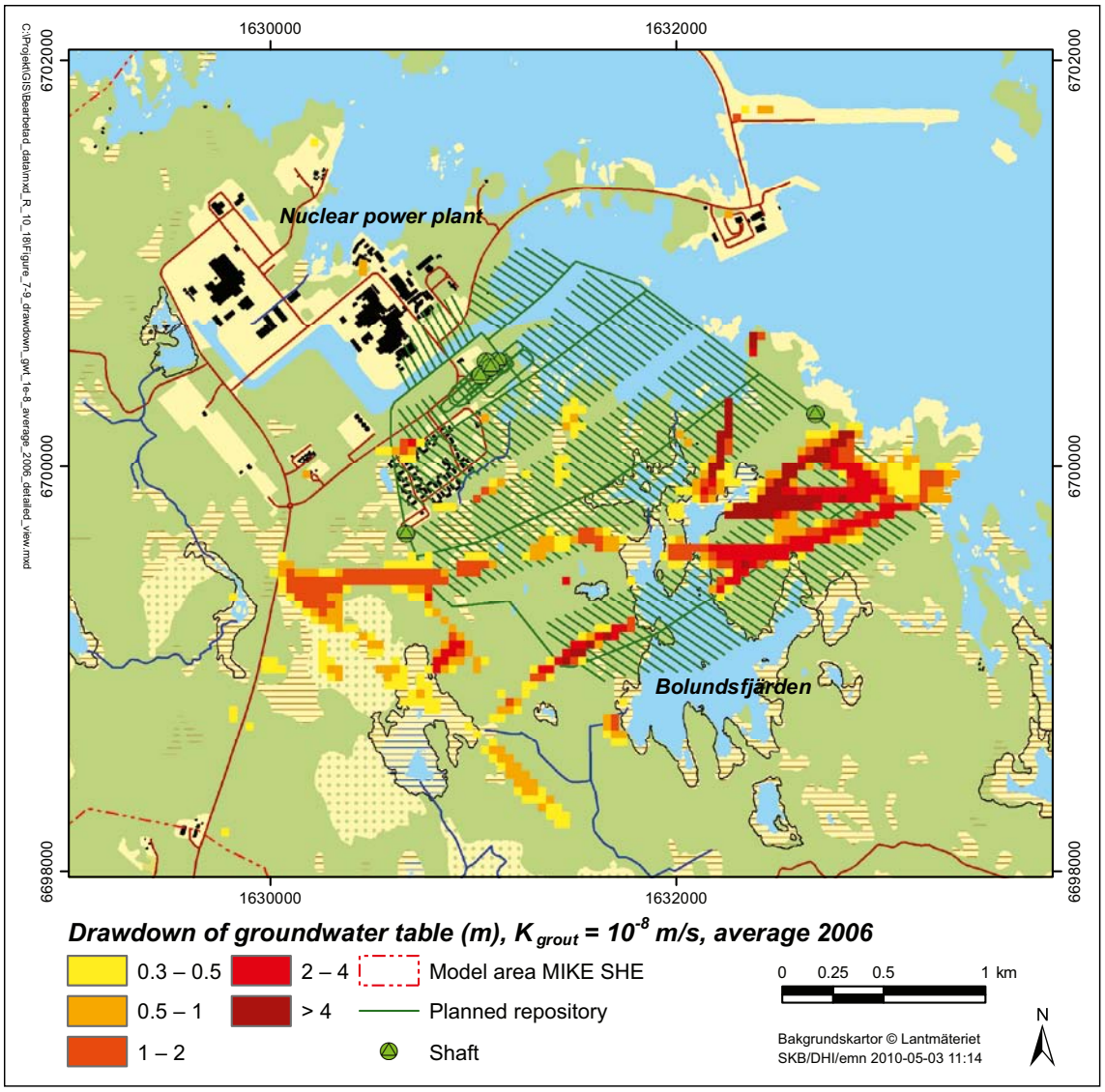

Figure 7-17. *Groundwater-table drawdown, $K_{grout} = 10^{-8}$ m/s (enlargement of Figure 7-16).*

7.5.2 Drawdown of hydraulic heads in the bedrock

As described in Section 7.5.1, the inflow to the repository yields a drawdown of the groundwater table mainly in areas in which the upper part of the bedrock contains fracture zones with high vertical hydraulic conductivity. As will be described in this section, the inflow yields a hydraulic-head drawdown of different magnitude at different levels in the bedrock.

Figure 7-18 shows the model-calculated hydraulic-head drawdown at the level 50 m.b.s.l. for grouting case $K_{grout} = 10^{-8}$ m/s. Compared to the drawdown of the groundwater table (cf. Figure 7-17), the hydraulic-head drawdown in the bedrock is considerably larger and has a larger influence area. This is also illustrated in Figures 7-19 and 7-20, which show model-calculated hydraulic heads at different levels for disturbed conditions ($K_{grout} = 10^{-8}$ m/s). Hydraulic heads are shown along two profiles through the model area and through the centre of the open repository, one south-to-north profile and one west-to-east profile. The figures also show maps of the model-calculated hydraulic-head drawdown at the level 50 m.b.s.l. As can be seen in Figures 7-19 and 7-20 the hydraulic-head drawdown is largest at repository level (450 m.b.s.l.). At the length-scale coordinates 1,900 m (Figure 7-19) and 3,000 m (Figure 7-20), respectively, the profiles cross areas in which there are no tunnels, which can be observed as a local increase of the hydraulic head.

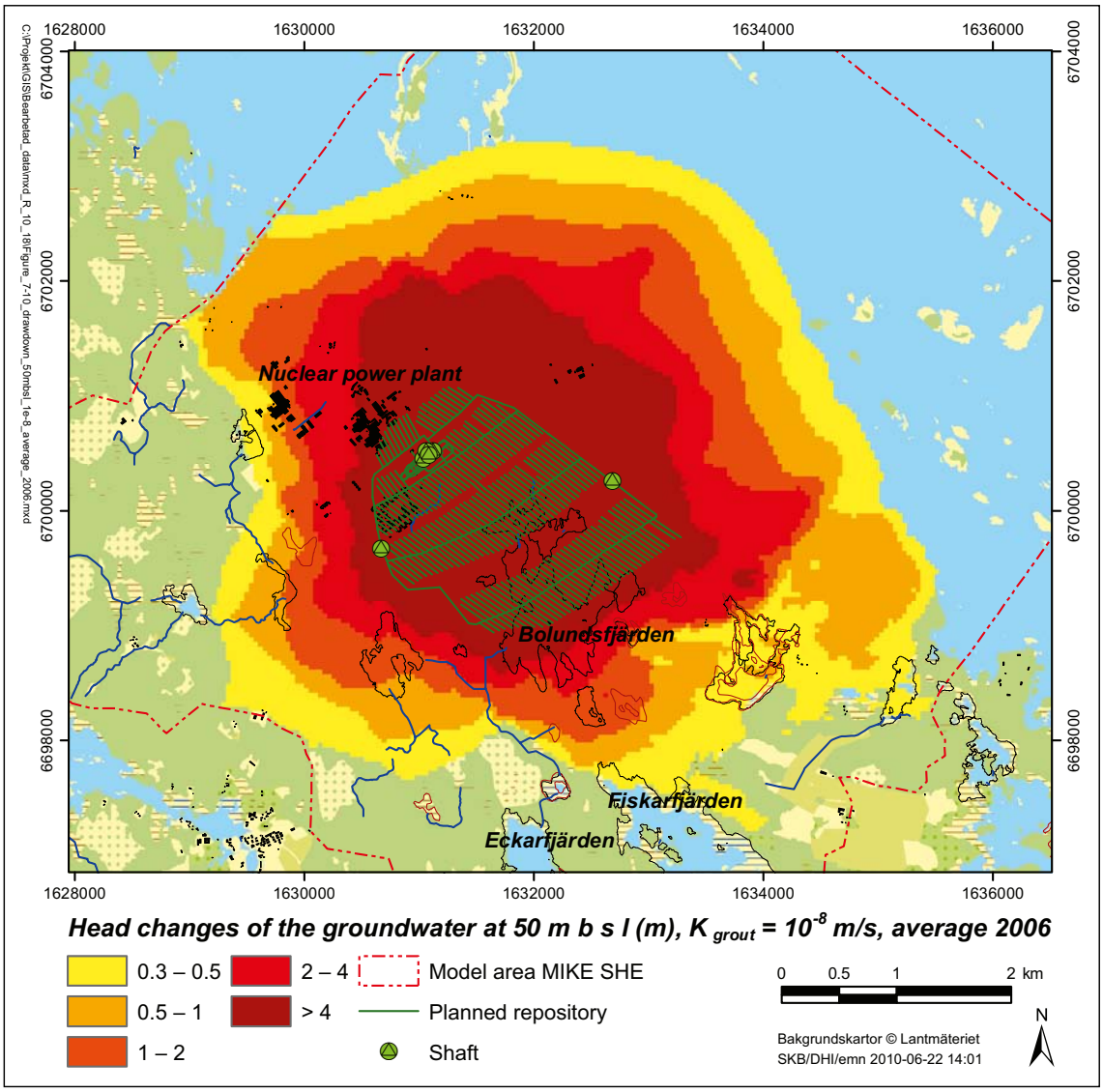

Figure 7-18. *Hydraulic-head drawdown at the level 50 m.b.s.l., $K_{grout} = 10^{-8}$ m/s.*

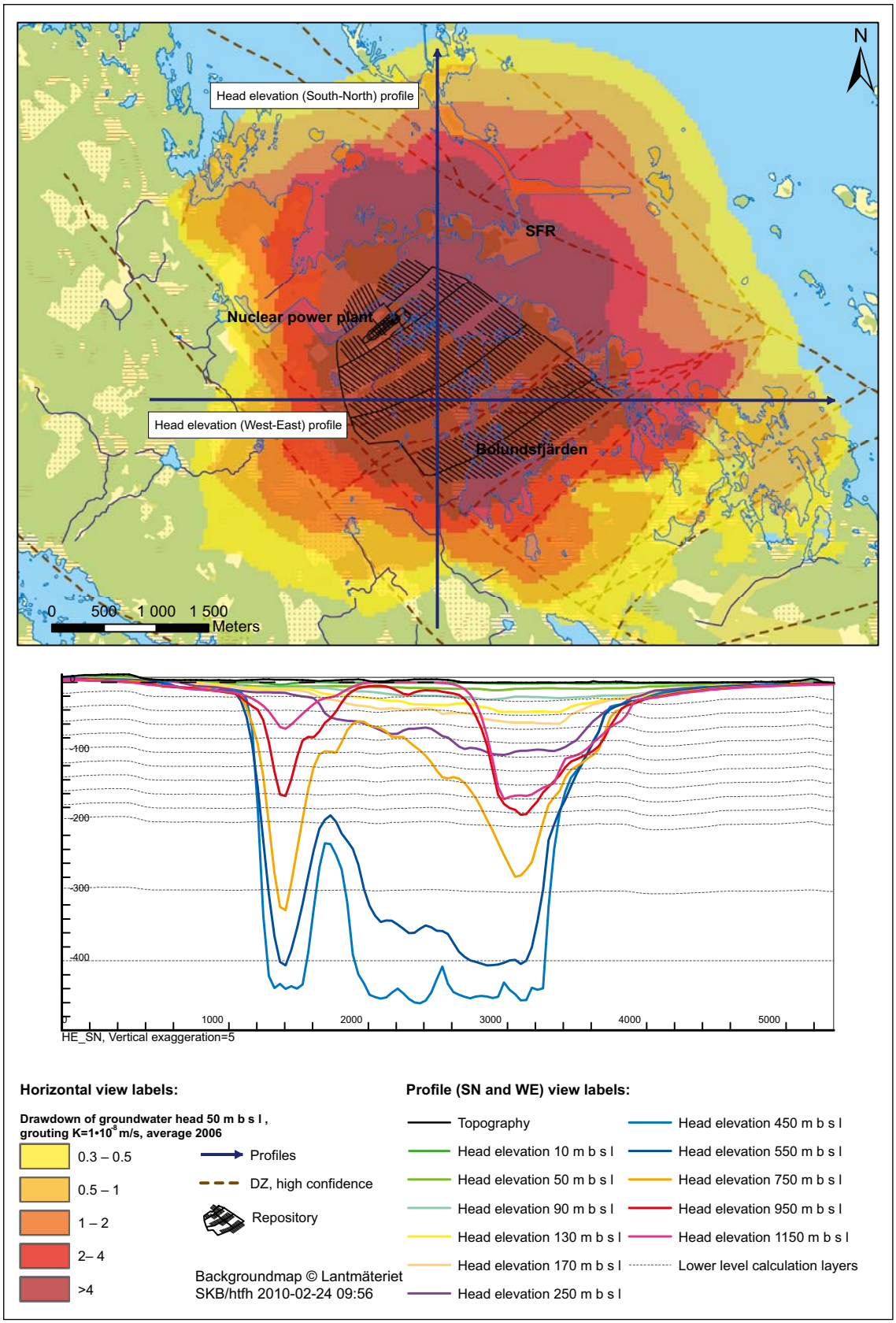

Figure 7-19. *Hydraulic heads in different calculation layers (coloured lines) in a south-to-north profile through the model area and the repository. The upper map shows the hydraulic-head drawdown at the level 50 m.b.s.l. for* $K_{grout} = 10^{-8}$ *m/s.*

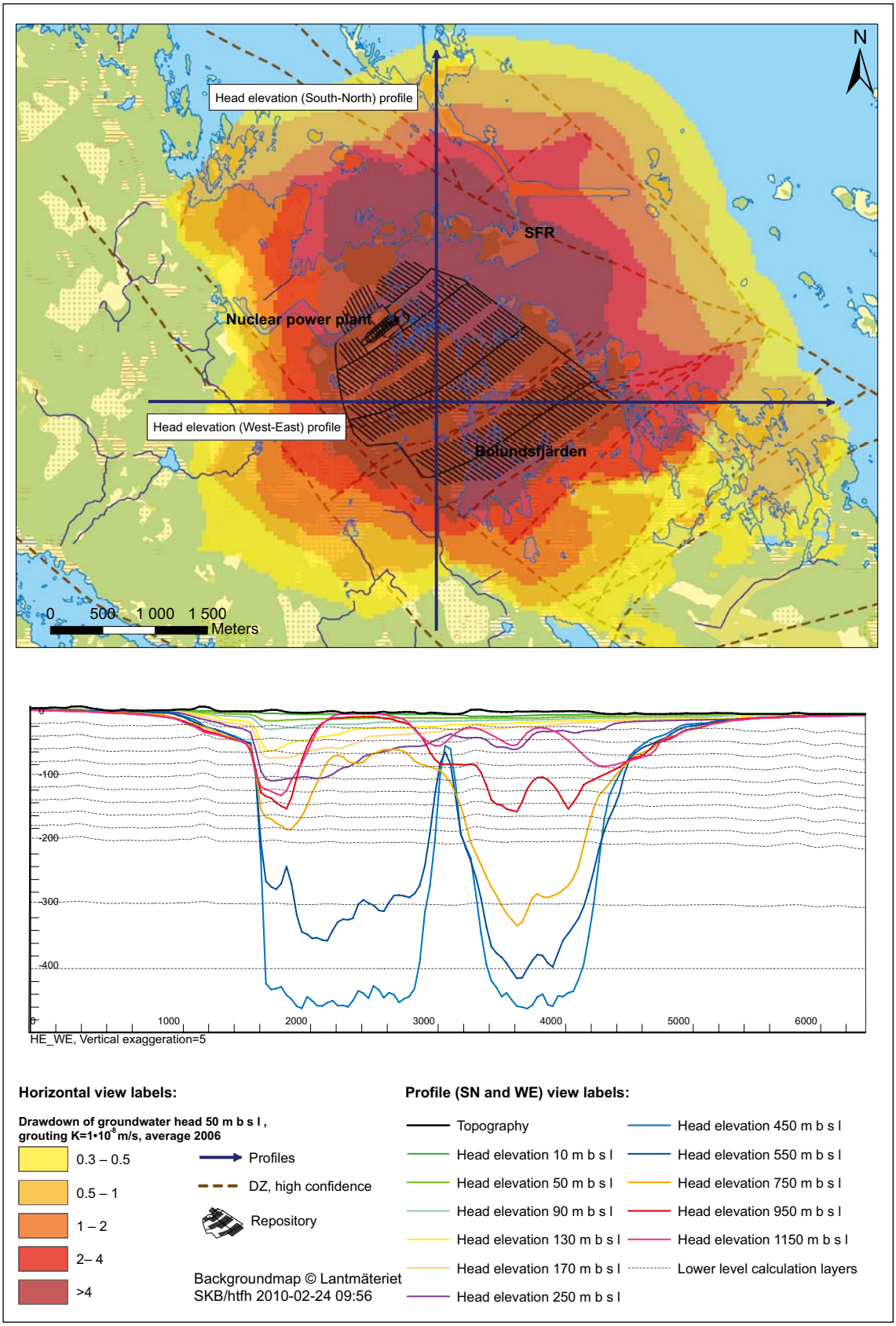

Figure 7-20. *Hydraulic heads in different calculation layers (coloured lines) in a west-to-east profile through the model area and the repository. The upper map shows the hydraulic-head drawdown at the level 50 m.b.s.l. for* $K_{grout} = 10^{-8}$ *m/s.*

Figure 7-21 shows the geographical location of the profile of Figures 7-22 and 7-23, which illustrate cross sections of the vertical (K_v) and horizontal hydraulic conductivity (K_h) in the upper 600 m of the model domain. The high-K_v fracture zones (Figure 7-22) connect the repository with the sheet joints in the upper bedrock. As can be seen in Figure 7-23, in the model the sheet joints are located at the levels 30, 70 and 110 m.b.s.l. The high horizontal hydraulic conductivity of the sheet joints explains the large size of the influence areas in the bedrock (Figure 7-18), whereas the drawdown of the groundwater table is limited to areas in which the upper part of the bedrock contains high-K_v fracture zones (Figure 7-17). The importance of these fracture zones for the directions and magnitude of vertical groundwater flow in the bedrock are further discussed in Section 7.6.3.

Table 7-12 presents the model-calculated hydraulic-head drawdown at the level 50 m.b.s.l. for different drawdown limits. For $K_{grout} = 10^{-7}$ m/s the influence area (drawdown > 0.3 m) covers more than 50% of the model area. The grouting case $K_{grout} = 10^{-7}$ m/s yields an influence area that is 12% and 50% larger than the influence area for $K_{grout} = 10^{-8}$ and 10^{-9} m/s, respectively.

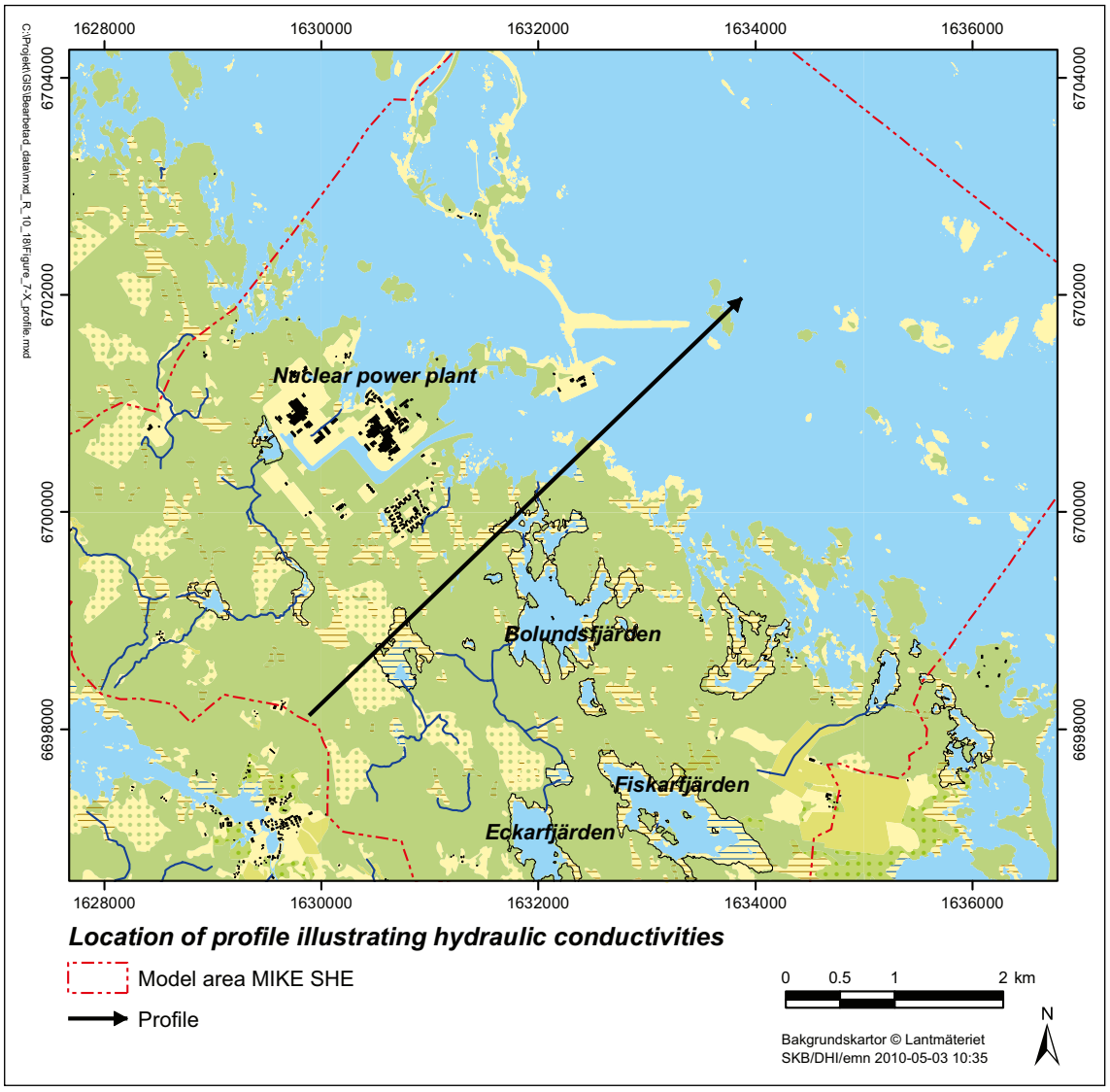

Figure 7-21. *Geographical location of the profile shown in Figures 7-22 and 7-23.*

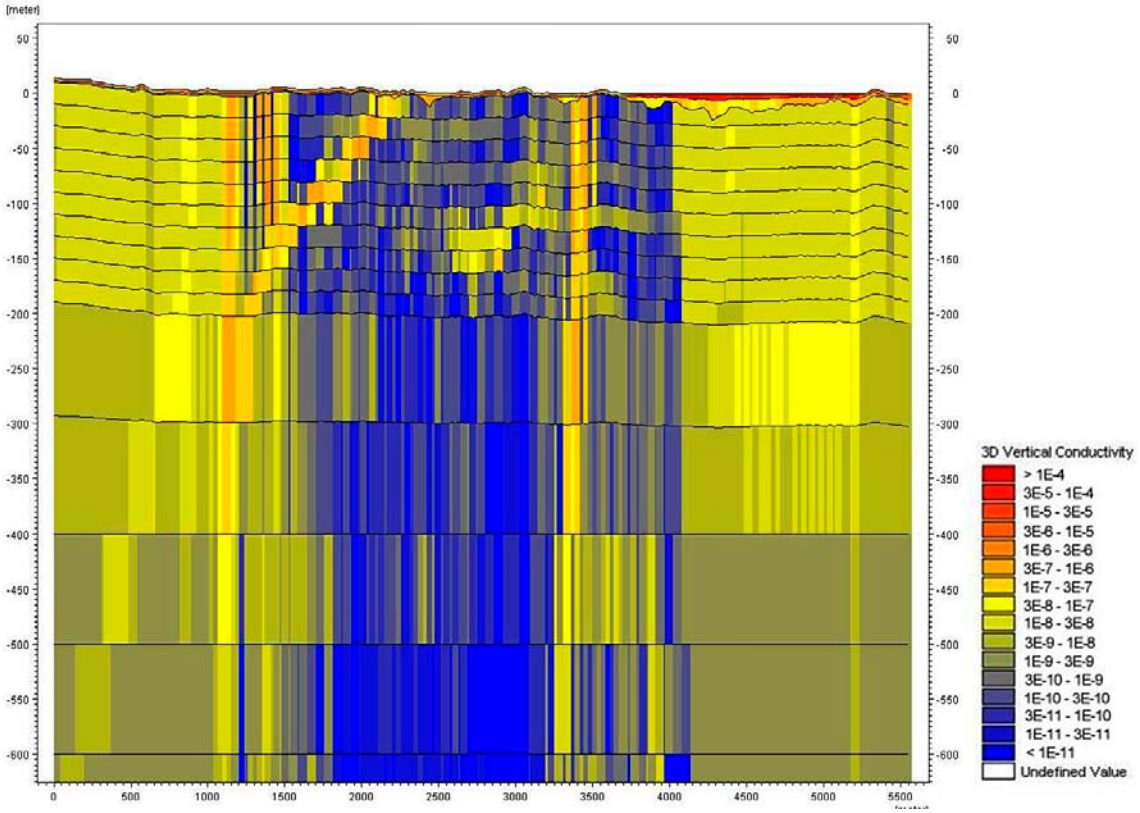

Figure 7-22. *Vertical hydraulic conductivity (K_v, m/s) in a southwest-to-northeast section through the repository. Red colours represent high values of K_v.*

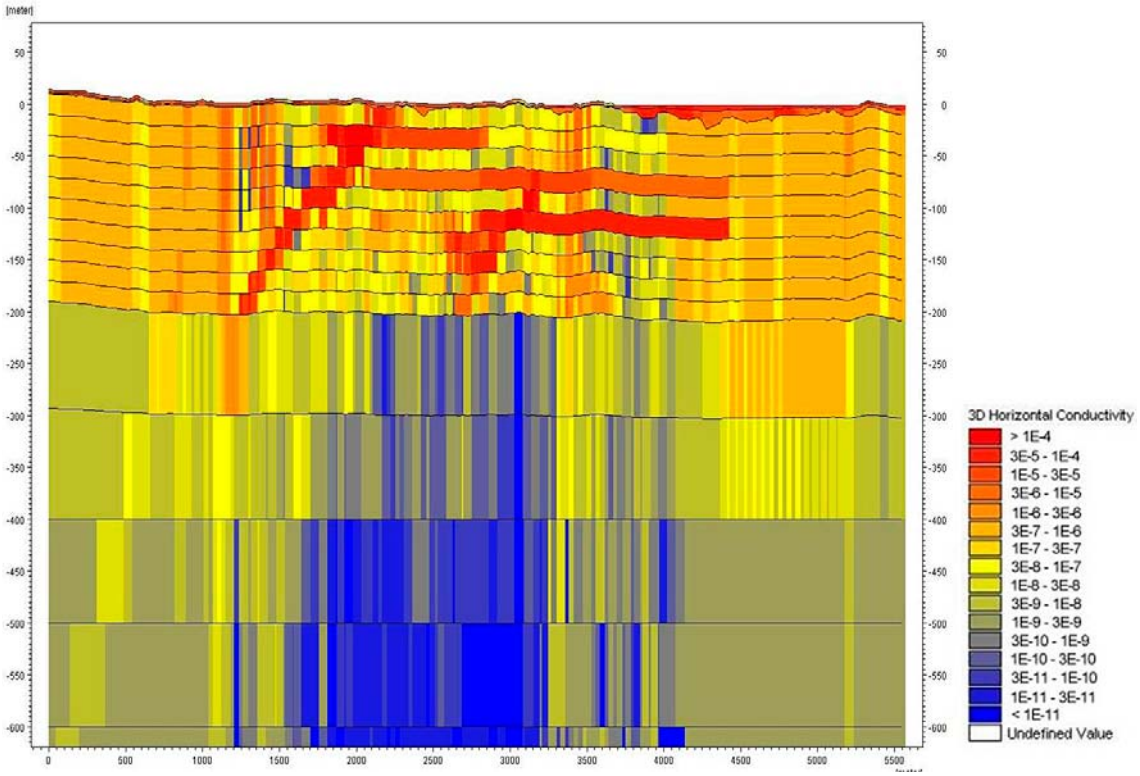

Figure 7-23. *Horizontal hydraulic conductivity (K_h, m/s) in a southwest-to-northeast section through the repository. Red colours represent high values of K_h. The high-K_h sheet joints in the upper part of the profile are generally not associated with high values of K_v (cf. Figure 7-22).*

Table 7-12. Influence areas (km²) for different limits of the hydraulic-head drawdown at the level 50 m.b.s.l.

Grouting case	Max. drawdown (m)	> 0.3 m	> 0.5 m	> 1 m	> 2 m	> 4 m	> 10 m
$K_{grout} = 10^{-7}$ m/s,	62.5	30.4	25.4	18.4	14.3	10.4	6.09
$K_{grout} = 10^{-8}$ m/s,	56.7	27.1	21.6	15.9	12.0	7.98	1.41
$K_{grout} = 10^{-9}$ m/s,	37.9	20.2	15.9	11.9	7.77	1.02	0.01

Figure 7-24 shows the influence area for all three studied grouting cases. For grouting cases $K_{grout} = 10^{-7}$ and 10^{-8} m/s, the influence area of the hydraulic-head drawdown reaches the model boundary in the northwest and southwest. The no-flow onshore boundary implies that areas outside of the boundary cannot contribute to the groundwater inflow to the repository. The importance of the boundary conditions is further investigated as a sensitivity case in Chapter 8. The results from this specific sensitivity analysis show that the boundary condition has minor importance for the inflow to the repository.

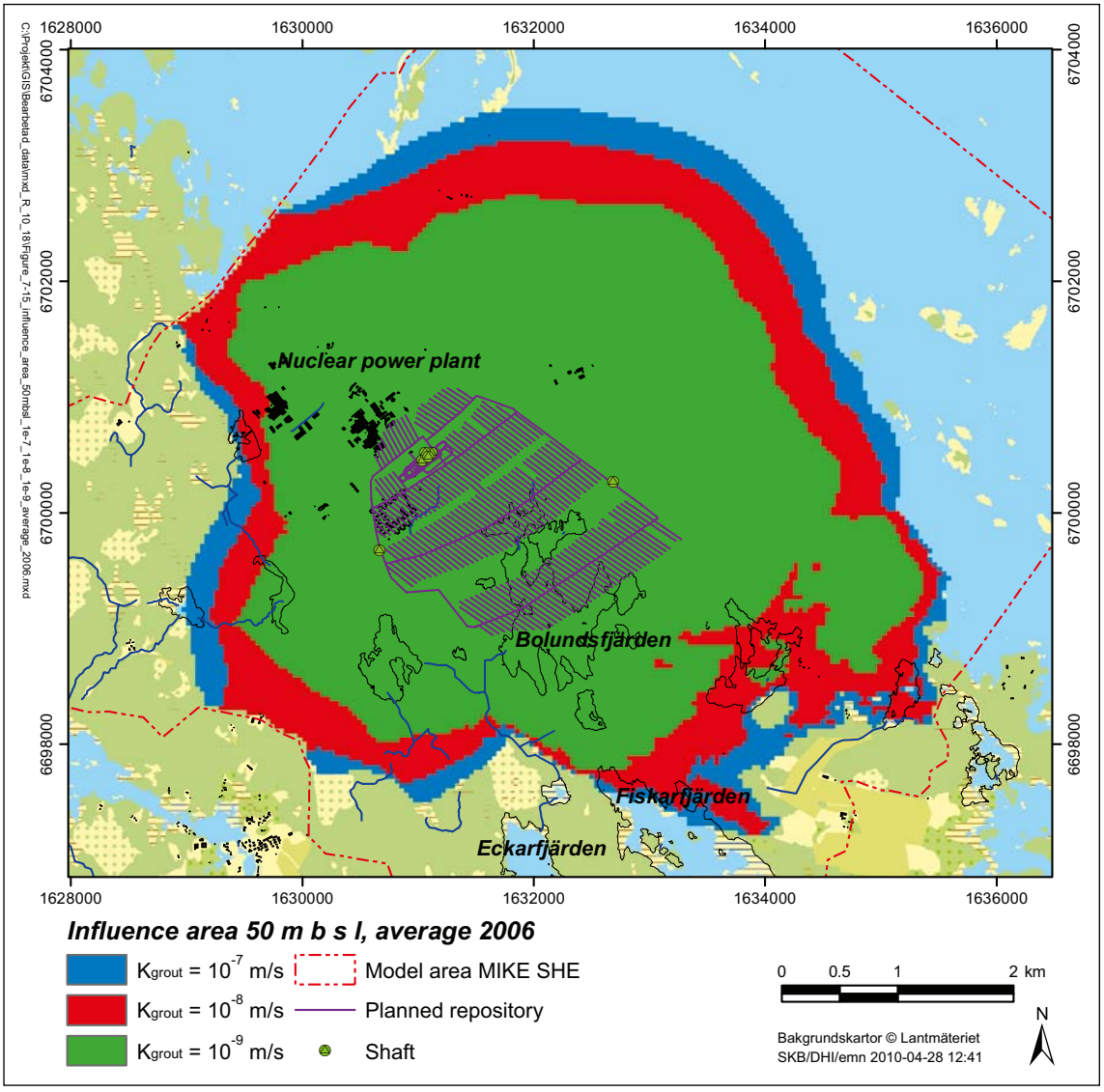

Figure 7-24. *Influence area for the model-calculated hydraulic-head drawdown > 0.3 m at the level 50 m.b.s.l. for $K_{grout} = 10^{-7}$ m/s (blue, red and green areas), 10^{-8} m/s (red and green areas) and 10^{-9} m/s (green areas).*

The magnitude of the present model-calculated hydraulic-head drawdowns and influence areas are larger compared to the results of /Gustafsson et al. 2009/. Compared to these previous results, the influence area at the level 50 m.b.s.l. is mainly extended to the northwest and southwest. In the /Gustafsson et al. 2009/ modelling, the influence area reached the model-area boundary in the sea, in which direction the present model area is extended. The main reasons for the different modelling results are the increased inflow to the repository and the updated hydrogeological model of the bedrock.

The results above refer to the hypothetical case with a fully open repository. Table 7-13 shows the annual hydraulic-head drawdown at the level 50 m.b.s.l. for the construction phase ($K_{grout} = 10^{-7}$ and 10^{-8} m/s), and for the hypothetical case with a fully repository excluding all main and deposition tunnels, development phase 3 and the case with a fully open repository ($K_{grout} = 10^{-8}$ m/s). In terms of the size of the influence area for the hydraulic-head drawdown, there are small differences (3%) between development phase 3 and the case with a fully open repository. The construction phase yields the smallest influence area, in size some 60% of the influence area for the case with a fully open repository.

Figures 7-25 to 7-27 show the hydraulic-head drawdown at the level 50 m.b.s.l. for the investigated phases ($K_{grout} = 10^{-8}$ m/s). The drawdown at this level reaches the model boundary also during the construction phase (phase 0) (Figure 7-25). Compared to phase 0, the influence area comprises areas further to the east and south during development phase 3.

7.5.3 Groundwater-table drawdown for different levels of grouting

This section studies the importance of the hydraulic conductivity of the grouted zone for the drawdown of the groundwater table. Figures 7-28 to 7-30 show the model-calculated drawdown of the groundwater table for the three grouting cases. As can be seen in these figures, the overall shape and size of the influence area is similar for all three grouting cases. Obviously, grouting case $K_{grout} = 10^{-7}$ m/s yields the largest drawdown and influence area, and as shown previously (Section 7.2) also the largest groundwater inflow to the repository.

Table 7-14 summarises the model-calculated groundwater-table drawdown and influence area for the three grouting cases. According to the table, $K_{grout} = 10^{-7}$ m/s yields an influence area (drawdown > 0.3 m) of 1.38 km^2, which is 31% and 116% larger than the influence area for the grouting cases $K_{grout} = 10^{-8}$ m/s and $K_{grout} = 10^{-9}$ m/s, respectively. Figure 7-31 shows the model-calculated influence area for all three grouting cases.

The maximum drawdown of the groundwater table occurs in areas north of Lake Bolundsfjärden, with an annual average drawdown of up to 16 m for grouting case $K_{grout} = 10^{-7}$ m/s. However, the drawdown exceeds 10 m only in a few, small areas.

Figure 7-32 shows model-calculated groundwater-table elevations along two profiles through the centre of the open repository, one south-to-north profile and one west-to-east profile. Results are shown for undisturbed conditions and for the three grouting cases for disturbed conditions. The figure also shows a map of the geographical locations of the two profiles and the groundwater-table drawdown for grouting case $K_{grout} = 10^{-8}$ m/s. For disturbed conditions there is no groundwater-table drawdown along most of the profiles, whereas at e.g. length coordinate 300 m in the south-to-north profile the drawdown is locally up to 10 m. The phenomenon with very local drawdowns can also be seen in Figure 7-31, and is due to the presence in some areas with fracture zones with high vertical hydraulic conductivity in the upper part of the bedrock.

Table 7-13. Influence areas (km^2) for different limits for the hydraulic-head drawdown at the level 50 m.b.s.l. for different development phases ($K_{grout} = 10^{-8}$ m/s).

Case	K_{grout} (m/s)	> 0.3 m	> 0.5 m	> 1.0 m	> 2 m	> 4 m	> 10 m
Construction phase	10^{-7}	21.3	18.5	14.2	10.6	7.44	3.27
Construction phase	10^{-8}	16.6	13.5	10.0	6.29	3.17	0.47
Fully open excl. main and deposition tunnels	10^{-8}	21.7	18.0	13.7	9.92	6.44	0.83
Development phase 3	10^{-8}	26.2	20.7	15.5	11.5	7.47	1.10
Fully open	10^{-8}	27.1	21.6	15.9	12.0	7.98	1.41

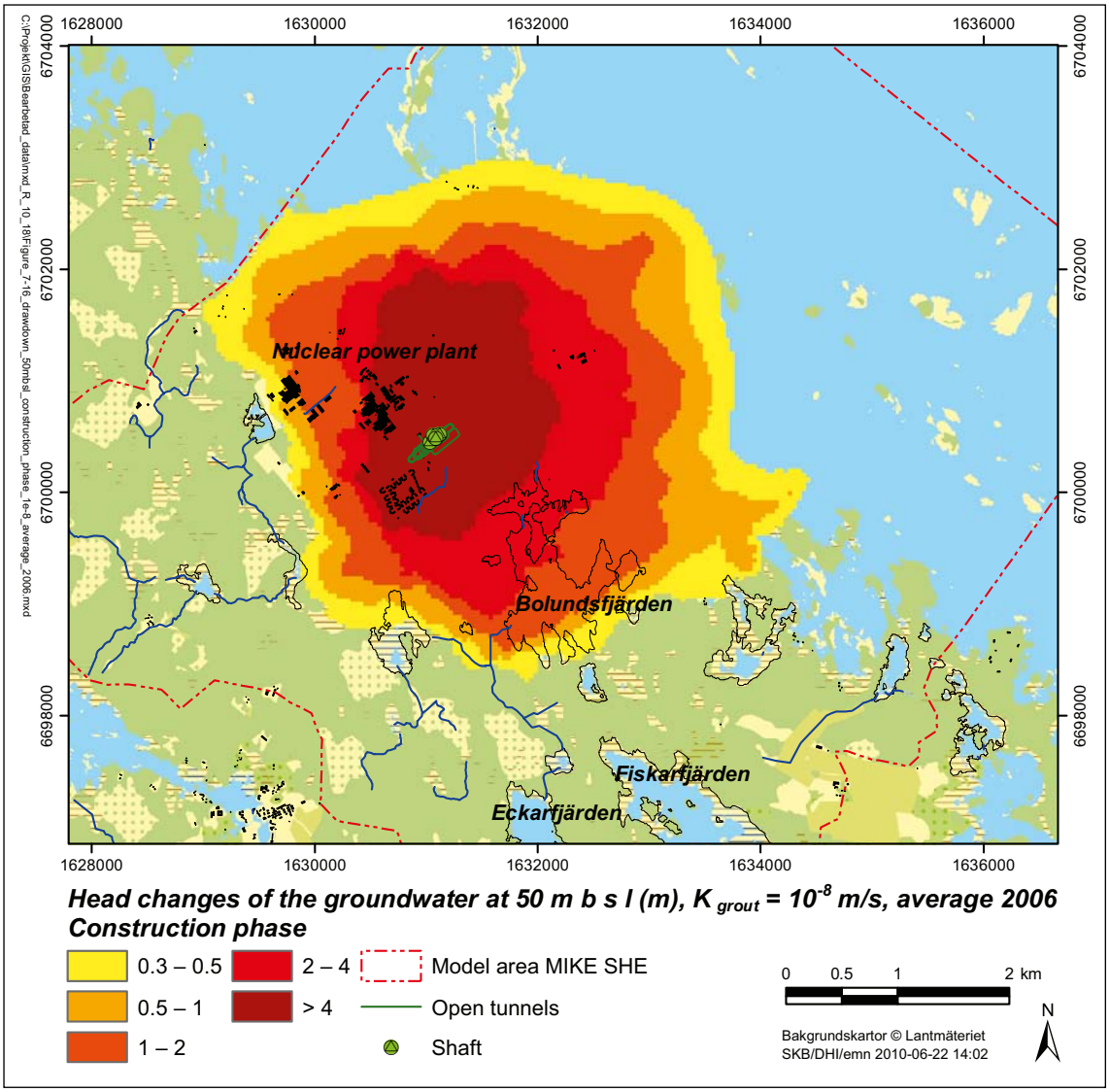

Figure 7-25. *Hydraulic-head drawdown during the construction phase, $K_{grout} = 10^{-8}$ m/s.*

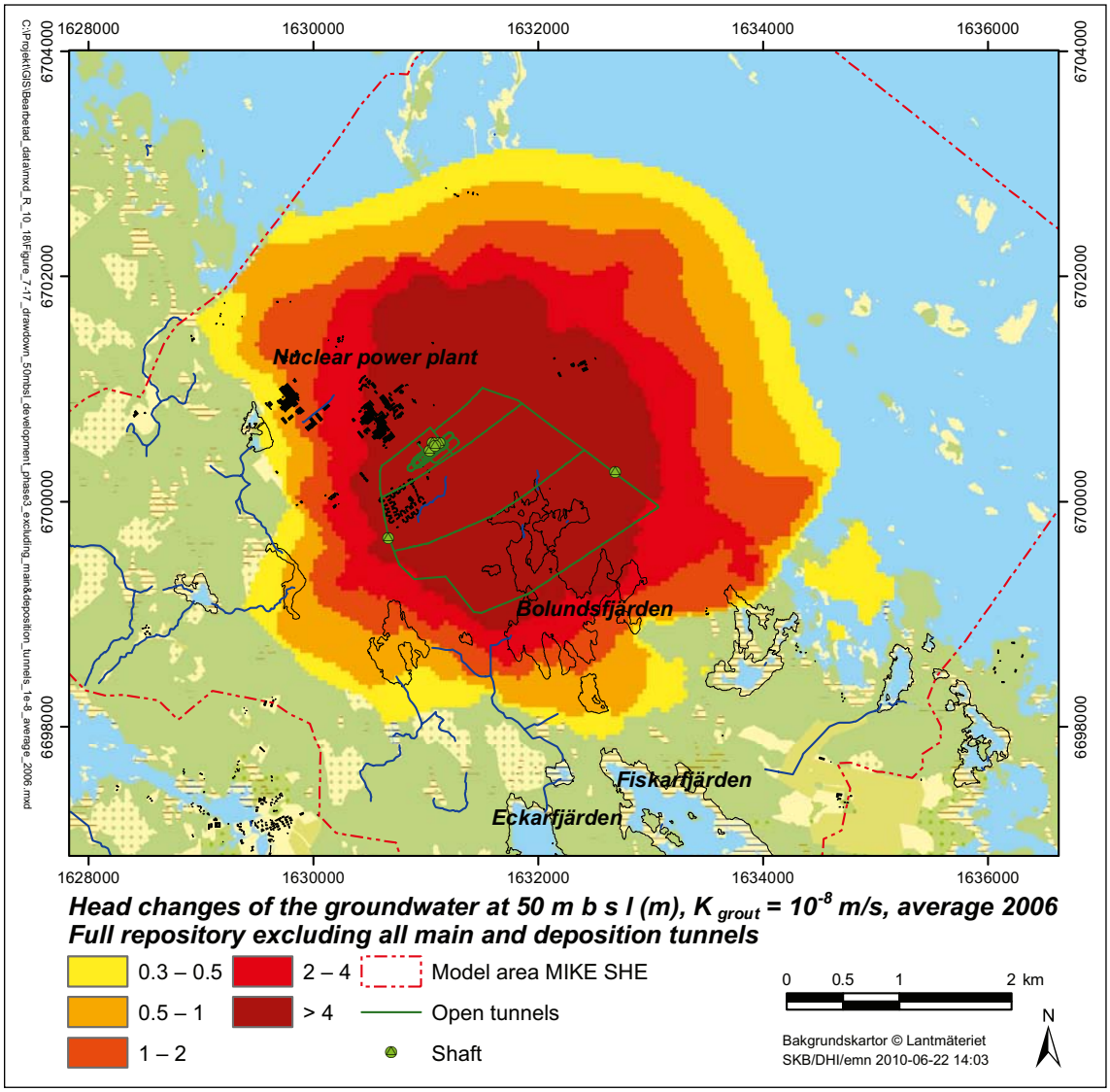

Figure 7-26. *Hydraulic-head drawdown for the hypothetical case of a fully open repository excluding main and deposition tunnels, $K_{grout} = 10^{-8}$ m/s.*

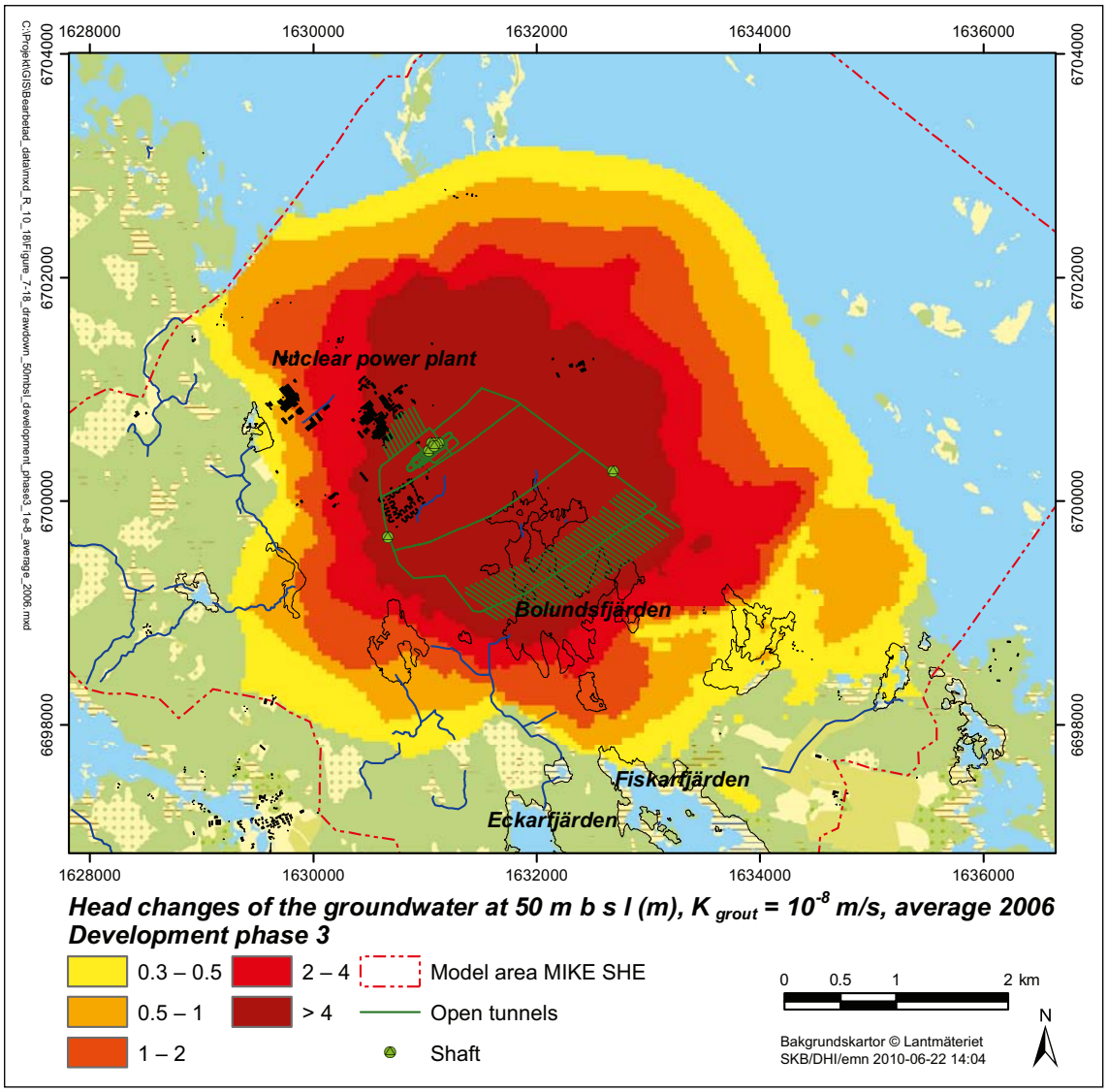

Figure 7-27. *Hydraulic-head drawdown during development phase 3, $K_{grout} = 10^{-8}$ m/s.*

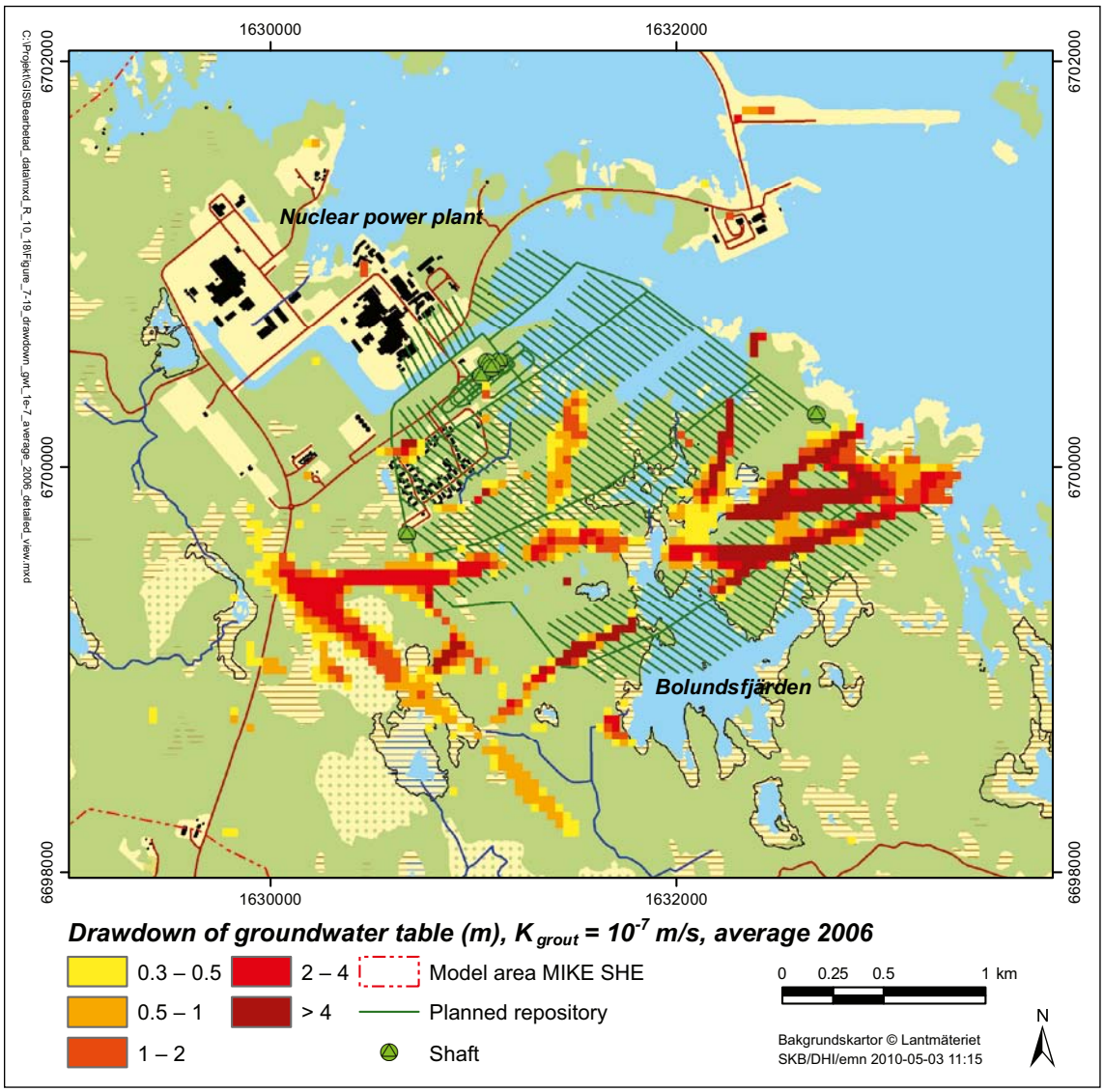

Figure 7-28. *Groundwater-table drawdown, $K_{grout} = 10^{-7}$ m/s.*

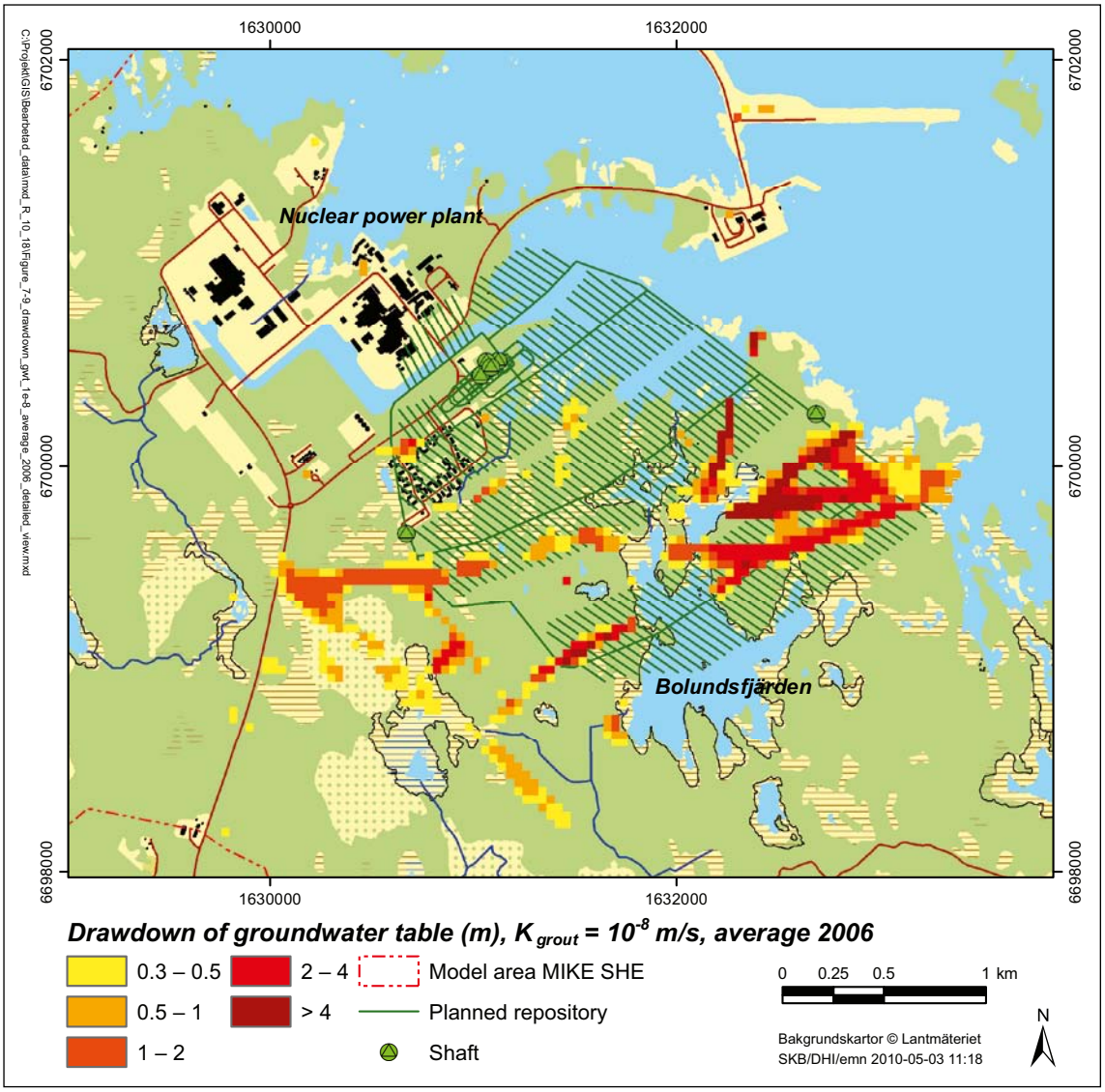

Figure 7-29. *Groundwater-table drawdown, $K_{grout} = 10^{-8}$ m/s.*

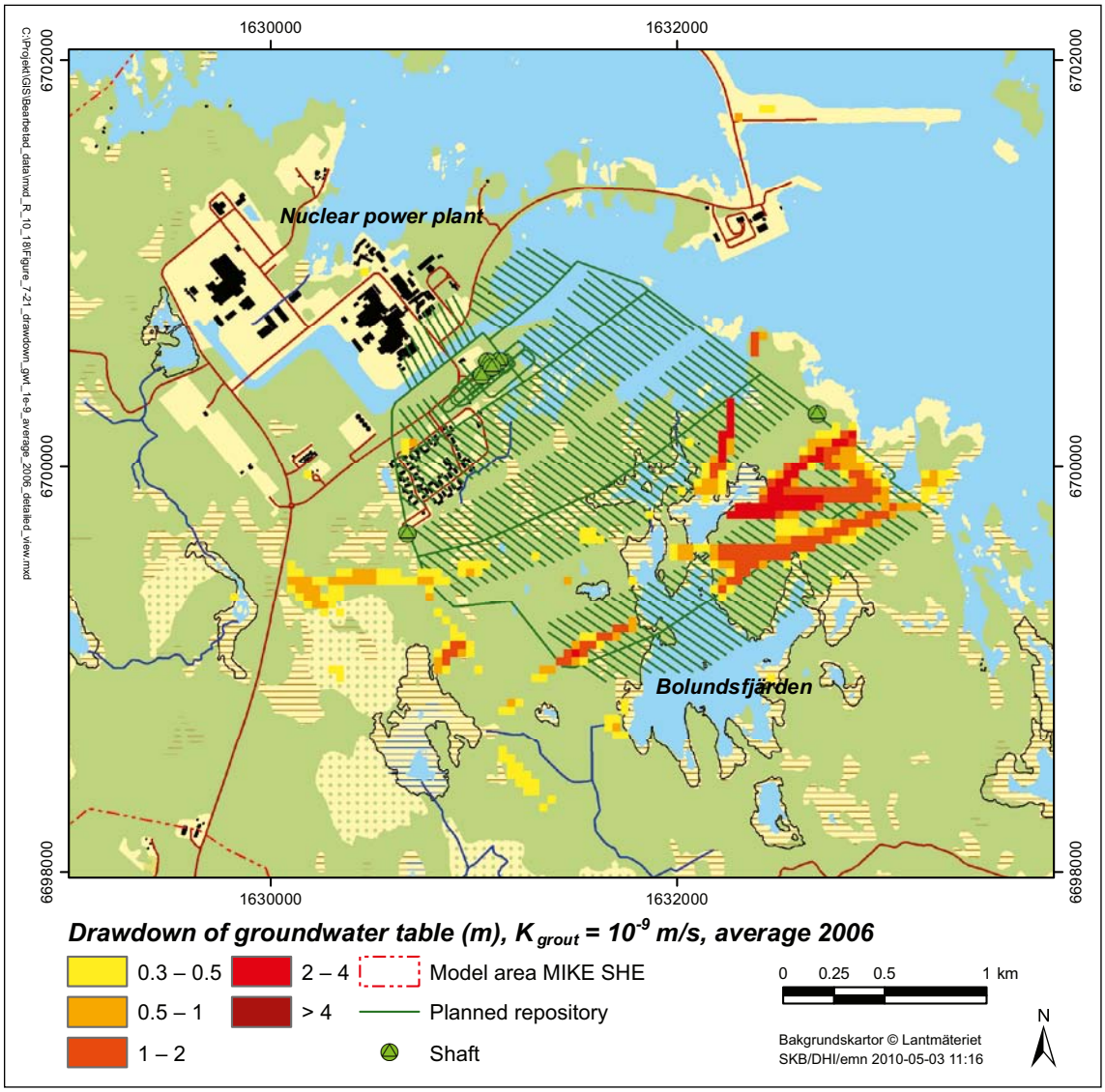

Figure 7-30. *Groundwater-table drawdown, $K_{grout} = 10^{-9}$ m/s.*

Table 7-14. Influence areas (km²) for different limits of the groundwater-table drawdown.

K_{grout} (m/s)	Max. gw. table drawdown (m)	> 0.1 m	> 0.3 m	> 0.5 m	> 1 m	> 2 m	> 4 m
10^{-7}	16.5	2.45	1.38	1.05	0.69	0.48	0.25
10^{-8}	9.2	1.96	1.05	0.72	0.47	0.27	0.10
10^{-9}	3.9	1.20	0.64	0.40	0.24	0.08	0.00

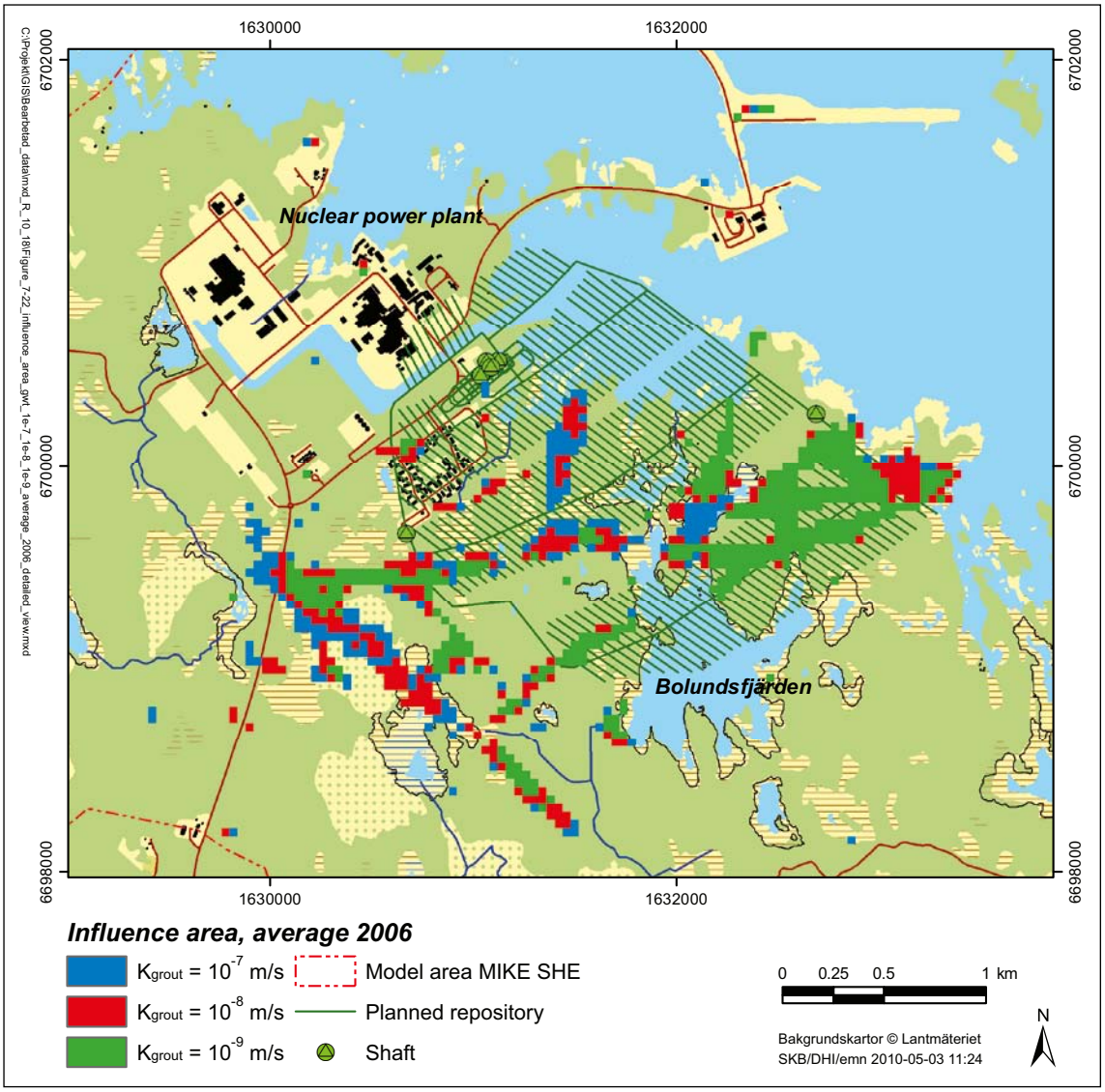

Figure 7-31. *Influence areas (groundwater-table drawdown > 0.3 m) for $K_{grout} = 10^{-7}$ m/s (blue, red and green areas), 10^{-8} m/s (red and green areas) and 10^{-9} m/s (green areas).*

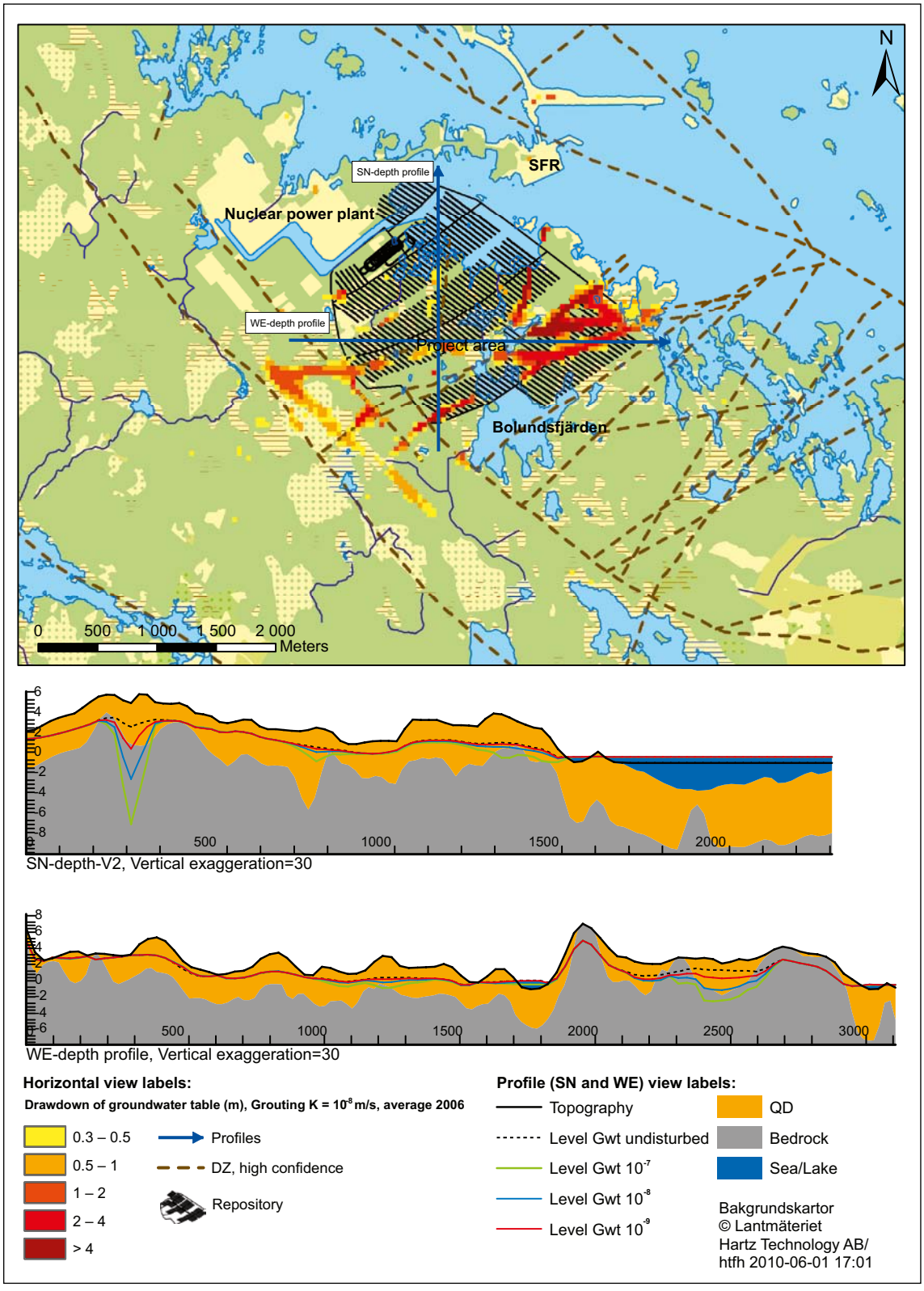

Figure 7-32. *Groundwater-table elevation (m.a.s.l.) along two profiles for undisturbed conditions (dotted line), and for disturbed conditions for K_{grout} = 10^{-7} m/s (green line), 10^{-8} m/s (blue line) and 10^{-9} m/s (red line). The upper map shows the geographical locations of the two profiles and the drawdown for K_{grout} = 10^{-8} m/s.*

Section 3.3 presents results using the MIKE SHE open repository model of /Gustafsson et al. 2009/ and the updated MIKE SHE-MOUSE coupling routine. Compared to these results the influence areas in Table 7-14 are smaller. Specifically, the influence area for $K_{grout} = 10^{-7}$ m/s is approximately 23% smaller compared to the results in Section 3.3, whereas the corresponding difference is 23% and 10% for $K_{grout} = 10^{-8}$ and 10^{-9} m/s, respectively. Hence, except for the updated coupling routine the present model updates yield a reduction of the influence area. The net effect of the updated MIKE SHE-MOUSE coupling routine and the other model changes (by comparison between Table 7-14 in this report and Table 5-13 in /Gustafsson et al. 2009/) is that the influence area for $K_{grout} = 10^{-7}$ m/s is 12% smaller, whereas it is 3% and 31% larger for grouting case $K_{grout} = 10^{-8}$ and 10^{-9} m/s, respectively.

One difference between the two models is that the band-shaped influence areas were somewhat wider in the /Gustafsson et al. 2009/ modelling. Another difference can be noted northeast of the nuclear power plant, with a significant drawdown in the /Gustafsson et al. 2009/ modelling but with no drawdown in that specific area according to the present results. This difference can be explained by the drainage system at the nuclear power plant, which was not implemented in the model of /Gustafsson et al. 2009/.

Figure 7-33 shows the model-calculated groundwater-table drawdown for grouting case $K_{grout} = 10^{-7}$ m/s, here also including areas with a drawdown in the interval 0.1–0.3 m. In this figure, one can note a small-magnitude drawdown along a band-shaped area with a length of 600–700 m northeast of Lake Fiskarfjärden. The maximum annual average drawdown in this specific area is 0.18 m for grouting case $K_{grout} = 10^{-7}$ m/s. For grouting case $K_{grout} = 10^{-8}$ m/s the size of this band-shaped area is somewhat smaller, whereas the drawdown is practically zero for $K_{grout} = 10^{-9}$ m/s. Figure 7-33 also shows a few scattered areas with a drawdown in the interval 0.1–0.3 m, north and northwest of the nuclear power plant. In the /Gustafsson et al. 2009/ modelling there is no drawdown in these areas, and neither in the area northeast of Lake Fiskarfjärden.

7.5.4 Groundwater-table drawdown for different development phases

As mentioned previously, the actual construction and operation of the repository imply that tunnel construction and backfilling will take place simultaneously in different parts of the repository area. In reality, the whole repository will therefore not be open at the same time. This section studies the groundwater-table drawdown for different development phases, which are approximations of reality. For further details on these different phases, see Section 4.3.2.

Figures 7-34 to 7-36 show the model-calculated groundwater-table drawdown for the construction phase, for a hypothetical case with a fully open repository excluding all main tunnels and deposition tunnels, and for development phase 3. All these phases were simulated for grouting case $K_{grout} = 10^{-8}$ m/s. As can be seen in these figures, the magnitude of the drawdown and the size of its influence area to some extent differ between the different development phases. However, the shape and size of the influence area is rather similar for all studied phases. This results shows that the specific parts of the repository area that are open are of minor importance for the groundwater-table drawdown. Rather, of importance for the drawdown is the total length of tunnels and in particular those that are located below or cross conductive fracture zones (see Figure 7-2 in Section 7.2). This is illustrated in Figure 7-37, which shows the model-calculated influence area for all studied development phases.

Table 7-15 present the model-calculated drawdown and associated influence areas for the different phases, including the case with a fully open repository. Obviously, the largest drawdown and influence area are obtained for the latter case. Concerning the three phases, the drawdown and the influence area are largest during development phase 3. For $K_{grout} = 10^{-8}$ m/s, the influence area (drawdown > 0.3 m) is 94% of that for the fully open repository. In the hypothetical case that excludes the main and deposition tunnels, the influence area is 72% of that for the fully open repository. The construction phase is associated with the smallest drawdown. For $K_{grout} = 10^{-8}$ m/s, during that phase the influence area is 43% of that for the fully open repository.

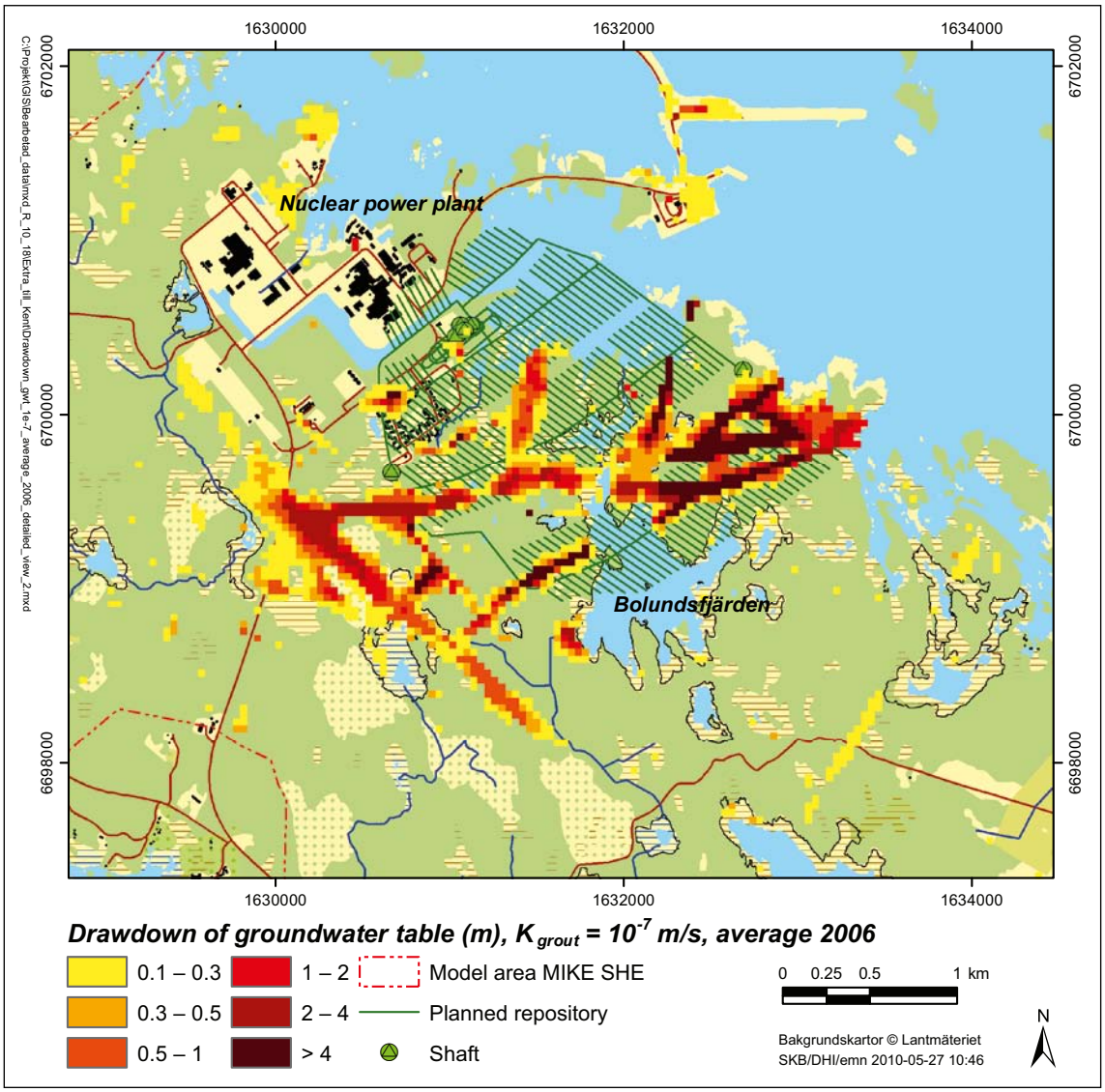

Figure 7-33. *Groundwater-table drawdown, $K_{grout} = 10^{-7}$ m/s. Note the different drawdown limits and the different map scale compared to Figure 7-28.*

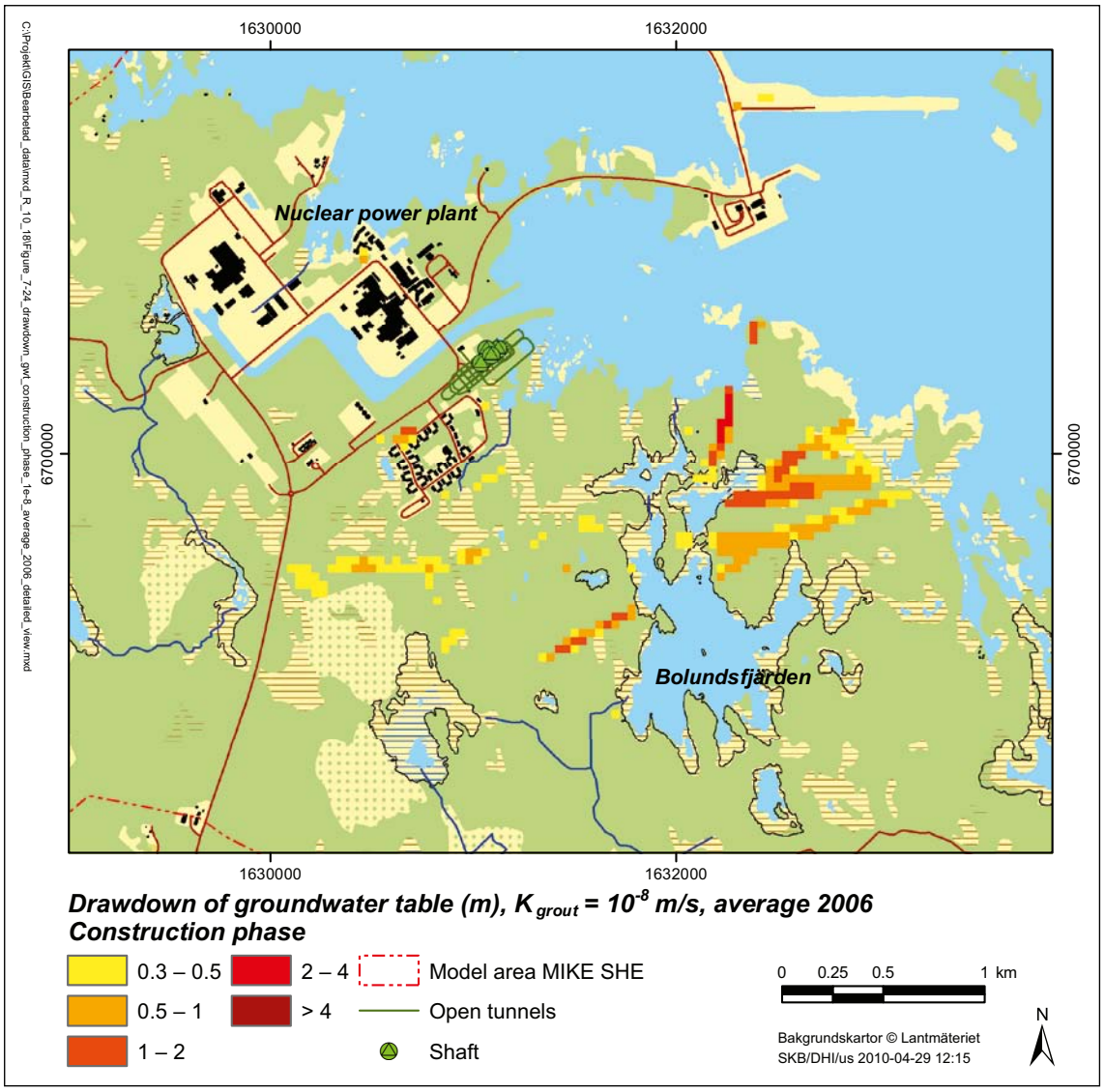

Figure 7-34. *Groundwater-table drawdown during the construction phase, $K_{grout} = 10^{-8}$ m/s.*

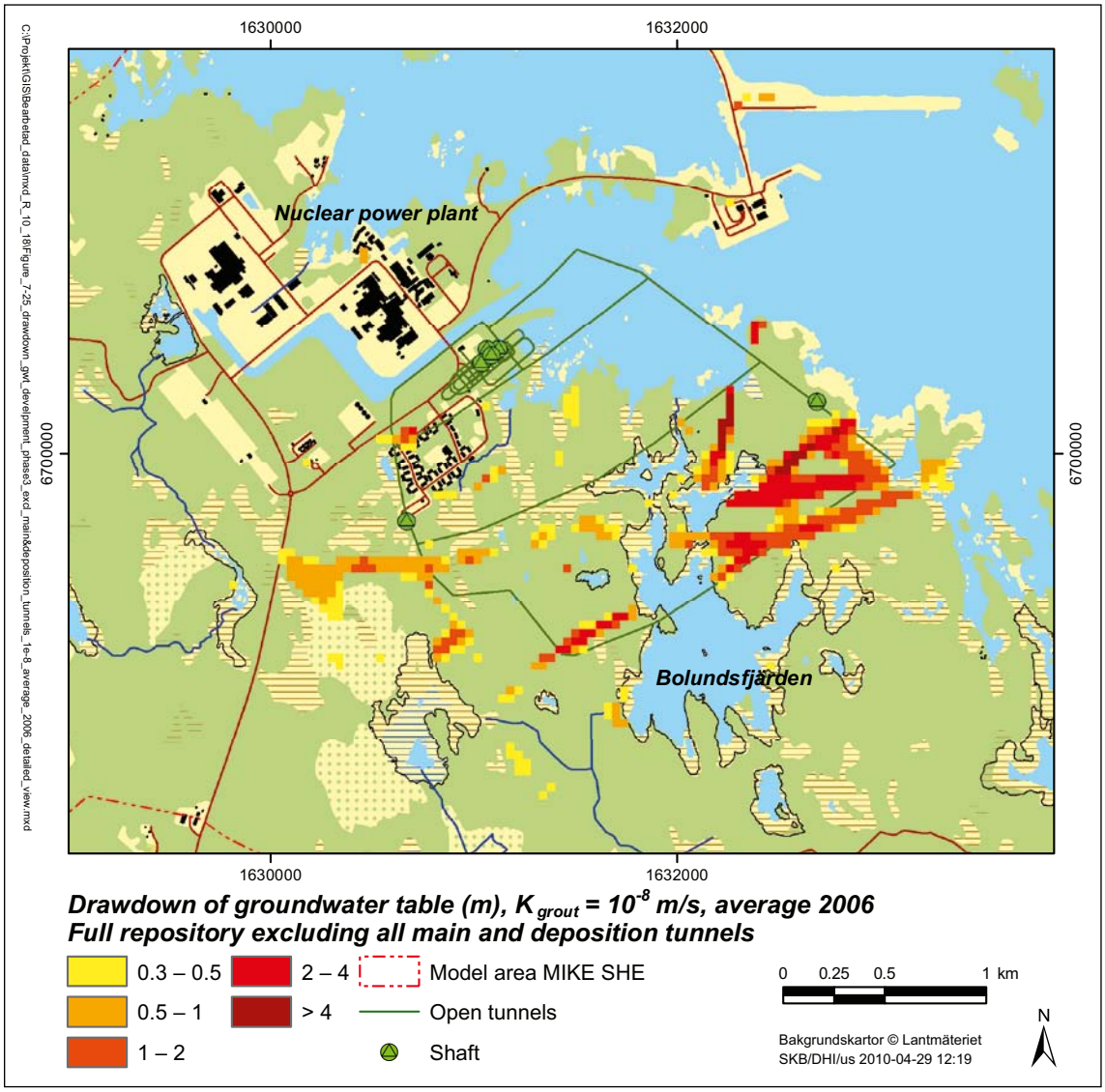

Figure 7-35. *Groundwater-table drawdown during development phase 3 excluding all main and deposition tunnels, $K_{grout} = 10^{-8}$ m/s.*

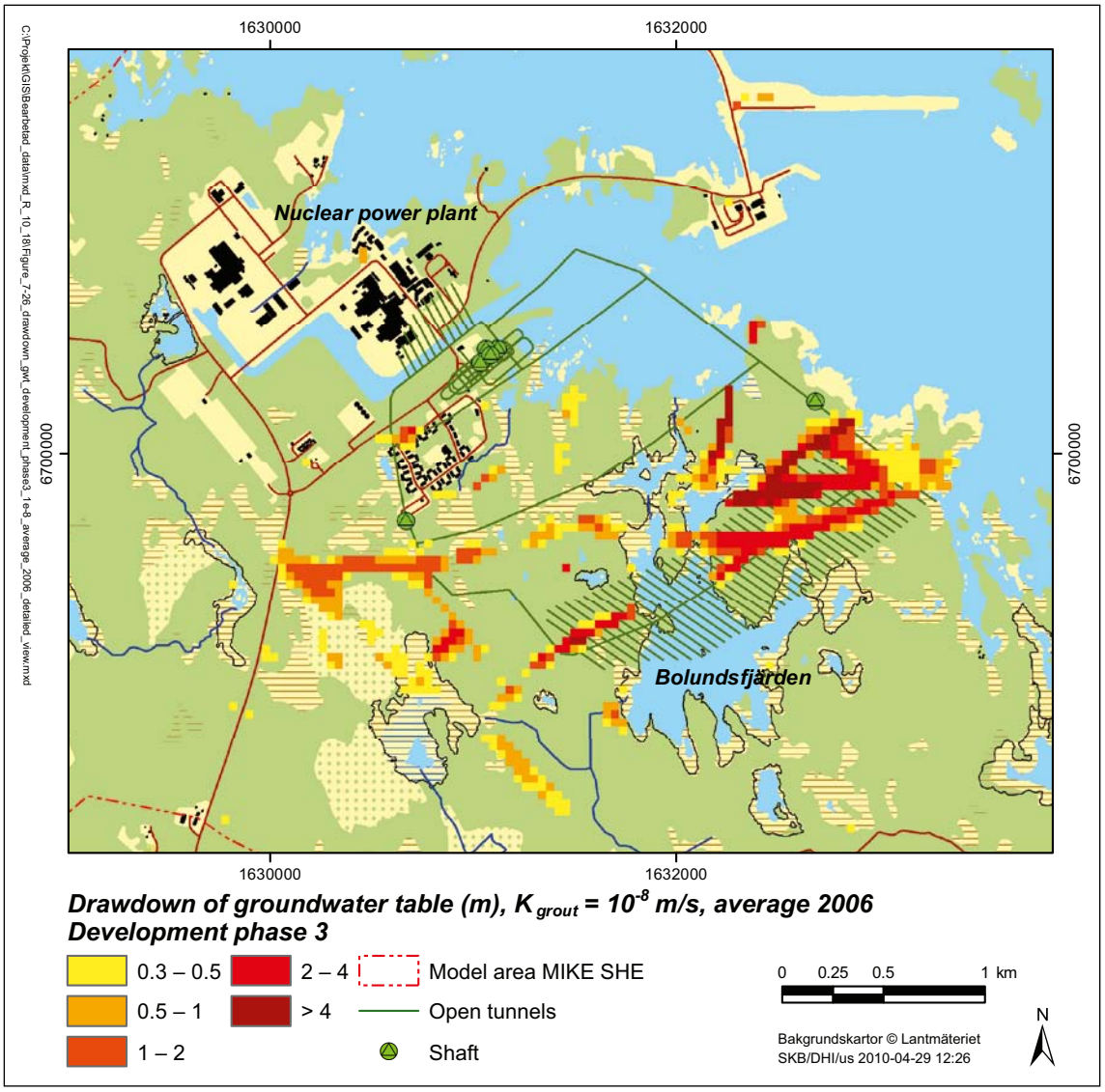

Figure 7-36. *Groundwater-table drawdown during development phase 3, $K_{grout} = 10^{-8}$ m/s.*

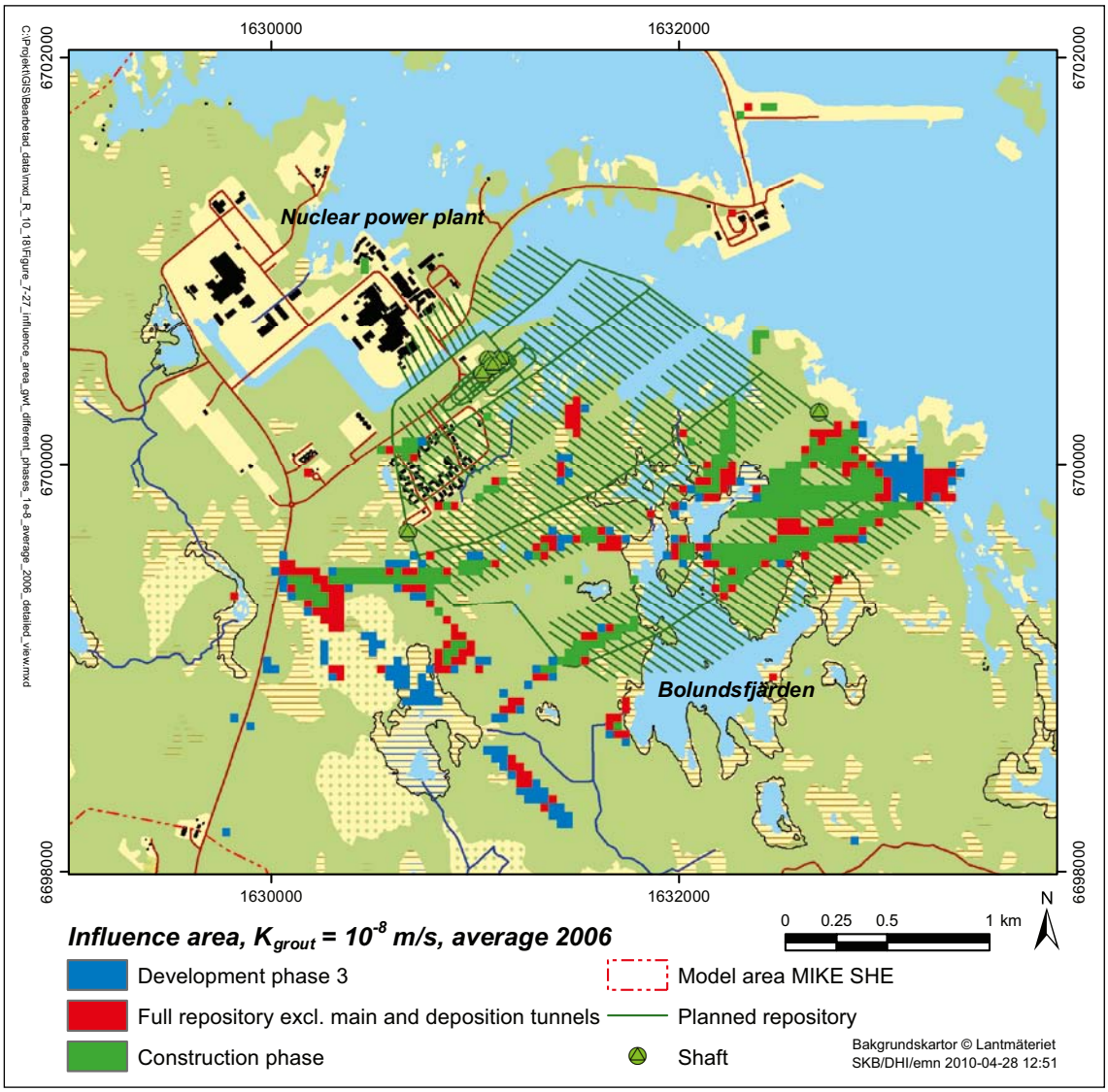

Figure 7-37. *Influence area (groundwater-table drawdown > 0.3 m) during development phase 3 (blue, red and green areas), development phase 3 excluding main and deposition tunnels (red and green areas) and the construction phase (green areas),* $K_{grout} = 10^{-8}$ *m/s.*

Table 7-15. Influence areas (km²) for different limits of the groundwater-table drawdown for different development phases and values of K_{grout}.

	K_{grout} (m/s)	> 0.1 m	> 0.3 m	> 0.5 m	> 1 m	> 2 m	> 4 m
Construction phase (phase 0)	10^{-7}	1.88	0.92	0.69	0.46	0.22	0.04
Construction phase (phase 0)	10^{-8}	0.93	0.45	0.25	0.08	0.01	0.00
Fully open, excl. main and deposition tunnels	10^{-8}	1.49	0.76	0.55	0.32	0.16	0.03
Development phase 3	10^{-8}	1.85	0.99	0.67	0.43	0.24	0.08
Fully open	10^{-8}	1.96	1.05	0.72	0.47	0.27	0.10

7.6 Present SFR and the SFR extension

As mentioned in Section 4.3.2 an extension of SFR (final repository for short-lived radioactive waste) is planned. The SFR repository is here simply referred to as "SFR", whereas the deep-rock repository for spent nuclear fuel is denoted "repository". The present SFR layout is implemented in the MIKE SHE model (using the modelling tool MOUSE), both for undisturbed (Chapter 6) and disturbed conditions (Chapter 7). This section investigates the impact of SFR and its planned extension in terms of the groundwater-table drawdown (Section 7.6.2) and drawdown of hydraulic heads in the upper part of the bedrock (Section 7.6.3). A simulation case for natural conditions is used as reference, i.e. the conditions without SFR. Moreover, simulations have been run considering an extended SFR, both with and without the repository. Section 7.6.1 presents the model-calculated groundwater inflow to each facility, including the present SFR, an extended SFR and the repository.

It should be noted that /Mårtensson et al. 2010/ present similar modelling results, using the model setup of /Gustafsson et al. 2009/. The present MIKE SHE model is an update compared to /Gustafsson et al. 2009/, including an improved coupling routine between MIKE SHE and MOUSE and an updated hydrogeological model of the bedrock (see Chapter 4). Therefore, the present SFR modelling results supersede those of /Mårtensson et al. 2010/.

7.6.1 Groundwater inflow to SFR and the repository

Table 7-16 presents the model-calculated groundwater inflow for different combinations of SFR and the repository. The measured groundwater inflow to SFR is 6 L/s /Johansson 2008/, whereas the calculated inflow is 5.7 L/s for a hydraulic conductivity of the grouted zone at the present SFR ($K_{grout, SFR}$) of $2.5 \cdot 10^{-9}$ m/s. More than 50% of the calculated inflow occurs in MIKE SHE layer 6 (60–80 m.b.s.l.) where most of the underground parts of SFR are located.

Table 7-16. Groundwater inflow (L/s) for different combinations of SFR and the repository, for $K_{grout, SFR\text{-}ext} = K_{grout} = 10^{-8}$ m/s. Results are presented for each MIKE SHE calculation layer.

Calculation layer	Lower level (m.b.s.l.)	Present SFR	Extended SFR	Present SFR and open repository	Extended SFR and open repository
Layer 1–3	20	0.1	0.1	0.1	0.1
Layer 4	40	0.4	0.4	1.0	1.0
Layer 5	60	0.7	4.4	1.2	4.7
Layer 6	80	3.3	4.5	5.1	6.2
Layer 7	100	0.3	0.3	1.2	1.2
Layer 8	120	0.6	0.5	5.5	5.4
Layer 9	140	0.4	0.4	0.8	0.8
Layer 10	160	0.0	0.0	0.5	0.5
Layer 11	180	0.0	0.0	0.5	0.5
Layer 12	200	0.0	0.0	0.6	0.6
Layer 13	300	0.0	0.0	0.7	0.7
Layer 14	400	0.0	0.0	0.8	0.8
Layer 15	500	0.0	0.0	18.0	18.0
Layer 16	600	0.0	0.0	0.0	0.0
Layer 17	700	0.0	0.0	0.0	0.0
Layer 18	800	0.0	0.0	0.0	0.0
Layer 19	900	0.0	0.0	0.0	0.0
Layer 20	1,000	0.0	0.0	0.0	0.0
Layer 21	1,100	0.0	0.0	0.0	0.0
Layer 22	1,200	0.0	0.0	0.0	0.0
Present SFR		5.7	5.4	5.3	5.1
SFR extension		–	5.1	–	4.8
Open repository		–	–	30.5	30.5
Sum		**5.7**	**10.5**	**35.9**	**40.4**

An extended SFR, with a hydraulic conductivity of the grouted zone at the extended part ($K_{grout, SFR\text{-}ext}$) of 10^{-8} m/s, yields a calculated total inflow of 10.5 L/s. About half of the total inflow (5.4 L/s) occurs at the present part of SFR and 5.1 L/s at the extension. Hence, in the case with an extended SFR the inflow to the present part of SFR decreases with 0.3 L/s compared to the present inflow. According to Table 7-16 the inflow to the SFR extension mainly occurs in layers 5 and 6 (40–80 m.b.s.l.).

The simulation case with an extended SFR and a fully open repository ($K_{grout} = 10^{-8}$ m/s) yields a total groundwater inflow to SFR and the repository of 40.4 L/s. In this case the inflow to the present part of SFR is 5.1 L/s, the inflow to the extension is 4.8 L/s, and the inflow to the repository is 30.5 L/s. The simulation case that combines the present SFR and the repository ($K_{grout} = 10^{-8}$ m/s) yields the same inflow to the repository, which shows that an extension of SFR will not affect the inflow to the repository compared to the situation with the present SFR. On the other hand, according to the modelling results the repository will affect the inflow to SFR and also the inflow to its planned extension.

7.6.2 Groundwater-table drawdown

Table 7-17 presents model-calculated influence areas for different limits of the groundwater-table drawdown, for different combinations of SFR and the repository. The simulation case with natural conditions (without SFR) is used as reference. As can be seen in Table 7-17 (see also Figure 7-38) the groundwater inflow to the present SFR yields a minor drawdown of the groundwater table in areas in the vicinity of SFR and in areas north of Lake Bolundsfjärden. Note that for visibility purposes the scale of Figures 7-38 to 7-40 and 7-42 differs compared to other similar figures in this report.

The inflow to an extended SFR also yields a minor drawdown of the groundwater table, however with an influence area (for a drawdown exceeding 0.3 m) that is twice the influence area for the present SFR. Figure 7-39 shows the annual average groundwater-table drawdown for an extended SFR, using natural conditions as reference. Figure 7-40 illustrates the drawdown specifically due to the inflow to the SFR extension (essentially, this figure is the difference between Figures 7-39 and 7-38). According to Figure 7-40, the inflow to the SFR extension yields a drawdown of the groundwater table that is limited to the SFR pier.

In the case with an extended SFR and a fully open repository ($K_{grout} = 10^{-8}$ m/s) the influence area has a size of 1.10 km^2 (Figure 7-41), using natural conditions as reference. The corresponding result for the simulation case with the present SFR and the repository is 1.08 km^2 (Figure 7-42), which illustrates the very limited drawdown of the groundwater table due to the inflow to the SFR extension.

7.6.3 Hydraulic-head drawdown and vertical groundwater flow patterns

As described in Section 7.6.2, the groundwater inflow to the present SFR and the inflow to an extended SFR only yield minor drawdown of the groundwater table. According to Figures 7-43 (present SFR) and 7-44 (extended SFR), compared to the groundwater-table drawdown the inflow yields larger drawdown of hydraulic heads at the level 50 m.b.s.l. In both these figures, natural conditions (without SFR) are used as reference. As expected, the hydraulic-head drawdown is largest in the vicinity of SFR. The influence area of the hydraulic-head drawdown also comprises the bedrock below the nuclear power plant and below Lake Bolundsfjärden. Compared to the case with the present SFR (Figure 7-43), the influence area is somewhat larger in the case with an extended SFR (Figure 7-44). Figure 7-45 specifically illustrates the additional hydraulic-head drawdown due to the inflow to the SFR extension (essentially, this figure is the difference between Figures 7-44 and Figure 7-43).

Table 7-17. Influence areas (km^2) of the groundwater-table drawdown for different drawdown limits ($K_{grout} = 10^{-8}$ m/s). Natural conditions (without SFR) are used as reference.

	> 0.1 m	> 0.3 m	> 0.5 m	> 1 m	> 2 m	> 4 m
Present SFR	0.16	0.02	0.01	0.00	0.00	0.00
Extended SFR	0.32	0.04	0.02	0.00	0.00	0.00
Present SFR & open repository	2.07	1.08	0.74	0.48	0.27	0.11
Extended SFR & open repository	2.12	1.10	0.78	0.49	0.28	0.12

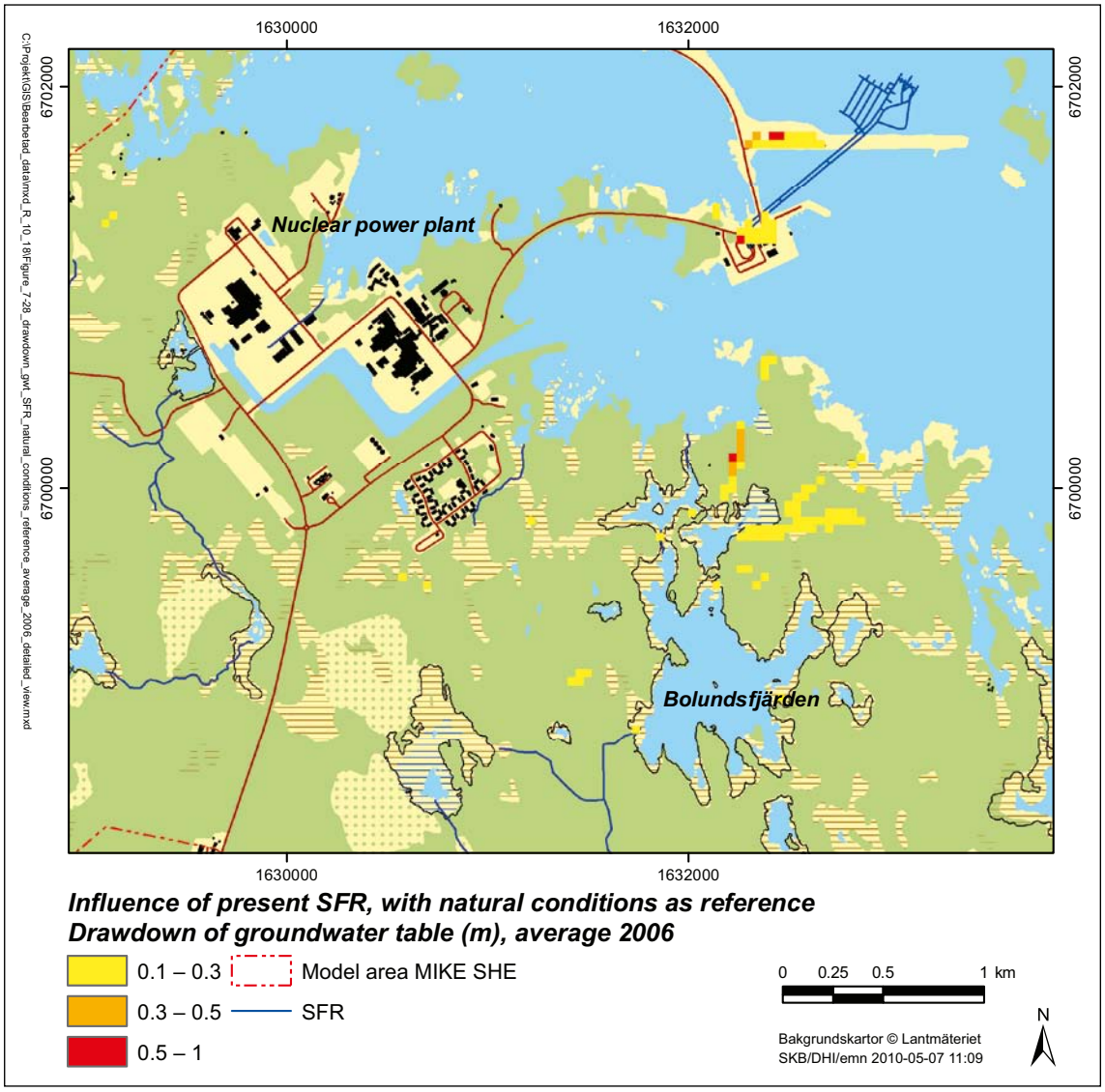

Figure 7-38. *Groundwater-table drawdown due to the groundwater inflow to the present SFR. Natural conditions (without SFR) are used as reference.*

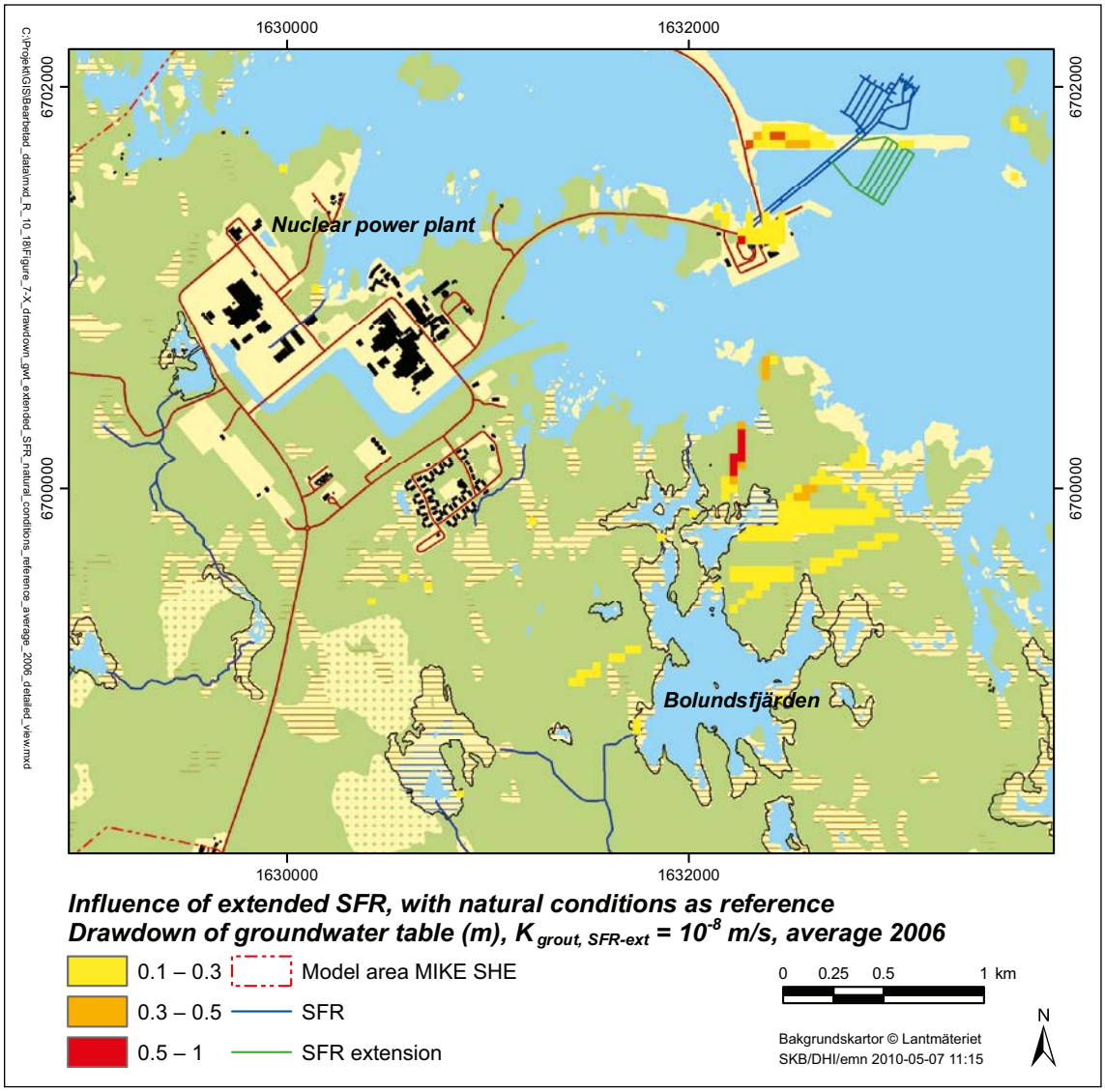

Figure 7-39. *Groundwater-table drawdown due to the groundwater inflow to an extended SFR, $K_{grout,\ SFR\text{-}ext} = 10^{-8}$ m/s. Natural conditions (without SFR) are used as reference.*

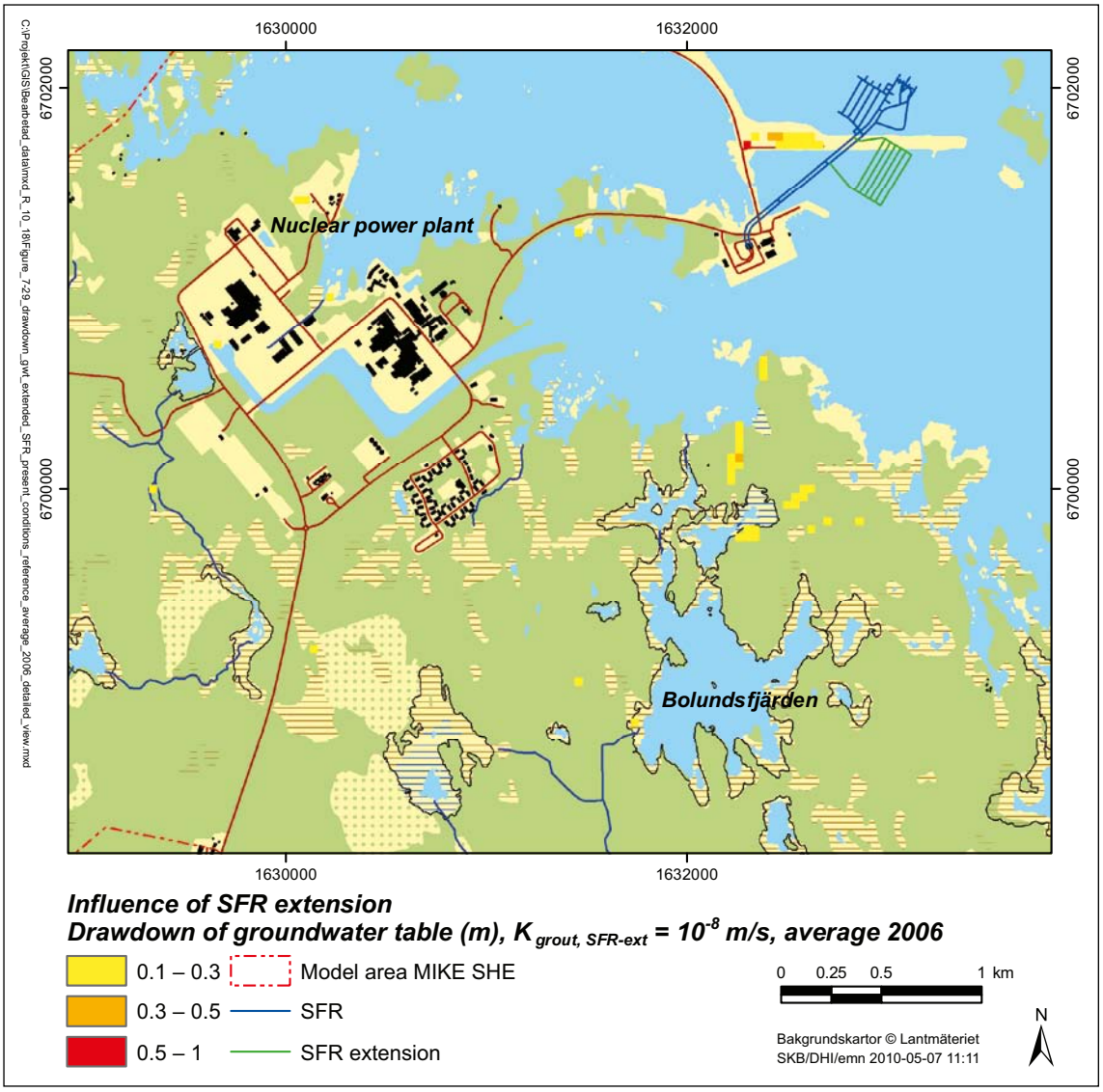

Figure 7-40. *Groundwater-table drawdown due to the groundwater inflow to the SFR extension, $K_{grout, SFR\text{-}ext} = 10^{-8}$ m/s. Present conditions (with present SFR) are used as reference.*

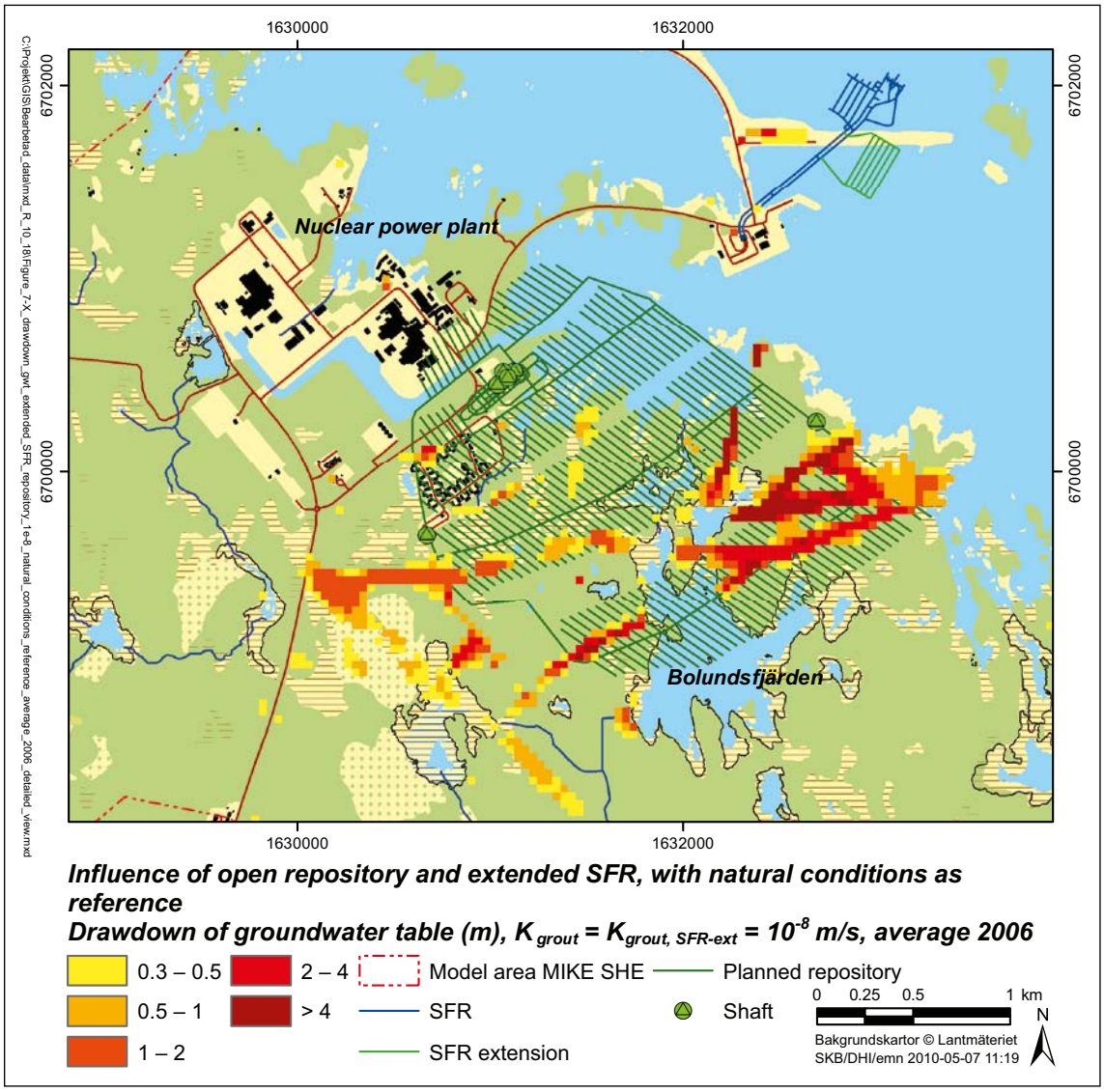

Figure 7-41. *Groundwater-table drawdown due to the groundwater inflow to the repository and an extended SFR, $K_{grout} = K_{grout,\ SFR\text{-}ext} = 10^{-8}$ m/s. Natural conditions (without SFR) are used as reference.*

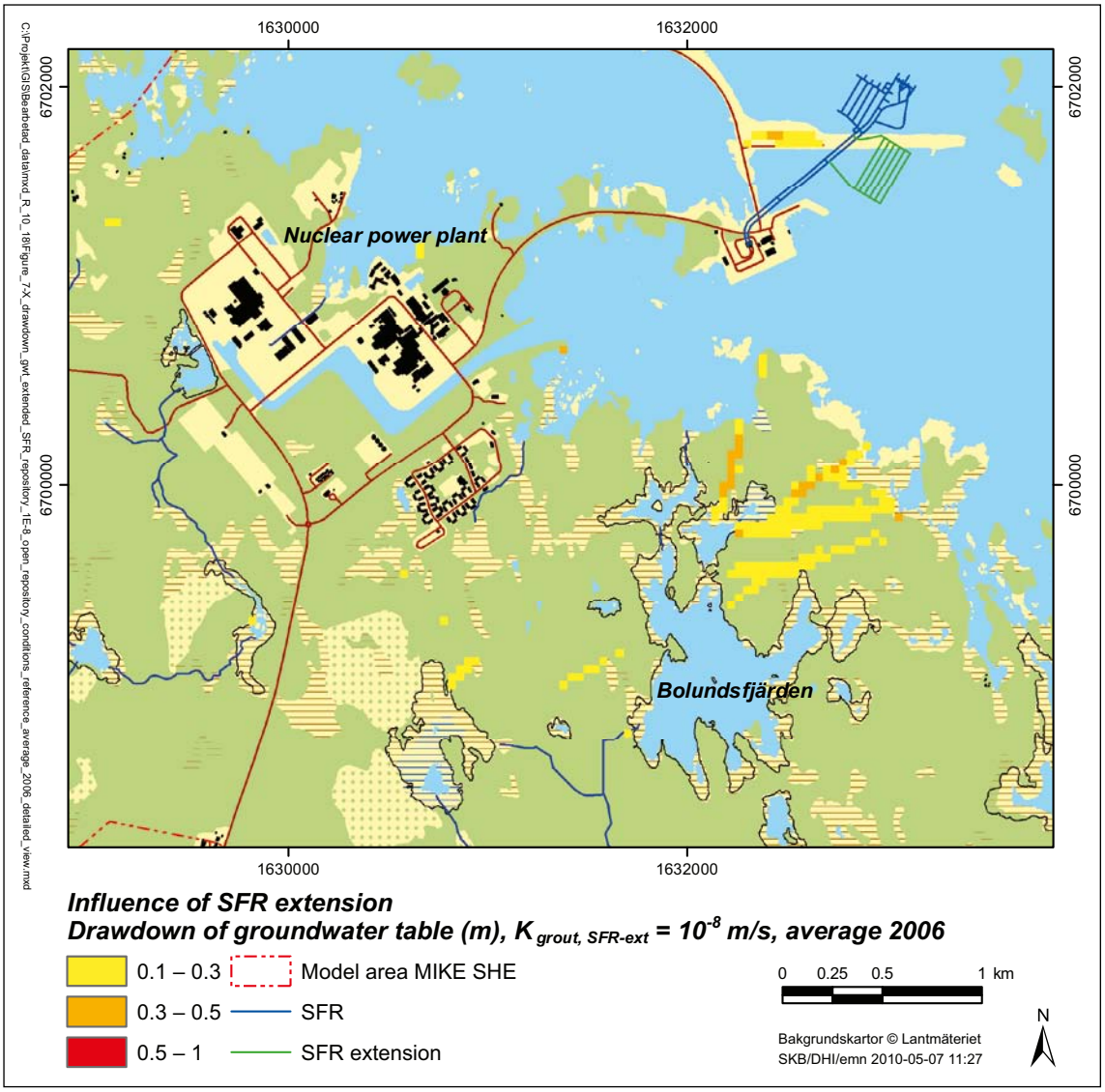

Figure 7-42. *Groundwater-table drawdown due to the groundwater inflow to the SFR extension, with the repository and an extended SFR, $K_{grout} = K_{grout,\ SFR\text{-}ext} = 10^{-8}$ m/s. The conditions with the repository and the present SFR are used as reference.*

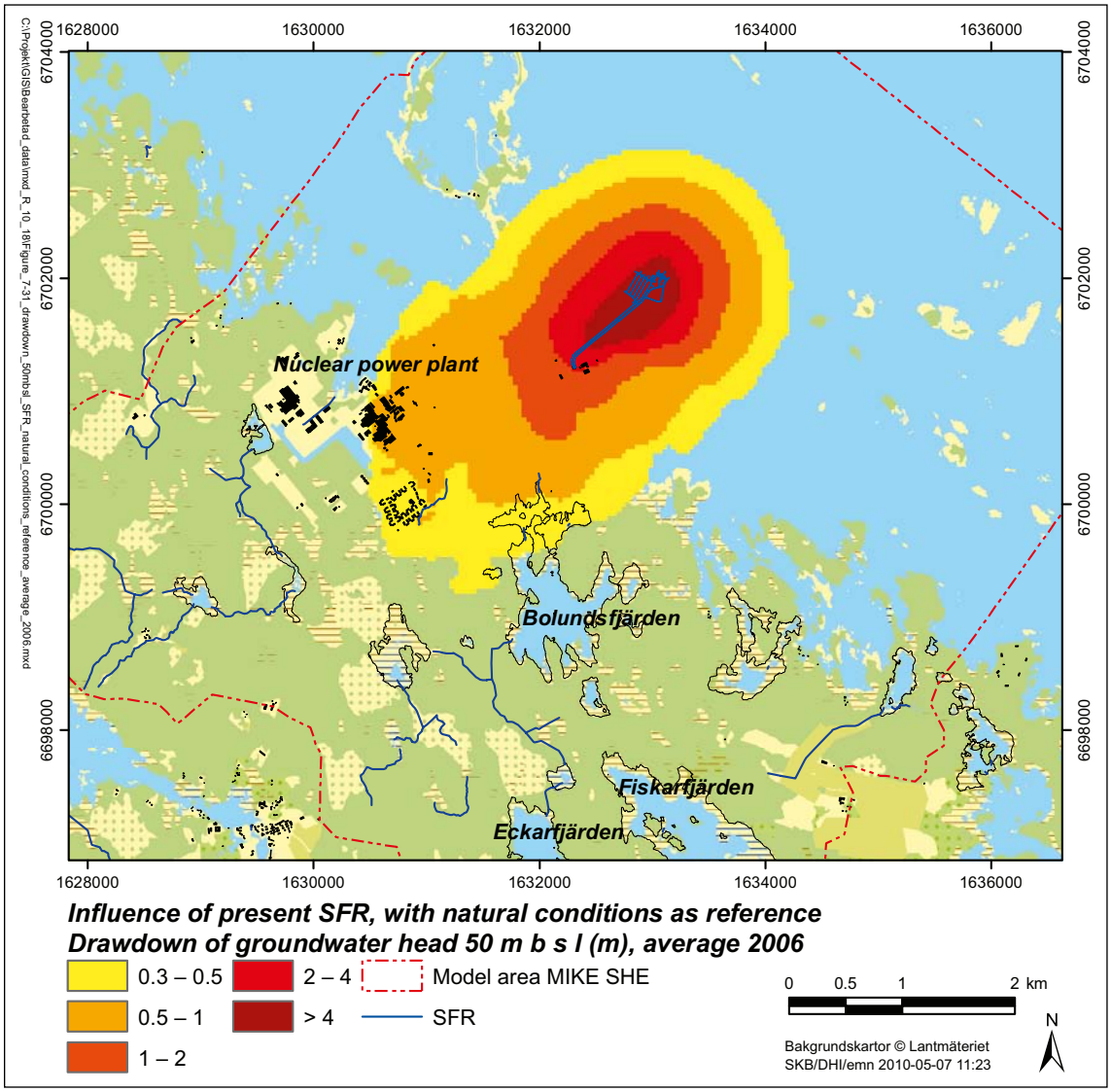

Figure 7-43. *Hydraulic-head drawdown at the level 50 m.b.s.l. due to the groundwater inflow to the present SFR. Natural conditions (without SFR) are used as reference.*

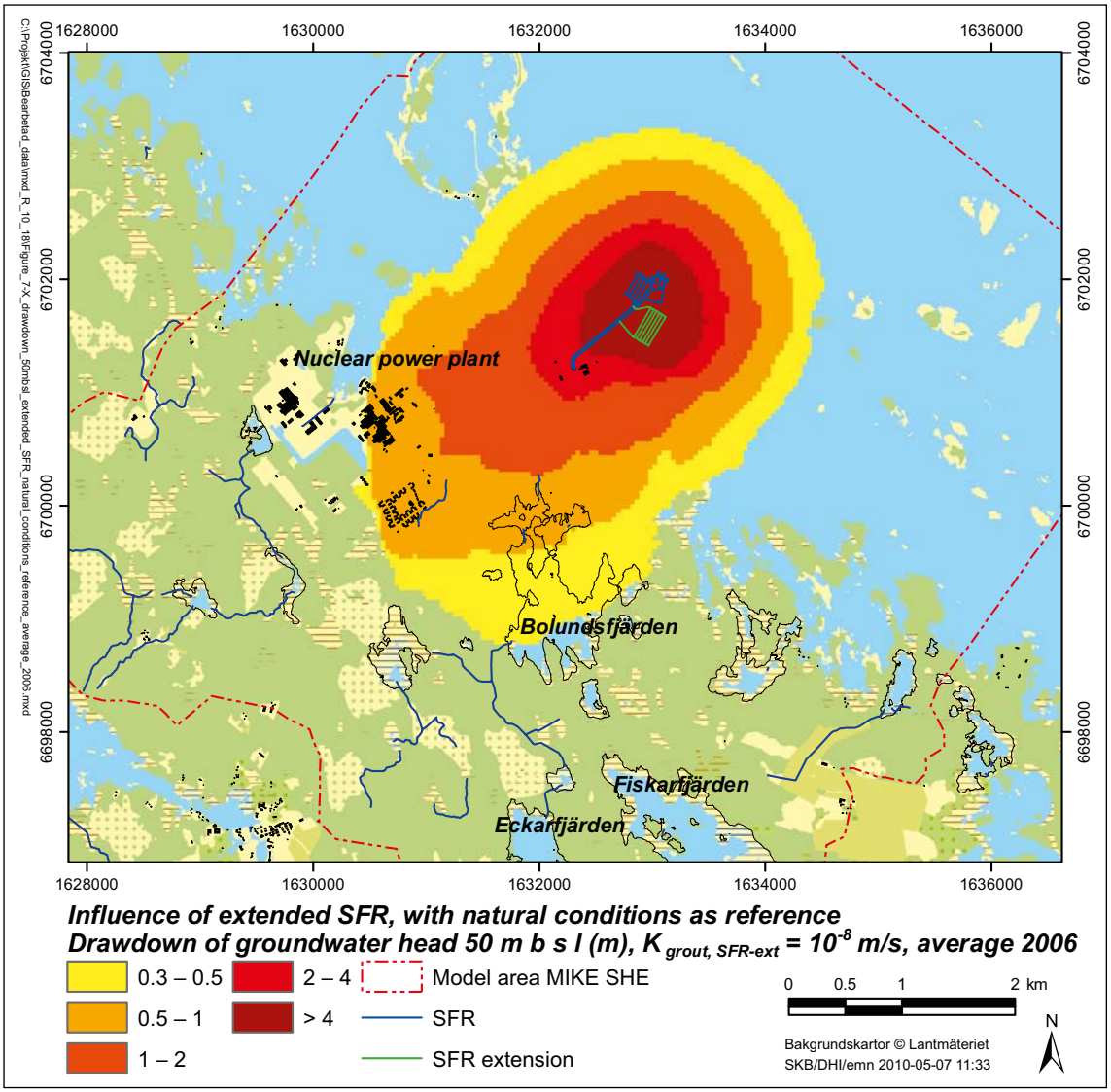

Figure 7-44. *Hydraulic-head drawdown at the level 50 m.b.s.l. due to the groundwater inflow to an extended SFR, $K_{grout,\ SFR\text{-}ext} = 10^{-8}$ m/s. Natural conditions (without SFR) are used as reference.*

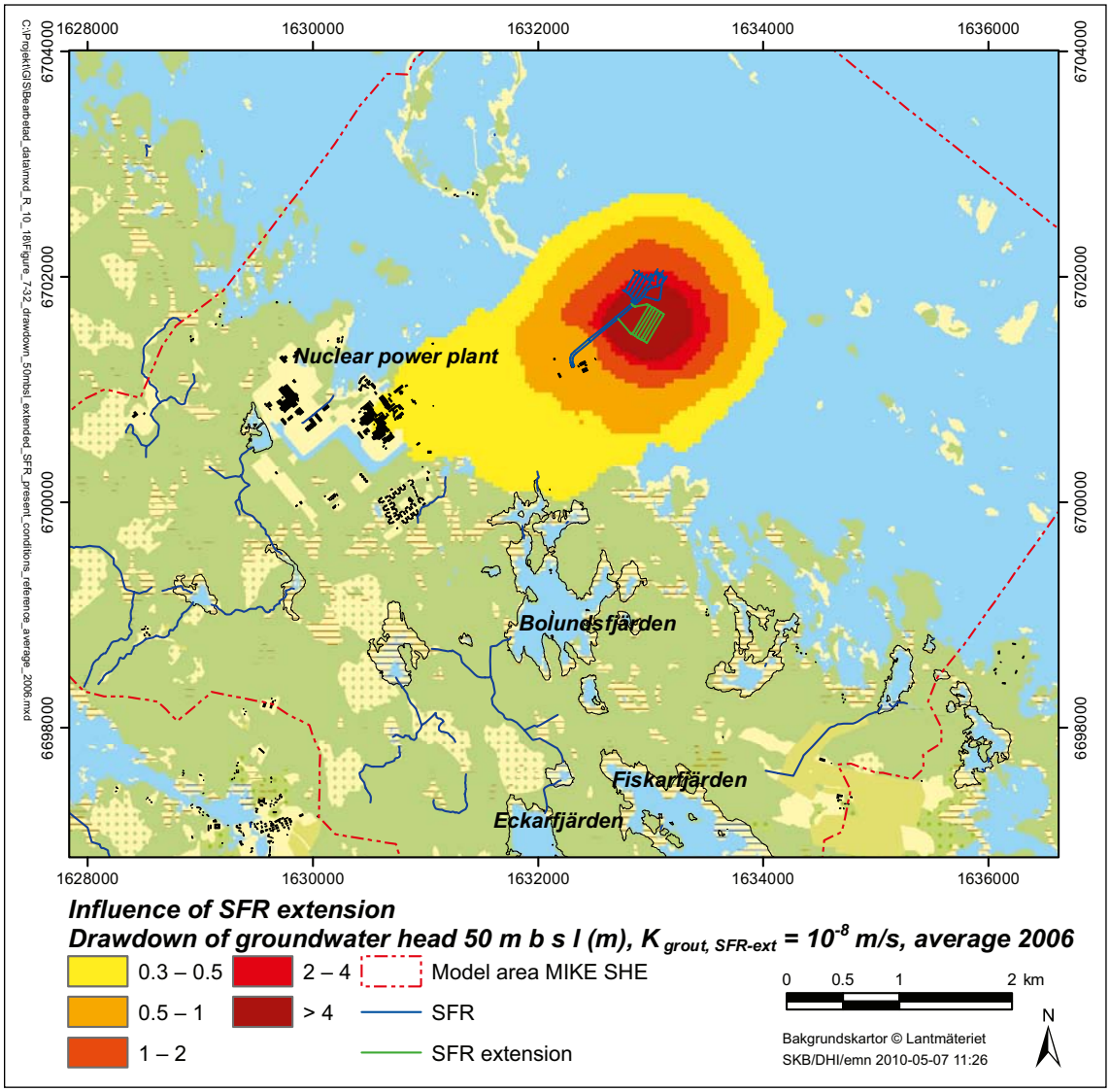

Figure 7-45. *Hydraulic-head drawdown at the level 50 m.b.s.l. due to the groundwater inflow to the SFR extension, $K_{grout,\ SFR\text{-}ext} = 10^{-8}$ m/s. Natural conditions (without SFR) are used as reference.*

Figure 7-46 shows the hydraulic-head drawdown for the simulation case that combines an extended SFR and the repository, using natural conditions as reference. According to the figure, the drawdown reaches the model boundary in the northwest and southwest. Compared to the case that combines the present SFR and the repository (Figure 7-18), for the former case the influence area is 4% larger, which hence is due to the inflow to the SFR extension. Figure 7-47 specifically illustrates the drawdown due to the SFR extension.

Section 7.5 discusses the importance of fracture zones with high vertical hydraulic conductivity and the importance of the sheet joints for the drawdown of hydraulic heads in the bedrock. Figure 7-48 shows model-calculated vertical groundwater flow rates (mm/day) at the level 50 m.b.s.l. for natural conditions (upper map) and for present conditions (lower map), i.e. with the existing SFR. According to this figure, both upward and downward flow rates are highest along the vertical fracture zones. For natural conditions (without SFR and the repository) there is upward groundwater flow below most of the sea within the model area. For the simulation case with the present SFR, the situation is the opposite with downward groundwater flow below the sea and a "cone" of downward flow in the bedrock around SFR. The small area with upward flow in the southern part of SFR is due to the inflow to those parts of SFR that are located above 50 m.b.s.l. The inflow to SFR has an impact of vertical groundwater-flow directions also in areas at the MIKE SHE model boundary.

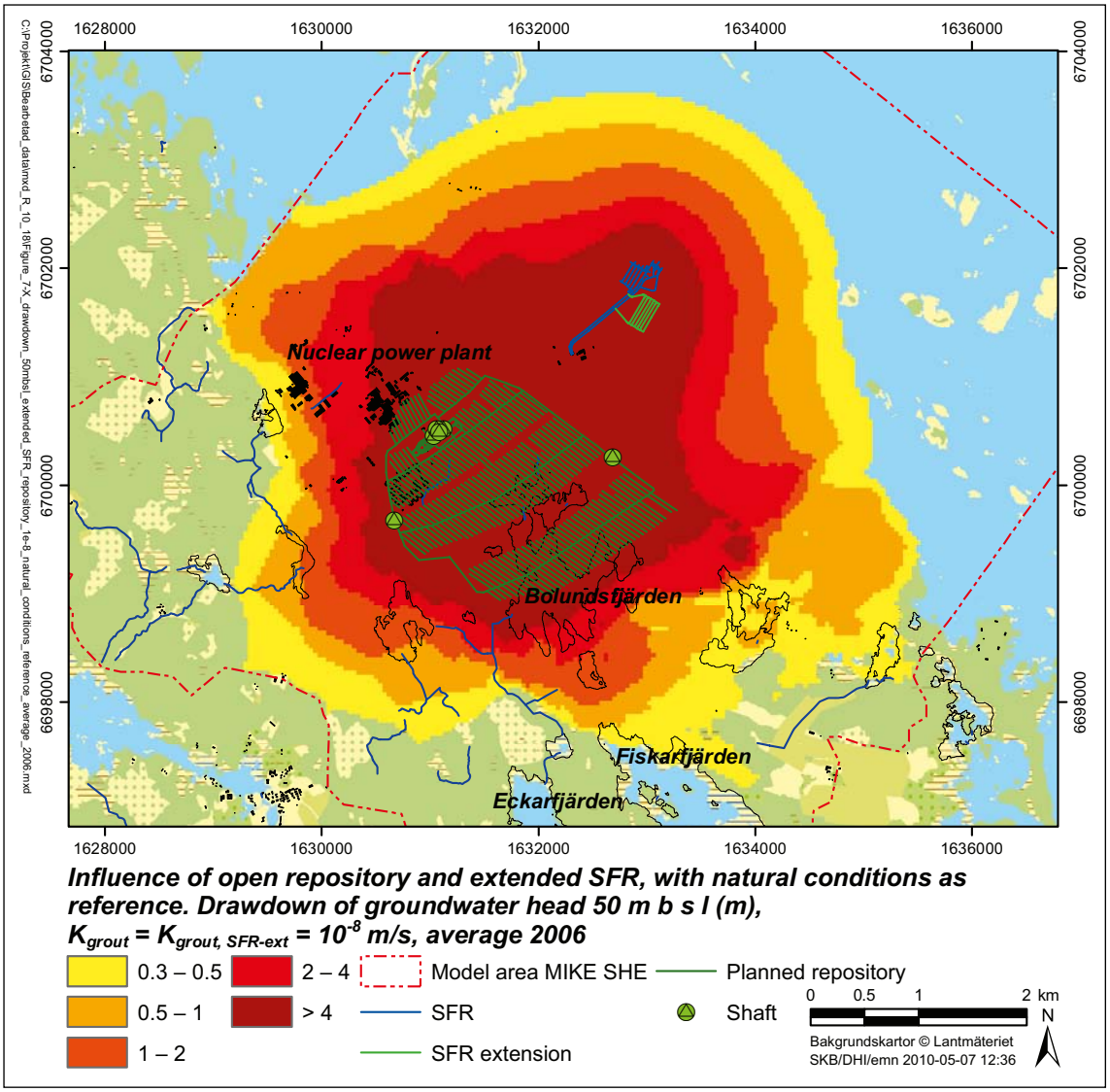

Figure 7-46. *Hydraulic-head drawdown at the level 50 m.b.s.l. due to the groundwater inflow to the repository and an extended SFR, $K_{grout} = K_{grout, SFR-ext} = 10^{-8}$ m/s. Natural conditions (without SFR) are used as reference.*

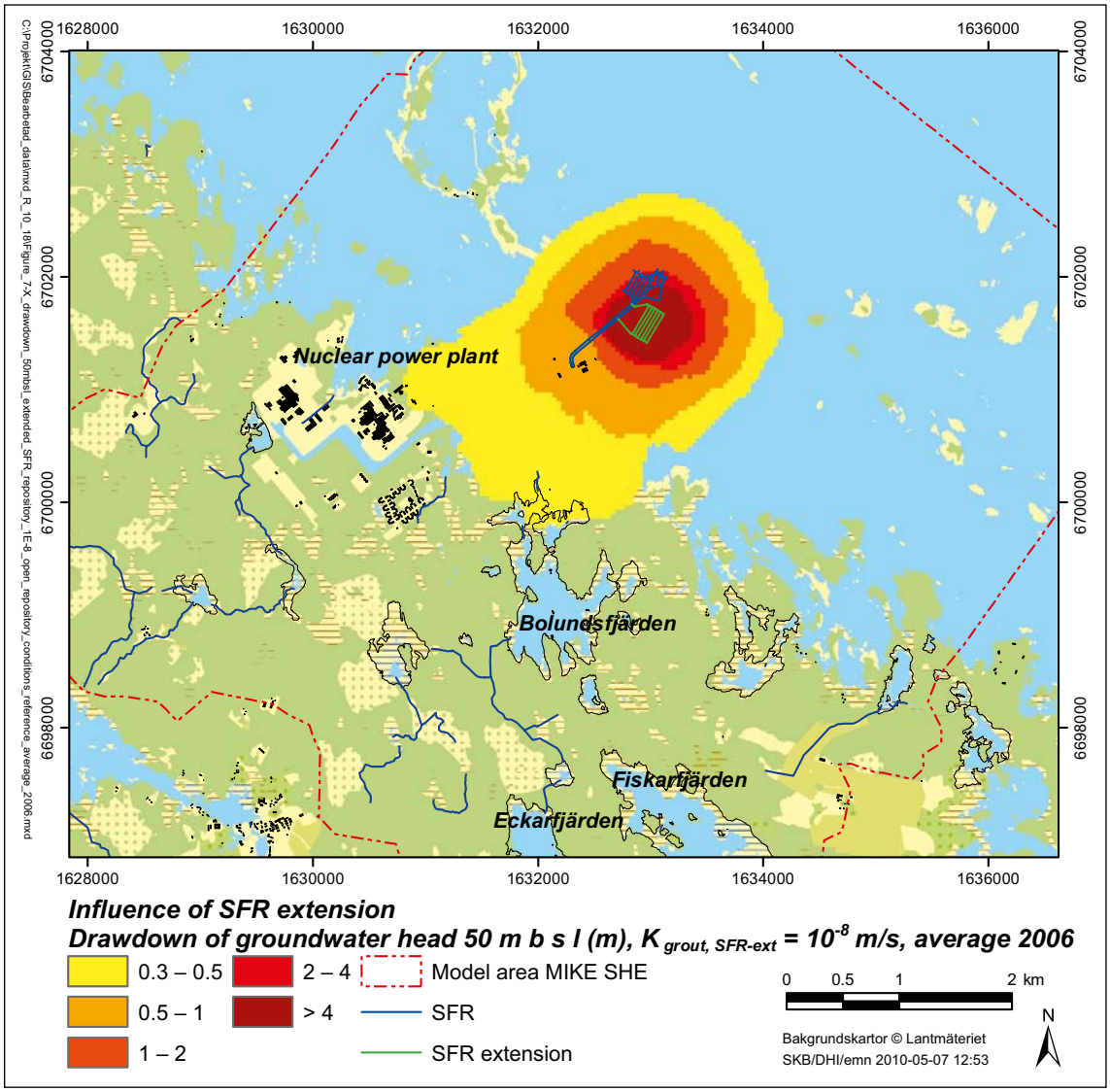

Figure 7-47. *Hydraulic-head drawdown at the level 50 m.b.s.l. due to the groundwater inflow to the SFR extension, for a simulation case that includes the repository and an extended SFR, $K_{grout} = K_{grout,\ SFR\text{-}ext} = 10^{-8}$ m/s. The conditions with the repository and the present SFR are used as reference.*

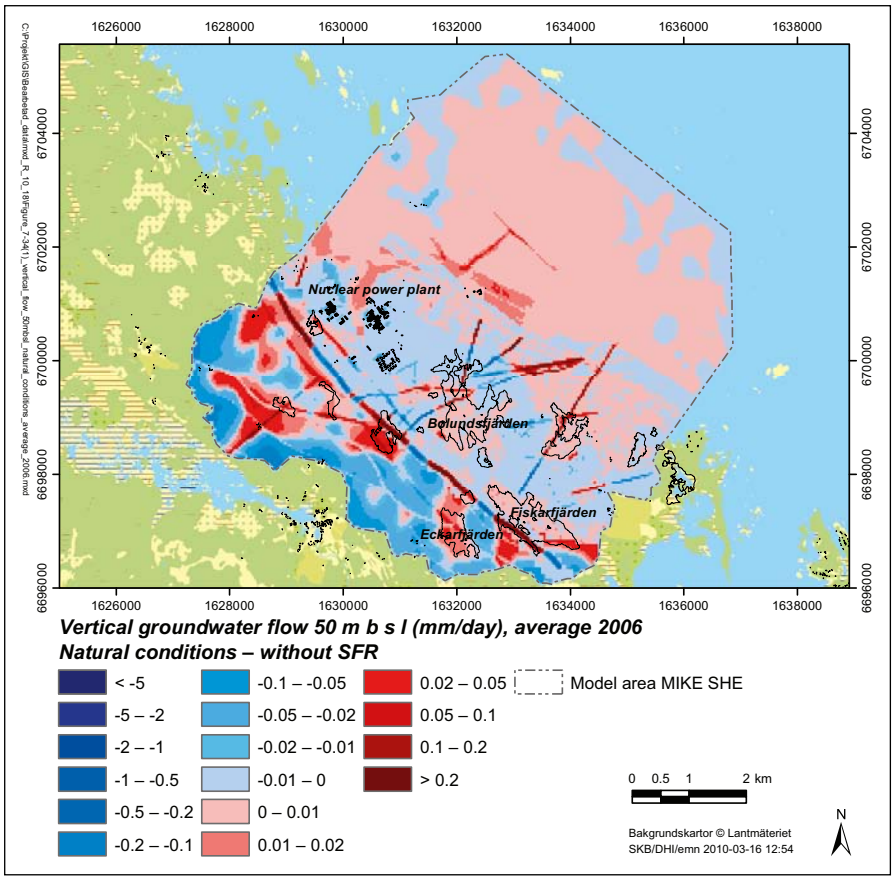

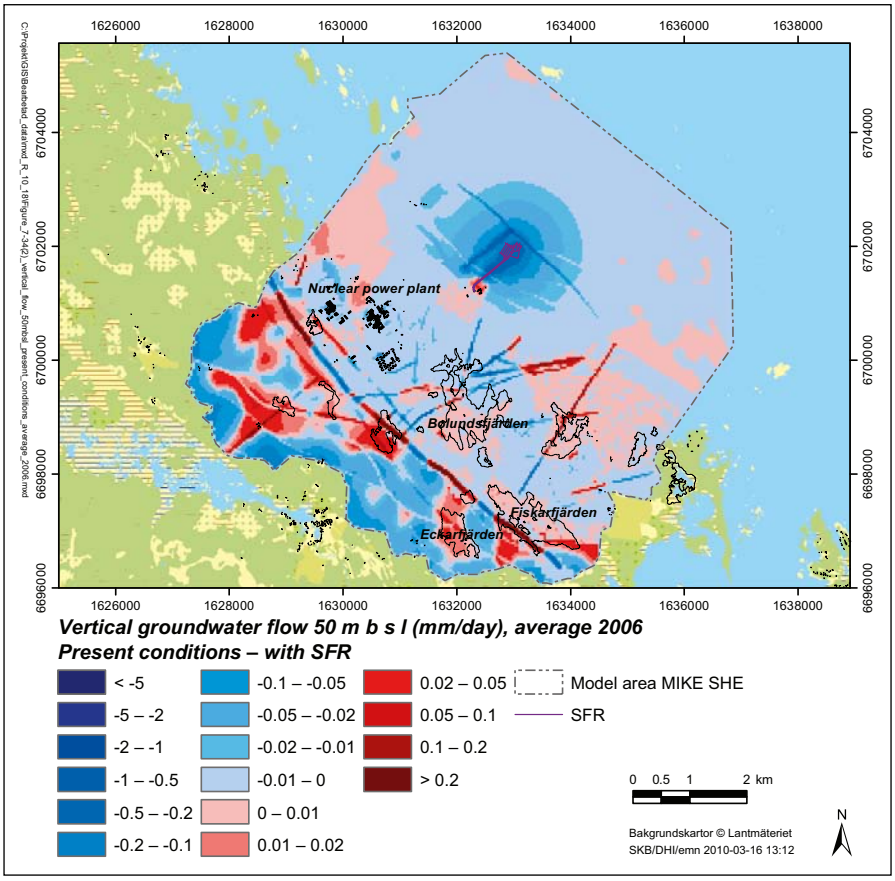

Figure 7-48. *Vertical groundwater flow (mm/day) in calculation layer 5 (50 m.b.s.l.), for natural conditions without SFR (upper map) and present conditions with existing SFR (lower map). Blue colours indicate downward flow and red colours indicate upward flow.*

However, the modelling results presented in Section 7.1 (Table 7-3) show that for undisturbed conditions, the horizontal groundwater flow across the model boundary is very small.

The upper map of Figure 7-49 shows the model-calculated vertical groundwater flow for the simulation case with an extended SFR, whereas the lower map shows the corresponding results for the simulation case also including the repository ($K_{grout} = 10^{-8}$ m/s). In the case with an extended SFR, the downward flow around SFR is larger compared to present conditions with present SFR (lower map of Figure 7-48). In this simulation case, there is no upward groundwater flow at the southern part of SFR. In the land area close to the sea, in some fracture zones the vertical groundwater flow has a different direction compared to the case with the present SFR.

The inflow to the repository has relatively large influence on the vertical groundwater-flow pattern in the bedrock (lower map of Figure 7-49), except for the southernmost and westernmost parts of the model area. The inflow to the repository increases the magnitude of the downward groundwater flow in areas above the repository, and in this simulation case there is downward flow in the bedrock in most of the model area.

7.7 Saturation of backfill and groundwater-level recovery

7.7.1 Modelling of the backfill-saturation process

Subsequent to the operation phase the underground parts of the repository will be backfilled. The pumping that drains the repository and maintains atmospheric pressure will end, which implies that the inflowing groundwater will gradually saturate the backfill material. A modelling study was performed to evaluate the time scale of the backfill saturation process and the groundwater-level recovery. The methodology is described in Appendix 4. It should be noted that the study does not take into account the buffer that surrounds the deposited canisters in deposition holes, and neither plugs that separate tunnels.

The methodology implies that the tunnel volume is reduced to represent the total pore volume of the backfill. This is done by separating the pore volume and the solid volume of the backfill. The pore volume is used to calculate a reduced tunnel radius, whereas the solid volume is implemented as a layer with a hydraulic conductivity equal to the hydraulic conductivity of the backfill. This layer is then added to the grouted zone, which has hydraulic conductivity K_{grout} (grouting case $K_{grout} = 10^{-8}$ m/s was used here). Based on the total pore volume of the preliminary materials to be used for backfilling the repository in Forsmark, the reduced tunnel volume is c. 1 Mm^3 or slightly less than 50% of the total volume of the whole repository.

Different types of backfill materials will be used for different types of tunnels. For instance, according to preliminary plans deposition tunnels will be filled with bentonite blocks and tunnels within the central area with crushed rock (Appendix 4). If the hydraulic conductivity of the backfill for a certain tunnel is higher than K_{grout}, no additional layer is added and only the tunnel radius is reduced. It should be noted that an important simplification made in the modelling is that the whole repository is backfilled simultaneously. In reality, tunnels will continuously be backfilled during the operation phase. In addition, in order to study a worst case the initial degree of saturation in the tunnels in MOUSE was set to zero.

In MIKE SHE, the initial conditions were taken from the last time step (January 14, 2007) of a simulation for disturbed conditions with a fully open repository ($K_{grout} = 10^{-8}$ m/s) and an extended SFR. However, in the simulation neither the present SFR nor the SFR extension was included, as SFR will not be in operation at the time when the repository is backfilled. The simulation was done for a six-year period (input data from the years 2005–2006 were cycled three times). The results of a reference simulation were used as a basis for calculation of residual drawdowns. The initial conditions for the reference simulation were taken from the end of a simulation without a repository but with an extended SFR. Also in the reference simulation, neither the present SFR nor the SFR extension was included. Hence, the reference simulation represents a situation with groundwater-level recovery subsequent to the decommissioning of SFR. This approach facilitates evaluation of the groundwater-level recovery that is specifically due to the termination of the groundwater diversion from the repository.

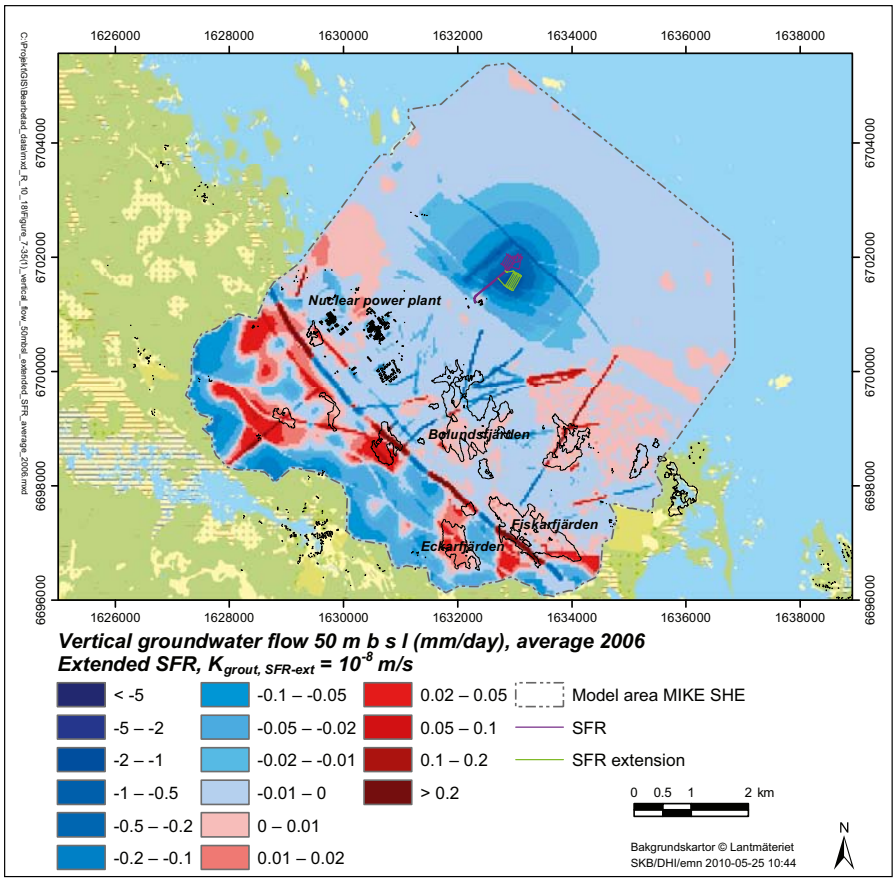

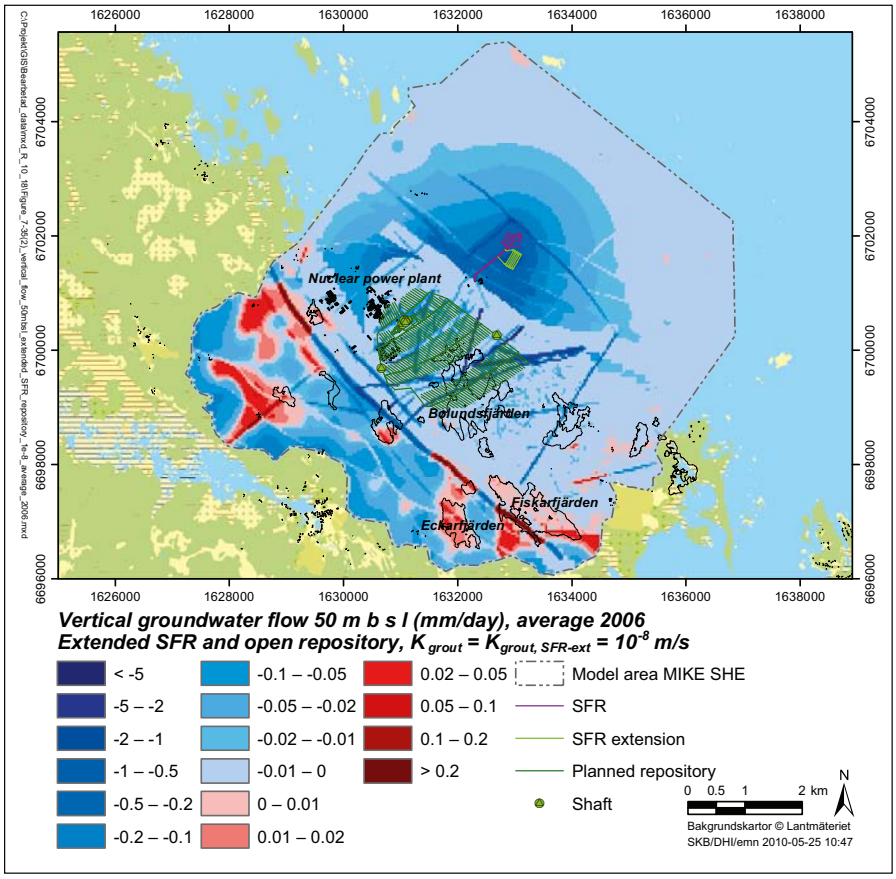

Figure 7-49. *Vertical groundwater flow (mm/day) in calculation layer 5 (50 m.b.s.l.), with an extended SFR (upper map) and an extended SFR and the repository (lower map), $K_{grout} = 10^{-8}$ m/s. Blue colours indicate downward flow and red colours indicate upward flow.*

Figure 7-50 displays the model-calculated degree of backfill saturation as a function of time after the end of groundwater diversion (time = 0 days). Unfortunately, due to numerical instabilities the simulation terminated at time = 10.5 months (c. 300 days) at which time the degree of saturation was 66%, i.e. 2/3 of the reduced tunnel volume was filled with water. It can then be estimated that the backfill is fully saturated after 14.5 months, based on an extrapolation (the dotted line) of the completed modelling results.

The model-calculated groundwater inflow to the repository (excluding the shafts) is 27.3 L/s for $K_{grout} = 10^{-8}$ m/s (see Table 7-7). With an assumed instantaneous backfilling of the repository, the groundwater inflow to the repository initially decreases as a result of the flow resistance of the backfill. This leads to an increase of the hydraulic head at repository depth, which in turn leads to an increase of the inflow. The inflow subsequently stabilises and continues at 25.9 L/s (i.e. 95% of the inflow to an open repository) until the backfill is fully saturated and the inflow drops to zero.

7.7.2 Groundwater-level recovery

In order to evaluate the recovery of the groundwater table, a separate simulation was done in which the repository simply was removed from the model. This simulation was started from the time when the saturation simulation terminated (time = 10.5 months) and the degree of saturation is 2/3 (Section 7.7.1). It is assumed that the hydraulic head in the bedrock at repository level at this time is similar to the situation with a fully saturated backfill. This assumption is based on Figure 7-50, which shows that the groundwater inflow to the repository is rather constant during the first ten months of the saturation process. When the backfill is fully saturated the groundwater inflow will terminate and the repository can hence be removed from the model.

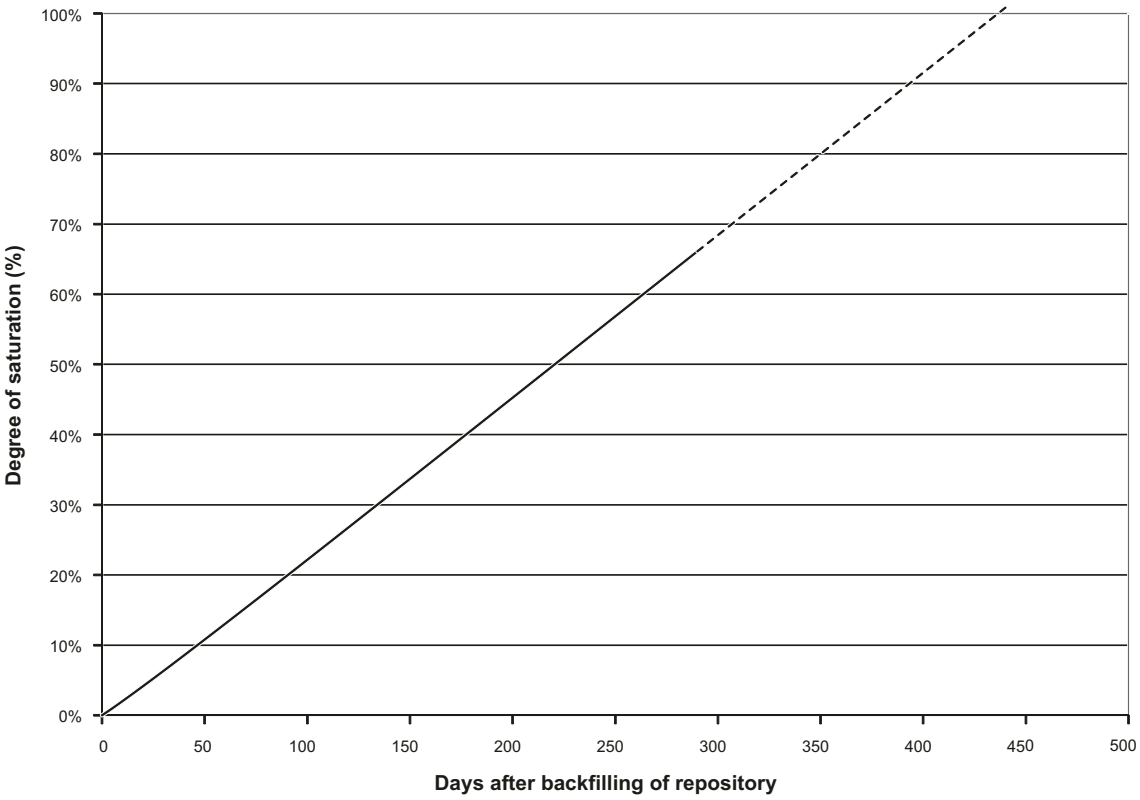

Figure 7-50. *Time-series plot of the degree of saturation (%) of the backfill after termination of pumping.*

Table 7-18 shows "residual" influence areas for a groundwater-table drawdown exceeding 0.3 m at different times after full saturation of the backfill (see the assumption above). The results show that one year after cessation of the groundwater inflow to the repository, the residual influence area is approximately one third of the influence area for disturbed conditions with inflow to the repository (columns 1 and 2). After an additional eighteen months, the residual influence area is reduced to less than 5%, mainly located to an area northeast of Lake Bolundsfjärden. According to the simulation results, full recovery of the groundwater table takes approximately three years after cessation of the inflow to the repository. It can hence be concluded that full recovery of the groundwater table takes some four years after termination of pumping from the repository.

Compared to the recovery of the groundwater table, there is a slower hydraulic-head recovery at repository level. Table 7-19 and Figures 7-51 to 7-53 show results in terms of the residual influence area for a hydraulic-head drawdown exceeding 0.3 m at the level 450 m.b.s.l., at time of full saturation of the backfill and also at subsequent times. As mentioned previously, it is assumed that the residual hydraulic-head drawdown at repository level at 2/3 degree of backfill saturation is equal to the residual drawdown at full saturation. Table 7-19 shows that the residual influence area decreases somewhat during the saturation process. According to Figure 7-51 (upper map) at full backfill saturation the influence area extends to the model boundary in the southwest, southeast and northwest. Figures 7-51 (lower map) to 7-53 show the hydraulic-head drawdown at the times 0.5, 1, 2, 4 and 6 years after full backfill saturation. After two years (Figure 7-52, lower map) the residual influence area is c. 20% of the influence area at the start of the recovery. After an additional four years (Figure 7-53, lower map) the influence area is limited to an area between the nuclear power plant and Lake Bolundsfjärden. Hence, a few more years are required for the hydraulic-head at repository level compared to the recovery of the groundwater table.

Table 7-18. Residual influence area (km^2) of the groundwater-table drawdown at different times after full saturation of the backfill. The influence area with groundwater inflow to the repository is shown for comparison (left side, $K_{grout} = 10^{-8}$ m/s).

Simulation with an open repository		Simulation of recovery after full saturation	
Date	**Influence area, drawdown > 0.3 m**	**Months after closure (October 21, 2005)**	**Influence area, drawdown > 0.3 m**
November 20th, 2006	1.28	1	1.06 (83%)
January 19th, 2006	1.04	3	0.71 (68%)
April 19th, 2006	0.93	6	0.48 (52%)
October 21th, 2006	1.33	12	0.42 (32%)
April 19th, 2006	0.93	18	0.12 (13%)
October 21th, 2006	1.33	24	0.17 (13%)
April 19th, 2006	0.93	30	0.05 (5%)

Table 7-19. Residual influence area (km^2) of the hydraulic-head drawdown at repository level prior to backfilling, at full backfill saturation and at different times after full saturation. The table also shows average and maximum hydraulic-head drawdown (m) within the influence area.

	Influence area, drawdown > 0.3 m	**Average drawdown (m)**	**Max. drawdown (m)**
Prior to backfilling	41.8	47.5	499
At full backfill saturation	41.0	46.1	472
Time after full saturation			
0.5 year	24.9	22.1	439
1 year	15.2	11.2	329
2 years	8.13	4.95	67.6
4 years	4.08	2.49	15.9
6 years	2.79	1.63	6.98

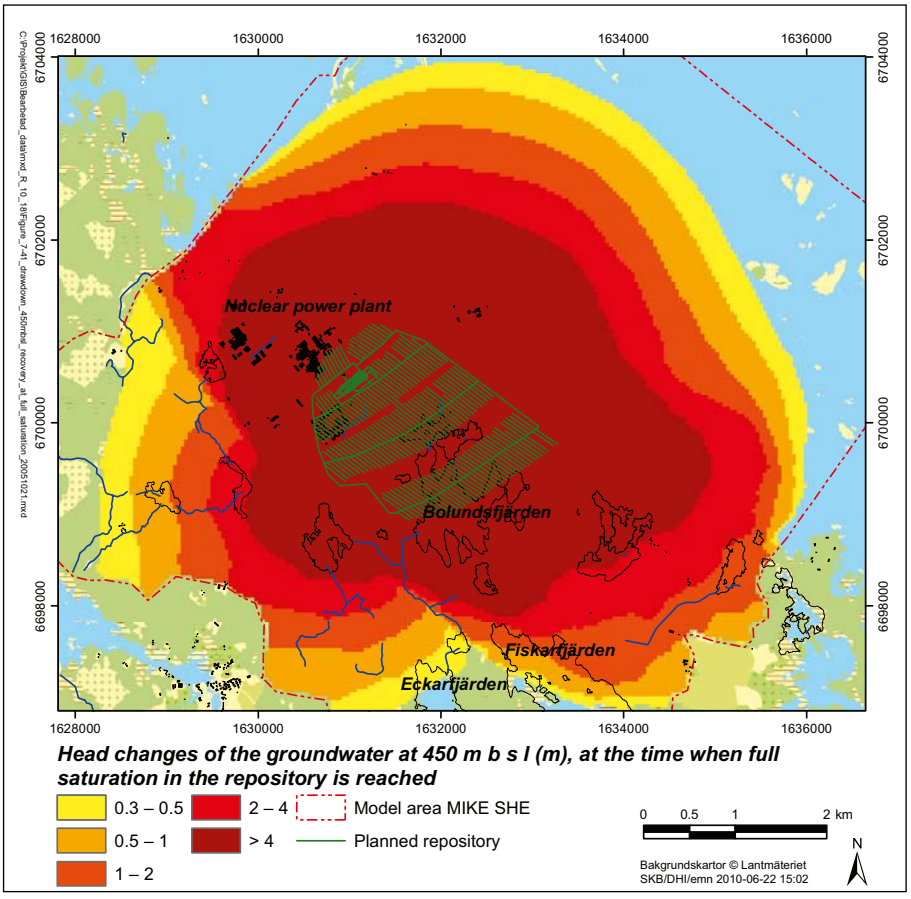

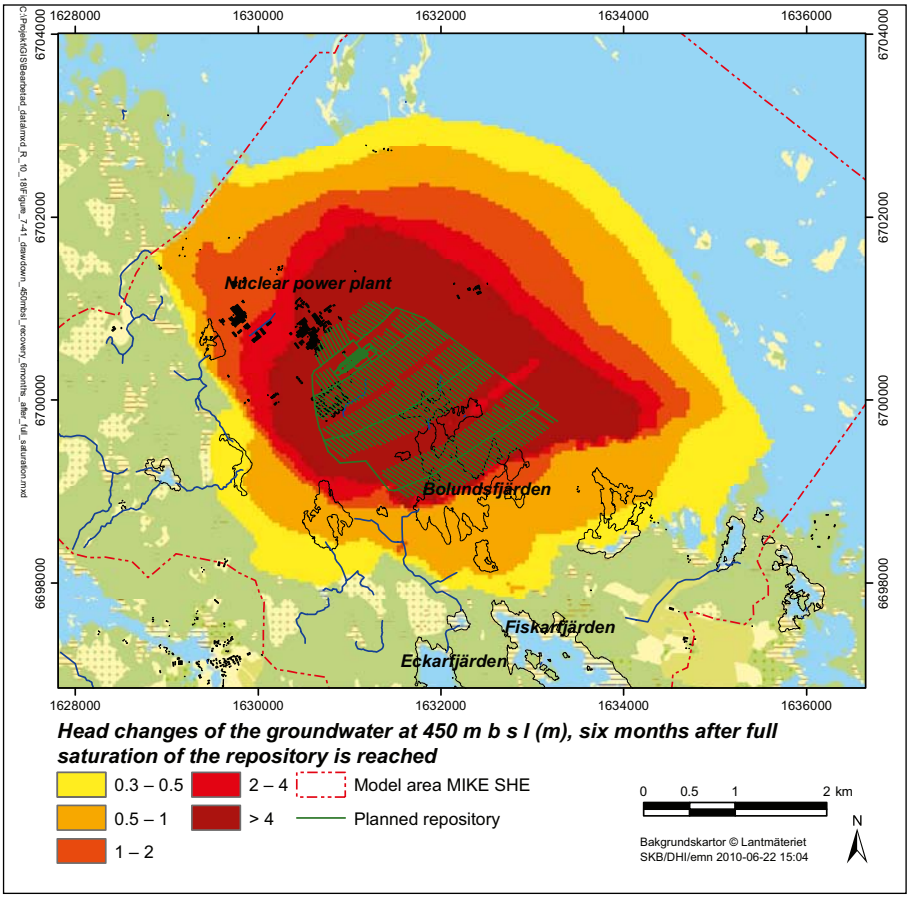

Figure 7-51. *Residual hydraulic-head drawdown at the level 450 m.b.s.l. at time of full backfill saturation (upper map) and six months after full saturation (lower map).*

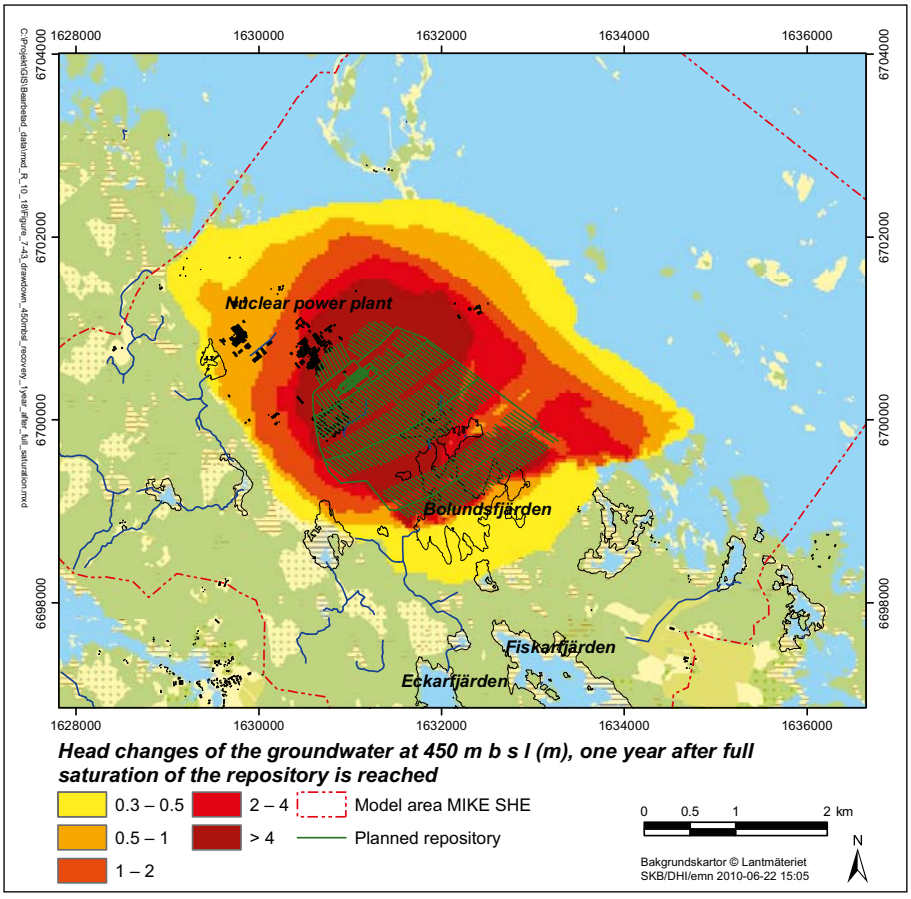

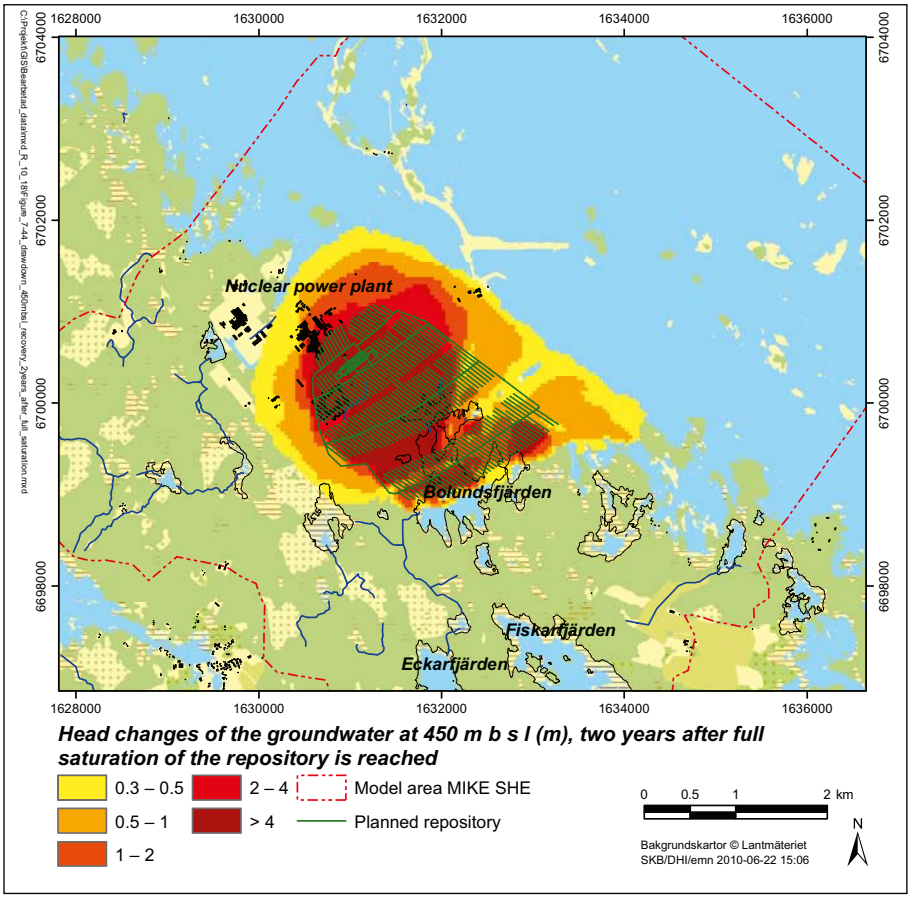

Figure 7-52. *Residual hydraulic-head drawdown at the level 450 m.b.s.l. one year (upper map) and two years (lower map) after full backfill saturation.*

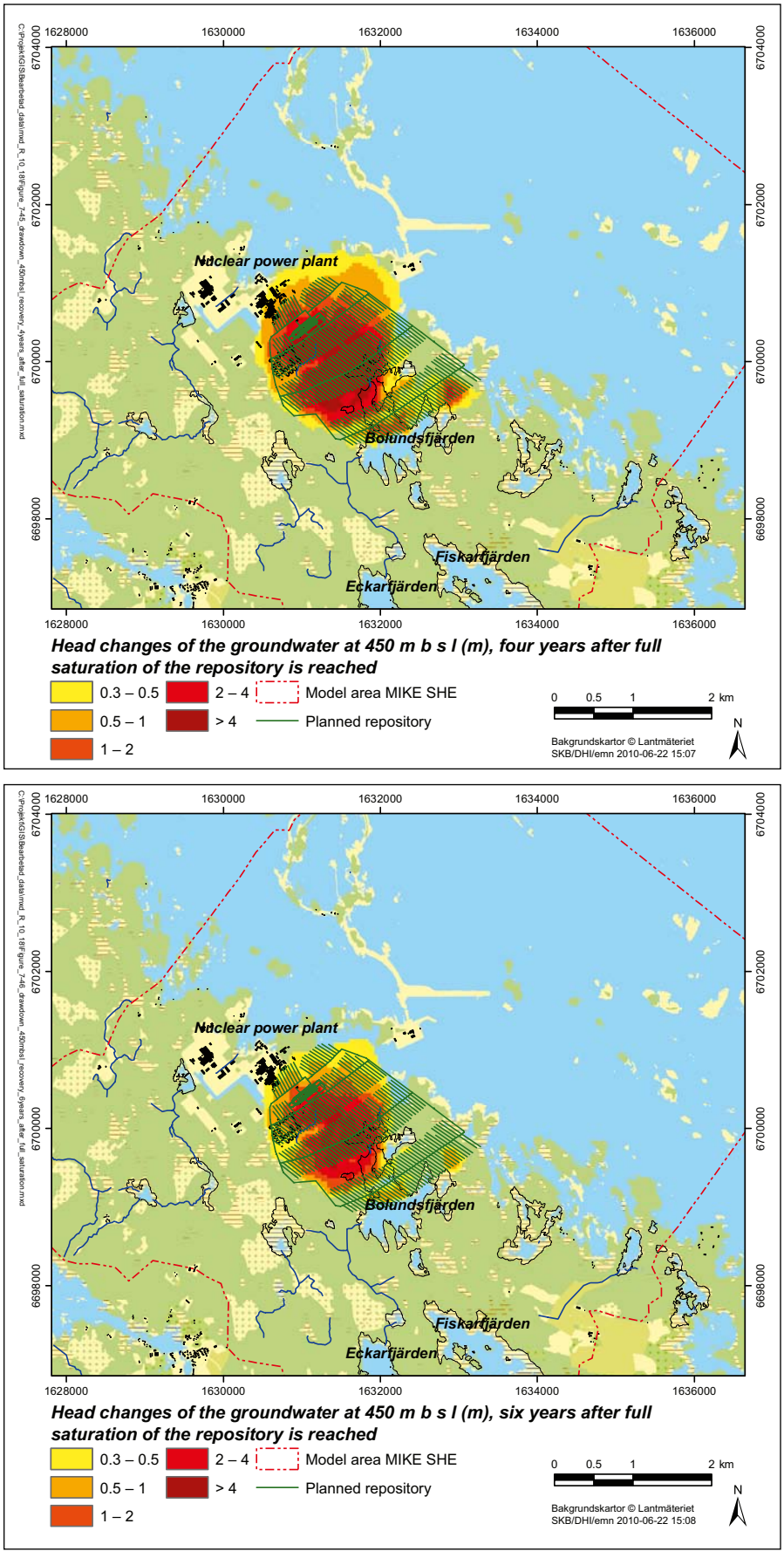

Figure 7-53. *Residual hydraulic-head drawdown at the level 450 m.b.s.l. four years (upper map) and six years (lower map) after full backfill saturation.*

8 Sensitivity analysis

The last step in the modelling process was to analyse the sensitivity of the modelling results to the hydrogeological properties of the upper bedrock, the boundary conditions, the procedure for modelling of water flow in the unsaturated zone, and a possible future scenario with an increased average sea level. A comparison was also made between the base case MIKE SHE model and a model with the upper 20 m of the model domain parameterised according to the DarcyTools model, developed in a parallel modelling activity.

8.1 Definition of simulation cases

Seven sensitivity cases have been defined and studied, both for disturbed (with the repository) and undisturbed conditions (without the repository). The sensitivity cases involve various changes of the hydrogeological properties of the bedrock and the Quaternary deposits, the boundary conditions, the procedure for modelling of water flow in the unsaturated zone, and the average sea level. The sensitivity cases are defined in Table 8-1. The "reference model" used for comparison is the updated version of the SDM-Site Forsmark MIKE SHE model described and used in Chapters 4 and 5.

It should be noted that the calibration of the MIKE SHE model (Chapter 5) also involves changes of the hydrogeological properties dataset delivered from the CONNECTFLOW modelling team, here referred to as "the original bedrock model". These changes were included in order to improve the model performance in terms of surface-water discharges and groundwater levels in the Quaternary deposits and the bedrock. For further details regarding the model calibration, see Chapter 5. The differences between the original bedrock model and the bedrock model used in the reference model are as follows:

- The horizontal hydraulic conductivity in the upper 200 m of the bedrock was increased by a factor of 5.
- The vertical hydraulic conductivity in the upper 200 m of the bedrock was decreased by a factor of 5.
- The specific storage coefficient was set to $5 \cdot 10^{-8}$ m^{-1} in all bedrock layers.

Table 8-1. Definition of simulation cases in the sensitivity analysis. Changes are compared to the reference model (i.e. the updated version of the MIKE SHE SDM-Site Forsmark model).

Sensitivity case	Description	Horizontal hydr. cond., upper 200 m of bedrock	Vertical hydr. cond., upper 200 m of bedrock
BRO-HV-Ss	Original bedrock model	K_h / 5	$K_v \cdot 5$
BRO-HV	Original bedrock model with constant specific storage	K_h / 5	$K_v \cdot 5$
BR-HV	Increased horizontal conductivity and decreased vertical conductivity	$K_h \cdot 2$	K_v / 2
BR-boundary	Specified head boundary	–	–
Darcy-20m	Parameterisation of the upper 20 m according to the DarcyTools model /Svensson and Follin 2010/	See Table 8-2	See Table 8-2
UZ-all	Simulation of all grid cells in the unsaturated zone	–	–
Sealevel-high	Increased sea level (+0.56 m) and simulation of all grid cells in the unsaturated zone	–	–

The names of the sensitivity cases listed in Table 8-1 are based on the abbreviations BRO = original bedrock, BR = bedrock, H = horizontal hydraulic conductivity, V = vertical hydraulic conductivity, Ss = specific storage, Darcy = DarcyTools, and UZ = unsaturated zone. In all cases the simulation period comprises the period 2005–2006. All of the sensitivity cases, except for case *BR-boundary*, are modelled for both undisturbed and disturbed conditions ($K_{grout} = 10^{-7}$ m/s) in order to enable calculations of drawdowns and influence areas. However, case *BR-boundary* is only modelled for disturbed conditions as the undisturbed case yields exactly the same results as the reference case.

In the first two sensitivity cases in Table 8-1 (*BRO-HV-Ss* and *BRO-HV*) the hydraulic conductivity of the bedrock are reset to those of the original bedrock model. In case *BRO-HV-Ss*, the specific storage coefficient is also reset to a spatially varying value. During the calibration process (Chapter 5) the horizontal and vertical hydraulic conductivities were changed by a factor of 10 (compared to the original bedrock model) in one of the calibration cases. The impact of these changes on the results are tested in sensitivity case *BR-HV* using a constant specific storage coefficient ($S_s = 5 \cdot 10^{-8}$ m^{-1}) in the whole bedrock.

The effect of the inflow on hydraulic heads in the bedrock is substantial, and the influence area at the level 50 m.b.s.l. reaches the model boundary, see e.g. Figure 7-18 in Section 7.5.2. Due to the no-flow boundary condition in the on-shore part of the model area, it is not possible for the repository to draw any groundwater from the model boundary. This motivates sensitivity case *BR-boundary*, in which all no-flow boundaries are changed to a prescribed head boundary condition. Time-varying hydraulic heads are for each layer obtained from the results of the reference simulation for undisturbed conditions. The boundary towards the sea is unchanged, since this boundary has a time-varying head also in the reference case.

The DarcyTools open repository modelling is focused on the bedrock and the conditions at repository depth, and includes a simplified hydrogeological description of the upper part of the bedrock and the Quaternary deposits /Svensson and Follin 2010/. Table 8-2 shows parameter values that are used for the upper 20 m of the DarcyTools model domain. As can be seen from this table the vertical hydraulic conductivity has a constant value of $K_v = 10^{-6}$ m/s, which implies that DarcyTools does not take into account the presence of vertical fracture zones in the upper 20 m of the bedrock. Sensitivity case *Darcy-20m* aims to compare the two models (MIKE SHE and DarcyTools), specifically the influence of the parameterisation of the upper 20 m of the model domain.

In order to save simulation time, only a limited number of grid cells are used in the simulation of water flow in the unsaturated zone in MIKE SHE. In the model, vertical unsaturated zone columns with the same conditions (i.e. the same soil profile, land use and depth to the groundwater table) are aggregated. From each such group, water flow is simulated along one single column (selected randomly). This is obviously a simplification, since there is a variability of the depth to the groundwater table in each group that is represented by a single column. The exceptions from this approach are areas with ponded water, i.e. lakes and wetlands (excluding the sea) in which each grid cell is used in the simulations to ensure a proper calculation of the actual evapotranspiration. Sensitivity case *UZ-all* implies that all grid cells of the unsaturated zone are used in the simulation, in order to evaluate the influence of the simplified approach with aggregated soil columns.

Table 8-2. Summary of hydraulic properties in the upper 20 m of the model in sensitivity case Darcy-20m.

Hydraulic property	Unit	Value
K_h	(m/s)	$\max[10^{-7}, 5 \cdot 10^{-3} \cdot 10^{-depth/3}]$
K_v	(m/s)	10^{-6}
Porosity	(–)	$\max[10^{-3}, 5 \cdot 10^{-2} \cdot 10^{-depth/20}]$
Specific storage	(m^{-1})	10^{-9}

Increasing temperatures due to global warming could result in a sea-level rise by thermal expansion of water and through the addition of water from the melting of continental ice. Sensitivity case *Sealevel-high* investigates the influence of an increased sea level. This was done by adding a possible sea-level rise up to year 2100 (0.56 m) to the measured sea level time-series /Brydsten et al. 2009/. In the model, the changed sea level concerns the prescribed head boundary condition in the sea part of the uppermost calculation layer and the outer sea boundary for all calculation layers. All grid cells in the unsaturated zone are simulated in this sensitivity case, similar to sensitivity case *UZ-all*. Hence, sensitivity case *UZ-all* is used as reference to case *Sealevel-high* specifically in order to evaluate the effect of an increased sea level.

8.2 Results from the sensitivity analysis

8.2.1 Evaluated output parameters

This section analyses the results of the sensitivity cases in terms of the calculated groundwater inflow to the repository, hydrological effects and drawdown of the groundwater table. The results are summarised in Table 8-3 in the form of annual averages of various output parameters (see list below), based on the abbreviations OR = open repository, Q = discharge, H = water level, S = surface water, G = groundwater.

In order to assess whether the various sensitivity cases are realistic, Table 8-3 includes comparisons of measured and model-calculated data for undisturbed conditions for the whole simulation period (the years 2005–2006). The parameters in the table are abbreviated R = correlation coefficient, ME = mean error, MAE = mean absolute error, PFM = surface-water discharge gauging station, SFM = groundwater-monitoring well (installed in the Quaternary deposits), and HFM = percussion borehole (in the bedrock). Note that a positive mean error (ME) implies that model-calculated values on average are below measured values, and the opposite for a negative ME. Also note that sensitivity case *Sealevel-high* represents a future scenario. For this case, Table 8-3 only show results concerning the influence of the open repository.

- OR Q: Groundwater inflow to a fully open repository.
- OR G 0.3: Influence area with a drawdown of the groundwater table > 0.3 m.
- OR G 1.0: Influence area with a drawdown of the groundwater table > 1.0 m.
- OR S dH: Drawdown of the surface-water level in Lake Bolundsfjärden.
- OR S dQ: Relative change of the surface-water discharge in the stream upstream from Lake Bolundsfjärden.
- R PFM S: Average correlation coefficient for the four surface-water discharge gauging stations.
- ME SFM S: Average mean error for the four surface-water level monitoring stations.
- MAE SFM S: Average mean absolute error for the four surface-water level monitoring stations.
- ME SFM G: Average mean error for groundwater-monitoring wells.
- MAE SFM G: Average mean absolute error for groundwater-monitoring wells.
- ME HFM G: Average mean error for percussion boreholes.
- MAE HFM G: Average mean absolute error for percussion boreholes.

The upper part of Table 8-3 shows the open repository results, whereas the lower part compares measured and model-calculated data for undisturbed conditions. The largest differences compared to the reference case are highlighted.

8.2.2 Deviations from measured data for undisturbed conditions

The sensitivity cases *BRO-HV-Ss* (original bedrock model) and *BRO-HV* (original bedrock model in terms of hydraulic conductivities) yield too high hydraulic heads in the bedrock compared to measurements (cf. Chapter 5). Case *BR-HV* gives a lower mean error (ME) for the percussion boreholes compared to the reference case. Sensitivity case *Darcy-20m* yields too low groundwater levels, both for the groundwater-monitoring wells and the percussion boreholes. For all other sensitivity cases, the fit to measurements is similar in terms groundwater levels measured in groundwater-monitoring wells. The influence on model-calculated stream discharges and lake levels is small in all sensitivity cases. The exception is the case *Darcy-20m,* which does not match measured stream discharges as well as the other sensitivity cases. This is likely due to the simplified parameterisation of the upper 20 m of the model domain, which for that specific part does not fully reproduce the conceptual hydrogeological model.

Table 8-3. Summary for different output parameters (see definitions in the text) for different sensitivity cases. In the simulations of disturbed conditions, $K_{grout} = 10^{-7}$ m/s. The largest differences compared to the reference case are highlighted.

Output parameter	Reference	BRO-HV-Ss	BRO-HV	BR-HV	BR-boundary	Darcy-20m	UZ-all	Sealevel-high
OR Q (L/s)	47.4	37.9	37.3	53.3	47.4	52.8	47.2	47.5
OR G 0.3 (km^2)	1.38	1.32	1.35	1.55	1.32	2.83	1.52	1.36
OR G 1.0 (km^2)	0.69	0.71	0.74	0.69	0.68	1.12	0.77	0.67
OR S dH (m)	0.021	0.018	0.019	0.020	0.014	0.054	0.029	0.011
OR S dQ (%)	–13	–4	–5	–19	–1	–24	–18	–16
R PFM S (–)	0.73	0.73	0.73	0.72	–	0.31	0.76	–
ME SFM S (m)	0.03	0.03	0.03	0.03	–	0.00	0.04	–
MAE SFM S (m)	0.07	0.07	0.07	0.07	–	0.09	0.07	–
ME SFM G (m)	–0.02	–0.02	–0.02	–0.01	–	0.44	–0.02	–
MAE SFM G (m)	0.30	0.29	0.29	0.30	–	0.58	0.31	–
ME HFM G (m)	–0.22	–0.44	–0.45	0.01	–	0.37	–0.21	–
MAE HFM G (m)	0.42	0.56	0.57	0.41	–	0.59	0.41	–

The motivation for the changes of the horizontal and vertical hydraulic conductivities in the upper 200 m of the bedrock during the calibration is the results obtained in the interference test (Chapter 5). Case *BR-HV* (which is identical to sensitivity case 4 in Chapter 5) yields poorer results compared to the reference case. Also, the changes to the delivered bedrock model should preferably be as small as possible.

8.2.3 Sensitivity to the bedrock properties

The influence area and the groundwater inflow are largest in sensitivity case *BR-HV*, in which the horizontal hydraulic conductivity is increased and the vertical hydraulic conductivity is decreased with a factor of two in the upper 200 m of the bedrock. In case *BR-HV* the influence area is 12% larger compared to the reference simulation. Case *BRO-HV-Ss* (original bedrock model) gives a slight reduction (4%) of the influence area compared to the reference case. Case *BRO-HV* uses horizontal and vertical hydraulic conductivities from the original bedrock model and a spatially constant specific storage coefficient (as in the reference case). This sensitivity case yields an influence area that is 2% smaller compared to the reference case. Actually, the influence area for a drawdown larger than 1 m is slightly larger in both cases *BRO-HV-Ss* and *BRO-HV*, compared to the reference case. The groundwater inflow to the repository decreases with approximately 20% in case *BR0-HV-Ss* (original bedrock model), and the reduction of the discharge in the stream upstream from Lake Bolundsfjärden is only 4%, compared to 13% in the reference case. In case *BR-HV* the groundwater inflow increases with 12% and the stream-discharge reduction is 19%.

8.2.4 Sensitivity to the boundary conditions

Based on the results presented in Chapter 7, it could be expected that the groundwater inflow to the repository would increase if the no-flow boundary condition in the on-shore part of the model is changed to a prescribed-head boundary. However, this is not the case, and the inflow is almost unaffected in the sensitivity case *BR-boundary*. This can be explained by the small impact of the boundary condition on the total vertical hydraulic gradient between the QD and the bedrock at repository level. Table 8-4 summarises calculated flow components that contribute to the groundwater inflow in the reference case and in sensitivity case *BR-boundary*. As can be seen from the table, the contribution from the horizontal net inflow (i.e. flow from the model boundary) in case *BR-boundary* increases with c. 8.5 L/s compared to the reference case. A corresponding decrease can be noted for the component that represents the vertical net inflow from the land area (excluding the influence area). All other flow components are more or less unchanged in case *BR-boundary*.

Table 8-4. Flow components (L/s) for the reference case and for sensitivity case *BR-boundary*.

Flow component	Reference case		BR-boundary	
	(L/s)	Relative contribution	(L/s)	Relative contribution
Vertical net inflow to bedrock in the influence area	12.7	27%	12.7	27%
Vertical net inflow to bedrock in the land area, excluding the influence area	11.5	24%	2.9	6%
Vertical net inflow to bedrock from the sea area	18.9	40%	18.9	40%
Horizontal net inflow to bedrock from the model boundary	0.5	1%	9.2	19%
Storage change in bedrock	–3.1	7%	–3.1	7%
Reduced inflow to SFR	–0.6	1%	–0.6	1%
Inflow to the open repository	47.2		47.3	

8.2.5 DarcyTools-parameterisation of the upper part of the model domain

As shown in Figure 8.1, if the upper 20 m of the model domain are described according to the DarcyTools model (sensitivity case *Darcy-20m*) the size of the influence area is doubled compared to the reference simulation. In this sensitivity case, the influence area is not concentrated to areas associated with vertical fracture zones. The reason is that no such zones are present in the upper 20 m in the DarcyTools model. Although the influence area is large, the maximum drawdown is only 7.0 m (16.5 m in the reference case) and the area where the drawdown exceeds 4 m is 25 times smaller compared to the reference simulation. This is due to the higher horizontal conductivity and lower vertical conductivity in the upper 20 m of the model domain in the case *Darcy-20m*.

Figure 8-1 also shows the influence area of the annual average groundwater-table drawdown (> 0.3 m) obtained using the DarcyTools model for development phase 3 and $K_{grout} = 10^{-7}$ m/s /Svensson and Follin 2010/. Even though the repository is fully open in case *Darcy-20m*, it is possible to compare the results from this sensitivity case with the results from the DarcyTools model. The influence areas in Figure 8-1 clearly show similarities regarding the horizontal extent. The groundwater inflow to the repository is 11% larger in sensitivity case *Darcy-20m* compared to the reference case. Most of the increase is noted in calculation layer 3 (lower level 20 m.b.s.l.), which is due to that the hydraulic conductivities are changed in this layer and the layers above.

The MIKE SHE model simulates transient ground- and surface water flow, whereas DarcyTools model calculates steady-state groundwater flow. This is an important difference between the models. In order to facilitate comparisons, sensitivity case *Darcy-20m* was also used to simulate steady-state flow. This was done using a temporally and spatially constant groundwater recharge in the land part of the model area, and with no simulation of water flow in the unsaturated zone and overland flow. The groundwater recharge (mean net precipitation) was set to 130 mm per year /Svensson and Follin 2010/, and the simulation was done for development phase 3 and grouting case $K_{grout} = 10^{-8}$ m/s.

Figure 8-2 shows the drawdown of the groundwater table in the steady state *Darcy-20m* case and the influence area calculated by DarcyTools. The results of the steady-state case show that MIKE SHE and DarcyTools produce different results, especially in terms of groundwater-table drawdown. The MIKE SHE-calculated influence area is considerably larger and more scattered. However, the groundwater table in the area northwest of Lake Bolundfjärden is strongly affected in both models.

In the steady-state *Darcy-20m* case, the groundwater inflow to the repository is 28.7 L/s (development phase 3, $K_{grout} = 10^{-8}$ m/s) compared to 28 L/s calculated by DarcyTools /Svensson and Follin 2010/ for the same development phase and value of K_{grout}. Hence, in terms of the model-calculated inflow the difference between the two models is in this case less than 3%.

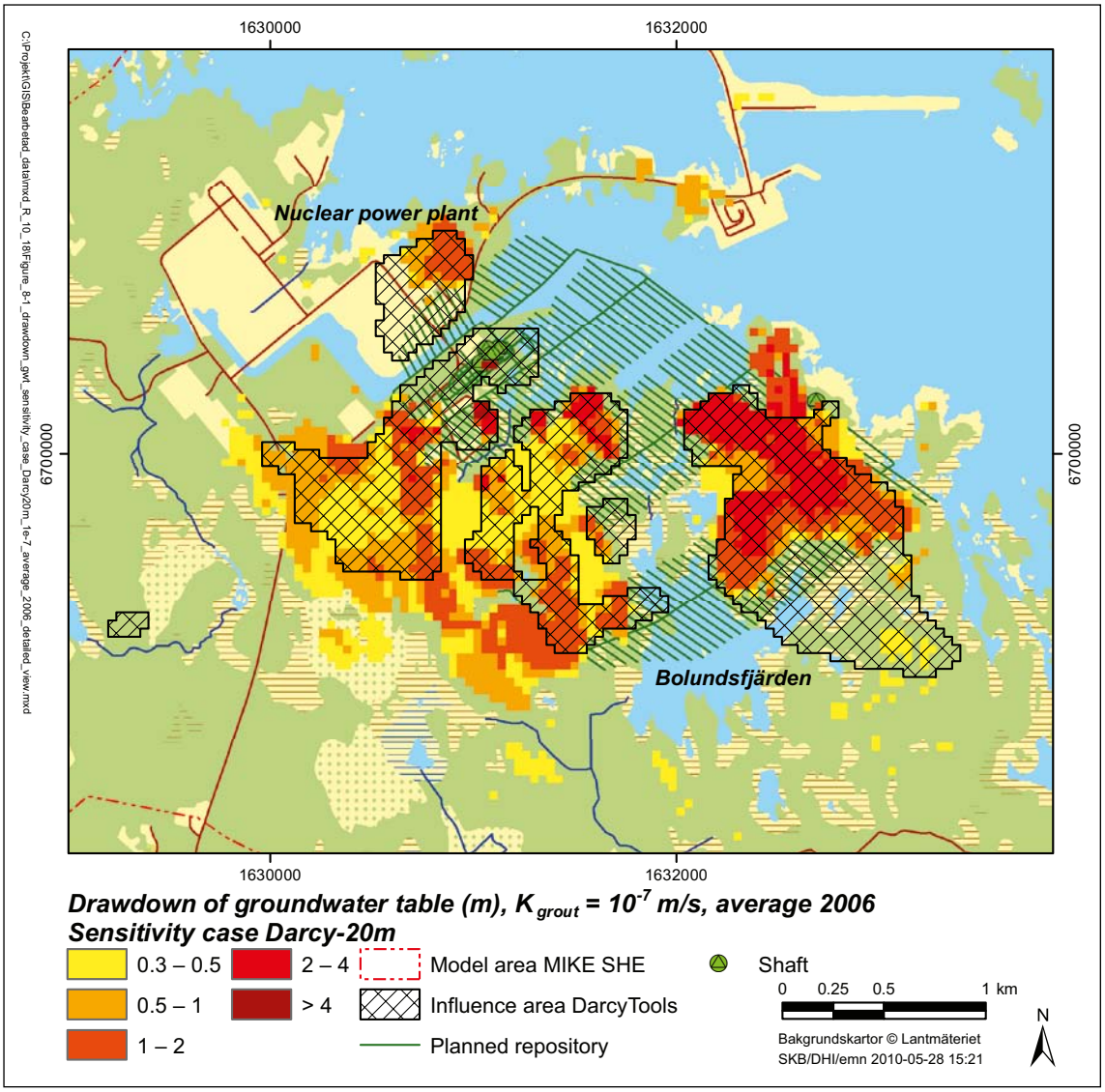

Figure 8-1. *Detailed view of the groundwater-table drawdown for sensitivity case Darcy-20m (K_{grout} = 10^{-7} m/s). The figure also shows the DarcyTools-calculated influence area for a drawdown > 0.3 m for the same grouting level (their grouting level I) for development phase 3 (their stage C) /Svensson and Follin 2010/.*

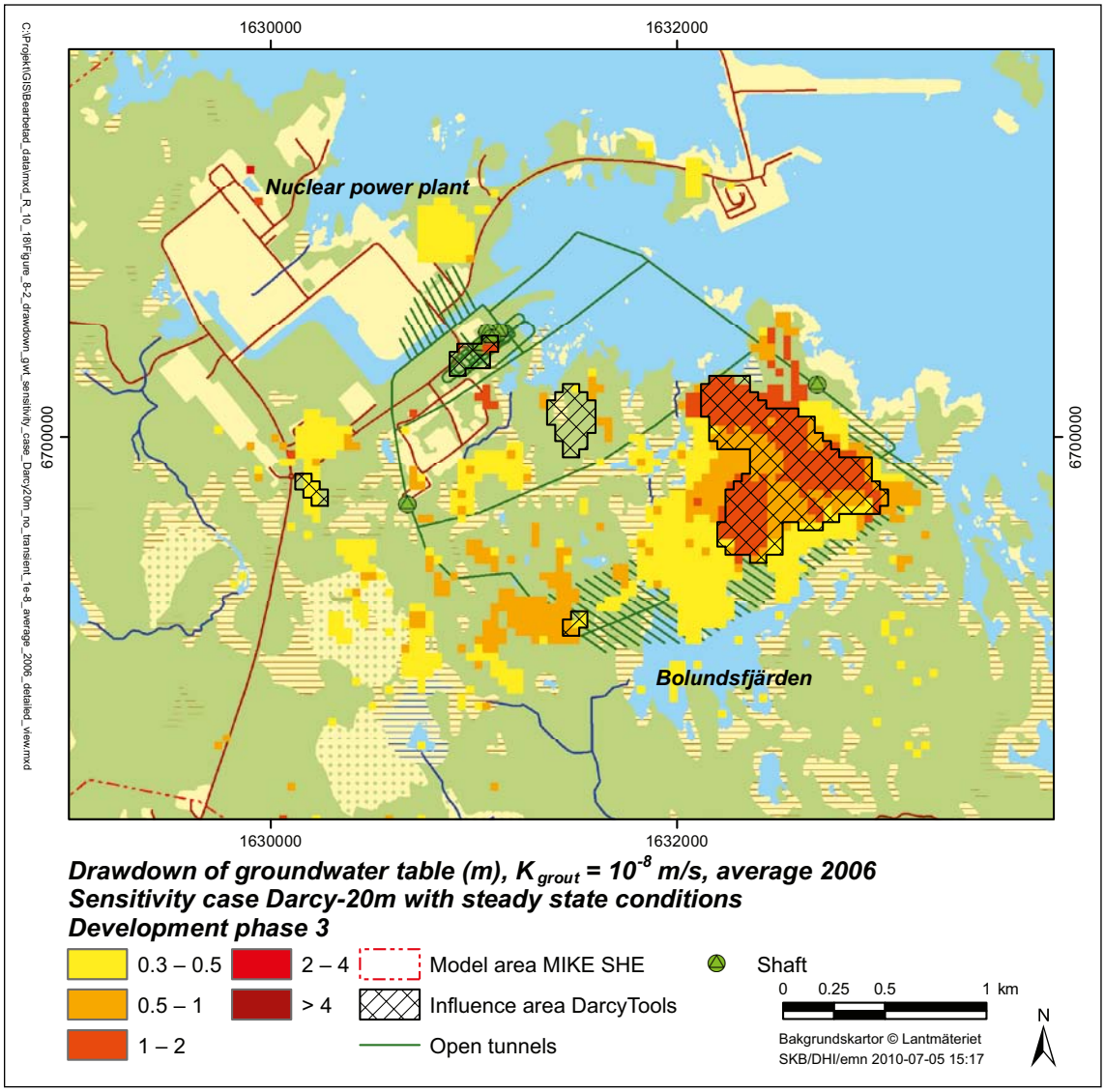

Figure 8-2. *Detailed view of the groundwater-table drawdown (K_{grout} = 10^{-8} m/s) for sensitivity case Darcy-20m with steady-state conditions. The influence area for a drawdown >0.3 m, calculated with the DarcyTools model for K_{grout} = 10^{-8} m/s (their grouting level II) for development phase 3 (their stage C) /Svensson and Follin 2010/ is also shown.*

8.2.6 Sensitivity to the methodology for modelling water flow in the unsaturated zone

Figure 8-3 shows the influence areas in sensitivity cases *UZ-all* and the reference case. The comparison shows that if water flow in the unsaturated zone is simulated in all grid cells in the unsaturated zone, instead of a limited number as in the reference case, the groundwater-table drawdown influence area increases with approximately 10%. Specifically, case *UZ-all* extends the influence area compared to the reference case. The results show that the groundwater inflow to the repository is not sensitive to the methodology for modelling of water flow in the unsaturated zone.

Compared to the reference case, in sensitivity case *UZ-all* there is a larger effect on the surface-water discharge in the stream upstream from Lake Bolundsfjärden and on the water-level in Lake Bolundsfjärden. In case *UZ-all*, the annually accumulated stream discharge and lake-water level decrease with 18% and 0.029 m, respectively, compared to 13% and 0.021 m in the reference simulation.

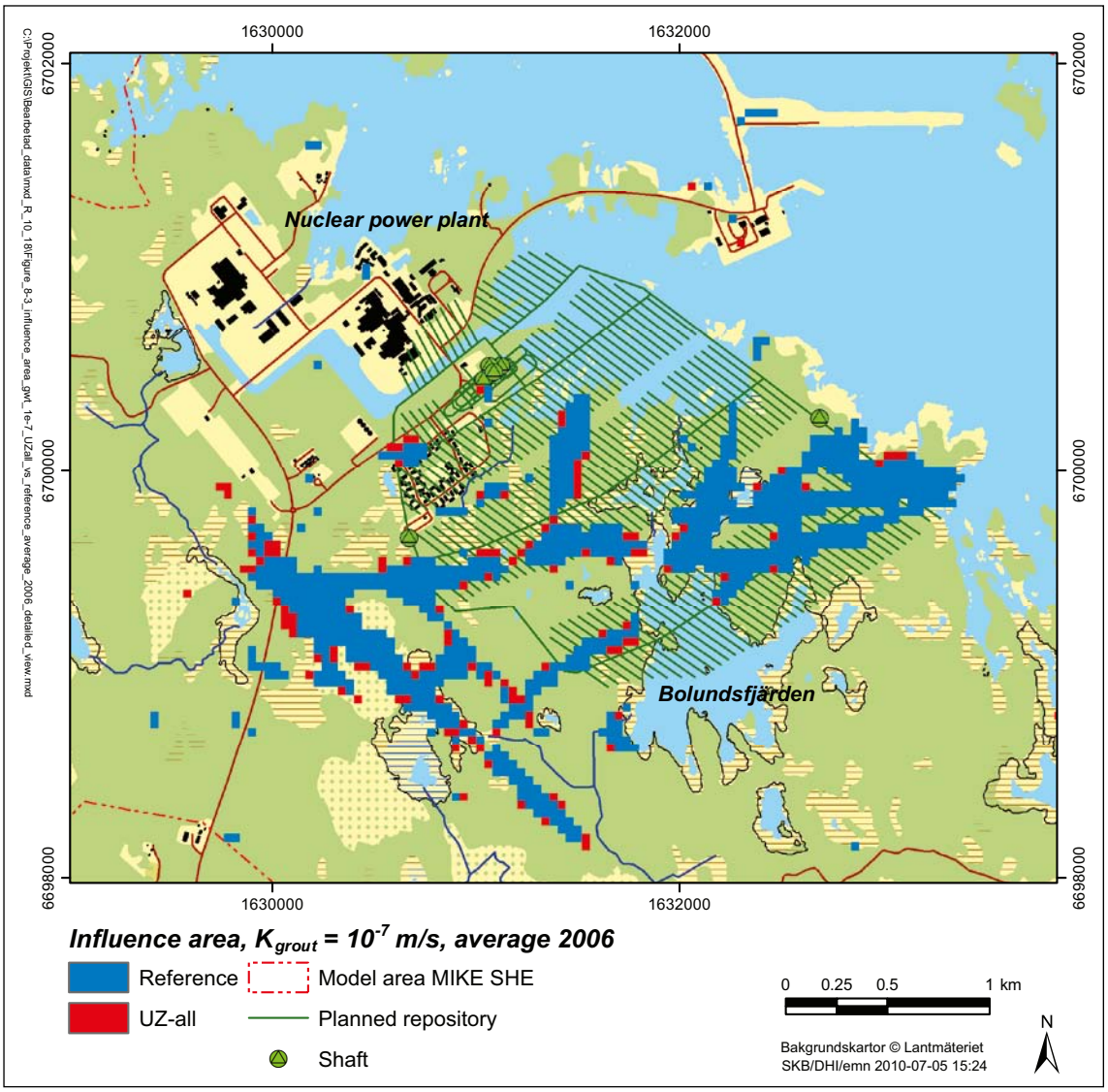

Figure 8-3. *Detailed view of the influence areas (groundwater-table drawdown > 0.3 m) for the reference case (blue areas) and sensitivity case UZ-all (red and blue areas) for K_{grout} = 10^{-7} m/s.*

8.2.7 Sensitivity to an increased sea level

In sensitivity case *Sealevel-high* the time-varying sea level is increased with 0.56 m and the unsaturated zone is simulated in all grid cells. Sensitivity case *UZ-all* is used as reference in order to evaluate the effect of the increased sea level only. It should be noted that this sensitivity case represents a possible future scenario of the sea-level rise until year 2100 /Brydsten et al. 2009/.

Figure 8-4 shows the influence areas in cases *UZ-all* and *Sealevel-high*. As can be seen in the figure and also in Table 8-3, the influence area decreases with approximately 11% when the sea level is increased. The difference in influence area is found in areas close to the sea. In sensitivity case *Sealevel-high,* these areas are either part of the sea or submerged most of the simulation time due to the higher sea level. The groundwater inflow to the repository appears not to be sensitive to the sea level.

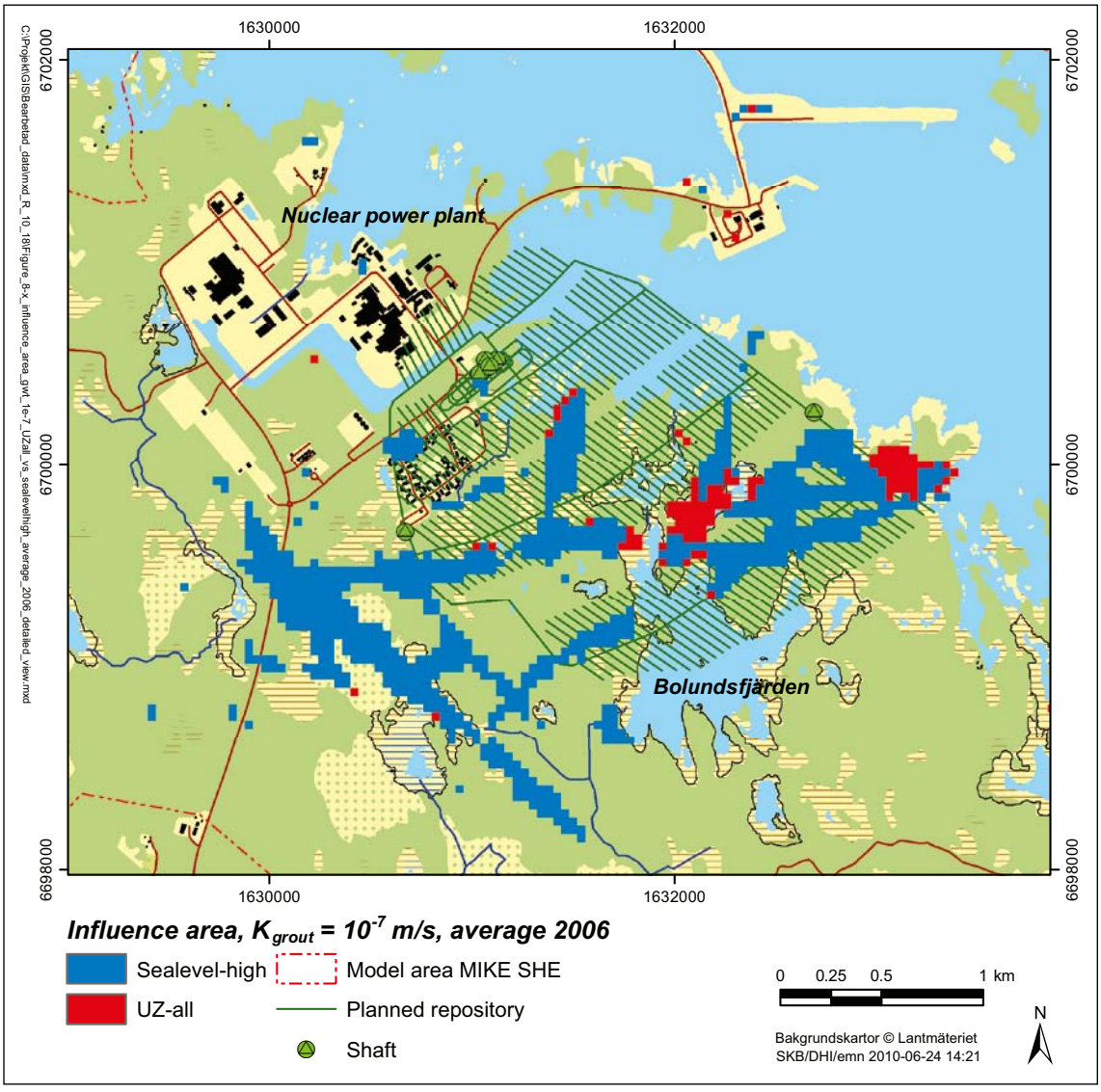

Figure 8-4. *Detailed view of the influence areas (groundwater-table drawdown > 0.3 m) for sensitivity cases Sealevel-high (blue areas) and UZ-all (red and blue areas) for* $K_{grout} = 10^{-7}$ *m/s.*

8.2.8 Conclusions of the sensitivity analysis

The following can be concluded from the sensitivity analysis:

- The inflow is sensitive to the hydrogeological properties of the bedrock but not to the boundary conditions, including the sea level.
- The size of the influence area of the groundwater-table drawdown shows little sensitivity to the hydrogeological properties of the deep bedrock and to the boundary conditions. However, a simplified description of the upper 20 m of the model domain (using DarcyTools data) yields a somewhat higher inflow. More important, it also yields a larger influence area, which indicates that the size of the influence area is sensitive to the hydrogeological properties of the upper part of the model domain.
- Simulating water flow in the unsaturated zone in all grid cells increases the size of the influence area of the groundwater-table drawdown, compared to the reference case in which grid cells are classified and aggregated. However, the inflow to the repository is not sensitive to the methodology for modelling water flow in the unsaturated zone.

9 Confidence and uncertainties

This chapter discusses uncertainties regarding conceptual models and the numerical models (MIKE SHE, MIKE 11 and MOUSE) that are used in this report to predict the groundwater inflow to the repository in Forsmark and associated hydrological and hydrogeological effects. Three different types of uncertainties of relevance in the present context are discussed in Sections 9.1 (conceptual uncertainty), 9.2 (parameter uncertainty), and 9.3 (numerical-model uncertainty).

9.1 Uncertainties related to conceptual models

9.1.1 The upper bedrock

According to the conceptual hydrogeological model of Forsmark, diversion of groundwater from the upper 200 m of the bedrock yields hydraulic-head drawdown in a large area around the diversion point. According to the conceptual model, this phenomenon is due to the high horizontal hydraulic conductivity of the sheet joints. Moreover, groundwater diversion yields a drawdown of the groundwater table mainly in areas in which the upper bedrock contains fracture zones with high vertical hydraulic conductivity that are in contact with the Quaternary deposits.

Based on site investigations in the Forsmark area, there is high confidence regarding the presence of high-transmissive (transmissivity = hydraulic conductivity times thickness) sheet joints in the upper part of the bedrock /Follin 2008, SKB 2008a/. There is also high confidence regarding locations of fracture zones with high vertical hydraulic conductivity that yield the “band shaped” influence area of the groundwater-table drawdown (e.g. Figure 7-17).

The high level of confidence on the matters above is explained by the extensive data set, the consistency in interpretations and conceptual models from different disciplines (e.g. geology and hydrogeology) and the fact that no significant conceptual-model adjustments have been considered necessary as new data gradually have been added during the site investigations. The site investigations have included studies of the hydrogeological effects of three large-scale interference tests, in which groundwater was pumped during two separate periods from percussion borehole HFM14 (for its location, see Figure 5-1 in Section 5.2) and during one period from HFM33 (not shown in Figure 5-1). During all these tests, one could observe hydraulic-head drawdown in the bedrock at distances on the order of 2 km from the percussion boreholes from which water was pumped.

In conclusion, the interference tests support the conceptual model, according to which groundwater diversion from the upper part of the bedrock “spreads” the hydraulic-head drawdown in the sheet joints due to their high horizontal hydraulic conductivity. Moreover, in connection to groundwater diversion from the bedrock, groundwater-table drawdown has been observed in groundwater-monitoring wells located in areas with fracture zones with high vertical hydraulic conductivity in the upper part of the bedrock.

9.1.2 The hydrogeological contact between Quaternary deposits and bedrock

The hydrogeological contact between the Quaternary deposits and the bedrock has large impact on the magnitude and geographical extent of the groundwater-table drawdown due to the groundwater inflow to the repository. The occurrence of thin layers of e.g. clay or silt in types of Quaternary deposits with otherwise high hydraulic conductivity (sand, gravel or coarse till) can limit or even prevent a drawdown of the groundwater table even in cases with substantial hydraulic-head drawdown in the underlying bedrock /Cesano et al. 2000, Olofsson 1994/.

The conceptual model of the Quaternary deposits is based on extensive and detailed field investigations. According to this conceptual model, the interface between the Quaternary deposits and the bedrock has a high hydraulic conductivity. In some areas the conceptual model includes a layer of dense, clayey and hence low-conductive till. The locations and hydrogeological properties of this type of till is well documented from the site investigations.

It can be concluded that the conceptual model in general does not assume any circumstances that would limit the hydrogeological contact between the Quaternary deposits and the bedrock, and that hence would prevent or limit the groundwater-table drawdown associated with the groundwater inflow to the repository. The contact may be overestimated at some locations, which implies that the model-calculated groundwater-table drawdown also may be overestimated locally.

9.1.3 Sea, lake and wetland sediments

Low-conductive sediments below the sea, lakes and wetlands limit the groundwater-surface water contact. According to the conceptual model, such low-conductive sediments are present below some parts of the sea, the lakes and the wetlands. The confidence regarding the geographical extents of such sediments is considered to be high /Hedenström and Sohlenius 2008/. However, there have been no complete geological investigations of all lakes and wetlands in Forsmark.

According to the conceptual model, low-conductive sediment layers limit the hydrogeological contact between surface waters and groundwater in the underlying till. Local conditions may yield a better or poorer hydrogeological contact than assumed in the conceptual model. Actual absence of low-conductive sediment layers in areas where they are assumed to be present is considered to be an uncertainty factor of minor importance in the present context.

9.2 Parameter uncertainty

9.2.1 Calibration of hydrogeological properties

The hydrogeological parameterisation of the Quaternary deposits and the bedrock is based on the site investigations. Model calibration and associated parameter adjustments have been important steps in the development of the MIKE SHE site descriptive model /Bosson et al. 2008/, the previous MIKE SHE open repository model /Gustafsson et al. 2009/ and the present MIKE SHE model (see Chapter 5). The model calibration has been performed using measurement data (long-term time series) on groundwater levels in groundwater-monitoring wells, percussion boreholes, lake-water levels and stream discharges. The MIKE SHE calibration process has also taken into account an interference test, including comparison between model-calculated and measured groundwater-level drawdowns for several percussion boreholes (see Section 9.2.2). It should be noted that model calibration has been performed using actual time-series data and not temporally averaged values.

In general, it has been possible to obtain reasonable agreement between model calculations and measurements without major changes of initial parameter values regarding the Quaternary deposits, the hydrogeological contact between the Quaternary deposits and the bedrock, and the corresponding contact between groundwater and surface water. In order to obtain proper calibration results regarding groundwater levels in the Quaternary deposits and the bedrock (see Chapter 5), it was required to change the hydrogeological parameterisation of the upper part of the bedrock (including fracture zones and sheet joints) delivered from the CONNECTFLOW modelling team. These adjustments also yield a quantification of vertical hydraulic gradients between the Quaternary deposits and the bedrock that better fits measurements.

9.2.2 Interference tests

As part of the both the present MIKE SHE model calibration (Chapter 5) and the calibration by /Bosson et al. 2008/, the three-week pumping test in percussion borehole HFM14 was simulated for different parameter combinations regarding the hydrogeological properties of the upper part of the bedrock. The model-calculated hydraulic responses (drawdowns) in percussion-borehole sections and also some groundwater-monitoring wells were then compared with measured responses. Based on these comparisons, it was possible to obtain and select the specific parameter combination that provided least difference between model calculated and measured drawdowns.

9.2.3 Sensitivity analyses

Numerous sensitivity analyses have been conducted as part of the present MIKE SHE modelling (Chapter 8) and also as part of the /Gustafsson et al. 2009/ modelling. Below follows a summary of the main important conclusions that can be drawn from these analyses, concerning the parameterisation of the upper part of the bedrock, the interface between the Quaternary deposits and the bedrock, and sediments below the sea, lakes and wetlands.

- ***The upper part of the bedrock:*** Several sensitivity cases in /Gustafsson et al. 2009/ and in the present report (Chapter 8) aim to investigate the sensitivity of the modelling results to the hydrogeological properties of the upper part of the bedrock, including fracture zones and sheet joints. The results of these analyses show that the parameterisation of the upper part of the bedrock is of importance for the model-calculated groundwater inflow to the repository and to some extent also for the size of the influence area of the groundwater-table drawdown. However, the hydrogeological properties of the bedrock are well-studied and, as mentioned previously, evaluation of these properties has been an integrated part of the model calibration. Hence, there is a good basis to assess parameter combinations that are reasonable in terms of their agreement between model-calculated and measured groundwater levels for undisturbed conditions (without the repository).
- ***Interface between the Quaternary deposits and the bedrock:*** /Gustafsson et al. 2009/ investigate the sensitivity of the modelling results to the hydraulic conductivity of the interface between the Quaternary deposits and the bedrock. It was found that this sensitivity was small in terms of the model-calculated inflow and groundwater-table drawdown. This indicates that the properties of this interface are not critical for the assessment of the inflow and the associated effects. However, the properties of this interface may be of importance locally (see further discussion in Section 9.3).
- ***Sediments below the sea, lakes and wetlands:*** In one sensitivity case /Gustafsson et al. 2009/ replaced the sediments in the model below the sea, lakes and wetlands with till. It was found that neither the inflow to the repository nor the influence area of the groundwater-table drawdown were sensitive to this change. This finding can be explained by the fact that the sediment layers in the model area are rather thin and of relatively high hydraulic conductivity ($1.5 \cdot 10^{-8}$–$3 \cdot 10^{-7}$ m/s). The properties of such sediments may be of importance locally (see further discussion in Section 9.3).

9.3 Uncertainty and confidence in the numerical models MIKE SHE and MOUSE

As mentioned previously, MIKE SHE is a distributed and physically based model. This means that the model can handle spatially variable hydrogeological properties and that water-flow processes are described by solutions of differential equations. However, any numerical model is a simplification of reality.

Even though the model can handle spatially variable hydrogeological properties, it is always necessary to make parameter adjustments of purely practical reasons. Sections 9.1 and 9.2 discuss the issue of deviations between the known reality and the true reality in terms of the function of the studied system (the conceptual model) and its hydrogeological properties (the parameterisation). Even if one in theory had complete knowledge of reality, the numerical-modelling methodology involves some degree of misrepresentation of this knowledge. Some fundamental reasons for this are discussed in the following sections.

9.3.1 Numerical concepts and spatial resolution

There are two types of groundwater models for bedrock that can be denoted DFN-models and CPM-models, respectively. DFN-models (discrete fracture network) are developed for quantification of groundwater flow in fractured bedrock. In such models, it is assumed that groundwater only can flow along fractures and deformation zones. CPM-models (continuum porous medium) are primarily developed for quantification of groundwater flow in porous media, such as Quaternary deposits and porous bedrock (e.g. limestone and sandstone). In such models, it is assumed that the groundwater can flow in all three directions and the hydrogeological properties can also be different in different directions. MIKE SHE is a type of CPM model, specifically a 3-dimensional continuum model with cubic calculation (grid) cells.

A 3-dimensional continuum model implies a simplified description of fracture zones and impermeable layers. The cubic grid cells of the MIKE SHE model domain are assigned average property values, i.e. parameter variability on scales smaller than the grid-cell size is replaced by spatial averages. This means that the use of large grid cells will even out property variations and hence possibly result in a simplification of reality. On the other hand, small grid cells will lead to long simulation times. In practice, the modeller therefore has to strike a balance between the representation of actual spatial variability and simulation time.

To address the above-mentioned issues, averages are calculated so that geological structures with high horizontal conductivity will have large influence on averages in the horizontal directions, whereas structures with low vertical conductivity will have large influence on the properties in the vertical direction. This approach reduces problems associated with scales. However, the approach is still is a simplification of reality and thus a source of uncertainty.

The issues discussed above imply that the size of the model-calculated influence area for the groundwater-table drawdown may be overestimated, whereas the magnitude of the drawdown may be underestimated locally. It is therefore of importance to verify the model using controlled and well-documented hydraulic disturbances such as pumping tests. As described previously such verifications have been done with good results (see Section 9.1, Chapter 5 and /Bosson et al. 2008/).

9.3.2 Calculation algorithms

One source of uncertainty is the calculation algorithms that describe various water-flow processes. In MIKE SHE most processes are described by well known differential equations, such as Saint Venant's equations for channel flow (in one dimension) and overland flow (two dimensions), Richards equation for flow in the unsaturated zone (one dimension) and Darcy's law for groundwater flow (three dimensions). The equations are solved using a finite-difference method, according to which the problem is solved iteratively until the residual error is below a specified threshold value. Increasing this threshold value yields a faster solution of the flow problem but also larger errors. Hence, the choice of threshold value is a matter of simulation time versus accuracy.

The description of some processes such as the evapotranspiration /Kristensen and Jensen 1975/ is based on empirical relationships. The description of such processes is hence not strictly based on physical laws, and the conditions for the studied problem may deviate from those on which the empirical relationship is based. However, the calculation algorithms are generally not considered to be a major source of uncertainty, and potential errors can be reduced by means of model calibration. The present model calibration provides a good agreement between model-calculated and measured data (Chapter 5).

A potential source of error is the methodology for calculation of the groundwater inflow to the repository. In the present modelling, the inflow equals the calculated water exchange between MIKE SHE and MOUSE (Section 2.3). For obvious reasons, the model-calculated inflow cannot yet be compared to the measured inflow. For a homogeneous system, the inflow algorithm (i.e., the MIKE SHE-MOUSE coupling routine) used in this study is compared with the results obtained by an analytical solution (Chapter 3) for different combinations of the hydraulic conductivity in the grouted zone (K_{grout}) and in the surrounding bedrock. This comparison shows very small differences between the numerically (MIKE SHE-MOUSE) and analytically calculated inflow, with a maximum difference of 7%.

Moreover, the MIKE SHE-calculated groundwater inflow has also been compared with the results from a parallel modelling activity using DarcyTools (Section 10.1). For repository development phase 3 and grouting case $K_{grout} = 10^{-8}$ m/s (a case that has been simulated using both models), the inflow difference between the models is only a few percent.

9.3.3 Model area, boundary conditions and input data

In principle, the present MIKE SHE model area equals the areal extent of the domain for the hydrogeological model of the bedrock that was delivered from the CONNECTFLOW modelling team. Moreover, the on-shore boundaries of the MIKE SHE model area follow surface-water divides. The on-shore boundary conditions imply that there is no groundwater flow across these

boundaries, whereas the boundary towards the sea is set equal to the measured transient sea level. If the hydraulic-head drawdown reaches the on-shore boundary (e.g. Figure 7-18 in Section 7.5.2), a no-flow boundary implies that the model may overestimate the magnitude of the drawdown, whereas the inflow to the repository and the geographical extent of the influence area may be underestimated. However, the results from one of the sensitivity cases in Chapter 8 (*BR-boundary*) show that the model-calculated inflow is not sensitive to the on-shore boundary condition.

The two-year period 2005–2006 is used as simulation period in the present study and also in /Gustafsson et al. 2009/. Hence, both studies are based on meteorological conditions for the same year (2006), whereas the preceding year 2005 is used as an initialisation period. /Mårtensson et al. 2010/ presents MIKE SHE modelling results for undisturbed and disturbed conditions, using meteorological data representing a statistically normal year, a dry year and a wet year. These results show large differences between various meteorological conditions in terms of the model-calculated groundwater-table drawdown. Based on that study, it can be concluded that the meteorological conditions may have large impact on the hydrological and hydrogeological effects of the groundwater inflow to the repository.

The value of K_{grout} has large impact on the model-calculated inflow to the repository and it also has impact on the calculated groundwater-table drawdown (see Chapter 7 and /Gustafsson et al. 2009/). In reality, the hydraulic conductivity of the grouted zone and its thickness may vary locally. The grouting cases studied here ($K_{grout} = 10^{-7}$, 10^{-8} and 10^{-9} m/s) are chosen to cover a reasonable range, and the modelling results provide a range of uncertainty in terms of the inflow to the repository and associated hydrological and hydrogeological effects.

10 Summary and conclusions

Unless stated otherwise, the results and conclusions discussed below are obtained using meteorological data and sea-level data from the two-year period 2005–2006. Moreover, the results refer to the hypothetical case with a fully open repository.

10.1 Water balance and inflow to the open repository

The groundwater inflow to the repository affects the total turnover of water in the model area. Considering the land part of the model area, depending on the hydraulic conductivity of the grouted zone (K_{grout}) the inflow is on the order of 9 to 28% of the total runoff for undisturbed conditions. Within the influence area (annual average drawdown exceeding 0.3 m) of the groundwater-table drawdown, the inflow has substantial effects on the water balance. Specifically, the inflow corresponds to up to 35% of the precipitation, depending on the value of K_{grout}.

The horizontal groundwater flow in the bedrock across the boundary between land and sea is much less than the vertical groundwater flow from the Quaternary deposits to the bedrock. Considering the whole model area, the model calculated vertical net inflow to the bedrock is in the range 20–48 L/s depending on K_{grout}, which can be compared to 5 L/s for undisturbed conditions. The corresponding horizontal net inflow to the bedrock across the boundary between land and sea is in the range 0.2–0.5 L/s, with a zero net flow for undisturbed conditions.

The model-calculated groundwater inflow to a fully open repository is in the range 15.5–47.5 L/s for K_{grout} in the range 10^{-9}–10^{-7} m/s. Compared to the results of /Gustafsson et al. 2009/, the present inflow is between 25% and 35% larger. This difference is most likely due to the use of different routines for coupling MIKE SHE and MOUSE. If the present, updated routine is applied to the MIKE SHE model used by /Gustafsson et al. 2009/, the difference in inflow is in the range 1–5%. This small, residual difference is due to other differences between the two models, e.g. in terms of the hydrogeological model of the bedrock and the size of the model domain. Test simulations for homogeneous conditions show that the model-calculated inflow only differ a few percent compared to an analytical solution if the updated MIKE SHE-MOUSE coupling routine is used, which further strengthens the reliability of the present results.

Some 50% of the inflow to the repository is related to an increased vertical groundwater flow from the Quaternary deposits to the bedrock in the land part of the model area. Specifically, about half of the increase within the land part pertains to the relatively small influence (annual average groundwater-table drawdown exceeding 0.3 m, $K_{grout} = 10^{-7}$ m/s). The remaining 50% of the inflow is mainly attributed to an increased vertical inflow from the part of the sea that is located within the model area. If the boundary condition for the on-shore part of the model area is changed from a no-flow boundary to a prescribed time-varying head boundary, the contribution from the land area (excluding the influence area) decreases, whereas the contribution from the model boundary increases with the same amount. However, the total inflow to the repository is not sensitive to the boundary conditions.

For grouting case $K_{grout} = 10^{-8}$ m/s the groundwater inflow for different simulated repository-development phases is between 37% and 89% of the inflow for the hypothetical case with a fully open repository. The smallest inflow is obtained for the (initial) construction phase. During this phase, the repository layout includes the access tunnel and the rock caverns, tunnels and shafts in the central area. The highest inflow is obtained for development phase 3, during which all transport tunnels and one deposition area (and its main tunnel) also are open.

The results of simulations concerning the planned SFR extension show that an extension yields a reduction of the groundwater inflow to the present part of SFR, from the calibrated inflow of 5.7 L/s to 5.4 L/s. The calculated inflow to the extended part of SFR is 5.1 L/s, using a hydraulic conductivity of $K_{grout, SFR\text{-}ext.} = 10^{-8}$ m/s for the extension. The total inflow to the SFR extension and the present part of SFR is reduced by 0.3 L/s when a fully open repository ($K_{grout} = 10^{-8}$ m/s) is included in the model. However, the inflow to the repository is unaffected by the SFR extension.

A sensitivity analysis shows that the inflow to the repository is reduced by approximately 20% if the vertical hydraulic conductivity is decreased to 1/5 and the horizontal hydraulic conductivity is increased by a factor of 5 in the upper 200 m of the bedrock. If the parameterisation of the upper 20 m of the model domain is described according to the DarcyTools model /Svensson and Follin 2010/, the inflow is 11% larger compared to the MIKE SHE reference case.

/Svensson and Follin 2010/ present the DarcyTools-calculated groundwater inflow for development phases 1–3 and for three grouting cases (K_{grout} = 10^{-7}, 10^{-8} and 10^{-9} m/s). The DarcyTools modelling has not considered the case with a fully open repository, which implies that the only possible inter-model comparison is that for development phase 3. For grouting case K_{grout} = 10^{-8} m/s the two models yield almost identical inflows, specifically 27.8 L/s (MIKE SHE) and 28 L/s (DarcyTools). However, the repository layout that is implemented in MIKE SHE includes two (reserve) sections of deposition tunnels in the north-western and southern corners of the repository area, whereas these sections are not implemented in DarcyTools.

10.2 Surface waters

According to the model calculations, the inflow to the repository has small effects on the water levels of most lakes in the model area. The inflow yields drawdown of hydraulic heads in the bedrock and groundwater-table drawdown below and around the lakes Bolundsfjärden, Gällsboträsket, Norra Bassängen and Puttan. These are the only studied lakes in which the annual average drawdown of the water level exceeds 0.01 m (using data for year 2006). In the model calculations, the maximum drawdown in these lakes occurs during the spring flood in April 2006.

The inflow has very small effects on model-calculated discharges in the streams. The exception is the stream upstream from Lake Bolundsfjärden, for which the annually accumulated stream discharge is reduced by 13% for grouting case K_{grout} = 10^{-7} m/s, which is due to the groundwater-table drawdown within the catchment area of the stream. The reduction of the stream discharge is less in a sensitivity case with a reduced vertical hydraulic conductivity and an increased horizontal hydraulic conductivity in the upper 200 m of the bedrock. In a sensitivity case with a prescribed time-varying head boundary, there is no reduction of the stream discharge (see Section 9.1).

10.3 Drawdown of the groundwater table and hydraulic heads

The groundwater inflow has largest effects on the location of the groundwater table in areas where the upper part of the bedrock contains fracture zones with high vertical hydraulic conductivity that are in contact with the Quaternary deposits. The size of the influence area (areas with an annual average groundwater-table drawdown exceeding 0.3 m) is 0.64 km^2 for grouting case K_{grout} = 10^{-9} m/s and 1.38 km^2 for grouting case K_{grout} = 10^{-7} m/s. The band-shaped extent of the influence area is relatively similar for the studied grouting cases. The influence area primarily includes areas around Lake Bolundsfjärden, and some small, scattered areas between the nuclear power plant and Lake Bolundsfjärden. In the model calculations, the largest drawdown of the groundwater table (4–17 m, depending on the value of K_{grout}) occurs north of Lake Bolundsfjärden.

The influence areas discussed above refer to a hypothetical case with a fully open repository. Considering separate development phases, the simulation results show that the groundwater-table drawdown is largest during development phase 3, with an influence area that is approximately 94% of that obtained for a fully open repository (K_{grout} = 10^{-8} m/s). The corresponding results for the construction phase and a hypothetical case with a fully open repository excluding all main and deposition tunnels are 43% and 72%, respectively. This is due to the fact that drawdown of the hydraulic head in the sheet joint layers, which occurs for all analysed stages, yields a groundwater-table drawdown in those areas in the vicinity of the repository that coincide with vertical fracture zones in the upper part of the bedrock.

In terms of the size and shape of the model calculated influence area, the present modelling results are similar to those of /Gustafsson et al. 2009/. For the hypothetical case with a fully open repository (and grouting case K_{grout} = 10^{-7} m/s), the presently model calculated influence-area size is 12% smaller

compared to that of /Gustafsson et al. 2009/, whereas it is 3% and 31% higher for the grouting cases $K_{grout} = 10^{-8}$ and 10^{-9} m/s, respectively. Northeast of the nuclear power plant, the groundwater-table drawdown was substantial in the /Gustafsson et al. 2009/ simulations. It was difficult to explain the large drawdown in that particular area, since there are no fracture zones with high vertical hydraulic conductivity. There is no groundwater-table drawdown in that area in the present modelling, which is likely due to the implementation of the subsurface drainage system below the nuclear power plant (this drainage system was not implemented by /Gustafsson et al. 2009/). There is hence larger confidence in the present modelling results concerning the effects of the inflow on the location of the groundwater table in that particular area.

There are differences between the present modelling results and those of /Gustafsson et al. 2009/ in terms of the hydraulic-head drawdown at different levels in the bedrock. Due to the enlargement of the model area, at the level 50 m.b.s.l. the presently calculated influence area for the hydraulic-head drawdown does not extend to the model boundary in the sea (this was the case in /Gustafsson et al. 2009/). The influence area at this level reaches the model boundary in the northwest and southwest and covers a larger area compared to /Gustafsson et al. 2009/. This is likely due to the larger calculated inflow in the present modelling.

Fracture zones with high vertical hydraulic conductivity connect the deep bedrock with the upper part of the bedrock where the sheet joints are located. Hydraulic-head drawdown that reaches a layer containing a sheet joint is transmitted in a large area. In the MIKE SHE model, there are no sheet joints in the upper 20 m of the bedrock, which implies that the hydraulic-head drawdown is transmitted to the Quaternary deposits along fracture zones with high vertical hydraulic conductivity.

MIKE SHE was also used to investigate potential cumulative effects of the planned extension of the underground SFR facility. Using natural conditions (i.e. without SFR) as reference, the modelling results indicate that the groundwater inflow to the present SFR yields a drawdown of the groundwater table only at the SFR pier and small areas north and northeast of Lake Bolundsfjärden. Concerning the SFR extension, the results indicate that the extension would only yield minor additional drawdown of the groundwater table, compared to present conditions.

The saturation of the repository backfill after termination of groundwater diversion was simulated in a simplified manner in MIKE SHE, by reducing the volume of the underground parts of the repository (reduction of tunnel radii). Further, a sealing layer was added to the grouted zone, which is assumed to have a hydraulic conductivity of $K_{grout} = 10^{-8}$ m/s. The hydraulic conductivity of the sealing layer was set according to preliminary data on the hydrogeological properties of the backfill. The simulation was initialised from the situation with a fully open repository and an extended SFR. According to the results, the backfill will be fully saturated approximately 14.5 months after termination of groundwater diversion. Moreover, for a case with substantial groundwater inflow during the saturation process, the results indicate that the groundwater table will be fully recovered within a few years after full saturation of the backfill. Further time is required for full recovery of the hydraulic head in the bedrock at repository level.

Sensitivity analyses show that the groundwater-table drawdown is relatively insensitive to the tested changes of the hydrogeological properties of the upper 200 m of the bedrock. The largest sensitivity in noted for a sensitivity case with a 50% reduction of the vertical hydraulic conductivity and 100% increase of the horizontal hydraulic conductivity. In this case, the influence area is 12% larger compared to that obtained using the MIKE SHE base-case parameterisation of the bedrock. A sensitivity case in which the upper 20 m of the model domain is parameterised in the same way as in the parallel DarcyTools modelling activity, the size of the influence area is twice as large and not band-shaped as in MIKE SHE. This is due to the absence of fracture zones with high vertical hydraulic conductivity in the upper 20 m of the DarcyTools model domain, which for that specific part does not fully reproduce the conceptual hydrogeological model. However, the total size of the model-calculated influence area and the magnitude of the groundwater-table drawdown show strong similarities between the two models, provided that the hydrogeological parameterisation of the upper 20 m of the bedrock is the same.

The MIKE SHE base-case model (i.e. not using DarcyTools data) yields an influence area of the groundwater-table drawdown that is very different to that reported for DarcyTools /Svensson and Follin 2010/. Figure 10-1 compares the results from the two models for development phase 3 and grouting case $K_{grout} = 10^{-8}$ m/s. As can be seen in this figure, both models predict drawdown in areas

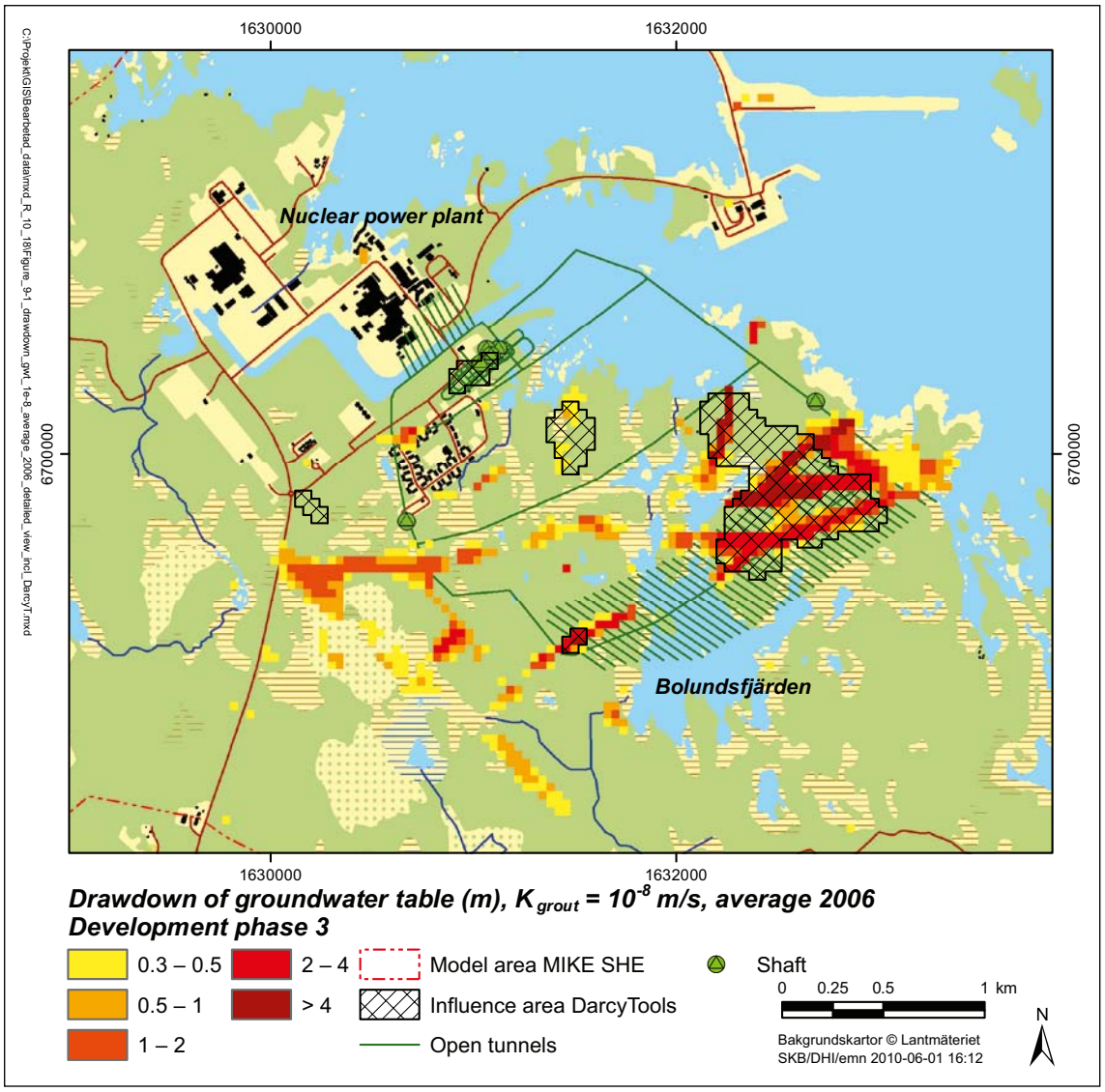

Figure 10-1. *Annual average MIKE SHE-calculated groundwater-table drawdown for development phase 3, $K_{grout} = 10^{-8}$ m/s. The figure also shows the DarcyTools-calculated influence area (drawdown >0.3 m) for $K_{grout} = 10^{-8}$ m/s (grouting level II of /Svensson and Follin 2010/) for development phase 3 (their stage C).*

north and northeast of Lake Bolundsfjärden. As mentioned previously, the shape of the influence area is very different in the two models. Moreover, in the DarcyTools simulations areas west of Lake Bolundsfjärden are more or less unaffected by the groundwater inflow, and the predicted maximum groundwater-table drawdown occurs at the central area. In the MIKE SHE simulations, there is no drawdown at this area.

10.4 Uncertainties

Chapter 9 discusses three types of uncertainty, namely conceptual uncertainty, parameter uncertainty and numerical-model uncertainty. In general, there is little conceptual uncertainty due to the extensive site investigations. For instance, this implies that there is high confidence concerning the locations of fracture zones with high vertical hydraulic conductivity, which causes the band-shaped pattern of the groundwater-table drawdown. The same applies to the locations of the horizontal sheet joints that transmit hydraulic-head drawdown in a large area in the bedrock.

Sensitivity analyses can be used as a tool to assess factors that are considered as uncertain. Sensitivity analyses presented in this report and in /Gustafsson et al. 2009/ demonstrate that the hydrogeological parameterisation of the bedrock is a potential source of uncertainty. However, the hydrogeological properties of the bedrock have been studied extensively within the framework of the site investigations and the site descriptive modelling, and evaluation of these properties has also been a key component in the MIKE SHE model calibration. As part of the present modelling, the hydraulic conductivity of the upper 200 m of the bedrock were adjusted by a factor of five compared to the data set delivered from the CONNECTFLOW modelling team (see Section 5.3). Back adjustments to original values yield a 20% reduction of the inflow to the repository compared to the MIKE SHE base case. The parameter adjustments made for the base case are motivated by the results from comparisons between model calculated and measured hydraulic heads for different parameter combinations describing the hydrogeological properties of the bedrock. The results of calibration using interference-test data (i.e. data from known hydraulic disturbances) further strengthens the rationale for the parameter adjustments. Despite what is said above, the hydrogeological parameterisation of the upper part of the bedrock is a potential uncertainty factor that cannot be ignored.

Errors in the calculation of the groundwater inflow to the repository (the MIKE SHE-MOUSE coupling routine) are now resolved (cf. /Gustafsson et al. 2009/) by the development and testing of the new coupling routine. Hence, this coupling routine is now considered as a minor source of uncertainty.

The meteorological conditions have large influence on the groundwater-table drawdown. All modelling results presented in this report are based on meteorological data for the two-year period 2005–2006. Comparing Forsmark modelling results for a statistically normal year and the year 2006, /Mårtensson et al. 2010/ report a difference is 36% in terms of the influence area for the groundwater-table drawdown. The size of the influence area varies also during an individual year. Focusing on the year 2006, /Mårtensson et al. 2010/ show that the influence area of the monthly average drawdown is approximately three times larger in November than in May. However, the inflow to the repository is not as sensitive to the meteorological conditions; the inflow difference between a dry and a wet year (each with a return period of 100 years) is only a few percent. This is due to similar vertical hydraulic gradients between the QD and the bedrock at repository level for different meteorological conditions.

10.5 Implications for Environmental Impact Assessment (EIA)

This report provides important background material for the EIA associated with the construction, operation and decommissioning of the repository in Forsmark. Specifically, the MIKE SHE modelling results and the findings from this study will be part of a permit application according to the Swedish Environmental Code, regarding water operations (Chapter 11 in the Environmental Code) in the form of diversion of groundwater from the repository. The report is therefore concluded by pointing out some findings that may be important to consider in the EIA and the permit application.

In terms of groundwater diversion, the results of the study can be used as a support for formulating suggested conditions in the water-operations permit application. Moreover, predicted groundwater inflows for different simulations cases are directly coupled to quantifications of the associated hydrogeological and hydrological effects in the surroundings of the repository, including effects on groundwater levels at different depths in the rock, the location of the groundwater table, stream discharges, and lake-water levels. These results can hence be used as direct input to analyses and descriptions of the consequences of the groundwater diversion.

The results of the study shows that to some degree, the rate of groundwater diversion that will be required to maintain the repository drained depends on both how large part of the repository that is open at a particular point in time and on the hydraulic conductivity of the grouted zone. Additional reasoning and expert judgement may be required if the modelling results are used to formulate suggested conditions in the water-operations permit application, because all possible combinations of development stages and values of K_{grout} have not been analysed explicitly in the modelling.

In terms of groundwater head changes in the rock and drawdown of the groundwater table, the size of the influence areas to some degree also depends on the above-mentioned factors. In general, this type of dependence would imply that different sets of e.g. private wells installed in Quaternary deposits would be affected during different development stages, hence also depending on the grouting level. However, the hydrogeological characteristics of the upper part of the bedrock in the Forsmark area imply that the size of the influence area for the groundwater-table drawdown is much smaller compared to the influence area for groundwater head changes in the rock. Further, the overall pattern of the groundwater-table influence area is to a large degree governed by the structural geology of the Forsmark area, specifically the presence of high conductive horizontal features (sheet joints) in the upper part of the bedrock that connect to fracture zones with high vertical hydraulic conductivity.

Based on these findings, it is suggested to use one or a few limited simulation cases as inputs to analyses and descriptions of the consequences of the groundwater diversion. For instance, in terms of groundwater inflow and resulting hydrogeological and hydrological effects, there are relatively small differences between the hypothetical case with a fully open repository and the more realistic cases that represent separate development stages. Moreover, depending on the type of consequence to be analysed, it may be possible to base the analysis on the modelling results obtained for grouting case $K_{grout} = 10^{-7}$ m/s. The study shows that in general terms, the case with a fully open repository and $K_{grout} = 10^{-7}$ m/s would provide a conservative, but not unrealistic, input to consequence analyses and descriptions. However, for specific areas and/or types of consequences, there is a need to be more elaborate in order to attain a reasonable and realistic basis for the consequence analysis.

11 References

SKB's (Svensk Kärnbränslehantering AB) publications can be found at www.skb.se/publications. References to SKB's unpublished documents are listed separately at the end of the reference list. Unpublished documents will be submitted upon request to document@skb.se.

Bosson E, Berglund S, 2006. Near-surface hydrogeological model of Forsmark. Open repository and solute transport applications – Forsmark 1.2. SKB R-06-52, Svensk Kärnbränslehantering AB.

Bosson E, Gustafsson L-G, Sassner M, 2008. Numerical modelling of surface hydrology and near-surface hydrogeology at Forsmark. Site descriptive modelling, SDM-Site Forsmark. SKB R-08-09, Svensk Kärnbränslehantering AB.

Bosson E, Sassner M, Sabel U, Gustafsson L-G, 2010. Modelling of present and future hydrology and solute transport at Forsmark. SR-Site Biosphere. SKB R-10-02, Svensk Kärnbränslehantering AB.

Brantberger M, Janson T, 2009. Underground design Forsmark, Layout D2. Grouting. SKB R-08-114, Svensk Kärnbränslehantering AB.

Brydsten L, Engqvist A, Näslund J-O, Lindborg T, 2009. Expected extreme sea levels at Forsmark and Laxemar–Simpevarp up until year 2100. SKB TR-09-21, Svensk Kärnbränslehantering AB.

Cesano D, Olofsson B, Bagtzoglou C, 2000. Parameters regulating groundwater inflows into hard rock tunnels – a statistical study of the Bolmen tunnel in southern Sweden. Tunnelling and Underground Space Tech. 15(2), 153–165.

DHI Software, 2010a. MIKE SHE – User Manual. DHI Water, Environment & Health, Hørsholm, Denmark.

DHI Software, 2010b. MOUSE PIPE FLOW – Reference Manual. DHI Water, Environment & Health, Hørsholm, Denmark.

Follin S, Johansson P-O, Hartley L, Jackson P, Roberts D, Marsic N, 2007. Hydrogeological conceptual model development and numerical modelling using CONNECTFLOW, Forsmark modelling stage 2.2. SKB R-07-49, Svensk Kärnbränslehantering AB.

Follin S, 2008. Bedrock hydrogeology Forsmark. Site descriptive modelling, SDM-Site Forsmark. SKB R-08-95, Svensk Kärnbränslehantering AB.

Follin S, Hartley L, Jackson P, Roberts D, Marsic N, 2008. Hydrogeological conceptual model development and numerical modelling using CONNECTFLOW, Forsmark modelling stage 2.3. SKB R-08-23, Svensk Kärnbränslehantering AB.

Gokall-Norman K, Ludvigson J-E, 2007. Forsmark site investigation. Hydraulic interference test in borehole HFM14. SKB P-06-196, Svensk Kärnbränslehantering AB.

Graham D N, Butts M B, 2005. Flexible, integrated watershed modelling with MIKE SHE. In: Watershed Models (Ch. 10), Singh V P, Frevert D K (eds.), 245–272, CRC Press.

Gustafsson L-G, Sassner M, Bosson E, 2008. Numerical modelling of solute transport at Forsmark with MIKE SHE. Site descriptive modelling, SDM-Site Forsmark. SKB R-08-106, Svensk Kärnbränslehantering AB.

Gustafsson L-G, Gustafsson A-M, Aneljung M, Sabel U, 2009. Effects on surface hydrology and near-surface hydrogeology of an open repository in Forsmark. Results of modelling with MIKE SHE. SKB R-08-121, Svensk Kärnbränslehantering AB.

Hedenström A, Sohlenius G, 2008. Description of regolith at Forsmark. Site descriptive modelling, SDM-Site Forsmark. SKB R-08-04, Svensk Kärnbränslehantering AB.

Johansson P-O, 2008. Description of surface hydrology and near-surface hydrogeology at Forsmark. Site descriptive modelling, SDM-Site Forsmark. SKB R-08-08, Svensk Kärnbränslehantering AB.

Joyce S, Applegate D, Hartley L, Hoek J, Simpson T, Swan D, Marsic N, Follin S, 2010. Groundwater flow modelling of periods with temperate climate conditions – SR-Site Forsmark. SKB R-09-20, Svensk Kärnbränslehantering AB.

Kristensen K J, Jensen S E, 1975. A model for estimating actual evapotranspiration from potential evapotranspiration. Nordic Hydrology, vol. 6, pp. 170–188.

Lindborg T (ed.), 2008. Surface system Forsmark. Site descriptive modelling, SDM-Site Forsmark. SKB R-08-11, Svensk Kärnbränslehantering AB.

Mårtensson E, Gustafsson L-G, Gustafsson A-M, Aneljung M, Sabel U, 2010. Hydrologiska och hydrogeologiska effekter på våtmarker och skogsområden av slutförvarsanläggningen i Forsmark. Resultat från modellering med MIKE SHE. SKB R-10-19, Svensk Kärnbränslehantering AB. (In Swedish.)

Odén M, 2009. Site investigation SFR. Hydrogeological modelling at SFR using DarcyTools. Site description SFR version 0.0. P-08-94, Svensk Kärnbränslehantering AB.

Olofsson B, 1994. Flow of groundwater from soil to crystalline rock. Hydrogeol. J. 2(3), 71–83.

SKB, 2008a. Site description of Forsmark at completion of the site investigation phase. SDM-Site Forsmark. SKB TR-08-05, Svensk Kärnbränslehantering AB.

SKB, 2008b. Geovetenskapligt undersökningsprogram för utbyggnad av SFR. SKB R-08-67, Svensk Kärnbränslehantering AB. (In Swedish.)

Svensson U, Follin S, 2010. Groundwater flow modelling of the excavation and operation phases – SR-Site Forsmark. SKB R-09-19, Svensk Kärnbränslehantering AB.

Unpublished documents

SKBdoc id	Title	Issuer, year
1177184 ver 0.20	Design, production and initial state of the backfill and plug in deposition tunnels for the safety assessment SR-Site	SKB, 20XX
1177186 ver 0.13	Closure production report	SKB, 20XX

Appendix 1

Surface-water discharges

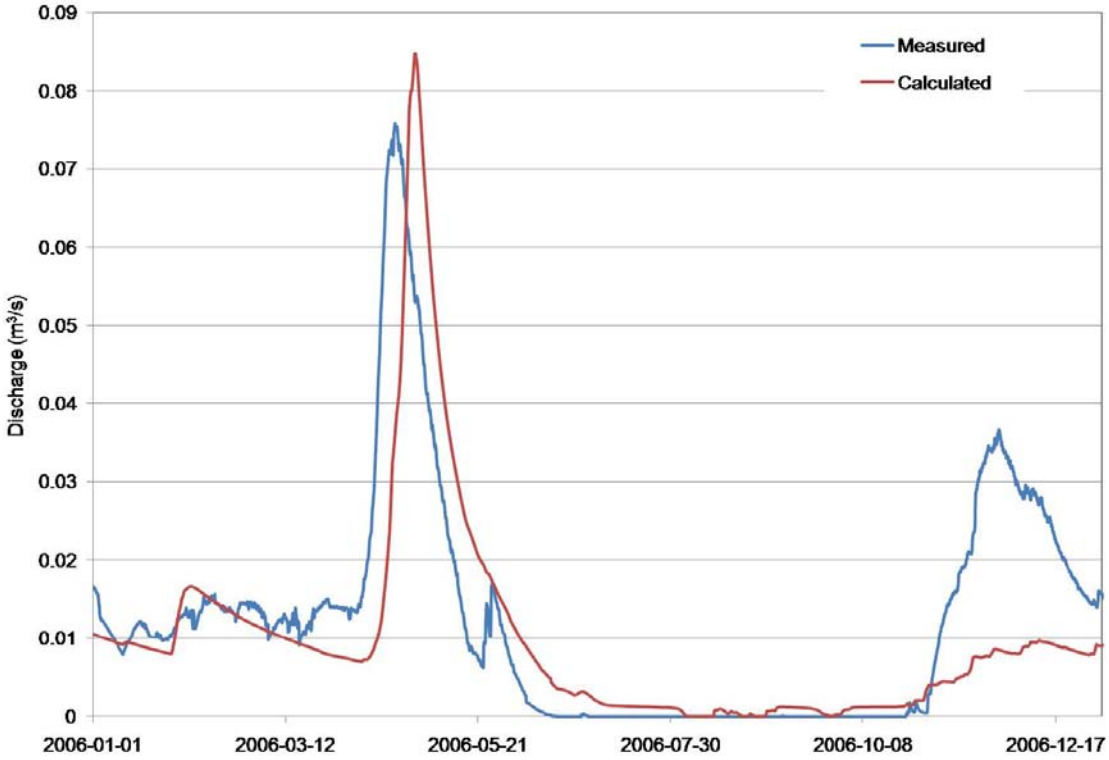

Figure A1-1. *Measured and calculated discharges (m^3/s) downstream Lake Eckarfjärden (reference simulation, undisturbed conditions).*

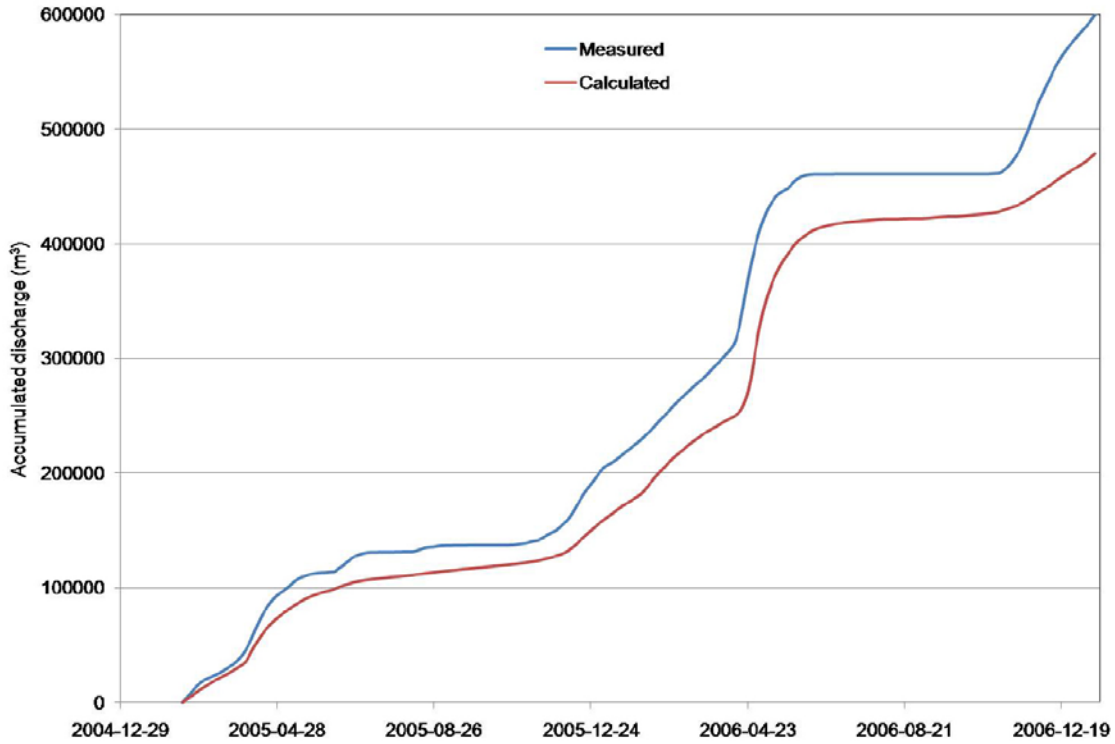

Figure A1-2. *Measured and calculated accumulated discharges (m^3) downstream Lake Eckarfjärden (reference simulation, undisturbed conditions).*

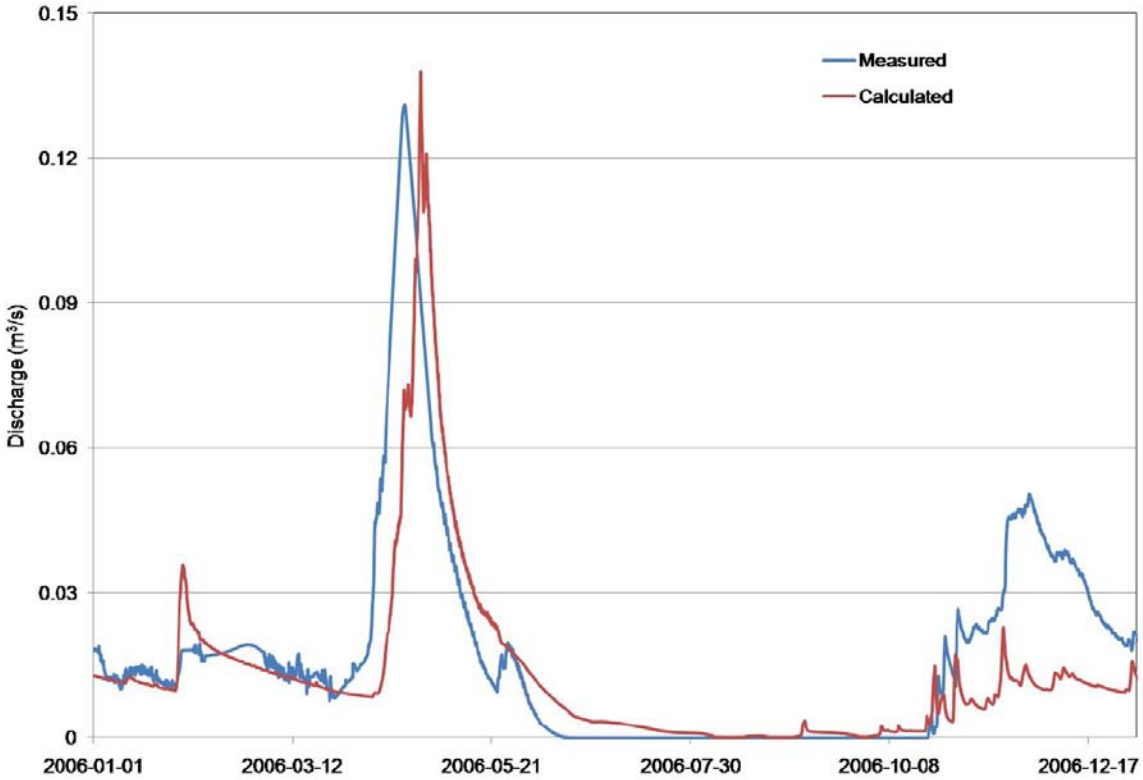

Figure A1-3. *Measured and calculated discharges (m^3/s) downstream Lake Stocksjön (reference simulation, undisturbed conditions).*

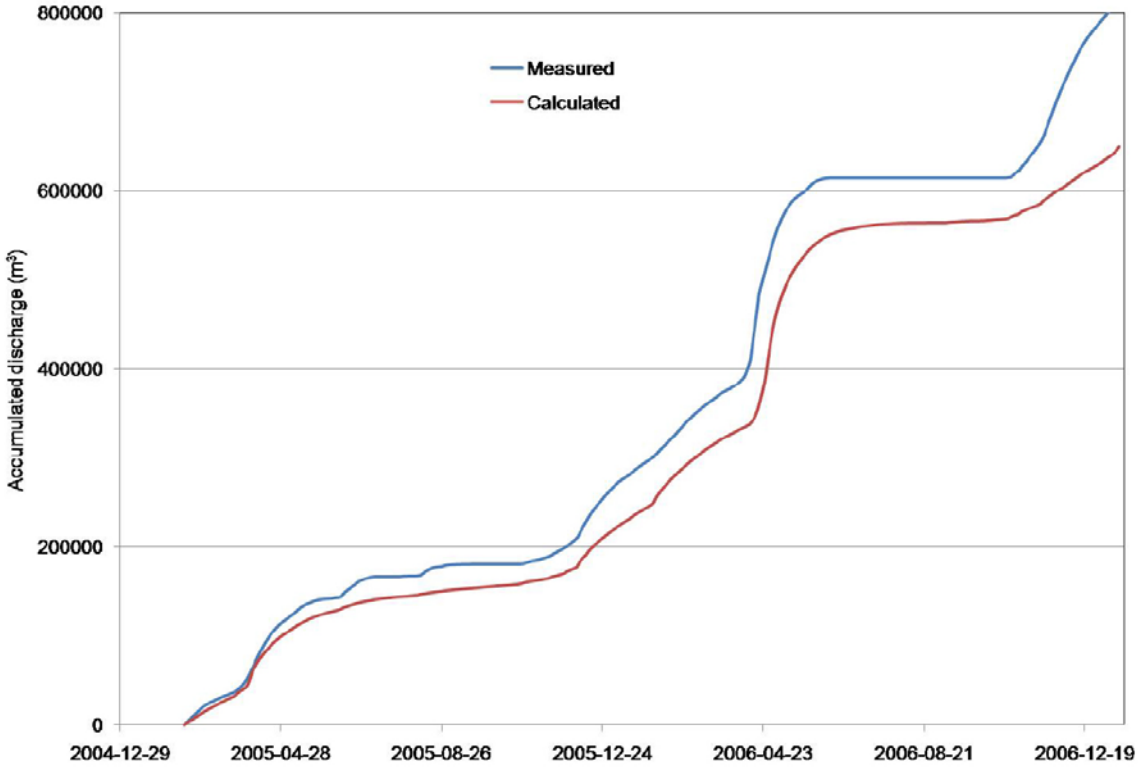

Figure A1-4. *Measured and calculated accumulated discharges (m^3) downstream Lake Stocksjön (reference simulation, undisturbed conditions).*

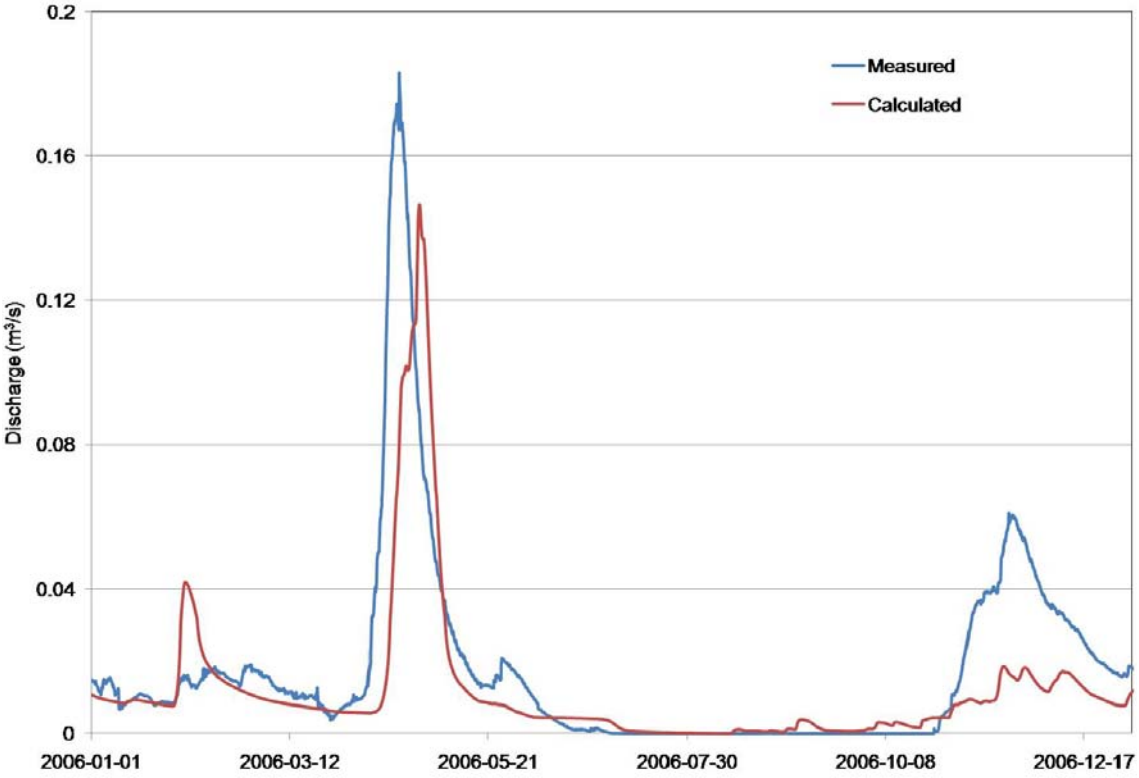

Figure A1-5. *Measured and calculated discharges (m^3/s) downstream Lake Gunnarsboträsket (reference simulation, undisturbed conditions).*

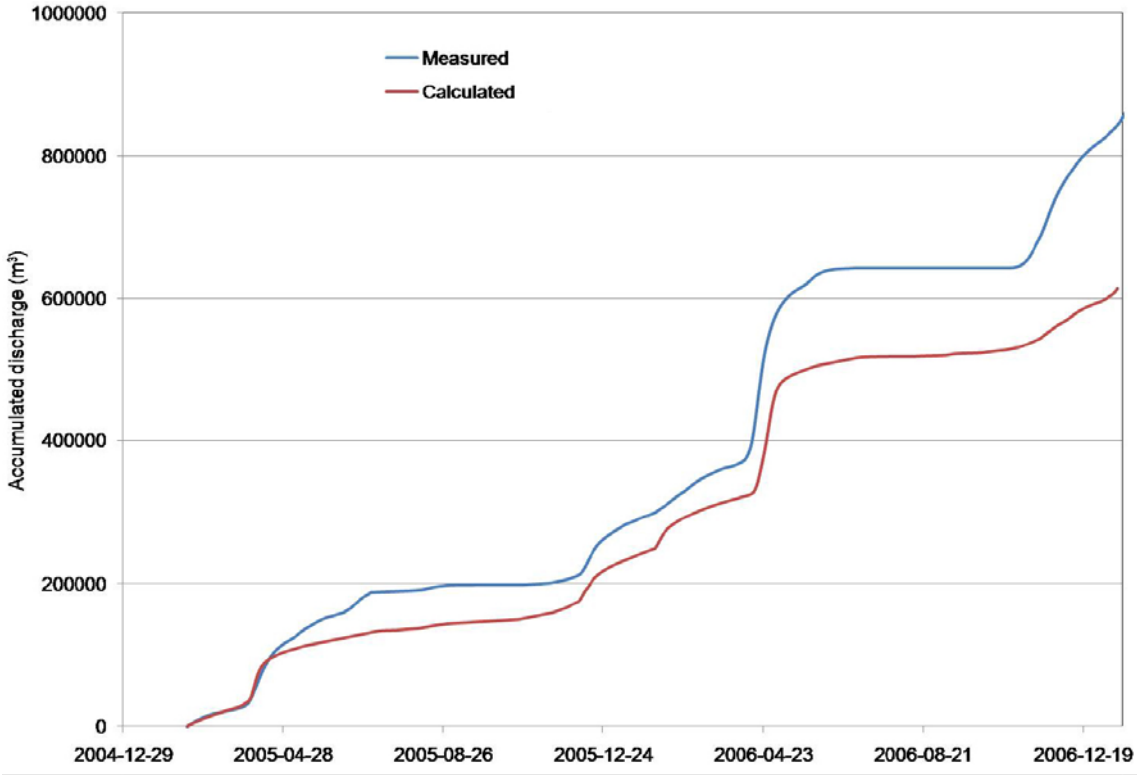

Figure A1-6. *Measured and calculated accumulated discharges (m^3) downstream Lake Gunnarsboträsket (reference simulation, undisturbed conditions).*

Appendix 2

Grouted-zone conductance for the shafts

The total conductance (C) of the grouted zone around the vertical shafts depends on the hydraulic conductivity (K_{grout}) and the thickness of this zone (d_{grout}). The values used for each shaft in the different grouting cases are listed in Tables A2-1 to A2-15. Two of the shafts (SF00 and ST00) are located very close to each other, which imply that a total conductance is calculated for both shafts. The method for calculation of the conductance C is described in Section 2.3.2.

Table A2-1. Geometry, hydraulic conductivity (K_h) and conductance (C) for shaft SA01, for $K_{grout} = 10^{-7}$ m/s.

Calc. layer	Shaft radius (m)	K_h (m/s)	Layer thickness (m)	D_{grout} (m)	K_{grout} (m/s)	Min(K_{grout}, K_h)	Conductance, C (m/s)
1	1.50	7.50E-06	2.59	5.00	1.00E-07	1.00E-07	1.11E-06
2	1.50	5.86E-06	2.69	5.00	1.00E-07	1.00E-07	1.15E-06
3	1.50	9.81E-12	18.80	5.00	1.00E-07	9.81E-12	7.90E-10
4	1.50	2.31E-09	20.00	5.00	1.00E-07	2.31E-09	1.98E-07
5	1.50	5.75E-08	20.00	5.00	1.00E-07	5.75E-08	4.93E-06
6	1.50	1.14E-07	20.00	5.00	1.00E-07	1.00E-07	8.57E-06
7	1.50	9.76E-09	20.00	5.00	1.00E-07	9.76E-09	8.36E-07
8	1.50	2.65E-08	20.00	5.00	1.00E-07	2.65E-08	2.27E-06
9	1.50	1.87E-08	20.00	5.00	1.00E-07	1.87E-08	1.60E-06
10	1.50	5.55E-09	20.00	5.00	1.00E-07	5.55E-09	4.76E-07
11	1.50	3.17E-09	20.00	5.00	1.00E-07	3.17E-09	2.72E-07
12	1.50	6.65E-09	20.00	5.00	1.00E-07	6.65E-09	5.70E-07
13	1.50	3.33E-10	98.59	5.00	1.00E-07	3.33E-10	1.41E-07
14	1.50	1.14E-09	102.59	5.00	1.00E-07	1.14E-09	5.01E-07
15	1.50	3.83E-10	61.82	5.00	1.00E-07	3.83E-10	1.01E-07

Table A2-2. Geometry, hydraulic conductivity (K_h) and conductance (C) for shaft SA02, for $K_{grout} = 10^{-7}$ m/s.

Calc. layer	Shaft radius (m)	K_h (m/s)	Layer thickness (m)	D_{grout} (m)	K_{grout} (m/s)	Min(K_{grout}, K_h)	Conductance, C (m/s)
1	1.50	2.81E-06	2.24	5.00	1.00E-07	1.00E-07	9.60E-07
2	1.50	1.00E-07	1.00	5.00	1.00E-07	1.00E-07	4.28E-07
3	1.50	2.67E-07	20.71	5.00	1.00E-07	1.00E-07	8.87E-06
4	1.50	3.65E-08	20.00	5.00	1.00E-07	3.65E-08	3.13E-06
5	1.50	5.79E-07	20.00	5.00	1.00E-07	1.00E-07	8.57E-06
6	1.50	1.14E-06	20.00	5.00	1.00E-07	1.00E-07	8.57E-06
7	1.50	2.44E-09	20.00	5.00	1.00E-07	2.44E-09	2.09E-07
8	1.50	9.18E-06	20.00	5.00	1.00E-07	1.00E-07	8.57E-06
9	1.50	5.23E-09	20.00	5.00	1.00E-07	5.23E-09	4.48E-07
10	1.50	1.20E-08	20.00	5.00	1.00E-07	1.20E-08	1.03E-06
11	1.50	2.31E-09	20.00	5.00	1.00E-07	2.31E-09	1.98E-07
12	1.50	5.72E-09	20.00	5.00	1.00E-07	5.72E-09	4.90E-07
13	1.50	1.44E-08	97.10	5.00	1.00E-07	1.44E-08	5.99E-06
14	1.50	1.72E-08	101.10	5.00	1.00E-07	1.72E-08	7.45E-06
15	1.50	1.75E-09	65.21	5.00	1.00E-07	1.75E-09	4.89E-07

Table A2-3. Geometry, hydraulic conductivity (K_h) and conductance (C) for shaft SB00, for $K_{grout} = 10^{-7}$ m/s.

Calc. layer	Shaft radius (m)	K_h (m/s)	Layer thickness (m)	D_{grout} (m)	K_{grout} (m/s)	Min(K_{grout}, K_h)	Conductance, C (m/s)
1	3.00	9.53E-05	2.36	5.00	1.00E-07	1.00E-07	1.51E-06
2	3.00	5.56E-06	1.00	5.00	1.00E-07	1.00E-07	6.41E-07
3	3.00	5.81E-08	20.20	5.00	1.00E-07	5.81E-08	7.52E-06
4	3.00	1.92E-06	20.00	5.00	1.00E-07	1.00E-07	1.28E-05
5	3.00	3.80E-07	20.00	5.00	1.00E-07	1.00E-07	1.28E-05
6	3.00	7.28E-07	20.00	5.00	1.00E-07	1.00E-07	1.28E-05
7	3.00	2.92E-08	20.00	5.00	1.00E-07	2.92E-08	3.74E-06
8	3.00	8.02E-08	20.00	5.00	1.00E-07	8.02E-08	1.03E-05
9	3.00	2.84E-08	20.00	5.00	1.00E-07	2.84E-08	3.64E-06
10	3.00	1.28E-07	20.00	5.00	1.00E-07	1.00E-07	1.28E-05
11	3.00	8.26E-07	20.00	5.00	1.00E-07	1.00E-07	1.28E-05
12	3.00	4.19E-08	20.00	5.00	1.00E-07	4.19E-08	5.37E-06
13	3.00	1.76E-08	96.35	5.00	1.00E-07	1.76E-08	1.09E-05
14	3.00	5.16E-10	100.35	5.00	1.00E-07	5.16E-10	3.32E-07
15	3.00	1.95E-11	89.74	5.00	1.00E-07	1.95E-11	1.12E-08

Table A2-4. Geometry, hydraulic conductivity (K_h) and conductance (C) for shaft SC00, for $K_{grout} = 10^{-7}$ m/s.

Calc. layer	Shaft radius (m)	K_h (m/s)	Layer thickness (m)	D_{grout} (m)	K_{grout} (m/s)	Min(K_{grout}, K_h)	Conductance, C (m/s)
1	2.75	7.50E-06	2.34	5.00	1.00E-07	1.00E-07	1.42E-06
2	2.75	5.05E-06	1.22	5.00	1.00E-07	1.00E-07	7.40E-07
3	2.75	3.59E-09	20.24	5.00	1.00E-07	3.59E-09	4.41E-07
4	2.75	1.10E-06	20.00	5.00	1.00E-07	1.00E-07	1.21E-05
5	2.75	2.19E-07	20.00	5.00	1.00E-07	1.00E-07	1.21E-05
6	2.75	2.00E-07	20.00	5.00	1.00E-07	1.00E-07	1.21E-05
7	2.75	1.07E-07	20.00	5.00	1.00E-07	1.00E-07	1.21E-05
8	2.75	9.00E-07	20.00	5.00	1.00E-07	1.00E-07	1.21E-05
9	2.75	3.03E-09	20.00	5.00	1.00E-07	3.03E-09	3.67E-07
10	2.75	2.55E-09	20.00	5.00	1.00E-07	2.55E-09	3.09E-07
11	2.75	3.19E-09	20.00	5.00	1.00E-07	3.19E-09	3.87E-07
12	2.75	5.33E-07	20.00	5.00	1.00E-07	1.00E-07	1.21E-05
13	2.75	1.02E-09	97.11	5.00	1.00E-07	1.02E-09	6.01E-07
14	2.75	1.74E-09	100.11	5.00	1.00E-07	1.74E-09	1.06E-06
15	2.75	7.62E-11	100.00	5.00	1.00E-07	7.62E-11	4.62E-08
16	2.75	1.07E-11	18.98	5.00	1.00E-07	1.07E-11	1.23E-09

Table A2-5. Geometry, hydraulic conductivity (K_h) and conductance (C) for shafts SF00 and ST00, for $K_{grout} = 10^{-7}$ m/s.

Calc. layer	Shaft radius (m)	K_h (m/s)	Layer thickness (m)	D_{grout} (m)	K_{grout} (m/s)	Min(K_{grout}, K_h)	Conductance, C (m/s)
1	3.50	8.50E-06	2.62	5.00	1.00E-07	1.00E-07	1.86E-06
2	3.50	6.76E-06	2.12	5.00	1.00E-07	1.00E-07	1.50E-06
3	3.50	4.81E-08	19.25	5.00	1.00E-07	4.81E-08	6.56E-06
4	3.50	2.37E-06	20.00	5.00	1.00E-07	1.00E-07	1.42E-05
5	3.50	1.21E-06	20.00	5.00	1.00E-07	1.00E-07	1.42E-05
6	3.50	1.70E-06	20.00	5.00	1.00E-07	1.00E-07	1.42E-05
7	3.50	3.72E-08	20.00	5.00	1.00E-07	3.72E-08	5.27E-06
8	3.50	1.69E-06	20.00	5.00	1.00E-07	1.00E-07	1.42E-05
9	3.50	1.06E-09	20.00	5.00	1.00E-07	1.06E-09	1.50E-07
10	3.50	7.03E-08	20.00	5.00	1.00E-07	7.03E-08	9.96E-06
11	3.50	1.88E-08	20.00	5.00	1.00E-07	1.88E-08	2.66E-06
12	3.50	6.81E-07	20.00	5.00	1.00E-07	1.00E-07	1.42E-05
13	3.50	4.16E-10	96.34	5.00	1.00E-07	4.16E-10	2.84E-07
14	3.50	7.11E-10	100.34	5.00	1.00E-07	7.11E-10	5.05E-07
15	3.50	1.28E-10	41.53	5.00	1.00E-07	1.28E-10	3.76E-08

Table A2-6. Geometry, hydraulic conductivity (Kh) and conductance (C) for shaft SA01, for $K_{grout} = 10^{-8}$ m/s.

Calc. layer	Shaft radius (m)	K_h (m/s)	Layer thickness (m)	D_{grout} (m)	K_{grout} (m/s)	Min(K_{grout}, K_h)	Conductance, C (m/s)
1	1.50	7.50E-06	2.59	5.00	1.00E-08	1.00E-08	1.11E-07
2	1.50	5.86E-06	2.69	5.00	1.00E-08	1.00E-08	1.15E-07
3	1.50	9.81E-12	18.80	5.00	1.00E-08	9.81E-12	7.90E-10
4	1.50	2.31E-09	20.00	5.00	1.00E-08	2.31E-09	1.98E-07
5	1.50	5.75E-08	20.00	5.00	1.00E-08	1.00E-08	8.57E-07
6	1.50	1.14E-07	20.00	5.00	1.00E-08	1.00E-08	8.57E-07
7	1.50	9.76E-09	20.00	5.00	1.00E-08	9.76E-09	8.36E-07
8	1.50	2.65E-08	20.00	5.00	1.00E-08	1.00E-08	8.57E-07
9	1.50	1.87E-08	20.00	5.00	1.00E-08	1.00E-08	8.57E-07
10	1.50	5.55E-09	20.00	5.00	1.00E-08	5.55E-09	4.76E-07
11	1.50	3.17E-09	20.00	5.00	1.00E-08	3.17E-09	2.72E-07
12	1.50	6.65E-09	20.00	5.00	1.00E-08	6.65E-09	5.70E-07
13	1.50	3.33E-10	98.59	5.00	1.00E-08	3.33E-10	1.41E-07
14	1.50	1.14E-09	102.59	5.00	1.00E-08	1.14E-09	5.01E-07
15	1.50	3.83E-10	61.82	5.00	1.00E-08	3.83E-10	1.01E-07

Table A2-7. Geometry, hydraulic conductivity (K_h) and conductance (C) for shaft SA02, for $K_{grout} = 10^{-8}$ m/s.

Calc. layer	Shaft radius (m)	K_h (m/s)	Layer thickness (m)	D_{grout} (m)	K_{grout} (m/s)	Min(K_{grout}, K_h)	Conductance, C (m/s)
1	1.50	2.81E-06	2.24	5.00	1.00E-08	1.00E-08	9.60E-08
2	1.50	1.00E-07	1.00	5.00	1.00E-08	1.00E-08	4.28E-08
3	1.50	2.67E-07	20.71	5.00	1.00E-08	1.00E-08	8.87E-07
4	1.50	3.65E-08	20.00	5.00	1.00E-08	1.00E-08	8.57E-07
5	1.50	5.79E-07	20.00	5.00	1.00E-08	1.00E-08	8.57E-07
6	1.50	1.14E-06	20.00	5.00	1.00E-08	1.00E-08	8.57E-07
7	1.50	2.44E-09	20.00	5.00	1.00E-08	2.44E-09	2.09E-07
8	1.50	9.18E-06	20.00	5.00	1.00E-08	1.00E-08	8.57E-07
9	1.50	5.23E-09	20.00	5.00	1.00E-08	5.23E-09	4.48E-07
10	1.50	1.20E-08	20.00	5.00	1.00E-08	1.00E-08	8.57E-07
11	1.50	2.31E-09	20.00	5.00	1.00E-08	2.31E-09	1.98E-07
12	1.50	5.72E-09	20.00	5.00	1.00E-08	5.72E-09	4.90E-07
13	1.50	1.44E-08	97.10	5.00	1.00E-08	1.00E-08	4.16E-06
14	1.50	1.72E-08	101.10	5.00	1.00E-08	1.00E-08	4.33E-06
15	1.50	1.75E-09	65.21	5.00	1.00E-08	1.75E-09	4.89E-07

Table A2-8. Geometry, hydraulic conductivity (K_h) and conductance (C) for shaft SB00, for $K_{grout} = 10^{-8}$ m/s.

Calc. layer	Shaft radius (m)	K_h (m/s)	Layer thickness (m)	D_{grout} (m)	K_{grout} (m/s)	Min(K_{grout}, K_h)	Conductance, C (m/s)
1	3.00	9.53E-05	2.36	5.00	1.00E-08	1.00E-08	1.51E-07
2	3.00	5.56E-06	1.00	5.00	1.00E-08	1.00E-08	6.41E-08
3	3.00	5.81E-08	20.20	5.00	1.00E-08	1.00E-08	1.29E-06
4	3.00	1.92E-06	20.00	5.00	1.00E-08	1.00E-08	1.28E-06
5	3.00	3.80E-07	20.00	5.00	1.00E-08	1.00E-08	1.28E-06
6	3.00	7.28E-07	20.00	5.00	1.00E-08	1.00E-08	1.28E-06
7	3.00	2.92E-08	20.00	5.00	1.00E-08	1.00E-08	1.28E-06
8	3.00	8.02E-08	20.00	5.00	1.00E-08	1.00E-08	1.28E-06
9	3.00	2.84E-08	20.00	5.00	1.00E-08	1.00E-08	1.28E-06
10	3.00	1.28E-07	20.00	5.00	1.00E-08	1.00E-08	1.28E-06
11	3.00	8.26E-07	20.00	5.00	1.00E-08	1.00E-08	1.28E-06
12	3.00	4.19E-08	20.00	5.00	1.00E-08	1.00E-08	1.28E-06
13	3.00	1.76E-08	96.35	5.00	1.00E-08	1.00E-08	6.17E-06
14	3.00	5.16E-10	100.35	5.00	1.00E-08	5.16E-10	3.32E-07
15	3.00	1.95E-11	89.74	5.00	1.00E-08	1.95E-11	1.12E-08

Table A2-9. Geometry, hydraulic conductivity (K_h) and conductance (C) for shaft SC00, for $K_{grout} = 10^{-8}$ m/s.

Calc. layer	Shaft radius (m)	K_h (m/s)	Layer thickness (m)	D_{grout} (m)	K_{grout} (m/s)	Min(K_{grout}, K_h)	Conductance, C (m/s)
1	2.75	7.50E-06	2.34	5.00	1.00E-08	1.00E-08	1.42E-07
2	2.75	5.05E-06	1.22	5.00	1.00E-08	1.00E-08	7.40E-08
3	2.75	3.59E-09	20.24	5.00	1.00E-08	3.59E-09	4.41E-07
4	2.75	1.10E-06	20.00	5.00	1.00E-08	1.00E-08	1.21E-06
5	2.75	2.19E-07	20.00	5.00	1.00E-08	1.00E-08	1.21E-06
6	2.75	2.00E-07	20.00	5.00	1.00E-08	1.00E-08	1.21E-06
7	2.75	1.07E-07	20.00	5.00	1.00E-08	1.00E-08	1.21E-06
8	2.75	9.00E-07	20.00	5.00	1.00E-08	1.00E-08	1.21E-06
9	2.75	3.03E-09	20.00	5.00	1.00E-08	3.03E-09	3.67E-07
10	2.75	2.55E-09	20.00	5.00	1.00E-08	2.55E-09	3.09E-07
11	2.75	3.19E-09	20.00	5.00	1.00E-08	3.19E-09	3.87E-07
12	2.75	5.33E-07	20.00	5.00	1.00E-08	1.00E-08	1.21E-06
13	2.75	1.02E-09	97.11	5.00	1.00E-08	1.02E-09	6.01E-07
14	2.75	1.74E-09	100.11	5.00	1.00E-08	1.74E-09	1.06E-06
15	2.75	7.62E-11	100.00	5.00	1.00E-08	7.62E-11	4.62E-08
16	2.75	1.07E-11	18.98	5.00	1.00E-08	1.07E-11	1.23E-09

Table A2-10. Geometry, hydraulic conductivity (K_h) and conductance (C) for shafts SF00 and ST00, for $K_{grout} = 10^{-8}$ m/s.

Calc. layer	Shaft radius (m)	K_h (m/s)	Layer thickness (m)	D_{grout} (m)	K_{grout} (m/s)	Min(K_{grout}, K_h)	Conductance, C (m/s)
1	3.50	8.50E-06	2.62	5.00	1.00E-08	1.00E-08	1.86E-07
2	3.50	6.76E-06	2.12	5.00	1.00E-08	1.00E-08	1.50E-07
3	3.50	4.81E-08	19.25	5.00	1.00E-08	1.00E-08	1.36E-06
4	3.50	2.37E-06	20.00	5.00	1.00E-08	1.00E-08	1.42E-06
5	3.50	1.21E-06	20.00	5.00	1.00E-08	1.00E-08	1.42E-06
6	3.50	1.70E-06	20.00	5.00	1.00E-08	1.00E-08	1.42E-06
7	3.50	3.72E-08	20.00	5.00	1.00E-08	1.00E-08	1.42E-06
8	3.50	1.69E-06	20.00	5.00	1.00E-08	1.00E-08	1.42E-06
9	3.50	1.06E-09	20.00	5.00	1.00E-08	1.06E-09	1.50E-07
10	3.50	7.03E-08	20.00	5.00	1.00E-08	1.00E-08	1.42E-06
11	3.50	1.88E-08	20.00	5.00	1.00E-08	1.00E-08	1.42E-06
12	3.50	6.81E-07	20.00	5.00	1.00E-08	1.00E-08	1.42E-06
13	3.50	4.16E-10	96.34	5.00	1.00E-08	4.16E-10	2.84E-07
14	3.50	7.11E-10	100.34	5.00	1.00E-08	7.11E-10	5.05E-07
15	3.50	1.28E-10	41.53	5.00	1.00E-08	1.28E-10	3.76E-08

Table A2-11. Geometry, hydraulic conductivity (K_h) and conductance (C) for shaft SA01, for $K_{grout} = 10^{-9}$ m/s.

Calc. layer	Shaft radius (m)	K_h (m/s)	Layer thickness (m)	D_{grout} (m)	K_{grout} (m/s)	Min(K_{grout}, K_h)	Conductance, C (m/s)
1	1.50	7.50E-06	2.59	5.00	1.00E-09	1.00E-09	1.11E-08
2	1.50	5.86E-06	2.69	5.00	1.00E-09	1.00E-09	1.15E-08
3	1.50	9.81E-12	18.80	5.00	1.00E-09	9.81E-12	7.90E-10
4	1.50	2.31E-09	20.00	5.00	1.00E-09	1.00E-09	8.57E-08
5	1.50	5.75E-08	20.00	5.00	1.00E-09	1.00E-09	8.57E-08
6	1.50	1.14E-07	20.00	5.00	1.00E-09	1.00E-09	8.57E-08
7	1.50	9.76E-09	20.00	5.00	1.00E-09	1.00E-09	8.57E-08
8	1.50	2.65E-08	20.00	5.00	1.00E-09	1.00E-09	8.57E-08
9	1.50	1.87E-08	20.00	5.00	1.00E-09	1.00E-09	8.57E-08
10	1.50	5.55E-09	20.00	5.00	1.00E-09	1.00E-09	8.57E-08
11	1.50	3.17E-09	20.00	5.00	1.00E-09	1.00E-09	8.57E-08
12	1.50	6.65E-09	20.00	5.00	1.00E-09	1.00E-09	8.57E-08
13	1.50	3.33E-10	98.59	5.00	1.00E-09	3.33E-10	1.41E-07
14	1.50	1.14E-09	102.59	5.00	1.00E-09	1.00E-09	4.40E-07
15	1.50	3.83E-10	61.82	5.00	1.00E-09	3.83E-10	1.01E-07

Table A2-12. Geometry, hydraulic conductivity (K_h) and conductance (C) for shaft SA02, for $K_{grout} = 10^{-9}$ m/s.

Calc. layer	Shaft radius (m)	K_h (m/s)	Layer thickness (m)	D_{grout} (m)	K_{grout} (m/s)	Min(K_{grout}, K_h)	Conductance, C (m/s)
1	1.50	2.81E-06	2.24	5.00	1.00E-09	1.00E-09	9.60E-09
2	1.50	1.00E-07	1.00	5.00	1.00E-09	1.00E-09	4.28E-09
3	1.50	2.67E-07	20.71	5.00	1.00E-09	1.00E-09	8.87E-08
4	1.50	3.65E-08	20.00	5.00	1.00E-09	1.00E-09	8.57E-08
5	1.50	5.79E-07	20.00	5.00	1.00E-09	1.00E-09	8.57E-08
6	1.50	1.14E-06	20.00	5.00	1.00E-09	1.00E-09	8.57E-08
7	1.50	2.44E-09	20.00	5.00	1.00E-09	1.00E-09	8.57E-08
8	1.50	9.18E-06	20.00	5.00	1.00E-09	1.00E-09	8.57E-08
9	1.50	5.23E-09	20.00	5.00	1.00E-09	1.00E-09	8.57E-08
10	1.50	1.20E-08	20.00	5.00	1.00E-09	1.00E-09	8.57E-08
11	1.50	2.31E-09	20.00	5.00	1.00E-09	1.00E-09	8.57E-08
12	1.50	5.72E-09	20.00	5.00	1.00E-09	1.00E-09	8.57E-08
13	1.50	1.44E-08	97.10	5.00	1.00E-09	1.00E-09	4.16E-07
14	1.50	1.72E-08	101.10	5.00	1.00E-09	1.00E-09	4.33E-07
15	1.50	1.75E-09	65.21	5.00	1.00E-09	1.00E-09	2.79E-07

Table A2-13. Geometry, hydraulic conductivity (K_h) and conductance (C) for shaft SB00, for $K_{grout} = 10^{-9}$ m/s.

Calc. layer	Shaft radius (m)	K_h (m/s)	Layer thickness (m)	D_{grout} (m)	K_{grout} (m/s)	Min(K_{grout}, K_h)	Conductance, C (m/s)
1	3.00	9.53E-05	2.36	5.00	1.00E-09	1.00E-09	1.51E-08
2	3.00	5.56E-06	1.00	5.00	1.00E-09	1.00E-09	6.41E-09
3	3.00	5.81E-08	20.20	5.00	1.00E-09	1.00E-09	1.29E-07
4	3.00	1.92E-06	20.00	5.00	1.00E-09	1.00E-09	1.28E-07
5	3.00	3.80E-07	20.00	5.00	1.00E-09	1.00E-09	1.28E-07
6	3.00	7.28E-07	20.00	5.00	1.00E-09	1.00E-09	1.28E-07
7	3.00	2.92E-08	20.00	5.00	1.00E-09	1.00E-09	1.28E-07
8	3.00	8.02E-08	20.00	5.00	1.00E-09	1.00E-09	1.28E-07
9	3.00	2.84E-08	20.00	5.00	1.00E-09	1.00E-09	1.28E-07
10	3.00	1.28E-07	20.00	5.00	1.00E-09	1.00E-09	1.28E-07
11	3.00	8.26E-07	20.00	5.00	1.00E-09	1.00E-09	1.28E-07
12	3.00	4.19E-08	20.00	5.00	1.00E-09	1.00E-09	1.28E-07
13	3.00	1.76E-08	96.35	5.00	1.00E-09	1.00E-09	6.17E-07
14	3.00	5.16E-10	100.35	5.00	1.00E-09	5.16E-10	3.32E-07
15	3.00	1.95E-11	89.74	5.00	1.00E-09	1.95E-11	1.12E-08

Table A2-14. Geometry, hydraulic conductivity (K_h) and conductance (C) for shaft SC00, for $K_{grout} = 10^{-9}$ m/s.

Calc. layer	Shaft radius (m)	K_h (m/s)	Layer thickness (m)	D_{grout} (m)	K_{grout} (m/s)	Min(K_{grout}, K_h)	Conductance, C (m/s)
1	2.75	7.50E-06	2.34	5.00	1.00E-09	1.00E-09	1.42E-08
2	2.75	5.05E-06	1.22	5.00	1.00E-09	1.00E-09	7.40E-09
3	2.75	3.59E-09	20.24	5.00	1.00E-09	1.00E-09	1.23E-07
4	2.75	1.10E-06	20.00	5.00	1.00E-09	1.00E-09	1.21E-07
5	2.75	2.19E-07	20.00	5.00	1.00E-09	1.00E-09	1.21E-07
6	2.75	2.00E-07	20.00	5.00	1.00E-09	1.00E-09	1.21E-07
7	2.75	1.07E-07	20.00	5.00	1.00E-09	1.00E-09	1.21E-07
8	2.75	9.00E-07	20.00	5.00	1.00E-09	1.00E-09	1.21E-07
9	2.75	3.03E-09	20.00	5.00	1.00E-09	1.00E-09	1.21E-07
10	2.75	2.55E-09	20.00	5.00	1.00E-09	1.00E-09	1.21E-07
11	2.75	3.19E-09	20.00	5.00	1.00E-09	1.00E-09	1.21E-07
12	2.75	5.33E-07	20.00	5.00	1.00E-09	1.00E-09	1.21E-07
13	2.75	1.02E-09	97.11	5.00	1.00E-09	1.00E-09	5.89E-07
14	2.75	1.74E-09	100.11	5.00	1.00E-09	1.00E-09	6.07E-07
15	2.75	7.62E-11	100.00	5.00	1.00E-09	7.62E-11	4.62E-08
16	2.75	1.07E-11	18.98	5.00	1.00E-09	1.07E-11	1.23E-09

Table A2-15. Geometry, hydraulic conductivity (K_h) and conductance (C) for shafts SF00 and ST00, for $K_{grout} = 10^{-9}$ m/s.

Calc. layer	Shaft radius (m)	K_h (m/s)	Layer thickness (m)	D_{grout} (m)	K_{grout} (m/s)	Min(K_{grout}, K_h)	Conductance, C (m/s)
1	3.50	8.50E-06	2.62	5.00	1.00E-09	1.00E-09	1.86E-08
2	3.50	6.76E-06	2.12	5.00	1.00E-09	1.00E-09	1.50E-08
3	3.50	4.81E-08	19.25	5.00	1.00E-09	1.00E-09	1.36E-07
4	3.50	2.37E-06	20.00	5.00	1.00E-09	1.00E-09	1.42E-07
5	3.50	1.21E-06	20.00	5.00	1.00E-09	1.00E-09	1.42E-07
6	3.50	1.70E-06	20.00	5.00	1.00E-09	1.00E-09	1.42E-07
7	3.50	3.72E-08	20.00	5.00	1.00E-09	1.00E-09	1.42E-07
8	3.50	1.69E-06	20.00	5.00	1.00E-09	1.00E-09	1.42E-07
9	3.50	1.06E-09	20.00	5.00	1.00E-09	1.00E-09	1.42E-07
10	3.50	7.03E-08	20.00	5.00	1.00E-09	1.00E-09	1.42E-07
11	3.50	1.88E-08	20.00	5.00	1.00E-09	1.00E-09	1.42E-07
12	3.50	6.81E-07	20.00	5.00	1.00E-09	1.00E-09	1.42E-07
13	3.50	4.16E-10	96.34	5.00	1.00E-09	4.16E-10	2.84E-07
14	3.50	7.11E-10	100.34	5.00	1.00E-09	7.11E-10	5.05E-07
15	3.50	1.28E-10	41.53	5.00	1.00E-09	1.28E-10	3.76E-08

Appendix 3

Results of particle-tracking simulations

Tables A3-1 and A3-2 present the distribution of particles on different registration zones/sinks after a simulation period of 100 years with a fully open repository (Table A3-1) and for the construction phase (Table A3-2). One particle was initially released in each MIKE SHE grid cell, and the model-calculated transient groundwater flow field for the year 2006 was cycled 100 times. Table 7-10 in Section 7.3 provides a summary of the information in Tables A3-1 and A3-2.

Table A3-1. Particle distribution on registration zones/sinks after a simulation period of 100 years for a fully open repository, $K_{grout} = 10^{-8}$ m/s. NOP = number of particles, NPP = Forsmark nuclear power plant.

Calc. layer	Unsaturated zone		River		Drain to river		Sea		Drain to boundary		Drainage at NPP		SFR		Repository		Left in the model	
	NOP	%	NOP	%	NOP	%	NOP	%	NOP	%	NOP	%	NOP	%	NOP	%	NOP	%
Layer 1	16,337	59	467	2	640	2	106	0	351	1	19	0	74	0	629	2	8,896	32
Layer 2	13,057	38	709	2	619	2	644	2	763	2	72	0	3,125	9	7,531	22	7,608	22
Layer 3	6,776	20	627	2	505	1	281	1	208	1	43	0	3,959	12	12,992	38	8,737	26
Layer 4	4,861	14	479	1	418	1	269	1	82	0	6	0	3,984	12	15,140	44	8,889	26
Layer 5	3,982	12	335	1	314	1	192	1	17	0			3,922	11	15,372	45	9,994	29
Layer 6	3,521	10	207	1	239	1	129	0	4	0			3,730	11	16,043	47	10,255	30
Layer 7	3,021	9	41	0	161	0	36	0					3,514	10	16,510	48	10,845	32
Layer 8	2,489	7	27	0	110	0	20	0					3,213	9	17,014	50	11,255	33
Layer 9	1,818	5	18	0	62	0	70	0					2,829	8	16,207	47	13,124	38
Layer 10	1,392	4	8	0	16	0	44	0					2,352	7	15,648	46	14,668	43
Layer 11	964	3	3	0			4	0					1,522	4	14,420	42	17,215	50
Layer 12	529	2											603	2	12,349	36	20,647	60
Layer 13	41	0											10	0	9,500	28	24,577	72
Layer 14															9,353	27	24,775	73
Layer 15															9,508	28	24,620	72
Layer 16															9,817	29	24,311	71
Layer 17															10,358	30	23,770	70
Layer 18															10,844	32	23,284	68
Layer 19															10,880	32	23,248	68
Layer 20															10,573	31	23,555	69
Layer 21															10,148	30	23,980	70
Layer 22															9,189	27	24,939	73
Total	**58,788**	**8**	**2,921**	**0**	**3,084**	**0**	**1,795**	**0**	**1,425**	**0**	**140**	**0**	**32,837**	**4**	**260,025**	**35**	**383,192**	**51**

Table A3-2. Particle distribution on registration zones/sinks after a simulation period of 100 years for the construction phase, $K_{grout} = 10^{-8}$ m/s. NOP = number of particles, NPP = Forsmark nuclear power plant.

Calculation layer	Unsaturated zone		River		Drain to river		Sea		Drain to boundary		Drainage at NPP		SFR		Repository		Left in the model	
	NOP	%	NOP	%	NOP	%	NOP	%	NOP	%	NOP	%	NOP	%	NOP	%	NOP	%
Layer 1	16,622	60	461	2	637	2	115	0	391	1	19	0	71	0	363	1	8,870	32
Layer 2	14,415	42	728	2	638	2	739	2	824	2	72	0	3,860	11	5,152	15	7,700	23
Layer 3	8,952	26	747	2	649	2	290	1	527	2	50	0	6,239	18	9,444	28	7,230	21
Layer 4	7,488	22	607	2	566	2	348	1	330	1	6	0	6,726	20	11,445	34	6,612	19
Layer 5	6,031	18	513	2	482	1	303	1	168	0			6,788	20	12,204	36	7,639	22
Layer 6	4,961	15	470	1	361	1	233	1	127	0			6,695	20	12,902	38	8,379	25
Layer 7	4,104	12	357	1	254	1	156	0	62	0			6,602	19	13,462	39	9,131	27
Layer 8	3,470	10	67	0	232	1	83	0	49	0			6,450	19	13,518	40	10,259	30
Layer 9	2,890	8	35	0	168	0	78	0	13	0			6,134	18	12,324	36	12,486	37
Layer 10	2,230	7	45	0	141	0	94	0	7	0			5,600	16	11,750	34	14,261	42
Layer 11	1,672	5	14	0	61	0	88	0					4,690	14	11,163	33	16,440	48
Layer 12	837	2	1	0	27	0	58	0					2,902	9	10,756	32	19,547	57
Layer 13	67	0	1	0	1	0	18	0					1,007	3	7,655	22	25,379	74
Layer 14							31	0					759	2	6,872	20	26,466	78
Layer 15							8	0					322	1	5,044	15	28,754	84
Layer 16							4	0					216	1	3,781	11	30,127	88
Layer 17							11	0					30	0	3,116	9	30,971	91
Layer 18							29	0							2,561	8	31,538	92
Layer 19							2	0							1,897	6	32,229	94
Layer 20															1,060	3	33,068	97
Layer 21															602	2	33,526	98
Layer 22															283	1	33,845	99
Total	**73,739**	**10**	**4,046**	**1**	**4,217**	**1**	**2,688**	**0**	**2,498**	**0**	**147**	**0**	**65,091**	**9**	**157,354**	**21**	**434,457**	**58**

Appendix 4

Saturation of backfill

Subsequent to the operational phase of the repository, the underground parts of the repository will be backfilled and the diversion of groundwater from the repository is terminated. This appendix describes the methodology used in MIKE SHE to study the backfill saturation process.

A simplified approach is used which implies that the pore volume of the backfill is lumped in the centre of the MOUSE pipe segments that represent the tunnels of the repository (see illustration in Figure A4-1). The solid mass of the backfill is modelled as a sealing layer, which is added to the grouted zone. The porosity of the backfill is used to calculate the reduced tunnel radius, $r_{red,}$ according to Equation A4-1.

$$r_{red} = r \cdot \sqrt{p} \qquad \text{A4-1}$$

r Original tunnel radius (m).

p Porosity of backfill material (–).

The thickness of the sealing layer, d_{seal}, is calculated separately. It is set so that the "backfill area" inside of d_{seal} in a cross section of the tunnel is equal to the area between d_{seal} and the tunnel wall. This yields the expression for d_{seal} as a function of the original tunnel radius (r) shown in Equation A4-2. According to preliminary plans, the backfill material to be used in the deposition tunnels (which constitute the largest part of the total volume of the repository) will have a porosity of 46%. If p = 0.46 is used in Equation A4-1, the sum of the reduced tunnel radius, r_{red}, and the thickness of the sealing layer, d_{seal}, will be very close to the original tunnel radius r (see Equation A4-3):

$$d_{seal} = r\ \left(1 - \frac{1}{\sqrt{2}}\right) \qquad \text{A4-2}$$

$$r\left(1 - \sqrt{0.46}\right) \cong r\left(1 - \frac{1}{\sqrt{2}}\right) \rightarrow r_{red} + d_{seal} \cong r \qquad \text{A4-3}$$

The exchange flow between MIKE SHE and MOUSE is calculated according to Equation 2-4. However, this equation needs to be changed for the case with a backfilled tunnel. Specifically, the tunnel radius (r) is replaced by the reduced tunnel radius (r_{red}), and the thickness of the sealing layer (d_{seal}) is added to the thickness of the grouted zone (d_{grout}), see Equation A4-4.

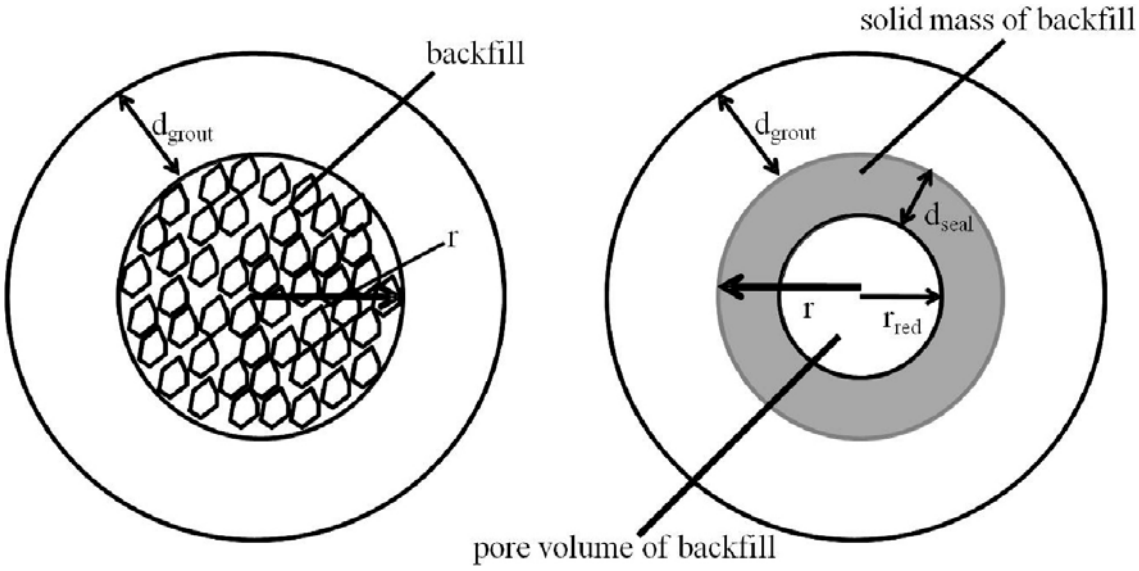

Figure A4-1. *Illustration of an actual backfilled tunnel (left) and the simplified approach used here (right).*

$$Q_{cell} = dh \cdot \frac{K \cdot 2 \cdot \pi}{\ln(\frac{r_{red} + (d_{grout} + d_{seal})}{r_{red}})} \cdot L \qquad \text{A4-4}$$

The total (lumped) hydraulic conductivity of the grouted zone and the sealing layer, K_{tot}, is calculated according to Equation A4-5, and then used in Equation A4-6 to determine the hydraulic conductivity, K, to be used in Equation A4-4.

$$K_{tot} = \frac{(d_{grout} + d_{seal})}{(\frac{d_{grout}}{K_{grout}} + \frac{d_{seal}}{K_{seal}})} \qquad \text{A4-5}$$

$$K = \min [K_{tot}, \max [K_h, K_v]] \qquad \text{A4-6}$$

Table A4-1 summarises the parameterisation of the backfill, based on preliminary plans /SKBdoc id 1177184, SKBdoc id 1177186/. Note that there are different requirements in terms of the hydraulic conductivity of the backfill material for different types of tunnels. In the tunnels and rock caverns within the central area and in the access tunnel above 200 m.b.s.l., according to the preliminary plans the backfill material will actually have a higher hydraulic conductivity compared to the grouted zone (grouting case $K_{grout} = 10^{-8}$ m/s was studied here). For those parts of the repository, the tunnel radius is reduced but the model does not take into include a sealing layer.

Table A4-1. Parameterisation of backfill materials, based on preliminary plans /SKBdoc id 1177184, SKBdoc id 1177186/.

	Porosity (–)	K_{seal} (m/s)
Deposition tunnels	0.46	10^{-10}
Main and transport tunnels	0.475	10^{-8}
Tunnels and rock caverns within central area	0.30	–
Access tunnel (below 200 m.b.s.l.)	0.475	10^{-8}
Access tunnel (above 200 m.b.s.l.)	0.40	–